The University Of Sheffield.

Reactions of Sydnones toward Pyrazole- and Sydnone-Based Analogues of CA4P

Author: Andrew W. Brown

August 2016

Submitted to the University of Sheffield in partial fulfilment of the requirements for the award of Doctor of Philosophy

Abstract

Sydnones represent versatile intermediates for the highly-regioselective synthesis of pyrazoles. The Buchwald ligand XPhos in conjunction with palladium catalysis facilitated the direct arylation of sydnones with aryl chlorides. Both *N*-aryl- and *N*-alkylsydnones were tolerated and the scope with respect to the aryl coupling partner was impressively broad.

The combretastatins are a class of tumour Vascular Disrupting Agents (VDAs) that have shown promise in the clinic for cancer therapy. Sydnone-based analogues of the lead compound, combretastatin A4 (CA4) were successfully prepared using the newly-developed direct arylation methodology. The compounds were evaluated *in vitro* using human umbilical vein endothelial cells (HUVECs) and the most active exhibited moderately high activity. The most active compound, **58**, was shown to activate the RhoA/ROCK pathway in a similar manner to CA4. **58** was phosphorylated to improve solubility and tested *in vivo*. However, the compound was completely inactive in the mouse model used.

Sydnones were used to prepare pyrazole-based analogues of CA4 in a highly-regioselective manner. Each possible structural isomer around the pyrazole core was successfully synthesised. The direct arylation methodology developed earlier was integral to the synthesis of 1,5- and 4,5-disubstituted analogues. In addition, an interesting monofluoromethylation reaction was also discovered and mechanistic insights obtained.

Similarly to sydnone analogues, the compounds were evaluated *in vitro* and exhibited modest to high activity. The most active compound, **85**, appeared at least as potent as CA4 in all the cell-based assays conducted. **85** was then analysed *in vivo*, and instigated an apparent increase in tumour cell necrosis in the mouse model used. Furthermore, it appeared equipotent to CA4P *in vivo*.

Directed cycloadditions offer a means to reduce the typically high temperatures and long reaction times required in dipolar cycloadditions. Typically, a Lewis acidic alkynylborane is generated in situ and paired with a Lewis basic directing group on the substrate. The methodology was successfully applied to sydnones with reaction temperatures decreased from 180 ^{o}C for the thermal reaction to 25 ^{o}C in the directed cycloaddition. Furthermore, reaction times were reduced to 2 hours from 48 hours in thermal reactions and afforded excellent yields of the pyrazole products. Interestingly, the sole products of the reactions were dialkynylboranes, which had only ever been observed as minor products in previous directed cycloadditions. The dialkynylboranes underwent typical reactions of organoboranes

including oxidation and Suzuki-Miyaura coupling. Mechanistic studies were undertaken and provided some insight into the unusual aspects of the reaction.

Acknowledgements

I am grateful to Cancer Research UK and Yorkshire Cancer Research for funding my studies and giving me the fantastic opportunities that the past 4 years have provided.

Joe – Thanks for putting up with me for 4 years! I wouldn't be half the chemist I am today without your continued input and wouldn't hate DFT half as much without the last few years... I truly appreciate all the opportunities you have given me throughout my time here and converting me to the boron-loving psychopath I am today. I also recognise just how much time you have invested in me, no one works harder for their students and I don't think you are always credited for that. I am sure the years will bring further successes (probably not for Celtic) and I look forward to keeping track of future group publications. I guess all that's left to say is "BINGO".

Chryso – Thank you for your endless patience in dealing your "resident chemist". I'd almost go as far as saying that I quite enjoy biology now… maybe not all the practical side (WESTERNS COUGH), but I have very much enjoyed learning from you. I must admit you were right, immunofluorescence pictures do make my thesis look pretty! Thank you for your superhuman effort as supervisor, lab technician, lab security, lab cleaner and every other job that you do, but isn't necessarily in your job description!

Gill – Thanks for all your input in group meetings, it has been an honour to be a part of your research group and see things from "the other side". Thank you for all the time you have invested in helping prepare the papers from this project, I am aware of how tight and precious your time is! I am sure you and the group will have continued success in the future.

Mum and Dad – No one has ever had more supportive parents, particularly at times when they didn't deserve it (I know I can be an awkward sod). This thesis is as much a reflection on you both as it is on me. I wouldn't be who I am today without you and have led me to success, often in spite of myself. I owe you both more than I can ever repay and will never forget the fantastic start (and boots up the backside) you have given me. I love you both and thank you.

Katy – What can I say Sis? Would I even have put myself through this if I didn't have such an amazingly talented little sister showing me up? Who knows… Although I may not always show it, you have been a constant source of inspiration to me. You could have excelled in anything you chose, and have quite successfully done so in your chosen field. Keep it up and I might even one day admit that you have more brains… In all seriousness, I couldn't be more proud of the woman you've become. Good luck Tom.

Grandma – You have always been a pillar of joy and inspiration in my life. Your support during my PhD has kept me upbeat in the bad times and I know the only person who wanted me to get this more than myself is you. Nothing brightens a bad day more than remembering that you are “as pure as the driven snow.”

Tracy – You make me a better chemist and a better person. It’s been a crazy 4 years and I still can’t quite believe my luck. It’s probably not healthy how much we talk about chemistry, but I’m not going to pretend that’s going to change. Every impact you have made on my life has been infinitely positive. I dread to think of the state of this thesis without you in my life. Now this monster is out of the way and yours is soon to follow, I am looking forward to actually having a life together.

Dave – Thank you for all your support through the years, you are a very important member of our family. Plus, I am pretty sure my love of chemistry stems from all those maths lessons years ago… I hope you’ve got over the disappointment of me choosing science over maths!

Rose and Ted – Thank you for accepting me into the family and all the times you have regularly helped both Tracy and myself out with either food and support during the course of our PhDs. Thank you for letting me marry your daughter, I will take good care of her.

Sally – Thanks for all your support and cooking during the past 4 years big sis! It’s been an awful few years for you in particular, but you have been so good by us both. I can only say thank you.

Josh, Mil and Toby – Thanks for being my surrogate family before the PhD and continuing afterwards. Although visits might be less frequent than they were, I still always enjoy coming round. Josh, the race is on for submission.

Nick – Thanks for all your help during my MChem and for being my independent advisor. I still try to solve problems by trying to think “how would Nick approach this”.

Dave Alker – Thanks for all your help Dave. Your input each year had a big impact on how I have approached my PhD and work.

Dr. Edeson – You’ve been the constant push I have needed to improve and not just teaching me how to oxidise and alcohol. I guess your company has been alright over the 4 years as well… Thank the Gods that I soon won’t have to listen to you hark on about having 2 degrees all the time.

Júlia – HOMA, TSP it's been a pleasure. Certainly not been the smoothest sailing in terms of our joint piece of work, but let's be fair, completely not our fault! I hope your postdoc is everything you want and gets you where you want to go.

Wheatos and Milk – The lab was a better place with you in it. I wish you all the success in the future. Banter king 2015-2016.

Noma – Just remember I always win buddy and I got outta there before you. Stinky Büchi queen 2016.

Matt Connolly – The knowledge bank! Oh how much better I could have been if you were around for all my PhD!

Anne-Chloe – I think I am right in saying that rule of the iron fist was greatly missed in the final couple of years. Our time together has definitely swayed me toward autocracy… Lab 2nd in command 2013-2014.

Damien – DAAAAAAAMMMIIIIIIIIIIIIENNNNN! Hangover hero 2013.

Wes – Probably the most unique individual I have met in my time here…

Kat – Thanks for putting up with me in the early days! It was never the same when you weren't around!

JK – One day we will have a contest to see who loves boron more…

Jean-Oliver – I'll always remember that time you tried to kill us all vaccing off bromine. It's fiiiiiiine, it's fiiiiiine.

Rob – Thanks for showing me the sydnone ropes and teaching me the apathy required for PhD work.

Malcolm – So much wisdom in such a short time! Stealth comedian 2015.

Jokin – Lab X Factor winner 2015-2016.

Elvis – Lab social media expert 2012, 2013, 2014, 2015.

Sylvestre – Winner of best French accent 2014, 2015, 2016.

Ben – Lab PoKeMoN Master 2016.

Helena – Tell me! Enjoy the rest of your PhD.

Prisca – Remember pyrazole TFBs are nearly as good as sydnones.

Taban – Keep happy and enjoy the Münchnones!

Andrew Reeder – Thanks for being my surrogate postdoc!

Jonny – The end of 8 long years doing chemistry at Sheffield together… I almost feel like going to population…

Pete and Nick – Thanks for all the help, laughs and chats. You are cracking lads and made everything easier.

Jez – PhD nutritional expert! What the hell am I meant to do for dinner after the past 8 years!?

Sam and Matt – Thanks for managing to put up with me as a supervisor. I'm sure it wasn't easy!

Abbreviations

1,2-DCE – 1,2-dichloroethane

1,2-DME – 1,2-dimethoxyethane

BMECs – bovine microvascular endothelial cells

BSA – bovine serum albumin

CA1P – combretastatin A1 phosphate

CA4 – combretastatin A4

CA4P – combretastatin A4 phosphate

DAPI – diamidino-2-phenylindole

DBH – 1,3-dibromo-5,5-dimethylhydantoin

DFT – density functional theory

DIBAL-H – diisobutylaluminium hydride

DIPEA – diisopropylethylamine

DMF – dimethylformamide

DMPK – drug metabolism and pharmacokinetics

DMSO – dimethylsulfoxide

DMXAA – 5,6-dimethyl-9-oxo-9H-xanthene-4-acetic acid

EBM – endothelial cell basal medium

ECGS – endothelial cell growth supplement

ECL – enhanced chemiluminescence

EDTA – ethylenediaminetetraacetic acid

F-Actin – filamentous actin

FCS – foetal calf serum

FITC – fluorescein isothiocyanate

GAPDH – glyceraldehyde 3-phosphate dehydrogenase

GI_{50} – concentration for 50% of maximal inhibition of cell proliferation

H & E – hematoxylin and eosin

hbFGF – human basic fibroblast growth factor

hEGF – human epidermal growth factor

HEPES – 4-(2-hydroxyethyl)-1-piperazineethanesulfonic acid)

HPV – human papillomavirus

HRP – horseradish peroxidase

HUVECs – human umbilical vein endothelial cells

IAN – *iso*amyl nitrite

IMS – industrial methylated spirit

LDS – lithium dodecyl sulfate

MLC – myosin light chain

MTD – maximum tolerated dose

N/A – not available

PAGE – polyacrylamide gel electrophoresis

PBS – phosphate buffered saline

PET – polyethylene terephthalate

PK/PD properties – pharmacokinetic/pharmacodynamic properties

pMLC – phosphorylated myosin light chain

PMP – 4-methoxyphenyl

rpm – revolutions per minute

SAR – structure activity relationship

SCID – severe combined immunodeficiency

SDS – sodium dodecyl sulfate

SW1222 – human colorectal adenocarcinoma

TBAF – tetrabutylammonium fluoride

TBS – *tert*butyldimethylsilyl

TBSCl – *tert*butyldimethylsilyl chloride

TBST – tris-buffered saline

TLC – thin layer chromatography

THF – tetrahydrofuran

TMEDA – *N*,*N*,*N'*,*N'*-tetramethylethylenediamine

TMP – 3,4,5-trimethoxyphenyl

TNF-alpha – tumour necrosis factor alpha

VDA – vascular disrupting agent

VEGF – vascular endothelial growth factor

Contents

Chapter 1: Introduction

1.1: Cancer

The cells that make up multicellular organisms do not comply with Darwin's rule of "survival of the fittest." Instead, these cells form collaborative assemblies, or tissues in which self-sacrifice for the good of the collective is the rule.[1] Ultimately, the somatic cells dedicate their entire existence to the support of germ cells (sperm or egg cells), and they alone have the chance of continued survival. Unlike bacteria that compete to survive cells of multicellular organisms collaborate. They send, receive, and react to a vast array of extracellular signals which act as a social control. As a result, these cells respond in a way that prevents, as far as possible, adverse effects on their neighbours. Such cells will grow, divide, and die as needed for the good of the organism. A disturbance in these controls can be disruptive for a multicellular society. This is particularly the case if one cell gains an advantage over its neighbours by growing and dividing more rapidly, or by having a better chance of survival through a mutation. This cell can then be the founder of a new colony of mutant cells that do not act in the best interests of the collective. A cell which prospers at the expense of its neighbours is at the core of cancer.

An individual's perception of cancer is often based upon their own experiences and knowledge. One possible definition of cancer is "a group of ~200 conditions which exhibit malignant behaviour, including inappropriate cell growth and survival leading to invasion and/or metastasis."[2] The causes of cancer are numerous and varied; environmental and lifestyle factors, such as smoking and diet, can vastly increase the risk of specific cancers. Certain chemical agents can be carcinogenic, an example being benzene, which can lead to acute leukaemia. Radiation has also been known for many years to cause cancer.[3] Certain viruses, known as oncoviruses, can also cause cancer. They do this by infiltrating cells and forcing them to proliferate rapidly. A particularly well known example is the human papillomavirus (HPV) which causes cervical carcinomas.[4] Furthermore, genetics play a pivotal role in determining if a person is likely to experience the disease in their lifetime. Certain genetic defects can make cancer far more likely in certain individuals. For example, a woman carrying a mutation in the $BRCA_1$ or $BRCA_2$ gene has an 84% chance of developing breast cancer by the age of seventy.[5] Ultimately, it is often a combination of factors that leads to the first dangerous genetic mutation on the path to cancer.

Not only are the causes varied, but the types of disease encompassed under the title of "cancer" are hugely diverse and complex. Indeed, even cancers of the same histological type

can vary massively between different individuals. Despite these complexities, most cancerous cells do share some common traits, which are seen as being vital to the development of neoplastic disease. Hanahan and Weinberg proposed the six hallmarks of cancer in their comprehensive review of the field in 2000 (*figure 1*).[2] These hallmarks of cancerous cells include; the ability to produce growth signals in various conditions which would normally inhibit growth, and the capacity to ignore anti-growth signals leading to uninterrupted, harmful cell development. They are also characterised by the continuous stimulation of new blood vessel growth and a limitless cellular replication potential, again enhancing dangerous tumour cell proliferation. The continuous stimulation of new blood vessel growth is particularly important in establishing the tumour microenvironment, which will be discussed later. Two further hallmarks of cancerous cells are the ability to evade normal cellular death pathways causing growth without control. As well as, the capability to metastasise other tissues and colonise different areas of the body which is often the cause of cancer fatalities.

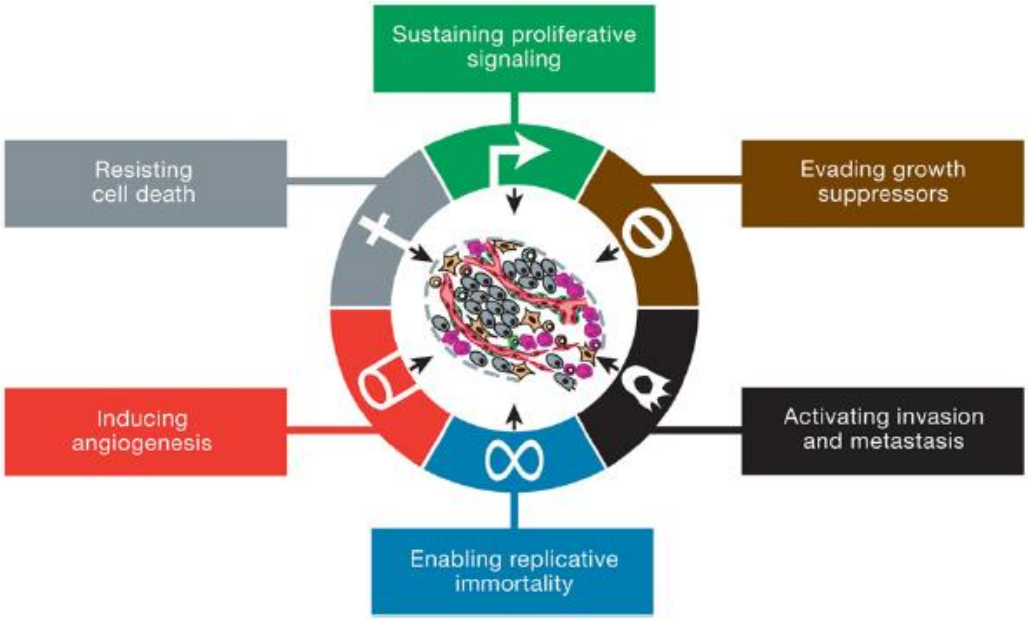

Figure 1*:* Hallmarks of cancer.

Hanahan, D.; Weinberg, R. A. The Hallmarks of Cancer. *Cell*, **2000**, *100*, 57-70 (Reproduced with the kind permission of Cell Press)

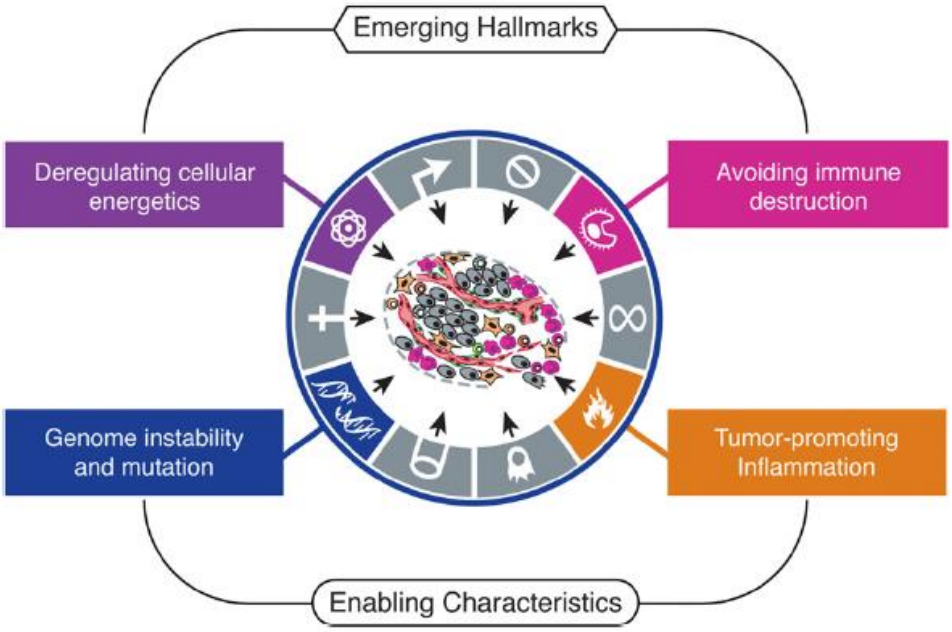

Figure 2*:* Emerging hallmarks of cancer.

Hanahan, D.; Weinberg, R. A. The Hallmarks of Cancer: the Next Generation. *Cell*, **2011**, *144*, 646-674

(Reproduced with the kind permission of Cell Press)

In their follow up review, in 2011, Hanahan and Weinberg described two more emerging hallmarks of cancer and two enabling characteristics of cancerous cells (*figure 2*).[6] The first emerging hallmark of cancerous cells is their ability to alter normal cellular energetic pathways. This enables energy production *via* different mechanisms to "normal" cells. This then fuels continuous growth and proliferation. The second emerging hallmark of cancerous cells is their ability to evade destruction by the body's immune system.

The first characteristic that allows tumour cells to prosper is a highly unstable genome. This leads to more mutations, which could allow more advantages to the cancerous cells. The second enabling characteristic of cancerous cells is the use of inflammation to promote tumour development and growth, thereby using the body's own defence mechanisms against it.

In essence, the hallmarks of cancer involve mutations which give a cell an advantage over its neighbours, leading to inappropriate growth at the expense of surrounding cells. Further mutations allow the deregulation of normal cellular growth controls, leading to dangerous levels of proliferation, and ultimately enabling invasion and metastasis.

1.2: The Tumour Microenvironment

It is important to recognise that tumours are more than just a colony of homogeneous cancer cells. Tumours are more like organs, whose complexity at least rivals that of healthy tissues.[6] Tumours contain numerous specialised cell types, not all of which are cancerous in nature. Non-cancerous cells in tumours (the stroma) include; endothelial cells, pericytes, tumour associated fibroblasts, and bone marrow derived cells such as neutrophils and macrophages. All of these contribute to tumour growth, progression and metastasis. It is therefore important in the study and treatment of neoplastic disease to not just consider the cancerous cells which are implicit in beginning tumour formation. It is equally important to examine the whole environment that is formed during tumourigenesis. A particularly significant way in which tumours differ from normal tissues is in their vasculature.

Tumour blood vessels have multiple structural and functional differences to normal blood vessels – often described as immaturity. Many of these differences stem from an increased rate of proliferation in tumour blood vessels compared to healthy vasculature.[7] Such tumour blood vessels tend to be irregularly shaped, convoluted, and less hierarchical than those in healthy tissues.[8] The diameter of these vessels is often irregular and the distances between branching points are often very long, resulting in geometrical resistance to blood flow. This means that a small decrease in perfusion pressure can have a radical effect in the tumour microenvironment, whilst leaving normal tissues relatively unaffected.[9] Tumour blood vessels also tend to have poorly developed walls, a discontinuous endothelial cell monolayer, a lack of good connections between endothelial cells and pericytes,[10] and a defective basement membrane.[11] The endothelial cells can themselves be irregularly shaped contributing to intercellular openings.[10] These factors play a major role in making tumour blood vessels intrinsically permeable to macromolecules, or "leaky."[12-13] This leads to a high interstitial fluid pressure.[14]

It is thought that "immaturity" of the tumour vasculature is caused by tumour-instigated, constant remodelling. As has been discussed earlier, continuous stimulation of new blood vessel growth in tumours is one of the hallmarks of cancer. Once a tumour exceeds a few millimetres in size, an "angiogenic switch" is triggered by hypoxia and nutrient deprivation.[15] Tumour cells exploit normal, quiescent cells around them by releasing cytokines and growth factors.[16] The combination of stimulatory signals leads to changes in multiple cell types which are "recruited" into the tumour microenvironment. An example of this is tumour-cell secreted, vascular endothelial growth factor (VEGF). VEGF stimulates the proliferation of endothelial cells and consequently, the formation of new vasculature. Although rapid

angiogenesis in the tumour does provide it with oxygen and nutrients, it is far from ideal and the differences between it and the vasculature of healthy tissues provides us with new avenues of research into cancer; for example, the selective targeting of tumour blood vessels. Due to the inherent “leakiness” of tumour blood vessels, a further increase in permeability upon treatment with a drug can be extremely damaging to tumour blood flow. This is particularly attractive, as without access to oxygen and nutrients, tumour cells will die.

1.3: Vascular Targeted Approach to Cancer Therapy

Targeting the tumour vasculature is becoming an increasingly important and effective area in the battle against cancer. Investigations are taking place at both basic and clinical levels of research.[17] Tumour blood vessels represent an attractive target for cancer therapy. This is because solid tumours require a functional supply of blood to provide nutrients and oxygen for continued growth and metastasis.[18] In theory, there are a number of advantages to this therapeutic approach. Firstly, this treatment should be effective on all solid tumours, independent of histological type.[19] Secondly, because a large number of tumour cells depend on this blood supply, damage to the vessels could lead to severe effects in both early stage tumour progression and in late stage tumours. Thirdly, targeting vascular endothelial cells is less likely to lead to acquired drug resistance than targeting the tumour cells directly, because endothelial cells are more genetically stable. Finally, targeting the vasculature rather than tumour cells themselves allows for the destruction of any tumour cells that have become resistant to conventional treatment.[20] Therapeutically, there are two distinct vascular-targeting approaches; antiangiogenic and vascular disruptive.

Antiangiogenesis

Angiogenesis is the formation of new blood vessels from pre-existing vessels - a process vital to tumour growth and metastasis.[21] Originally proposed by Folkman,[22] antiangiogenics prevent the formation of these vessels, which in turn prevents growth of the tumour and metastasis without eliminating the existing tumour mass. Antiangiogenic effects can be instigated by either blocking the response of endothelial cells to angiogenic factors, or by blocking the production, availability or activity of these factors, for example vascular endothelial growth factor (VEGF).[19,23] A therapeutic approach using these agents has been proposed to limit the growth of tumour mass and maintain metastasis in a dormant state. Therefore, it can be assumed that this approach will be most effective on small, early stage tumours, and the duration of the effect should last as long as the drug is present in the tumour at its effective dose.[24] However, this approach requires chronic treatment and has implications in terms of safety and side effects associated with prolonged use of a drug in treatment.[25] Although there is much potential in the use of antiangiogenic agents for the treatment of cancer, this report will focus on vascular disrupting agents (VDAs)

Vascular Disruption

Vascular disruptive approaches to cancer treatment were originally proposed by Denekamp.[26,27] Vascular disrupting agents cause rapid, selective collapse of the tumour

vascular network for a prolonged period of time, leading to widespread secondary tumour cell death *via* necrosis.[28] By definition, VDAs cause a much greater loss of blood flow in tumours than normal tissues.[29] Therapeutic agents of this type have the potential to have a significant impact on the treatment of cancer.[30] The therapeutic potential of VDAs lies not in their use as single agents, but in their combination with conventional and novel cancer treatments. As single agents, VDAs fail to prevent tumour regrowth and there is evidence that they actually boost tumour angiogenesis.[31] Clinical trials are currently underway utilising a number of VDAs in combination with traditional therapies, such as chemotherapy and radiotherapy.[32] A notable example of why combinational therapy is needed when using VDAs is the "viable peripheral rim of tumour cells." The survival of tumour cells at the peripheral rim of the tumour is a common feature of all VDAs and is relatively poorly understood. The reasons behind the periphery being less sensitive are probably due to higher interstitial fluid pressure in the centre of the tumour and differences in vascular architecture between the two regions.[28] Combining VDA treatment with antiangiogenic agents can eliminate the viable rim and improve tumour responses.[33]

There are two types of VDA; ligand-directed VDAs and low molecular weight VDAs. Ligand-directed VDAs use antibodies, peptides or growth factors to target toxins towards the tumour endothelium.[20] The focus of this report, low molecular weight VDAs, exploit differences between tumour and normal vasculature to selectively target tumour blood vessels. There are three classes of low molecular weight VDAs; *i*) the synthetic flavonoids, *ii*) the newly-discovered, cadherin targeting compounds and *iii*) the tubulin binding agents.

i) Synthetic Flavonoids

5,6-Dimethyl-9-oxo-9*H*-xanthene-4-acetic acid (DMXAA, *figure 3*) is a synthetic analogue of flavone-8-acetic acid (FAA, *figure 3*). DMXAA was shown to cause a significant reduction in blood flow *in vivo* and widespread tumour cell necrosis.[34] A 12-fold increase in tumour vascular endothelial cell apoptosis was observed, but no increase of apoptosis was seen in tissue from the heart, liver, spleen and brain.[35] The primary mode of the antitumour action of DMXAA was shown to be stimulation of the synthesis of tumour necrosis factor alpha (TNF-α).[36] DMXAA reached phase III clinical trials, before being dropped by Novartis in 2011.[20]

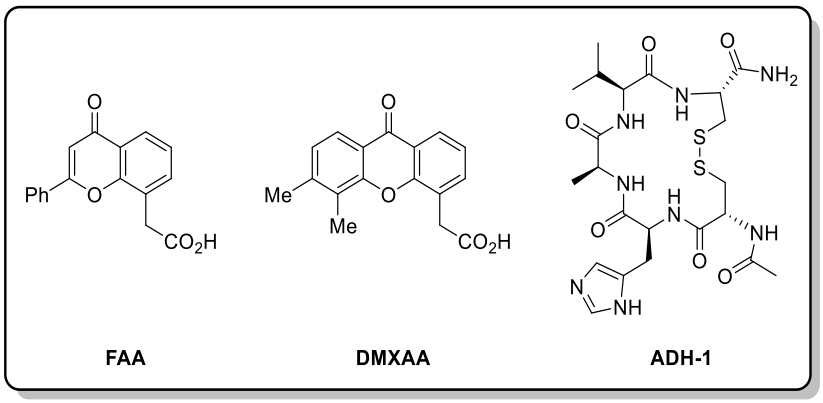

Figure 3: Structures of some flavonoid-based vascular disrupting agents and cadherin antagonists.

ii) Cadherin Antagonists

Type I and II cadherins are cell adhesion molecules linked to the microfilaments of the cytoskeleton.[37] Endothelial cells and pericytes which line the vasculature express cadherins. Endothelial cells express VE-cadherin and N-cadherin, whereas pericytes only express N-cadherin.[38] As the tumour vasculature is characterised by poor connections between endothelial cells and pericytes, further disruption of these connections by antagonists of N-cadherin or VE-cadherin has the potential to disrupt tumour blood vessels. The first cadherin antagonist to enter clinical trials was the synthetic cyclic pentapeptide ADH-1 (*figure 3*), discovered in 2000 by Blaschuk and Gour.[39] This compound was shown to inhibit tumour growth and metastasis in mouse models. However, effects on the tumour vasculature were not studied.[40]

iii) Tubulin Targeting Agents

Microtubules are tubulin polymers that play numerous, important roles in endothelial cell biology, and as endothelial cells are integral to the vascular network, it is unsurprising that tubulin binding drugs have the potential to target the tumour vasculature.[41] Of the three VDA families, tubulin binding agents are by far the most advanced and well researched. The structures of compounds that bind tubulin are quite diverse, but this report will focus solely on the combretastatins.

Targeting Microtubules

As previously stated, microtubules play numerous and diverse roles in cell biology. As well as characteristically forming the mitotic spindle to separate chromosomes during mitosis, microtubules have a number of other functions including regulation of cell structure, movement, adhesion and signalling. During the interphase, microtubules in cells are

cylindrical polymeric structures formed from α- and β-tubulin subunits. They originate from the centrosome and spread across the entire cell (*figure 4*). Microtubules exist in equilibrium between monomer and polymeric form, in a process known as dynamic instability.[42] The microtubules switch between phases of relatively stable length and phases of rapid shortening and lengthening. As the cell begins to enter mitosis, long interphase microtubules are converted into shorter spindle poles, eventually forming the mitotic spindle. Microtubule targeting agents bind to specific sites on the β-tubulin subunit and, therefore, alter microtubule dynamics and stability.[43] Interfering with the dynamic instability of microtubules at any stage of the cell cycle is likely to have an effect on normal cellular function.

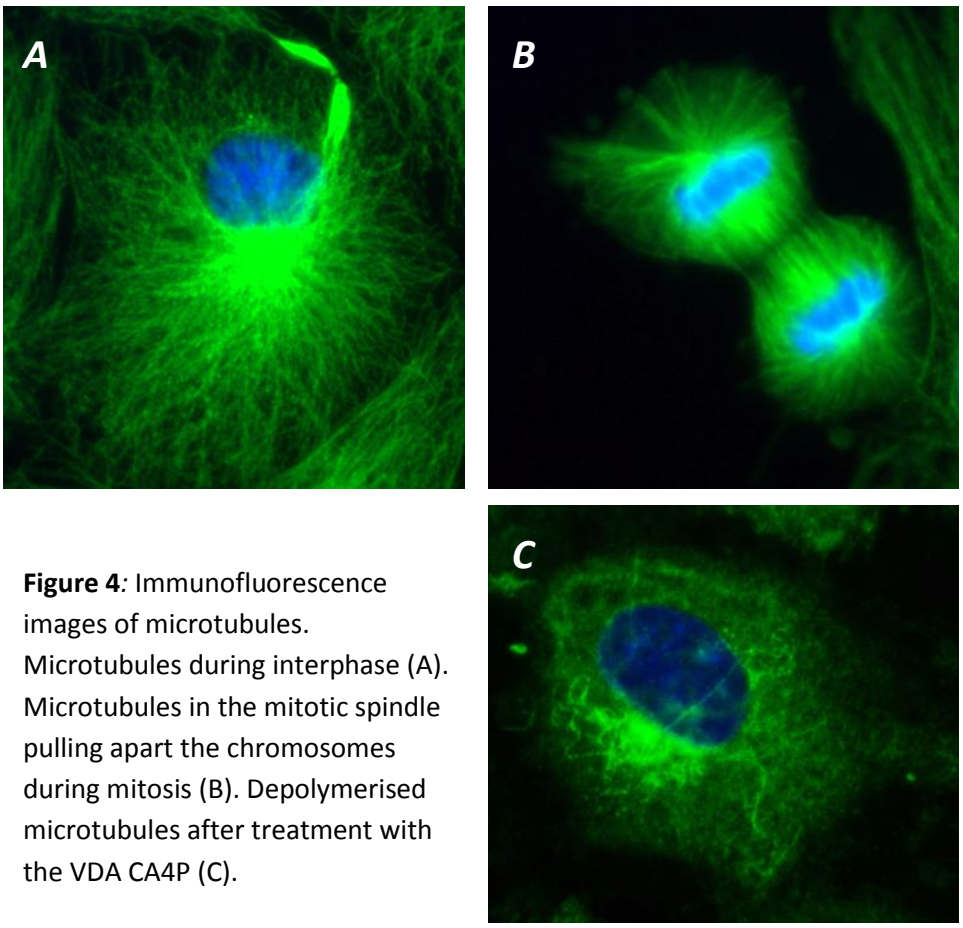

Figure 4*:* Immunofluorescence images of microtubules. Microtubules during interphase (A). Microtubules in the mitotic spindle pulling apart the chromosomes during mitosis (B). Depolymerised microtubules after treatment with the VDA CA4P (C).

Antiangiogenesis vs Vascular Disruption

There are two applications proposed for tubulin binding agents; as antiangiogenic agents, or as vascular disrupting agents (VDAs). Tubulin targeting agents, which affect microtubule dynamics, also inhibit endothelial cell functions - which are crucial to the formation of new tumour blood vessels (angiogenesis). This is the primary effect of microtubule stabilising agents such as taxanes.[44] In contrast to this, tubulin targeting agents, which target microtubule organisation, cause changes in endothelial cell shape by damaging the existing

tumour blood vessel network (vascular disruption) and inducing tumour cell necrosis. This is the principal effect of microtubule destabilising compounds, such as those related to colchicine and the *Vinca* alkaloids.[45,46,47] The majority of tubulin binding agents are being developed for vascular disruption, rather than for antiangiogenic therapy. These two processes are very different in terms of basic mechanism, effect on tumours, and therapeutic application. However, despite the differences between these two processes, the distinction is not always absolute. Drug concentration and *in vivo* setting can determine whether a specific drug acts as a VDA or an angiogenesis inhibitor.[48] Studies *in vitro* seem to indicate that microtubule depolymerising agents are effective as VDAs at relatively high doses by causing catastrophic microtubule network disruption. At lower doses they affect microtubule dynamics without actually destroying microtubules, leading to an antiangiogenic effect. The effectiveness of a drug as either a VDA or an angiogenesis inhibitor is, therefore, likely to be influenced by its pharmacokinetic (PK) and pharmacodynamic (PD) parameters, as well as how it binds to tubulin and by its cellular retention time.

1.4: The Combretastatins

One of the most important families of VDAs is the microtubule depolymerising agent family. The classic example of a microtubule depolymerising agent is the tubulin binding, antimitotic agent, colchicine (*figure 5*). Colchicine prevents cells from undergoing mitosis by inhibiting formation of the mitotic spindle, therefore preventing separation of the chromosomes on the spindle and causing the cells to arrest in the metaphase. The vascular disrupting properties of colchicine have been known since the 1930s. However, these effects are only seen at near to the maximum tolerated dose (MTD).[49,50] Structurally related stilbene compounds, the combretastatins, were isolated from the Cape Bush Willow tree, *Combretum caffrum* in the late 1980s.[51] These compounds were initially studied for their potential as antimitotic agents.[52] However, it later became apparent that combretastatins had great potential as VDAs.[53] The lead compound, combretastatin A-4 (CA4), was shown to be effective at causing selective tumour vascular collapse at non-toxic doses.[54] It was swiftly developed into a water-soluble, sodium phosphate salt prodrug, disodium combretastatin A-4 3-*O*-phosphate (CA4P). The prodrug CA4P is not, itself, active as a tubulin binding agent, but is rapidly cleaved in plasma to CA4.[55] CA4P is currently undergoing Phase II/III clinical trials in combination with other cancer therapies.[56] Another interesting member of the combretastatin family with VDA action, is the phosphate prodrug of combretastatin A-1.[57] CA1P is significantly more effective at shutting down tumour blood vessels than CA4P[58] and has entered Phase I clinical trials as a single agent treatment.[59]

The promising attributes of CA4P have led to a surge of interest in VDAs as potential anticancer agents. There have been numerous studies into the mode of action of combretastatins, but it is still not entirely clear how they act. A large proportion of literature is based around studies of CA4P, most probably because it was the first microtubule depolymerising VDA to enter clinical trials. Upon treatment with a clinically relevant dose of CA4P, a large reduction in tumour blood flow can be detected within minutes. After an hour, almost complete tumour vascular shutdown is observed with near undetectable levels of blood flow remaining for a number of hours.[60] A large proportion of the tumour (80-90%) can become necrotic within a few hours of a dose of CA4P.[54] The initial target of the combretastatins seems to be the endothelial cell microtubule cytoskeleton.[28] Due to the speed of vascular shutdown, the drugs must be disrupting the microtubules of endothelial cells during the interphase, rather than the classic interference with the mitotic spindle which is often characteristic of tubulin depolymerising agents.[43] As mentioned previously, it is likely that changes in endothelial cell size and shape, as a result of microtubule disruption, are integrally linked to vascular collapse.[47] The endothelial cells in immature vasculature have

also been shown to have a less developed actin cytoskeleton, and are thus more sensitive to microtubule depolymerising agents.[58]

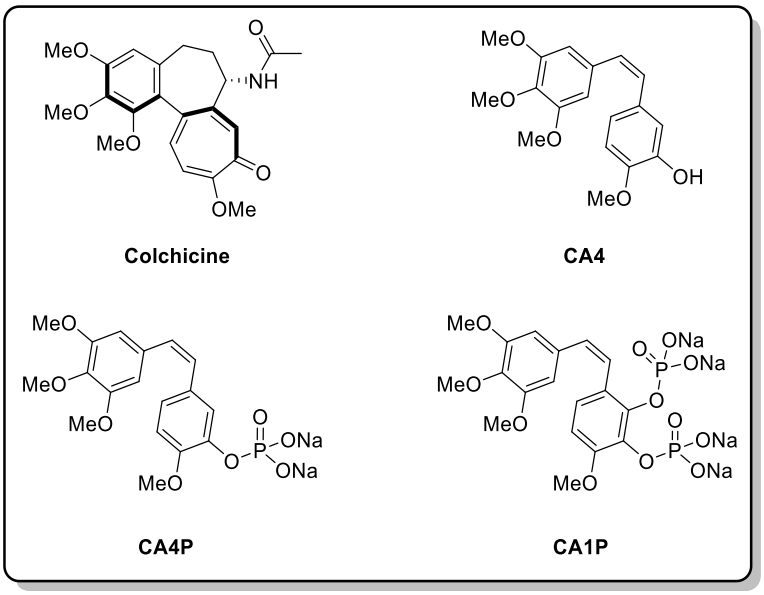

Figure 5: Structures of some tubulin-binding VDAs.

Action of the Combretastatins

The lower toxicity (and thus higher MTD) of CA4 compared to colchicine is attributed to CA4 binding reversibly to the β-tubulin subunit, as opposed to colchicine that binds pseudo-irreversibly.[61] This means that cells are not exposed to CA4 for long periods of time, which minimises toxic effects whilst continuing to be effective at initiating vascular collapse. Certain tumour cell types are, in fact, more sensitive to tubulin depolymerising drugs than endothelial cells.[62] This leads to the question of whether the toxicity of CA4P towards tumour cells plays a role in its effectiveness as a therapeutic agent. Recent work by Kanthou and Tozer *et al.* has demonstrated that it is vascular effects that dominate solid tumour response to CA4P.[63] They ascertained this by the development of a line of SW1222 human carcinoma cells which were resistant to CA4P. Subcutaneous injection of the resistant cells into mice alongside wild type SW1222 cell controls led to the development of solid tumours in the mice. Treatment with CA4P led to widespread tumour cell necrosis in both the wild type tumour bearing and CA4P resistant tumour bearing mice. The extent of tumour cell necrosis was similar in both sets of mice. A clear demonstration that, in the case of CA4P at least, it is vascular effects, not direct toxicity on tumour cells that dominates the activity of the drug *in vivo*.

Comparison of Combretastatin Analogues

Due to uncertainty over the mode of action of CA4P *in vivo*, it is important when comparing the relative activities of combretastatin analogues *in vitro* to consider antitubulin action of the compounds. However, it is also important to maintain awareness that these activities do not necessarily directly correspond to *in vivo* potential. Comparing drug activity to the activity of CA4/CA4P can also be difficult, as different laboratories report quite diverse IC_{50} values. For example, in the case of toxicity against cancerous cells (despite its lack of importance *in vivo*), IC_{50} values ranging between picomolar and micromolar have been reported. These differences stem from a number of factors including; the cell lines used in the assays, the purity of CA4 in various laboratories, the drug exposure time, as well as experimental set up.[64] Indeed, the use of different cell lines to calculate IC_{50} values for cytotoxicity in different studies makes them particularly difficult to compare. This problem is further exacerbated by the significant proportion of reports in this field that have not conducted tubulin polymerisation assays on compounds high IC_{50} values for toxicity against cancerous cells. Probably due to the cost of the high purity tubulin needed to conduct an assay. This is a particularly risky practice. For example, the cytotoxicity of CA1 is, in most cases, reported around the 1 μM range, whereas the cytotoxicity of CA4 is generally reported around 3 nM. However, CA1 is more effective at causing shutdown of the tumour vasculature than CA4. The poor profile of CA1 *in vitro* could have led to it being regarded as inactive in many studies, resulting in an incomplete investigation of its potential as a drug. This could be the case with many compounds that were not taken on for further testing. Also, as mentioned previously, ignoring compounds due to cytotoxicity data is not good practice, as cytotoxicity is not the primary mode of action of CA4.[63] Another issue arises in that few studies include data on the effect of the drugs on endothelial cells, for example, human umbilical vein endothelial cells (HUVECs). If the primary target of combretastatins is indeed the endothelial cell cytoskeleton, then assays involving HUVECs should be a more accurate *in vitro* model than traditional tubulin assays. Recently, the area has been made more complex to analyse by the development of a new, rapid screening system for tubulin binding compounds, using sea urchin embryos.[65] This technique allows analysis of antimitotic activity and tubulin destabilising effects. Developed by Semenova *et al.* in 2006, several recent papers have solely used this technique for compound screening, thus providing a further obstacle in comparing the performance of these compounds with previous drug candidates.[66,67]

Due to the structural simplicity of combretastatins, there have been numerous CA4 analogues synthesised throughout the past two decades. Synthetically, two main routes have

been utilised to create stilbene analogues; *i*) the Wittig reaction or *ii*) alkyne synthesis (for example *via* Sonogashira coupling) followed by reduction of the alkyne (*scheme 1*).

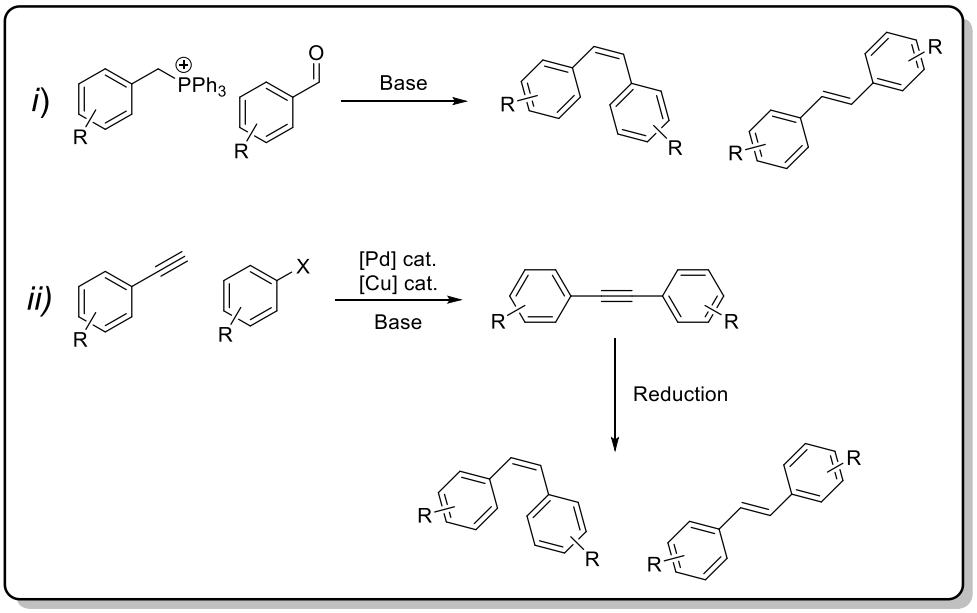

Scheme 1: Typical routes to combretastatin analogues.

Classically, the Wittig reaction has been used to synthesise stilbene analogues of combretastatins.[68,69,70] In terms of generating compound libraries, a particular advantage of the Wittig reaction is the generally poor *E*:*Z* selectivity achieved. This leads to the possible isolation of two potential drug compounds from each reaction. However, such an approach often requires non-trivial separation of the isomeric products. Furthermore, due to the near complete inactivity of the *E*-isomers compared to their *Z*-counterparts, there is little point in accessing them in modern analogue synthesis. The mixture of products obtained, also limits application of the Wittig reaction to scale up synthesis. Much higher stereoselectivity for the formation of *Z*-isomers can be achieved *via* the reduction of alkynes. Biaryl alkynes have been synthesised by transforming the corresponding aryl aldehyde into a terminal alkyne using Corey-Fuchs methodology, followed by palladium mediated Sonogashira cross-coupling with an aryl halide.[71,72] Petrov *et al.* also reported the formation of the biaryl alkyne intermediate of CA4 *via* the Colvin rearrangement from the biaryl ketone, phenstatin.[73] A number of methods for the *Z*-selective reduction of alkynes have been utilised in the synthesis of combretastatin analogues. In Petrov's report, reactions were carried out over Lindlar catalyst yielding a 94:6 ratio of *Z*-stilbene to the fully hydrogenated alkane. However, separation of the two compounds was not possible. Lawrence *et al.* reported the use of hydroboration/protonation for the reduction.[71] The method, developed by Zweifel *et al.*,[74] afforded a >99:1 mixture of *Z*-:*E*-stilbene. A related method, involving hydrosilylation/protodesilylation was developed by Alami *et al.*[75] The advantage of this

method is that the *Z*-product is formed with complete alkene stereocontrol. It is, however, relatively low yielding. The most effective *Z*-selective reduction of alkynes was reported by Lara-Ochoa *et al.*[72] This method involves the formation of a titanium(II)-alkyne complex, followed by hydrolysis (*scheme 2).* It is 100% *Z*-selective and high yielding (79-94%).

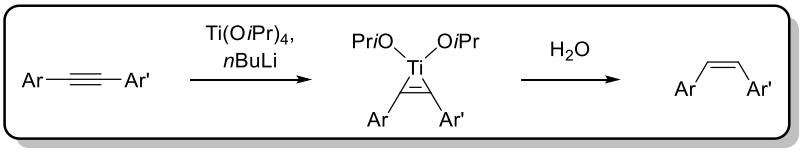

Scheme 2: Titanium tetra*iso*propoxide/*n*-butyllithium-mediated alkyne reduction.

Conceptually, the simplest way to analyse strategic approaches to combretastatin analogues is to split the molecules into 3 segments; the A ring, the B ring and the double bond (*figure 6*).

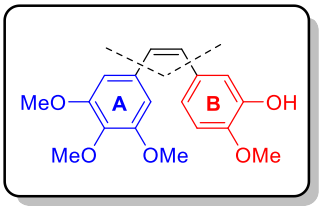

Figure 6: Structural identification of combretastatin analogues.

The A Ring

Compared to the other two segments of the molecule, modifications of the A ring has received relatively scant attention. The reasons for this are most likely due to the recurrence of the 3,4,5-trimethoxybenzene moiety in other naturally occurring antitubulin drugs (e.g. colchicine). Furthermore, a number of early compounds by Cushman and Hamel *et al.* with modifications of this motif led to a significant drop in activity.[76] It is not possible to state with certainty that the trimethoxybenzene ring is essential for desirable activity in combretastatin analogues as has often been alluded to. To gain a true insight into this area, further knowledge needs to be gathered as to the exact mode of action of these drugs. Without this knowledge, it is very difficult to grasp the full implications of results gained from *in vitro* assays without moving all compounds to *in vivo* studies. A practice that would be impractical, expensive, and potentially unethical.

The B ring

Classically, analogues of CA4 have been developed by utilising variations on the B ring. Examples of B ring modified combretastatins are widely reported in scientific literature.

These analogues can be broadly split into two categories: *i*) substituted phenyl rings and *ii*) substituted and non-substituted heterocyclic rings.

Since the discovery of combretastatins as potential anticancer agents, it has been clear that modifications of the B ring could lead to interesting changes in pharmacological and pharmacokinetic properties of the drugs. Indeed, work in the 1990s by Cushman and Hamel *et al.* gave early indications of the features that were important to activity.[68,76] However, despite the dozens of analogues synthesised, the most potent substitution pattern of the B ring remains unclear. A major issue is that much research has been based on structure activity relationships which are not necessarily valid for VDAs. However, within the plethora of compounds synthesised a number of exciting potential drugs have been discovered and have advanced to clinical trials, such as Sanofi-Aventis' prodrug Ombrabulin (*figure 7*).[30] The structures of these new, lead compounds are quite diverse and include substituted phenyl rings and heterocyclic rings. This is particularly promising for future compound design because the more diverse the motifs tolerated, the more potentially active combinations there are still available to find. The drawback, however, is the inability to pursue a more targeted approach to analogue design from previous findings. This problem is made all the more daunting by the often erratic biological studies reported. In particular, a number of early papers do not include data on activity against tubulin. Assuming that tubulin is the primary target of these VDAs, then SARs derived solely from cytotoxicity studies against cancerous cell lines do not offer a clear judgement on the vascular disruptive potential of these particular compounds. Also, as mentioned previously, the lack of accurate *in vitro* models prevents precise conclusions on VDA activity being drawn without the aid of *in vivo* studies. Therefore, although much work has been conducted in this area, important details could have been missed through incomplete research.

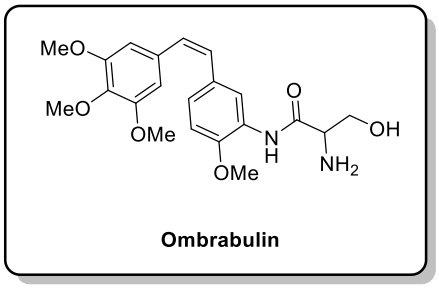

Figure 7: Aventis prodrug Ombrabulin.

The Olefin Bridge

Modifications of the olefinic component of CA4 have received most literature attention over the last quarter of a century. In part, this results from the widely accepted view that at the

biological site the double bond plays more of a structural than a binding role.[64] It is thought to position the aromatic rings at an appropriate angle for binding. If this is indeed the case, any bridge between the two rings which holds them at the correct angle would yield compounds of similar activity to CA4. The *Z* configuration of the double bond is fundamental to activity, as the *E*-isomer has little biological activity.[68] However, *Z*-stilbenes are known to undergo facile isomerisation when exposed to heat, light, and protic media. CA4 can metabolise to the inactive *E*-isomer in the body. Because of this, much work has been carried out to synthesise metabolically stable analogues. Research in this area can be classified in two broad categories: *i*) modified double bond and chain linked analogues, *ii*) ring-fixed analogues.

Modified Olefin and Chain Linked Analogues

Some particularly important early work on bridge-modified combretastatins was conducted by Hamel *et al.,*[77] focussing upon the effect of bridge length on activity. They found that reduction of the double bond of CA4 to an alkyl chain, **1**, (*figure 8*) resulted in a less than 2-fold loss of antitubulin action. This is to be expected with increased degrees of freedom lost on binding. A further 2-fold loss of activity was observed when the two carbon bridge was reduced to a single carbon, **2**. Interestingly, biaryl system, **3**, was inactive. Extending the bridge to three carbons, **4**, and four carbons, **5**, resulted in significant losses of activity. This work, in particular, has led to the majority of research focussing on one and two carbon bridged systems. However, there are examples of relatively potent compounds with longer bridges. These compounds are different to those synthesised and tested by Hamel *et al.*, as they include at least one double bond to introduce rigidity, therefore reducing the entropic cost of binding.

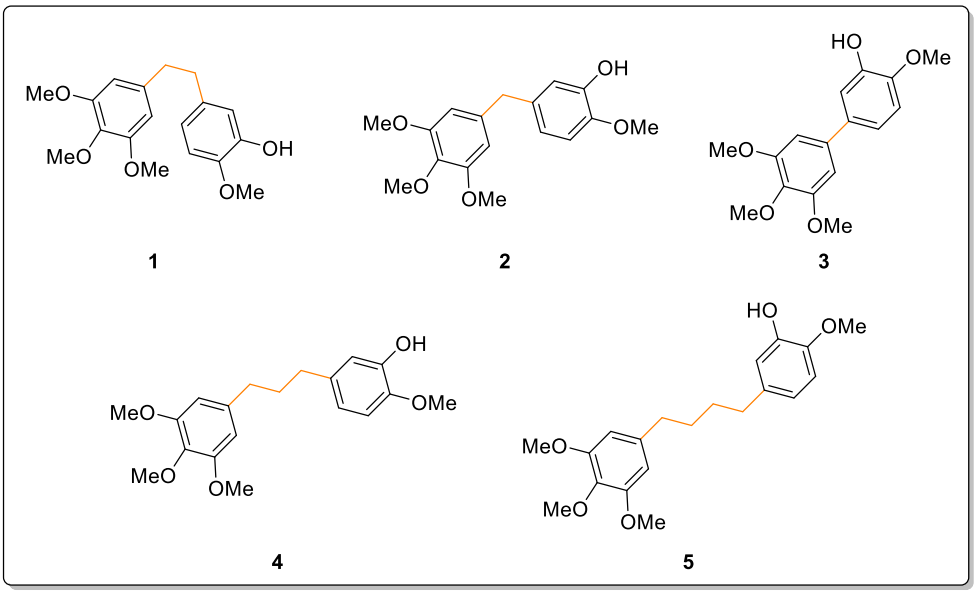

Figure 8: Contracted and extended linker analogues.

***Cis*-Fixed, Ring-Bridged Analogues**

Research into ring-bridged combretastatin analogues has been the fastest expanding area of investigation in the past ten years. This has been largely the result of a number of early positive results, and the potential advantages that a ring bridge provides. The main advantages of ring-bridged structures are threefold; *i*) *cis-trans* isomerisation is no longer an issue, *ii*) heterocyclic rings can offer a benefit to PK/PD properties and *iii*) they allow for functionalisation away from the key binding region of the A- and B-rings. Furthermore, from a purely synthetic point of view they allow research into new, potentially exciting methodologies to access them.

Arguably, it was a 1998 paper by Ohsumi *et al.* that initiated the explosion of research into ring-bridged analogues.[69] Their investigation demonstrated that a variety of 5-membered rings could be utilised to replace the olefinic bridge of ombrabulin's active fragment, **6**, (*figure 9*). Such modifications maintained or moderately lowered *in vitro* and *in vivo* activity (*table 1: entries 2 – 6 vs 1*). Most interestingly, 2-aminothiazole analogue, **7**, was as effective as the analogous stilbene, **6**, both *in vitro* and *in vivo*. It also contained functional handles on both the bridge and the B-ring (*figure 9*). The equivalent thiazole, without the 2-amino group, **8**, was slightly less active than **7**. However, **8** had a significantly higher MTD than **7** and thus, could be the more promising drug candidate. Triazole, **9**, was one of the least effective candidates against tubulin, but demonstrated potent *in vivo* activity, as well as low toxicity. Further triazole analogues were developed by Welsh *et al.*, some being more potent than **9**.[78] However, analogues synthesised by Hansen *et al.* demonstrated limited activity.[79] Other analogues were synthesised and tested by Romagnoli and Viola *et al.*[80] Myers *et al.* also

developed a number of triazoles, which demonstrated strong activity against tubulin and were effective in assays involving HUVECs.[81] Tetrazole, **10**, was relatively potent *in vitro*, but was incredibly potent *in vivo* and also had very low toxicity. This positive outcome prompted further investigation by Romagnoli and Viola *et al.*[82] The compounds were not quite as active as some thiazole and triazole analogues, but continued to demonstrate strong anti-tubulin activity.

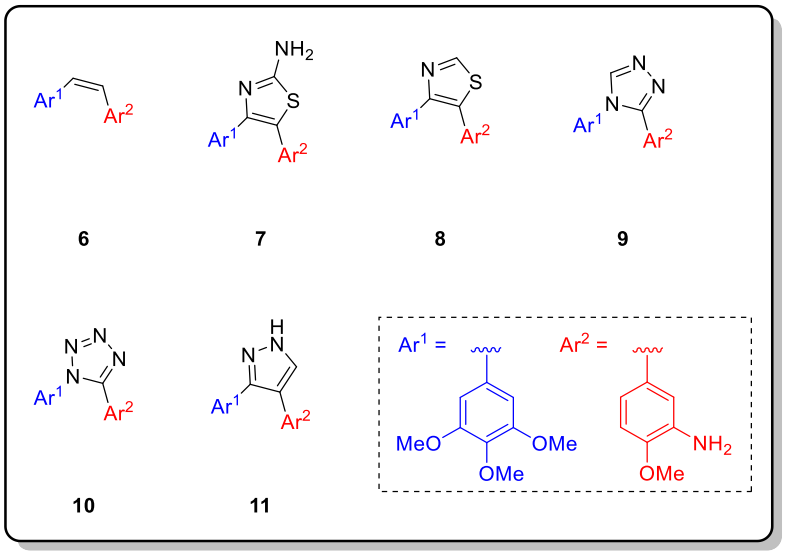

Figure 9: Ring-Bridged Combretastatins.

Entry	Compound	IC_{50} (Tubulin Assay)/μM	Antitumour IR[a] / % (dose)[b]
1	**6**	1	73% (40 mg/kg)
2	**7**	1	75% (40 mg/kg)
3	**8**	3	66% (160 mg/kg)
4	**9**	4	47% (160 mg/kg)
5	**10**	2	89% (160 mg/kg)
6	**11**	3	0% (20 mg/kg)

Table 1: *In vitro* and *in vivo* screening of ring-bridged analogues.

a) Inhibition ratio, compared to vehicle only. b) Maximum tolerated dose administered

Pyrazole, **11**, was 3-fold less effective against tubulin than **6**. It also showed the highest toxicity of the analogues synthesised and did not exhibit any tumour suppression properties *in vivo*. However, due to its toxicity, it was administered at a much lower dose than the other compounds. There are few examples of pyrazole analogues in the literature. This is

surprising, considering the success of marketed drugs that utilise this heterocyclic motif. In part, this could possibly be explained by the above findings, but also may be the result of difficulties associated with the selective synthesis of diarylpyrazoles. Reports by Dhar *et al.*[83] and Lee *et al.*[84] described pyrazoles with a three-atom-bridge (for example **12**, *figure 10*) – already shown to be less effective than molecules with a two-atom-bridge in the majority of cases. The compounds were not tested for activity against tubulin in either report. A single analogue with a two-atom-bridge, **13**, was reported by Wang *et al.* in 2002.[85] Again, however, neither tubulin depolymerisation effects nor effects on endothelial cells were not studied. More recently, Liu *et al.* investigated the activities of diaryl-3-aminopyrazoles.[86] They found **14** (*figure 10*) to be half as active against tubulin as CA4. These results are interesting because maintaining high activity whilst incorporating a functional handle away from the active site, could allow the incorporation of useful groups at the binding site. The groups incorporated would not necessarily have to be functional handles themselves. Even more recently, Pirali *et al.* reported the preparation and evaluation of pyrazole-based analogues of CA1.[87] The most active compound, **15**, demonstrated nanomolar cytotoxicity against neuroblastoma cells (SH-SY5Y), but was not tested in endothelial cells or against pure tubulin. A further report by Wu and Zhang *et al.* detailed a number of alkyl-substituted diarylpyrazoles, including direct CA4 analogues (for example **16** and **17**, *figure 10*).[88] However, the compounds exhibited unremarkable activity in the assays conducted and the majority of assays focussed on the treatment of cancerous cells. Despite the above reports, there has not been a systematic evaluation of substitution effects around the pyrazole core. Furthermore, simple pyrazole-based analogues of CA4 have not been reported.

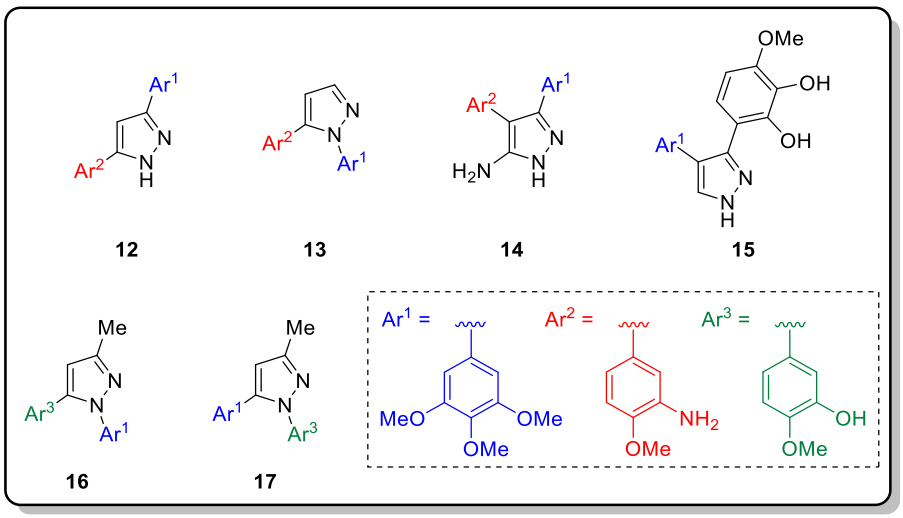

Figure 10: Pyrazole-bridged combretastatin analogues.

Summary of *Cis*-Fixed, Ring-Bridged Analogues

Replacing the olefinic bridge of combretastatins has proved to be an invaluable area of small molecule discovery chemistry in cancer research. A number of analogues have demonstrated high potency both *in vitro* and *in vivo* and 5-membered, nitrogen-containing rings seem to be the best candidates for incorporation. However, effective analogue screening is non-trivial and a generalised and accepted method for evaluation of VDAs *in vitro* has yet to be established. Future analogue synthesis should likely focus on 5-membered heterocycles, but also be coupled with investigations into a robust *in vitro* screening method for the compounds.

Summary of Combretastatin Research

Vascular disrupting agents are a highly promising group of potential cancer therapeutics. In this context, hundreds of combretastatin derivatives have been synthesised and screened for biological activity. Despite successful synthesis of numerous compounds with isosteric substitutions of the A ring, B ring, and double bond in the past twenty five years, it is not possible to draw definite conclusions of structure activity relationships for any area of these molecules. This failure is largely due to two factors: *i)* a continued lack of understanding of which *in vitro* characteristics make a successful VDA, *ii)* the reliance on cytotoxicity studies against cancerous cells as a defining factor in the determination of compound activity. Understanding just how tubulin depolymerising VDAs work is a vexing issue. In an ideal world, a compound's ability to depolymerise tubulin would correspond directly to its potential as a VDA. However, there are examples of compounds with much lower potency against tubulin than CA4 leading to marked reductions in tumour volume *in vivo*. The situation is further complicated by the fact that CA4P is more effective on certain tumour types than others, despite VDAs theoretically being effective on all solid tumours. This discrepancy is probably the result of how different tumour cells instigate the construction of their own microenvironment. If this is the case, then further understanding of the differences in tumour microenvironments created by different tumour cell types, is likely to be pivotal not only in VDA design, but also in the design of other anti-cancer agents. Addressing the over reliance on cytotoxicity studies would seem a simpler issue to solve. However, it is easy to state that cytotoxicity studies are invalid and should not be used in judgements of VDA potential. Which studies should be used to replace them is a more complex matter. Certainly qualitative or semi quantitative studies of a drug's effect on HUVEC morphology are very useful probes into vascular disruption potential. This is because changes in the morphology of endothelial cells seem to be integral to vascular collapse. Therefore, these simple tests at set concentrations could be a useful discriminator between compounds. One potential quantitative test of these

effects could be to use HUVEC permeability assays to observe the extent that a HUVEC monolayer is perturbed by a drug. However, these data should be utilised to determine which drugs should progress to *in vivo* testing, not necessarily as activity markers in their own right.

It is very difficult to apply specific levels of design to novel analogues. In terms of the A ring, the 3,4,5-trimethoxybenzene unit is the "go to" structure. It is not clear if a better structure exists for this position. In the majority of cases where detailed studies have been undertaken, the 3,4,5-trimethoxybenzene unit does seem to produce optimal activity. The B ring appears to be quite amenable to modification with a number of varied structures retaining or improving on the activity of CA4 *in vitro* and *in vivo*. Modification of the olefinic bridge seems to be a particularly relevant area of investigation. Indeed, replacing the olefinic bridge with a 5-membered ring is one of the most promising areas of combretastatin research. Numerous modifications of the B ring have further increased the library of potential therapeutics. It is likely that these structures will be the major focus of combretastatin research in the coming years. Combined with carefully designed testing, they will provide access to relevant structure activity relationships for 5-membered ring bridged compounds.

1.5: Introduction to the Project

Combretastatin derivatives have the potential to impact greatly on the treatment of cancer. Novel, potent analogues with desirable physical properties are therefore of great interest to medicinal chemists. In particular, 5-membered ring-bridged analogues have shown themselves to be particularly promising, versatile candidates. Accordingly, the aim of this project is to synthesise a number of novel combretastatin analogues based on a pyrazole bridge. Pyrazoles hold a privileged position in medicinal chemistry, as many biologically active molecules contain this motif. The structure's presence in a number of blockbuster drugs such as Celebrex and Viagra (*figure 11*) has led to widespread interest in the chemistry of pyrazoles.

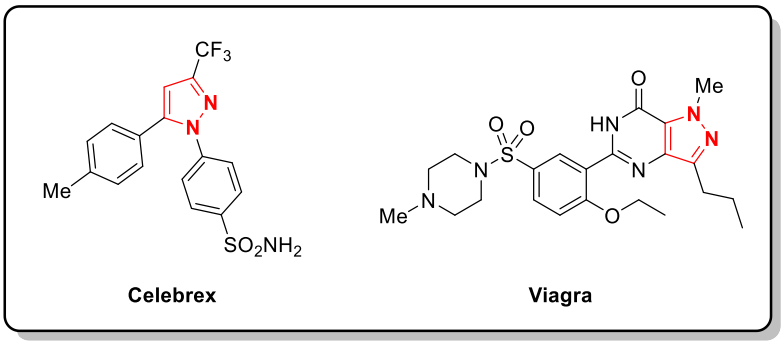

Figure 11: Commercial pyrazole-based therapeutics.

Pyrazoles are typically formed *via* one of two methods; condensation reactions with hydrazines (*scheme 3: a*) or 1,3 dipolar cycloadditions (*scheme 3: b*).[89] This report focuses on the synthesis of pyrazole analogues of combretastatins, *via* [3+2] cycloadditions of sydnones with alkynes.

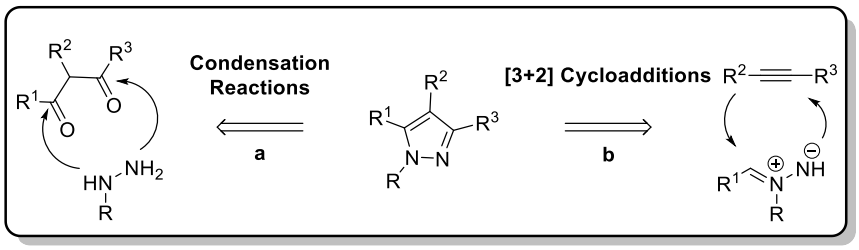

Scheme 3: Synthetic routes to pyrazoles.

1.6: Sydnones

Sydnones are heterocyclic, mesoionic compounds discovered by Earl and Mackney in 1935.[90] The term "mesoionic" describes dipolar five- or six-membered heterocycles for which an uncharged, covalent structure cannot be drawn and a single mesomeric structure is not sufficient.[91] These properties have led to much debate about the most appropriate structural representation of these molecules.[92] However, sydnones are generally represented by a negatively charged, exocyclic, enolate-type oxygen and a positively charged, trivalent oxygen within the ring (**18**, *figure 12*). Although this structure is widely adopted, it does not provide a comprehensive view of the properties of sydnones. Although carbon C4 is nucleophilic, like an enolic carbon, it also bears an acidic proton (pK_a 18-20).[93] The presence of a ketone-like function is supported by infrared spectral data of a number of sydnones, which have an absorbance at around 1730 cm^{-1}.[92] These odd properties make sydnones highly versatile and interesting substrates in chemical synthesis.

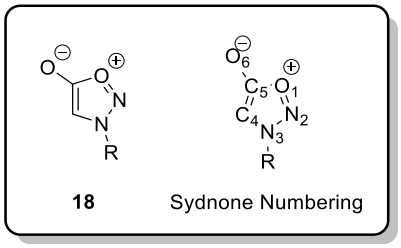

Figure 12: Sydnone structure and numbering nomenclature.

Synthesis of Sydnones

Sydnones can be easily synthesised from *N*-substituted amino acids. Classically, *N*-nitrosation with sodium nitrite in concentrated hydrochloric acid, followed by cyclodehydration using acetic anhydride, has been used to prepare these mesoionic compounds (*scheme 4*). These early methods have since been modified to give greater options in the synthesis of sydnones. Acid sensitive groups can be tolerated *via* the use of *iso*amyl nitrite (IAN) as an alternative nitrosation agent.[94] Due to an increased rate of cyclisation, trifluoroacetic anhydride has largely replaced the use of acetic anhydride in the cyclodehydration step.[95] More recently a "one pot" preparation of sydnones using 1,3-dibromo-5,5-dimethylhydantoin (DBH) was reported by Azarifar *et al.*[96] A one pot procedure is particularly advantageous in the synthesis of sydnones, by avoiding isolation of the highly toxic nitrosamine intermediate.

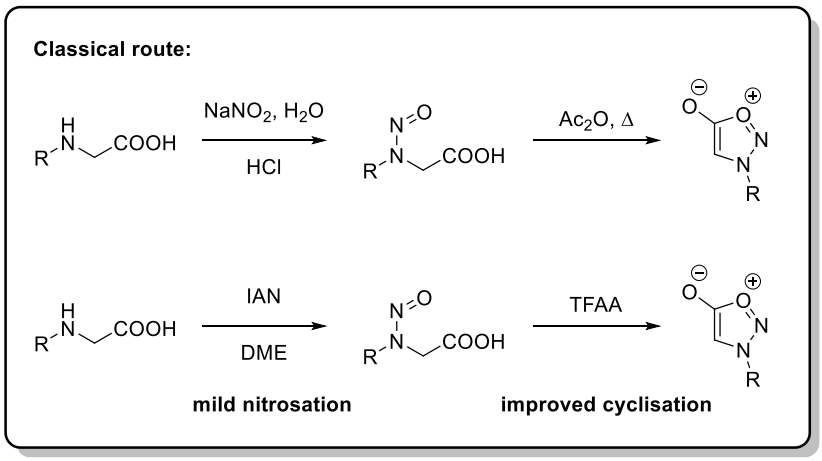

Scheme 4: Synthesis of sydnones.

1.7: Reactions of Sydnones

Sydnone functionalisation is dominated by reactions at the *C*4 carbon. Because sydnones are both nucleophilic and acidic, both electrophilic aromatic substitution and deprotonation followed by electrophile addition are available as methods of functionalisation.

Halogenation

Aryl halides hold a privileged position in organic chemistry due to their widespread use as partners in cross coupling reactions and other useful applications including, metal-halogen exchange. Unsurprisingly, a number of different methods for the halogenation of sydnones have been developed. Bromination in particular, has been studied extensively. The first methods for the halogenation of sydnones were developed by Baker, Ollis and Poole in the late 1940s.[97] They demonstrated that the bromination of sydnones occurred upon treatment of *N*-phenylsydnone with bromine in acetic anhydride at 0 °C, or with *N*-bromosuccinimide (NBS) in boiling chloroform. Kato *et al.* reported improved yields by treating *N*-phenylsydnone with bromine in ether, in the presence of sodium hydrogen carbonate.[98] More recent work by Dumitraşcu *et al.* demonstrated direct iodination of sydnones in good yields, using iodine monochloride in buffered acetic acid.[99] This was followed by the chlorination and bromination of a range of sydnones utilising similar conditions with chlorine and bromine respectively (*scheme 5*).[100]

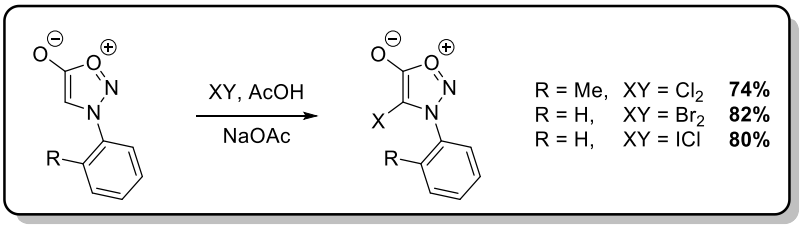

Scheme 5: Halogenation of sydnones.

Modification of *C*4 Halosydnones

Palladium-mediated Suzuki-Miyaura coupling of 4-bromosydnones was successfully achieved in the Harrity laboratories.[101] 4-Bromo-3-phenyl sydnone could be readily coupled with a large variety of aryl boronic acids, boronic esters, and trifluoroborate salts in good yields, with conventional heating and under microwave conditions (*scheme 6*). Turnbull *et al.* successfully demonstrated that Sonogashira coupling of 4-bromosydnones was possible.[102] However, portionwise addition of both catalyst and alkyne was necessary for full conversion.

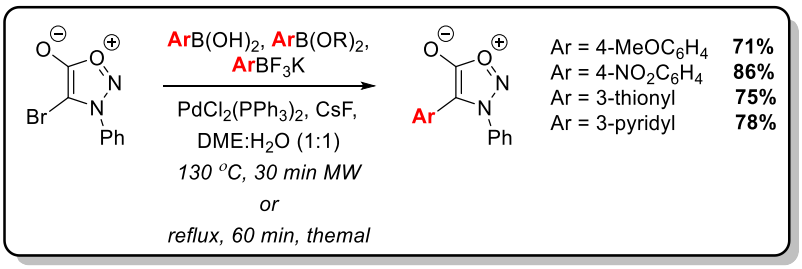

Scheme 6: Suzuki-Miyaura coupling of 4-halosydnones.

Moran *et al.* demonstrated that direct arylation of *C*4 unsubstituted sydnones with aryl bromides and iodides is possible in the presence of catalytic amounts of palladium and a base (*scheme 7*).[103] A subsequent paper reported the applicability of this approach to alkenyl- and alkynylation of sydnones.[104] Kuang *et al.* have since reported the direct arylation of sydnones with boronic acids.[105] However, this method does not seem to offer any advantages over Moran's method.

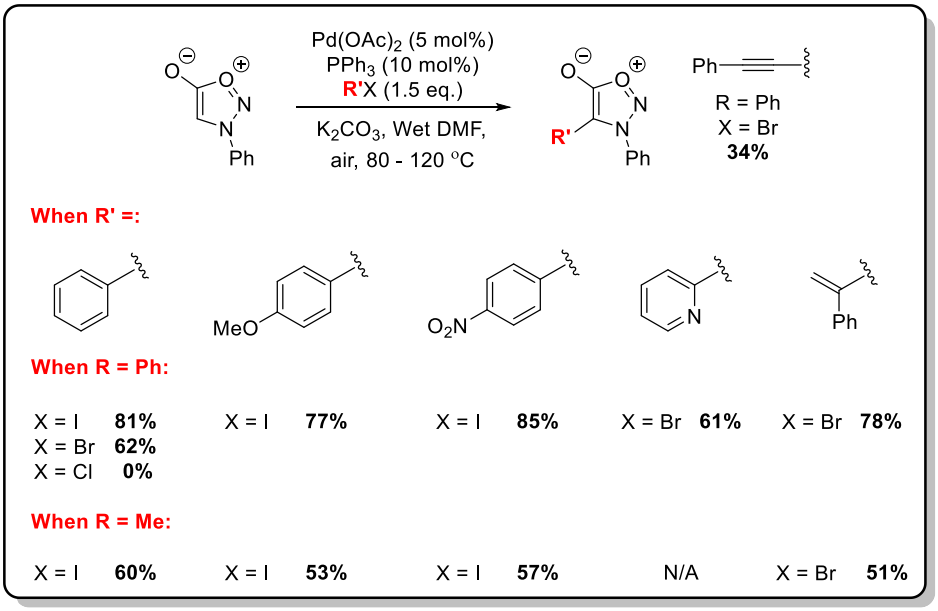

Scheme 7: Direct arylation of sydnones.

Alkyne Cycloadditions

Arguably, the most important property of sydnones, is their ability to undergo [3+2] cycloaddition – retrocycloaddition reactions with alkynes. The reactions produce pyrazoles after the expulsion of carbon dioxide.

The first report of sydnones undergoing cycloadditions with alkynes was by Huisgen *et al.* in the early 1960s.[106] In this study, a range of alkynes, bearing various functional groups were utilised to form pyrazoles in good to excellent yields. More recent studies have focussed on

the preparation of more heavily substituted pyrazoles, as well as regiocontrol of the cycloaddition. Electron deficient dienophiles react most readily with sydnones, hence, a number of studies have been reported using the activated alkyne dimethylacetylenedicarboxylate (DMAD).[99,107] Padwa *et al.* undertook cycloaddition studies of unsymmetrical alkyne, methyl propiolate, and a variety of *C*4-substituted sydnones.[108] However, these reactions proceeded in moderate yields and with low regiocontrol. A particularly interesting study of regioselectivity was undertaken by Wong and Yeh *et al.*[109] These authors undertook a systematic study of the components of the cycloaddition and how modifications affected regioselectivity. They found that various *C*4-substitutions had little effect on regioselectivity. However, varying the ester group of the propiolate led to changes in selectivity (*scheme 8*). The use of diphenylmethyl propiolate gave excellent levels of regiocontrol when used with 4-cyano-3-(4-ethoxyphenyl)sydnone. The reaction gave solely the 3,5 substituted pyrazole, a significant contrast to ethyl and benzyl propiolate that gave essentially no regioselectivity.

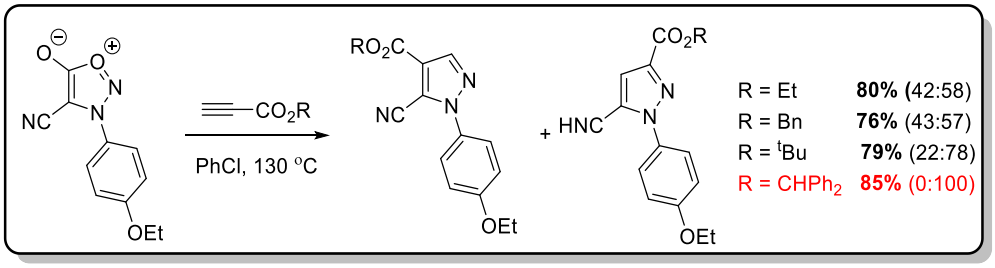

Scheme 8: Sydnone cycloadditions with propargyl esters.

A particularly interesting class of dienophiles are alkynylboronates. Cycloadditions with these substrates allow access to aromatic and heteroaromatic boronic esters. Boronic esters are attractive substrates because they can undergo a wide range of chemical transformations, a particularly important example being Suzuki-Miyaura coupling. Detailed studies in the Harrity group have previously found alkynylboronates to be competent partners in sydnone cycloadditions.[110,111,112] Cycloadditions of *C*4-unsubstituted sydnones with alkynylboronates can be undertaken with moderate to high regiocontrol (*scheme 9*). Substitution at the *C*4 position allows access to high levels of regiocontrol in the formation of both regioisomers (*scheme 10*). This strategy has shown itself to be a very powerful tool in the synthesis of pyrazoles.

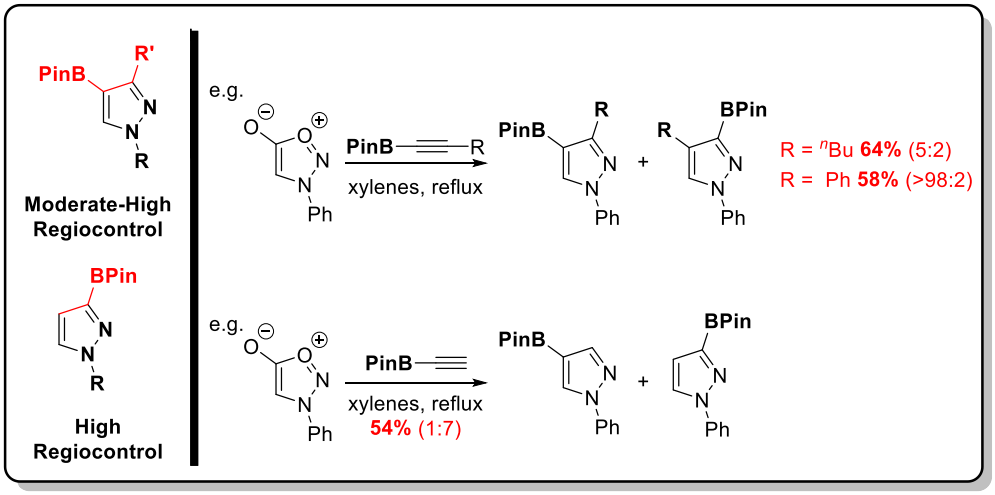

Scheme 9: Cycloaddition of unsubstituted sydnones with alkynylboronates.

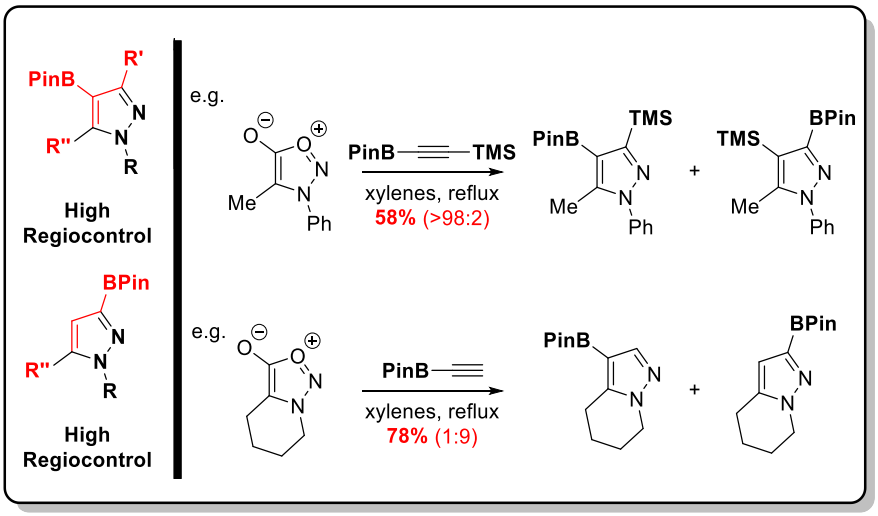

Scheme 10: Cycloaddition of substituted sydnones with alkynylboronates.

Particularly interesting recent developments in sydnone cycloadditions have seen both catalytic and stoichiometric copper used to improve reactivity and even alter regioselectivity. Seminal work by Taran *et al.* demonstrated that catalytic copper in the presence of phenanthroline and sodium ascorbate facilitated cycloadditions at 60 °C and inverted the natural regioselectivity of the cycloaddition. The 1,4-substituted pyrazole products were furnished as single regioisomers (*scheme 11*).[113,114] However, substrates were limited to *N*-arylsydnones and terminal alkynes. This chemistry has since been extended to tolerate bromine substitution at the sydnone *C*4 position, allowing access to 1,4,5-trisubstituted pyrazoles.[115] The proposed mechanism involves the formation of the copper acetylide which undergoes cycloaddition with the sydnones. Harrity *et al.* further studied the mechanism of these reactions and also found that the regioselectivity of the copper-promoted reaction could be altered by simply changing the copper salt used (*scheme 12*).[116] Copper triflate was

found to accelerate the reaction by Lewis acidic activation of the sydnones and preferentially give the 1,3-substituted pyrazoles. Copper acetate was found to accelerate the reaction and give the opposite regioselectivity by *in situ* formation of the appropriate copper acetylide.

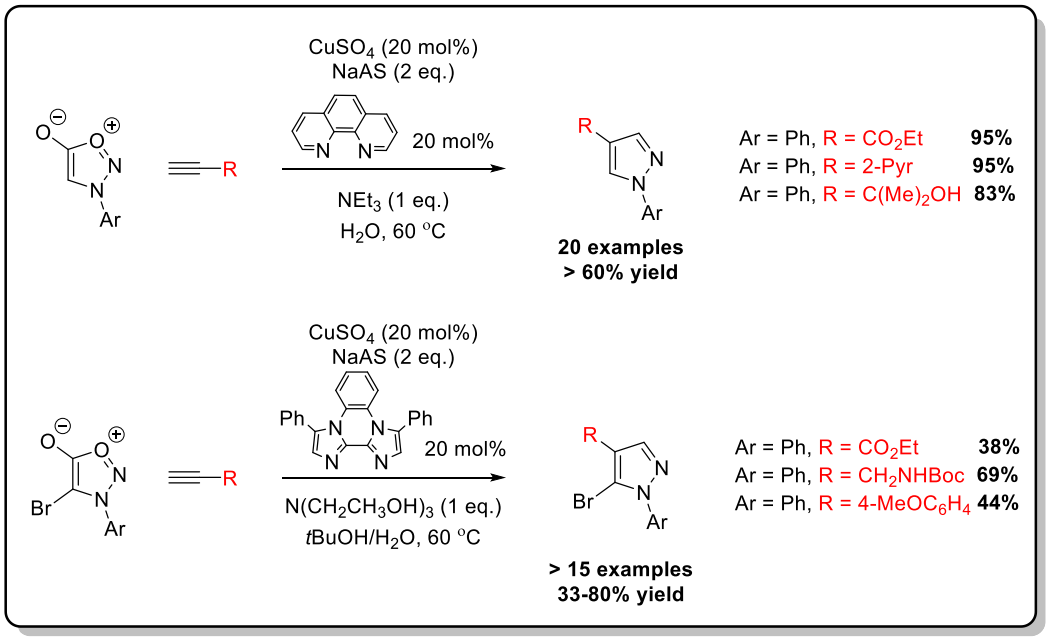

Scheme 11: Taran's copper-catalysed sydnone cycloaddition.

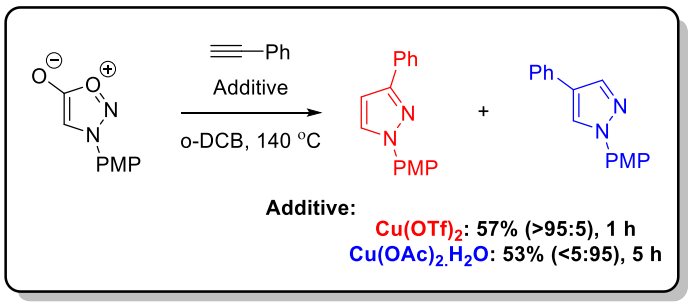

Scheme 12: Copper-controlled regioselectivity of sydnone cycloadditions.

Summary of Sydnone Chemistry

Sydnones are a highly versatile class of mesoionic compounds which undergo a wide variety of transformations. These unusual compounds have been shown to readily participate in modern synthetic techniques, such as metal-catalysed cross-coupling and direct arylation reactions. Recent studies into the control of regioselectivity of alkyne cycloadditions have provided more powerful strategies in the utilisation of sydnones as chemical intermediates. A combination of modern coupling methodology and regioselective cycloadditions with alkynylboronates allows access to highly-functionalised pyrazoles with high regiocontrol. Therefore, as well as having interesting biological activity, sydnones provide access to a wide range of useful pyrazoles.

1.8: Project Strategy

The aim was to utilise the three vicinal zones of the pyrazole ring to synthesise various combretastatin analogues (*figure 13*). This strategy gave the potential for a large compound library, as for every pair of aromatic rings used, 6 parent compounds could be prepared before further substitution of the pyrazole core was even considered. Attention was therefore focussed on accessing pyrazoles that were direct analogues to the parent CA4 compounds, with scope for alternative analogue synthesis based on biological screening results.

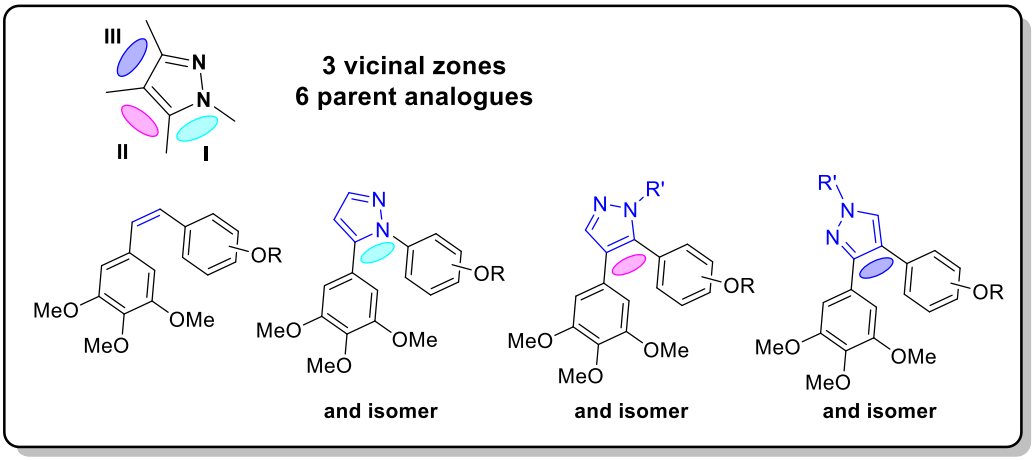

Figure 13: Pyrazole-based analogues of combretastatins.

Sydnones were chosen as the precursors to the target pyrazoles, because of their versatility in the preparation of pyrazoles and particularly because of their propensity to undergo highly regioselective cycloadditions to form the desired diazoles. Particularly attractive was the potential to prepare all synthetic targets from a small number of starting materials, using similar chemistry (*scheme 13*). However, this strategy raised a number of challenges that needed to be overcome. Firstly, access to 1,5-substituted pyrazoles theoretically required a high temperature cycloaddition with acetylene gas. Secondly, 4,5-substituted pyrazoles required the natural regioselectivity of the cycloaddition to be overcome. Typically, the largest substituent is incorporated at the *C*3. Finally, regioselectivity would be difficult achieve with biaryl alkynes for the preparation of 3,4-substituted pyrazoles. With these challenges in mind, initial investigations would focus on methods for the *C*4 arylation of sydnones. *C*4 arylated sydnones were required intermediates for the preparation of both the 1,5 analogues and the 4,5 analogues.

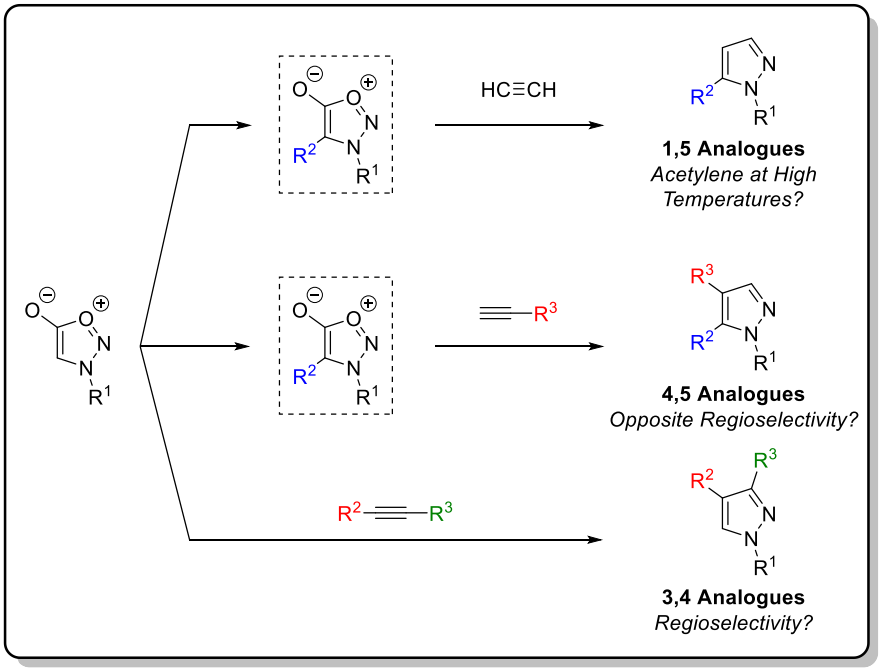

Scheme 13: Sydnone approach to pyrazole-based combretastatin analogues.

1.9: Initial Investigations into Sydnone *C*4 Arylation

A number of options were available in order to access the key intermediate *C*4-arylated sydnones. The first option was to obtain the desired compounds directly from the arylated amino acid using traditional sydnone synthesis techniques (*scheme 14, A*). This method was not particularly attractive as it required several arylated amino acids to be made available. Moreover, this approach would be quite linear and would require significant effort to make a large number of analogues available. The second option was to use classical cross coupling methods (*B*). As stated earlier, work in the Harrity group had demonstrated the feasibility of Suzuki-Miyaura coupling with bromosydnones.[101] As such, this approach seemed viable. The final option was to use direct arylation to access the compounds using the chemistry reported by Moran *et al.* (*C*).[103] This seemed an attractive prospect because it avoided the need for prefunctionalisation of the sydnones. However, only limited scope had been demonstrated in this process and aryl iodides seemed to be necessary to obtain the best yields. It was therefore decided to begin our investigations by exploiting the Suzuki-Miyaura coupling to access the key sydnone intermediates.

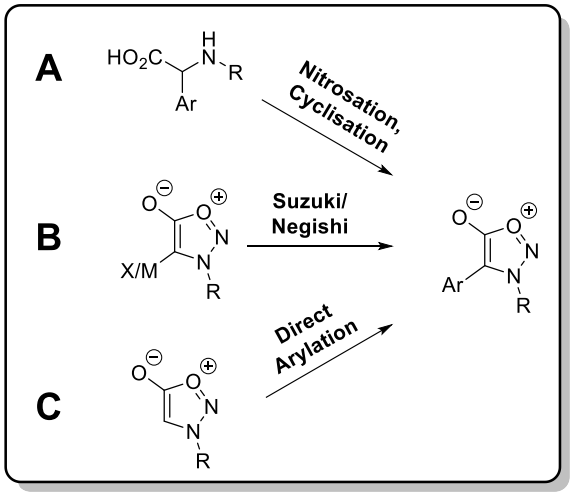

Scheme 14: Approaches to *C4*-arylation.

Suzuki-Miyaura Route to *C4*-Arylated Pyrazoles

Investigations began with the preparation of *N*-(3,4,5-trimethoxyphenyl)-4-bromosydnone **19** using bromination conditions previously employed on *N*-phenylsydnone (*table 2, entry 1*).[101] Unfortunately this method resulted in a 1:1 mixture of product:starting material. Resubjection of the crude material to the reaction conditions did result in full conversion of starting material, but the product was recovered in only 5% isolated yield. Increasing the reaction time did improve the product:SM ratio, but full conversion was not achieved (*entries 2-4*). Full conversion and clean product was obtained in 53% yield when 3 equivalents of

bromine were used over a reaction time of 30 minutes (*entry 5*). Unfortunately, this result was not reproducible on scale, with significant loss of material observed in these cases.

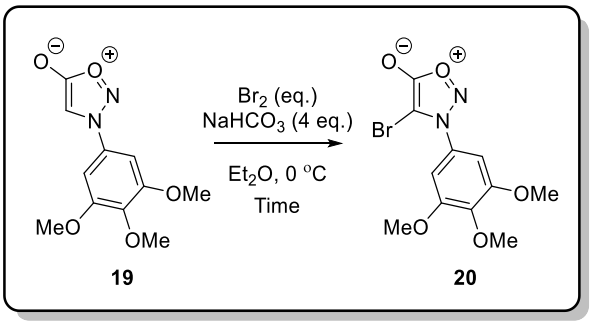

Entry	Time	Eq. Br_2	P:SM ratio in isolated material[a]	Yield
1	10 min	1.5	1:1 (1:0)[b]	(5%)[b]
2	15 min	1.5	6:4	57%
3	30 min	1.5	7:3	55%
4	60 min	1.5	7:3	83%
5	30 min	3	1:0	53%

a) Ratio determined from ^{1}H NMR spectrum of isolated material. b) Yield and conversion in parenthesis after resubjection of crude product to reaction conditions

Table 2: Optimisation of bromination.

In spite of continuing issues in the preparation of significant quantities of **20**, it was decided to attempt the Suzuki-Miyaura coupling of **20** with 3-hydroxy-4-methoxyphenylboronic acid pinacol ester (*scheme 15*). Cross-coupled product was not observed under conditions developed previously in the Harrity group. With the on-going issues of bromination and this discouraging cross-coupling result, a different strategy was devised. Unfortunately, attempts at Negishi coupling of *in situ* generated sydnonylzinc reagent were met with limited success and attempts at optimisation did not improve the reaction. It was therefore decided to use the direct arylation chemistry developed by Moran *et al.* to prepare the desired compounds.[103]

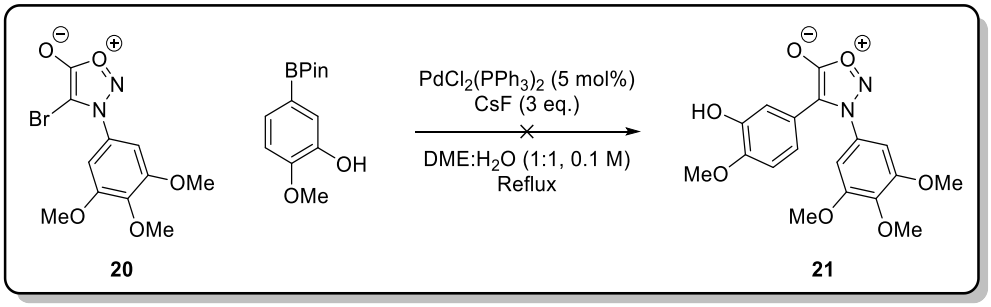

Scheme 15: Attempted Suzuki-Miyaura coupling of **20**.

Chapter 2: Palladium-Catalysed Direct Arylation of Sydnones

2.1: Direct Arylation

Introduction to Direct Arylation

Direct arylation is a particularly attractive technique for the preparation of biaryl molecules. It is more efficient than traditional coupling techniques, such as Suzuki-Miyaura, Negishi, and Stille coupling as it avoids the requirement for the pre-functionalisation of at least one coupling partner. There are three distinct types of direct arylation; oxidative direct arylation with organometallics, dehydrogenative direct arylation, and direct arylation with aryl halides (*scheme 16*).[117] Both oxidative direct arylation with organometallics and dehydrogenative arylation require an oxidant to render the reaction catalytic in the precious metal. Direct arylation with aryl halides does not require an added oxidant. The mechanism involves oxidative insertion of the metal catalyst into the aryl halide, followed by completion of the redox cycle in the product forming reductive elimination step.

Oxidative direct arylation with organometallics has been widely reported in the literature. It is valuable due to the versatility in the identity of the organometallic coupling partner. The use of aryl boronates, silanes, stannanes, Grignard reagents, and zinc reagents has been reported.[117] A wide range of metal catalysts have also been utilised, including those based on rhodium, ruthenium, palladium, and iron. For example, Nakamura *et al.* demonstrated that iron catalysts could be used in imine directed direct arylation with organozinc reagents (*scheme 17*).[118]

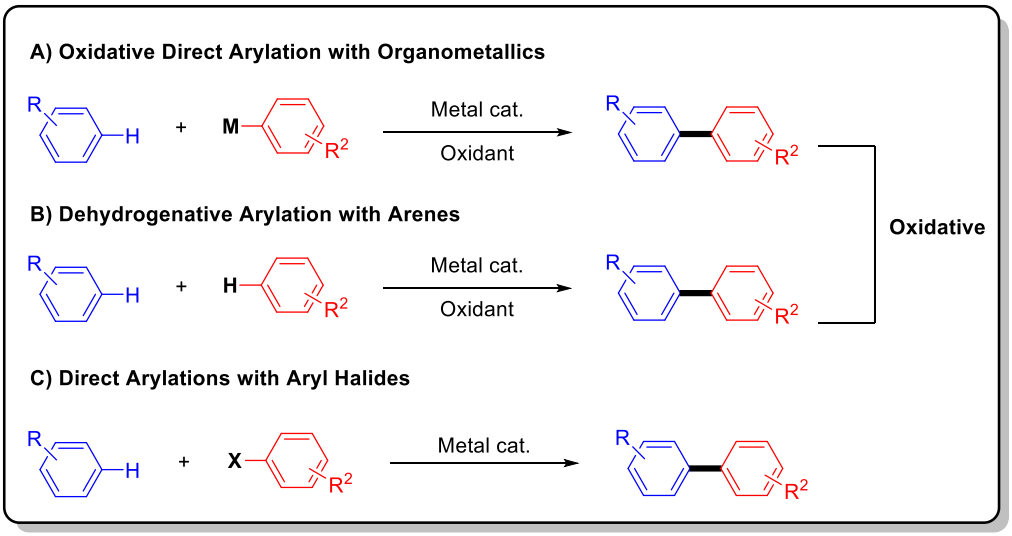

Scheme 16: Direct arylation methods.

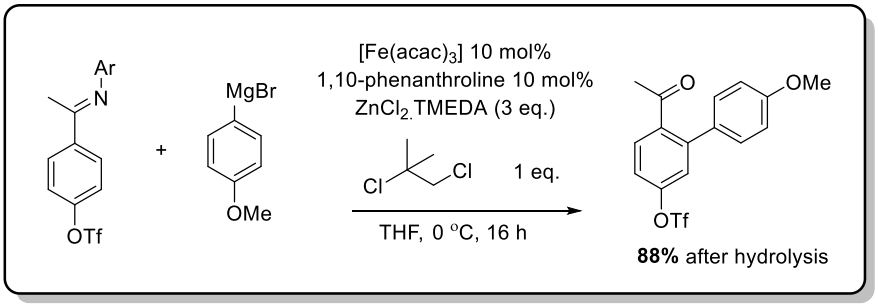

Scheme 17: Nakamura's iron-catalysed direct arylation.

Dehydrogenative arylation is perhaps the most attractive variant of direct arylation, particularly if molecular oxygen could be used as the oxidant. In this case, water would be the by-product of the reaction. However, these reactions are difficult to control. Interesting examples that exemplify the utility of this approach were described by Ohno *et al.* They demonstrated that Buchwald-Hartwig coupling, followed by the introduction of an atmosphere of oxygen and acetic acid resulted in the dehydrogenative coupling to the carbazole (*scheme 18, A*).[119] Elegant work by Larossa *et al.* achieved both chemo- and regioselectivity in dehydrogenative arylations by using heterocycles and perfluorobenzenes under gold catalysis (*scheme 18, B*). Although impressive, it highlighted the limitations of dehydrogenative coupling in the need to for significant differentiation of *C-H* bonds.

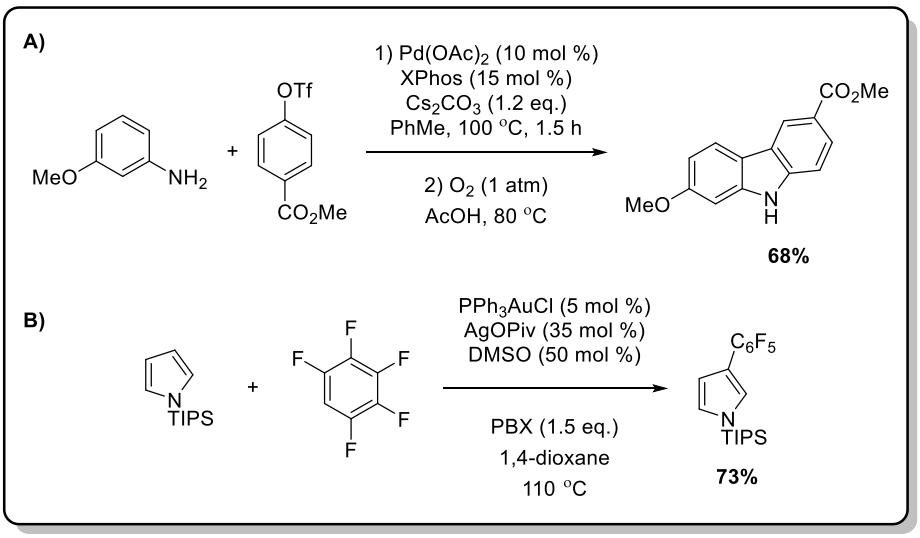

Scheme 18: Ohno's ring closing direct arylation and Larossa's dehydrogenative direct arylation.

Direct arylation with aryl halides has had arguably the greatest impact on the field of *C-H* arylation chemistry. The absence of the requirement for an oxidant, and the ready availability of cheap aryl halides and pseudo-halides have certainly kept this variant at the forefront of *C-H* functionalisation. An early example of chelation controlled *C-H* arylation of aryl iodides

was reported by Miura *et al.* (*scheme 19, A*).[120] The key step involved attack of the phenolate on the Pd(II) complex formed from the oxidative addition of the aryl halide. In recent years, much work has focused directed *C-H* activation. *Ortho*-directed and *meta*-directed *C-H* activation has become a powerful tool in synthetic organic chemistry.[121,122,123] The chemistry is not limited to arylation, examples of amidation,[124] alkylation,[125] oxidation[126] and many others have been reported, with a variety of directing groups and metal catalysts. Important contributions that avoid the need for a directing group have also been made. For example, Glorius *et al.* reported the regioselective direct arylation of benzothiophenes with aryl chlorides (*scheme 19, B*) using heterogeneous catalysis.[127] Ellman and Bergman *et al.* reported the direct arylation of pyridines and quinolines with aryl bromides using a rhodium catalyst (*scheme 19, C*).[128] Interestingly, the reaction required substitution in the 2-position of the pyridine for success. Substituents in this position alter the basicity of the pyridine nitrogen and can therefore help prevent unwanted ligation to metals. Very recently, Harrity *et al.* have exploited this phenomenon to realise the Rh-catalysed *C-H* amidation of 2-substituted pyridines (scheme 20).[129] As was to be expected, electron withdrawing substituents were most successful at deactivation of the pyridine nitrogen. What's more the reaction proceeded at mild temperatures of 40 ^{o}C.

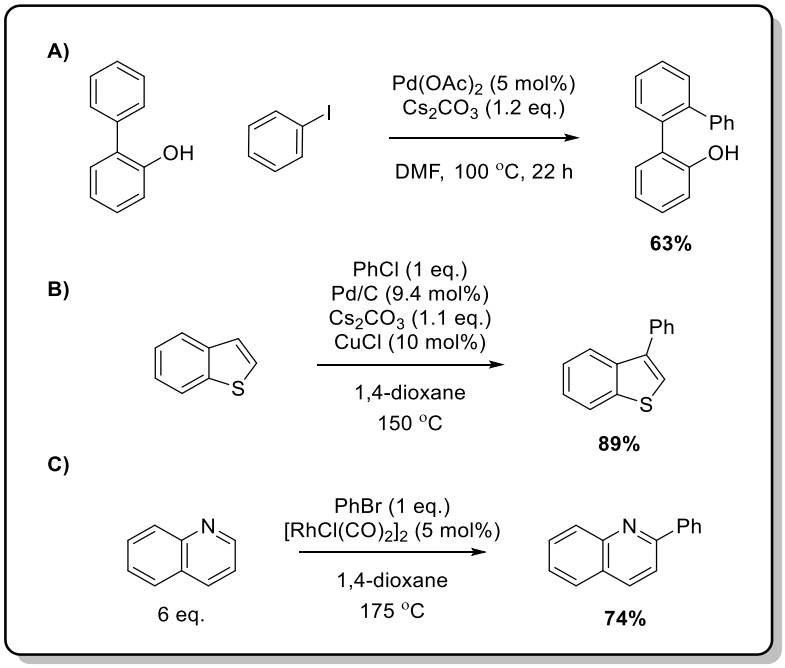

Scheme 19: Direct arylation examples by Miura, Glorius and Ellman.

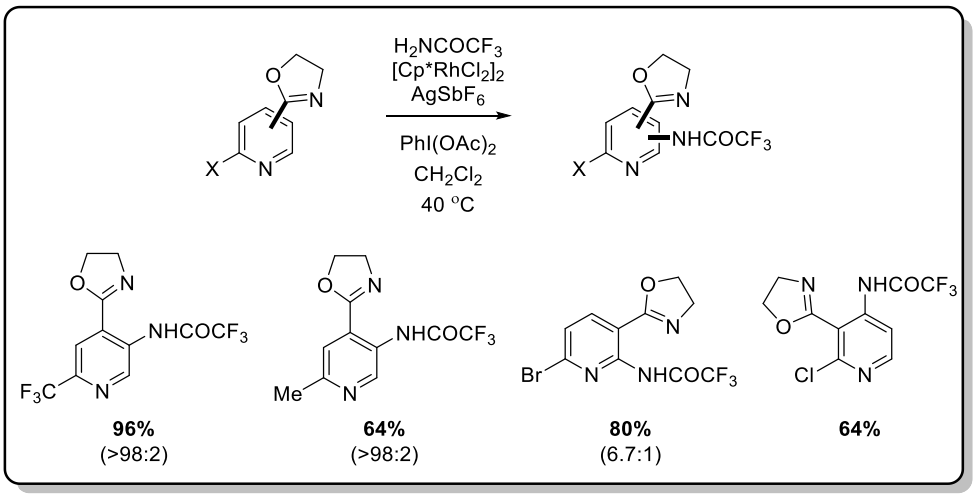

Scheme 20: Harrity's directed amidation of pyridines.

Mechanism of Direct Arylation with Aryl Halides

The mechanism of direct arylation with aryl halides is believed to initially proceed *via* oxidative addition of the palladium (0) catalyst. The subsequent functionalisation of the *C-H* bond could proceed *via* a number of mechanisms; electrophilic aromatic substitution (S_EAr) (*scheme 21, A*), Heck reaction (*B*), oxidative addition (*C*), concerted S_E3 process (*D*), or σ-bond metathesis (E).[130,131] The exact mechanism is clearly dependent on the reaction conditions, substrates and catalyst. Historically, the mechanisms of such reactions had been thought to proceed by either, S_EAr, the Heck reaction or by oxidative addition. More recent studies have indicated S_E3 processes and σ-bond metathesis to be the more likely pathways in many cases.[132,133] These mechanistic pathways have been termed concerted metalation-deprotonation (CMD) processes. The legitimacy of CMD mechanisms is supported by the significant rate enhancements seen when catalytic amounts of pivalic acid are added to certain *C-H* functionalisation reactions.[134,135]

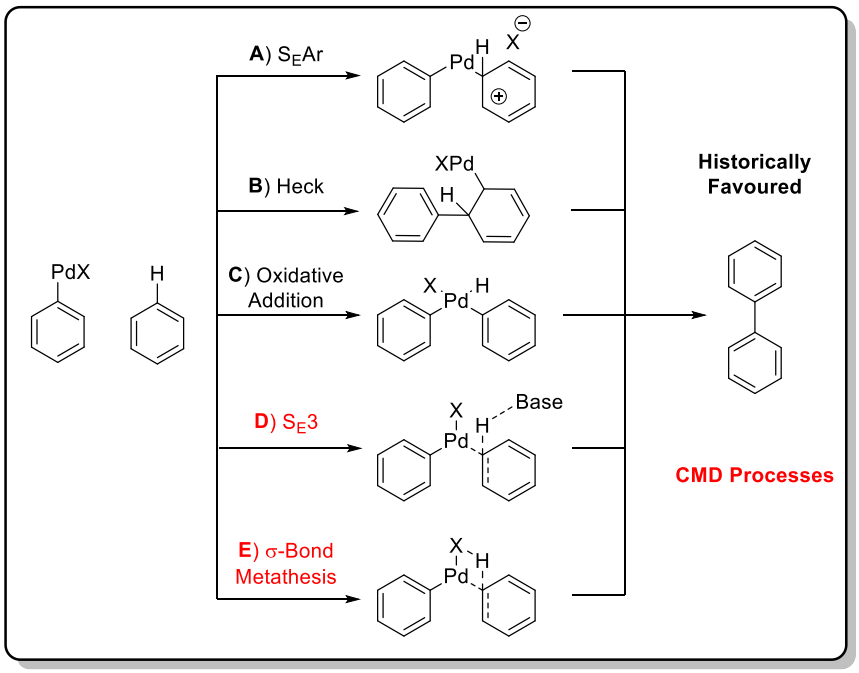

Scheme 21: Possible mechanisms of direct arylation.

2.2: Direct Arylation of Sydnones

Moran's Conditions for Direct Arylation of Sydnones

As previously mentioned, the direct arylation of sydnones was reported by Moran *et al.*[103] This convenient method seemed suitable to gain access to 3,4-diarylsydnones. Application of the reported conditions to **19** and 4-bromoanisole led to isolation of a 2% yield of the target arylated sydnone, **22**. A significant amount of the apparent sydnone decomposition product, **23** was also isolated (*scheme 22*). Repetition of the reaction under nitrogen resulted in a 55% yield of **22**, but also isolation of a 17% yield of phenylated by-product **24** (*scheme 23*).

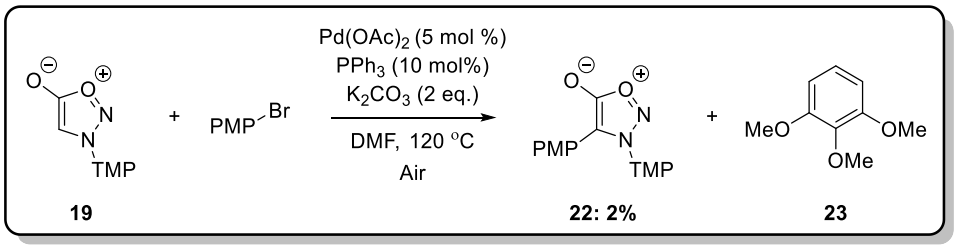

Scheme 22: Direct arylation under Moran's conditions.

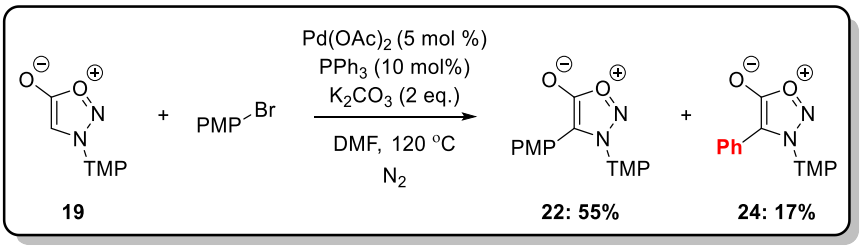

Scheme 23: Direct arylation using Moran's conditions under inert atmosphere.

Intriguingly, similar phenylated by-products were also observed in a number of related reactions, including those with *N*-(4-methoxyphenyl)sydnone, **25** (*table 3, entries 1, 2 and 4-6*). Most importantly, it was particularly difficult to separate the by-product from phenol **21**. In this reaction, the starting bromide was a TBS-protected phenol, which desilylated under the reaction conditions. The crude reaction mixture contained **21** and **24** in an 8:2 ratio (*table 3, entry 4*). Difficulty in separation resulted in a poor isolated yield of **21** in 11%.

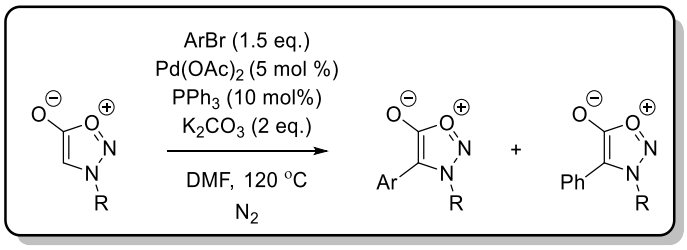

Entry	R	Ar	Product	Yield Product	By-product	Yield By-product
1	3,4,5-$MeOC_6H_2$	4-$MeOC_6H_4$	**22**	55%	**24**	17%
2	4-$MeOC_6H_4$	3,4,5-$MeOC_6H_2$	**26**	49%	**27**	Trace[a]
3	3,4,5-$MeOC_6H_2$	C_6H_5	**24**	61%	-	-
4	3,4,5-$MeOC_6H_2$	3-OTBS-4-$MeOC_6H_3$	**21**[b]	11% (8)[c]	**24**	(2)[c]
5	4-$MeOC_6H_4$	4-$MeOC_6H_4$	**28**	29%	**27**	9%
6	3,4,5-$MeOC_6H_2$	2-$MeOC_6H_4$	**29**	70%	**24**	Trace

a) Observed ^{1}H NMR of crude material, but not isolated b) Isolated product was the desilylated phenol.

c) Ratio observed in ^{1}H NMR of crude material.

Table 3: Application of Moran's conditions to other substrates.

The source of the by-product was an intriguing issue. Given the same 4-Ph-substituted by-product was observed from a variety of substrates, the only logical source of the phenyl group was the phosphine ligand. In this context, aryl-aryl exchange of phosphine ligands in metal-catalysed cross coupling has been known for a number of years.[136] When the transmetallation step is slow, competing reductive elimination of the phosphine and the aryl group to form a phosphonium salt can occur. During the direct arylation of sydnones, *C-H* insertion is effectively the transmetallation step. Therefore, it is likely to be slow because rather than an organometallic acting as the nucleophilic component, it is a relatively unpolarised *C-H* bond or the corresponding conjugate base. It was postulated that in the case of sydnones, reductive elimination of the phosphonium salt can occur (*scheme 24, II*). Oxidative addition into a different phosphorus-carbon bond generates the Pd(II) intermediate with phenyl group attached (*scheme 24, III*). This can then re-enter the catalytic cycle to form the phenylated by-product. Reductive elimination of phosphine ligands is promoted in polar solvents and inhibited by steric bulk and electron withdrawing substituents on the aryl group. It was therefore, unsurprising that the sterically hindered 2-

methoxyphenyl bromide coupled smoothly, with only trace amounts of the by-product being generated in this case (*table 3, entry 6*).

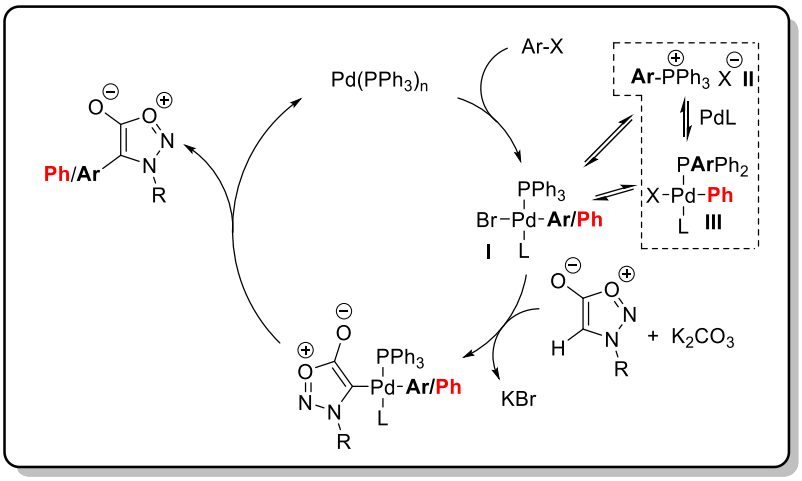

Scheme 24: Proposed mechanism and source of by-product.

To avoid the issue of aryl-aryl exchange, a number of options were considered. For example; the use of a less polar solvent, such as 1,2-dichloroethane, would inhibit the formation of the phosphonium salt. Another option was to use trimesitylphosphine to increase steric bulk and reduce the propensity for reductive elimination of the phosphonium salt. Instead, it was decided to use tributylphosphine, because even if reductive elimination of the phosphonium salt occurred, oxidative addition into sp^2C-P bond of the aryl group would be far more likely than the sp^3C-P alkyl bonds.

2.3: Direct Arylation of Sydnones with Tributylphosphine

Preliminary investigations employed the same conditions as Moran, but with tributylphosphine as ligand. Sydnone **25** was coupled with 4-bromoanisole affording **28** in a 27% yield (*table 4, entry 1*). Performing the reaction in a sealed tube slightly increased the yield to 31% (*entry 2*). Increasing the loading of the phosphine to 50 mol % increased the yield to 50% (*entry 3*). The requirement for increased ligand loading was likely due to the use of non-distilled tributylphosphine. It is therefore likely that the ligand contained significant amounts of tributylphosphine oxide, which is not a good ligand for palladium. Utilisation of the same reaction conditions with **19** and 4-bromophenetole only afforded 10% of the corresponding sydnone **30** (*entry 4*). Furthermore, the attempted coupling of *N*-(4-ethoxyphenyl)sydnone, **31**, with 5-bromo-1,2,3-trimethoxybenzene failed to afford more than trace amounts of product (*entry 5*).

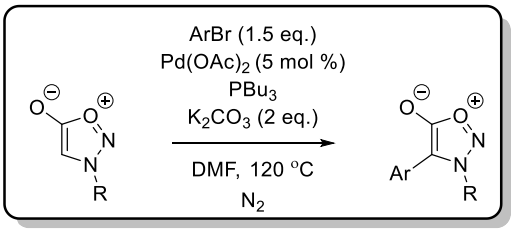

Entry	Starting Material	R	Bromide	Pbu_3	Product	Yield[a]
1	**25**	4-$MeOC_6H_4$	4-$MeOC_6H_4$	10%	**28**	27%
2	**25**	4-$MeOC_6H_4$	4-$MeOC_6H_4$	50%	**28**	31%
3	**25**	4-$MeOC_6H_4$	4-$MeOC_6H_4$	50%	**28**	50%[b]
4	**19**	3,4,5-$MeOC_6H_2$	4-$EtOC_6H_4$	50%	**30**	10%[b]
5	**31**	4-$EtOC_6H_4$	3,4,5-$MeOC_6H_2$	50%	**32**	Trace[b]

a) Isolated yields of purified compounds. b) Reaction performed in a sealed tube.

Table 4: Optimisation with tributylphosphine as ligand.

Although the problem of by-product formation had been eliminated, the consistent isolation of products in poor yields led to a change in direction. It was thought that a more powerful ligand would give higher yields and avoid by-product formation.

2.4: Direct Arylation of Sydnones with XPhos

For a number of years, Buchwald *et al.* have developed a series of electron rich phosphine ligands such as XPhos (*figure 14*). The ligands have a number of important structural features, which result in useful properties for transition metal catalysed reactions.[137] Alkyl groups increase electron density at phosphorus, which promotes oxidative addition; so much so, that aryl chlorides can be used as coupling partners.[138] The use of bulky alkyl groups creates a sterically crowded phosphorus centre, which promotes reductive elimination. The lower aryl ring of the biaryl promotes reductive elimination, as well as reducing the rate of oxidation of the phosphine[139] – often a significant problem with electron rich, alkyl phosphines. Bulky groups on the lower aryl ring prevent the formation of palladacycles, such as **33** (*figure 14*) which inhibit catalysis.[140] The bulky groups also favour formation of the active catalyst $L_1Pd(0)$ over $L_2Pd(0)$.

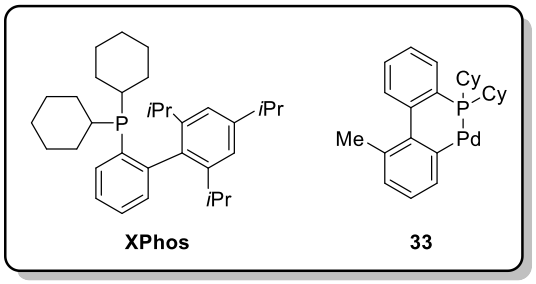

Figure 14: Buchwald ligands.

It was envisaged that the steric crowding around phosphorus would hinder formation of the unwanted phosphonium salt and that the increased electron density on phosphorus would increase the reactivity of the catalytic system. Gratifyingly, utilisation of 10 mol % XPhos in the reaction of sydnone **25** with 4-bromoanisole proceeded smoothly to form **28** in 86% yield (*table 5, entry 1*) without by-product formation. Moreover, use of 4-chloroanisole furnished the diarylsydnone in only slightly diminished yield (*entry 2*). This was particularly exciting as aryl chlorides had been unreactive reaction partners in Moran's investigations. Pleasingly, the reaction was scalable and gave the product in quantitative yield on gram scale.

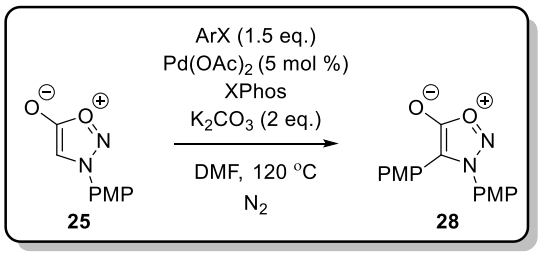

Entry	Ar-X	Yield 28[a]
1	4-$MeOC_6H_4Br$	86%
2	4-$MeOC_6H_4Cl$	79%
		97%[b]

a) Isolated yields of purified compounds. b) Reaction performed on 5 mmol scale.

Table 5: Initial investigations with XPhos.

It was decided to explore the scope of the direct arylation using 4-chlorotoluene and a series of sydnones (*table 6*). A range of *N*-aryl groups were well tolerated in the coupling (entries 1 – 5). However, it should be noted that 4-(4-methylphenyl)-*N*-(4-fluorophenyl)sydnone **39** (*entry* 5) was unstable in solution and decomposed in chloroform and dichloromethane. Pleasingly, *N*-alkylsydnones coupled smoothly (*entries 6-8*) when a reduced reaction temperature of 80 °C was used. This was consistent with Moran's observations that lower temperatures were required for the coupling of *N*-alkylsydnones, due to the thermal instability of these mesoionic compounds.[103]

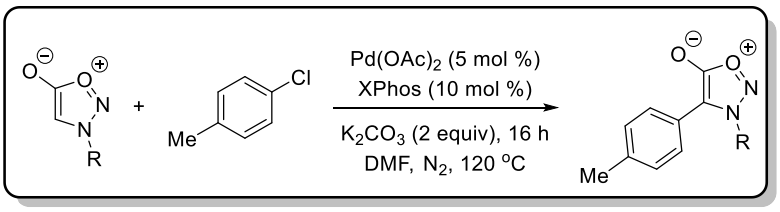

Entry	Starting Material	R	Product	Yield[b]
1	**25**	4-$MeOC_6H_4$	**33**	83%
2	**19**	3,4,5-$(MeO)_3C_6H_2$	**34**	96%
3	**31**	4-$EtOC_6H_4$	**35**	77%
4	**36**	Ph	**37**	83%
5	**38**	4-FC_6H_4	**39**	68%
6	**40**	Me	**41**	67%[c]
7	**42**	Et	**43**	72%[c]
8	**44**	Bn	**45**	61%[c]

a) Reaction conditions: **1a** (0.5 mmol), 4-MeC_6H_4Cl (0.8 mmol), $Pd(OAc)_2$ (0.025 mmol), XPhos (0.05 mmol) and K_2CO_3 (1.0 mmol) in DMF (2 mL) stirred at 120 °C for 16 hours. b) Isolated yields of purified compounds. c) Reaction conducted at 80 °C.

Table 6: Scope with respect to sydnone.

Next, the scope of the direct arylation reaction using a selection of aryl chlorides was explored (*table 7*). The cross-coupling was successful for a series of benzene derived (*entries 1-7*) and heteroaromatic substrates (*entries 8, 9*), although 4-chloroaniline and 4-chlorophenol provided the corresponding sydnones (**49** and **50**, respectively) in poorer yields. Fortunately however, these sydnones could be obtained in much higher yields when the corresponding aryl bromides were used instead (*scheme 25*).

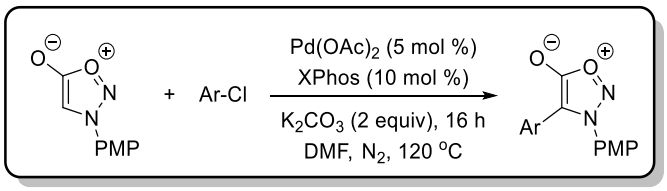

Entry	ArCl	Product	Yield[b]
1	Ph	**27**	83%
2	3-$O_2NC_6H_4$	**46**	85%
3	2-ClC_6H_4	**47**	94%
4	3-ClC_6H_4	**48**	79%
5	4-$H_2NC_6H_4$	**49**	22%
6	4-HOC_6H_4	**50**	Trace
7	2-Thiophenyl	**51**	89%
8	4-Pyridyl	**52**	78%[c]

a) Reaction conditions: **1a** (0.5 mmol), **2a(Br/Cl)** (0.8 mmol), $Pd(OAc)_2$ (0.025 mmol), XPhos (0.05 mmol) and K_2CO_3 (1.0 mmol) in DMF (2 mL) stirred at 120 °C for 16 hours. b) Isolated yields of purified compounds. c) 3 equivalents of K_2CO_3 used.

Table 7: Scope with respect to aryl chloride.

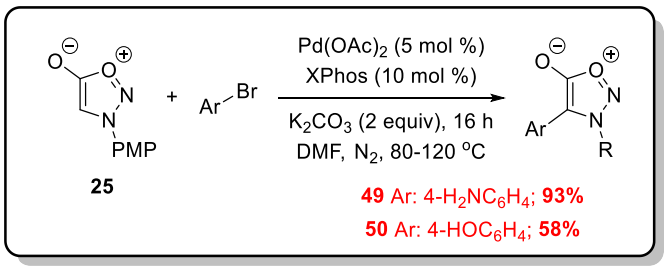

Scheme 25: Improved yields with aryl bromides.

With reliable conditions in hand for the direct arylation of sydnones, attention was turned to the preparation of sydnone-based analogues of CA4P. A range of analogues were readily prepared *via* the new protocol (*table 8*), including two direct analogues of CA4 **21** and **58** (*entries 9 and 10*). Romagnoli and Viola *et al.* had found 4-ethoxyphenyl B rings to be potent partners for the 3,4,5-trimethoxyphenyl A ring in 5-membered ring-bridged systems.[141,80] Analogues of this type, **30** and **32**, were prepared in excellent and good yields respectively

(*entries 6 and 12*). An analogue of Sanofi's AVE8062 was also prepared in excellent yield (**56**, *entry 8*).

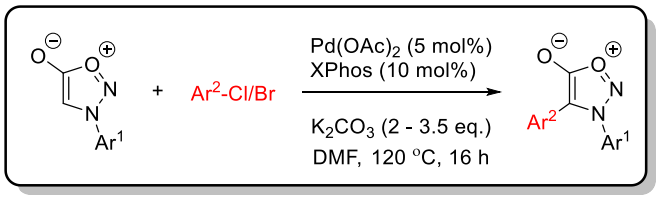

Entry	Compound	Ar^1	Ar^2	Product	Yield[a]
1	**19**	3,4,5-$MeOC_6H_2$	4-$MeOC_6H_4$	**22**	73%
2	**19**	3,4,5-$MeOC_6H_2$	2-$MeOC_6H_4$	**29**	71%
3	**19**	3,4,5-$MeOC_6H_2$	Ph	**24**	81%
4	**19**	3,4,5-$MeOC_6H_2$	3-$NO_2C_6H_4$	**53**	90%
5	**19**	3,4,5-$MeOC_6H_2$	2-Thiophenyl	**54**	81%
6	**19**	3,4,5-$MeOC_6H_2$	4-$EtOC_6H_4$	**30**	92%
7	**19**	3,4,5-$MeOC_6H_2$	2-ClC_6H_4	**55**	73%
8	**19**	3,4,5-$MeOC_6H_2$	3-H_2N-4-$MeOC_6H_3$	**56**	91%
9	**19**	3,4,5-$MeOC_6H_2$	3-HO-4-$MeOC_6H_3$	**21**	81%
10	**57**	3-HO-4-$MeOC_6H_3$	3,4,5-$MeOC_6H_2$	**58**	47%
11	**31**	4-$EtOC_6H_4$	3,4,5-$MeOC_6H_2$	**32**	76%
12	**25**	4-$MeOC_6H_4$	3,4,5-$MeOC_6H_2$	**26**	71%

a) Isolated yields of purified compounds

Table 8: Synthesis of sydnone-bridged combretastatin analogues.

In conclusion, triphenylphosphine was found to be the source of by-product formation in the direct arylation of sydnones. The Buchwald ligand XPhos was found to improve yields, prevent by-product formation, and extend the chemistry to previously unreactive aryl chlorides. The scope of the reaction was found to be impressively broad with a number of polar functional groups tolerated. A number of 3,4-diarylsydnones were successfully prepared using the procedure, including direct analogues of CA4. As well as providing compounds for biological testing, the procedure set itself as a solid, scalable platform to base the synthesis of pyrazole-bridged analogues of CA4 upon.

Chapter 3: Methods and Materials

3.1: General Cell Culture

Cell culture was undertaken in class II safety flow cabinets under aseptic conditions. Cabinet surfaces were wiped with 70% industrial methylated spirit (IMS) and left to run for ten minutes to minimise the risk of infections. Gloves were worn and sanitised with 70% IMS before conducting cell culture. All materials placed into the hood were wiped with 70% IMS.

All cell culture media, phosphate buffered saline (PBS) (Lonza; BE17-512F) and trypsin-EDTA (Lonza; 17161F) were warmed to 37 °C before use in cell culture, to prevent the cells being exposed to cold stress. All cells were maintained in humidified incubators at 37 °C in 5% CO_2.

The cells used in this study were Human Umbilical Vein Endothelial Cells (HUVECs). HUVECs are primary endothelial cells, which are isolated by dissociation from the inner surface of umbilical veins using a collagenase solution. HUVECs used in this study were obtained commercially from pooled donors (Promocell, C-12203). HUVECs were cultured in Endothelial Cell Basal Medium (EBM) (Promocell: C-22010) supplemented with Endothelial Cell Growth Supplement Mix (Promocell: C-39215). The supplemented medium contains 2% foetal calf serum (FCS), 0.4% Endothelial Cell Growth Supplement (ECGS), 0.1 ng/ml recombinant Human Epidermal Growth factor (hEGF), 1 ng/ml recombinant human Basic Fibroblast Growth Factor (hbFGF), 90 µg/ml heparin and 1 µg/ml hydrocortisone. Previous work in the group has shown that increasing the serum concentration in the EBM medium to 10% FCS led to improved cell proliferation and survival and therefore extra heat inactivated low endotoxin FCS (Sigma; F2442) was added to the medium to increase the concentration to 10% (v/v).

General Subculturing Conditions

Cell cultures were observed daily under a phase contrast microscope. Media changes were performed based on the growth rate of cells. Old media were carefully removed from the culture plate and new media preheated to 37 °C were added and the cells were returned to the incubator.

When cells reached 80-100% confluence, they were subcultured. Cell monolayers were washed twice with PBS and then covered with trypsin/EDTA and left in the incubator for 2-3 minutes. Trypsin is a proteolytic enzyme, which disrupts cell-cell junctions and integrin matrix interactions causing cells to detach from the growth surface. EDTA is used to chelate any metal ions, which strengthen matrix integrin protein interactions. Trypsin/EDTA can damage

cells with prolonged exposure so cells are exposed to these for the shortest possible time. The flask was gently tapped on a surface to dislodge the cells. Preheated media containing FCS was added to inhibit the action of trypsin. The cells were thoroughly mixed into a suspension. An aliquot of the cell suspension was counted on Biorad TC20 Cell Counter using Biorad Counting Slides (Biorad; 145-0011). A sample was prepared from a mixture of 50 µL of single cell suspension with 50 µL Trypan Blue (Biorad; 145-0013). Trypan blue is a diazo dye that stains dead cells therefore allowing viable cells to be distinguished. The Biorad Cell Counter provided cell numbers per mL as well as viable cells per mL. This information could be used to calculate seeding densities, and it was at this point that cells were seeded for bioassays. The remaining suspension was centrifuged for 5 minutes at 1000 rpm. The supernatant was carefully removed and the pellet resuspended in fresh EBM. The suspension was further diluted as required for the desired seeding densities. As HUVECs do not adhere well to plastic, culture plates were coated with 0.2% gelatin (Sigma; G1393) in PBS for a minimum of 30 minutes prior to plating. The gelatin was removed just before plating.

3.2: Cell Proliferation Studies

Studies of the effects of various drugs on cell proliferation were undertaken and GI_{50} data were obtained. The cells were grown for several days in the presence or absence of increasing concentrations of drug or vehicle control. The cells were then fixed, stained with crystal violet, a nuclear stain, and then lysed and dye absorbance analysed on a plate reader. Dye uptake correlates with DNA content and cell number and this assay is therefore used to establish effects on cell number/growth/proliferation.

Preparation of Culture Plates

Multi-well culture plates (96-well), were coated with 0.2% gelatin for at least 30 minutes prior to culture. Cells were plated at 5 x 10^4 cells/mL, 100 µL/well and left to adhere for 24 hours. Different concentrations of drugs were then added in 50 µL of EBM. A minimum of 9 wells containing cells were used to test each concentration and in parallel a similar number of wells containing cells were treated with vehicle control. In addition, several wells were left empty. The cells were incubated at 37 °C in a humidified incubator for 72 hours before the media were removed and cells were fixed with 3.7% formalin for 10 minutes. The wells were then washed four times with PBS and stained with 1% crystal violet (Sigma: C3886) solution in 10% ethanol for 20 minutes at room temperature. The plates were then repeatedly rinsed with water until no more dye was visibly staining the washes and then left to dry overnight. 100 µL of 10% acetic acid was added to each well and left for 30 minutes to lyse the cells. The absorbance of each well at 590 nm was then recorded by a plate reader. The absorbance data was corrected against background (wells with no cells but with 10% acetic acid) and transformed into the percentage growth inhibition for each drug concentration (*equation 1*). Where $\%inhib_x$ is the percentage growth inhibition at concentration x, abs_x is the absorbance at 590 nm of stained cells after treatment at concentration x and abs_0 is the absorbance at 590 nm of stained, untreated cells.

$$\%inhib_x = 100 - \left(\frac{abs_x}{abs_0}\right).100$$

Equation 1. Method of calculating percentage inhibition of growth.

The percentage growth inhibition was plotted against the logarithm of concentration using GraphPad Prism 6 software. The point at which y = 0.5 x $y_{max,}$ corresponds to log GI_{50}.

3.3: Immunofluorescence Staining of the Cell Cytoskeleton

Immunofluorescence staining was used to visualise changes in cell morphology and the cytoskeleton. A variety of proteins and filaments that make up the cellular cytoskeleton can be stained with a range of antibodies or fluorescently labelled probes that bind specifically these components. Fluorescently labelled phalloidin, which binds to filamentous actin and an antibody to β-tubulin were used in the study. In addition, the DNA binding dye diamidino-2-phenylindole (DAPI) was used to stain cell nuclei.

Preparation of Cells

HUVECs were cultured on 4 or 8 well Permanox chamber slides (Labtek), which were coated with 5 μg/mL fibronectin in PBS for a minimum of 30 minutes before plating. Cells were plated at 2.5 x 10^4 cells per slide well in 250 μL EBM for 8 well slides and 5 x 10^4 cells per well in 500 μL for 4 well slides. The cells were then kept at 37 °C in a humidified incubator until close to confluence.

a) *Drug activity studies:* Various concentrations of drugs were prepared in EBM *via* systematic dilutions from a 20 mM stock in DMSO. The cells were treated with the drug for 30 minutes in the incubator. The media were then discarded and the cells fixed with 3.7% formalin in PBS for 20 minutes. Formalin creates intermolecular bridges, cross-linking free amino acids whilst preserving overall cellular ultrastructure.
b) *Recovery studies:* A drug solution was prepared in EBM *via* systematic dilutions from a 20 mM stock in DMSO. In well 1 the cells were treated with a vehicle control for the duration of the experiment. In well 2 the cells were treated with the drug for 30 minutes. In well 3 the cells were treated with the drug for the duration of the experiment (90-150 minutes). In well 4 the cells were treated with the drug for 30 minutes, then the media were removed and cells were washed four times with media containing serum. The cells were then placed back in the incubator for 30 minutes, the washing procedure repeated and the cells incubated for a further 30-90 minutes. The media were then discarded and the cells fixed with 3.7% formalin in PBS for 20 minutes.

Staining Protocol

After fixation, the cells were washed 3 x with PBS with each wash lasting 5 minutes. The cells were permeabalised with 0.1% Triton in PBS for 10 minutes followed by a further three washes with PBS. Triton permeabilises the cell membrane allowing the fluorescently labelled probes and antibodies to enter the cell. The cells were then

incubated in a blocking solution of 2% bovine serum albumin (BSA, Sigma: A9647) and 5% horse serum (Vector Laboratories: S-2000) in PBS for one hour at room temperature. The blocking solution was removed and the cells incubated with anti-β-tubulin antibody (Sigma: T4026) at a 1:500 dilution in blocking solution for 2 hours at room temperature or overnight at 4 °C . The cells were subsequently washed four times with PBS to remove excess antibody. The cells were then incubated with a biotinylated anti-mouse anti-rabbit primary antibody (Vector Laboratories: BA-1400) at a 1:100 dilution in blocking solution for one hour. The cells were then washed again in PBS to remove excess antibody. The next steps were undertaken in dark conditions to minimise bleaching of fluorophores. The final incubation was with fluorescently labelled avidin (Vector Laboratories: A-2001) at a 1:250 dilution and Texas Red Phalloidin (Invitrogen: T7471) at a 1:100 dilution in 10 mM HEPES, pH 7.5, 0.15 M NaCl buffer for two hours at room temperature. Avidin binds with high affinity to the biotin on the secondary antibody and enhances the signal while Texas Red Phalloidin binds to filamentous actin (F-Actin). The cells were subsequently washed four times with PBS, the plastic chamber gaskets were removed and the slides mounted using Vectashield containing DAPI (Vector Laboratories: H-1200) and a cover slip. The cover slip edges were sealed using clear nail varnish and slides were stored at 4 °C in the dark until ready to image.

3.4: Monolayer Disruption/Permeability Experiments

To assess the potential of the compounds to disrupt the vasculature, experiments were undertaken to quantify the level of monolayer disruption induced by exposure to a potential VDA. Studies of this type offer a reasonably accurate *in vitro* assessment of vascular disruption potential.

Cell culture inserts (Falcon: 353492) with a PET track etched membrane with pore size of 3 μm ($2.0 \pm 0.2 \times 10^5$ pores/cm^2) were coated with fibronectin (5 μg/mL) for a minimum of 30 minutes before plating. Cells were plated at 5.0×10^4 cells per insert in 200 μL EBM. Each insert was placed in a well of a 24-multiwell companion plate, notched for use with cell culture inserts (Falcon: 353504) and 700 μL of EBM was added to the lower well. To one insert 200 μL EBM were added but without cells. The cells were kept at 37 °C in a humidified incubator for 24 hours before the media were changed in both the well and insert The cells were then kept at 37 °C in a humidified incubator for a further 4 days.

In each experiment three inserts were used as vehicle controls and a fourth insert, which did not contain any cells, was also treated with vehicle. Four inserts were treated with CA4P in EBM at a relevant dose and four inserts were treated with a relevant dose of test drug in EBM. The cells were incubated at 37 °C in a humidified incubator for 30 minutes. The media were removed from the inserts followed by washing with PBS. The inserts were then placed into the wells of a new 24-multiwell plate (Falcon: 353504) and 700 μL of EBM was added to each well. 200 μL EBM containing FITC-dextran (0.8 mg/mL) (Sigma: 46945) was added to each insert and the cells were incubated at 37 °C in a humidified incubator for 30 minutes. The inserts were removed from the wells and discarded. 5 x 100 μL aliquots of each well were placed into wells of a 96-multiwell plate. The fluorescence was measured on a plate reader at excitation 488, emission 525. The raw emission reading from each well was transformed into % emission relative to the well without cells (E_{100}), which was normalised to 100% emission (equation 2). Where E_x is the emission of the wells treated by drug x. The perturbation of the monolayer was proportional to the emission for FITC-dextran that passed through the insert into the well.

$$\%emission_x = 100 - \left(\frac{E_x}{E_{100}}\right).100$$

Equation 2. Transformation of raw emission readings to percentage relative emission.

3.5: Analysis of Protein Expression/Phosphorylation by Western Blotting

In order to assess if the compounds were activating similar signalling pathway(s) as CA4P,[47] studies were undertaken to quantify changes in protein expression/phosphorylation by Western blotting.

Preparation of Samples

HUVECs were cultured on 12-multiwell plates, which were coated with 0.2% gelatin for a minimum of 30 minutes before plating. Cells were plated at 5 x 10^4 cells per well in 500 µl EBM and kept at 37 °C in a humidified incubator for 7 days without media change. Various concentrations of drugs were prepared in EBM *via* systematic dilutions from a 20 mM stock in DMSO. The cells were treated with the drug or vehicle control for 10 minutes at 37°C. The media were then discarded and the cells lysed with 1 x NuPAGE LDS reducing sample buffer (ThermoFisher: NP0008). The cell lysates were syringed with a 27 G needle 5-6 times and briefly spun down in a centrifuge to reduce bubbles. The samples were then heated at 70 °C for 10 minutes prior analysis by polyacrylamide gel electrophoresis and western blotting.

Electrophoresis of Protein Samples

Polyacrylamide gels were freshly prepared on the day of use in 1.5 mm disposable cassettes (Novex: NC2015). To form the resolving gel a 20 mL stock of 12% gel was prepared using 8 mL Protogel (National Diagnostics: A2-0072), 6.7 mL dH_2O, 5 mL resolving buffer (National Diagnostics: B9-0010), 100 µL 10% glycerol, 200 µL 10% ammonium persulfate (Sigma: A3678) and 10 µL *N,N,N',N'*-tetramethylethylenediamine (TMEDA), (Sigma: T7024). The solution was poured into the cassette until ~75% full and a thin layer of *iso*propanol was applied to the top of the gel to exclude oxygen and facilitate polymerisation and ensure that a flat layer was achieved. The gel was allowed to set for at least 30 minutes then rinsed with dH_2O. To form the stacking gel, a 10 mL stock of 4% gel was prepared using 1.3 mL Protogel 30% (which is a mixture of 37.5:1 acrylamide to bisacrylamide stabilised solution) (National Diagnostics EC-890) 6.1 mL dH_2O, 2.5 mL stacking buffer (Protogel: B9-0014), 50 µL 10% glycerol, 50 µL 10% ammonium persulfate and 10 µL TMEDA. The gel solution was poured into the cassette and a 10-well comb inserted to construct the wells. The gel was allowed to set for at least 30 minutes before the comb was removed and the wells washed with dH_2O. The cassette was then assembled into an XCell SureLock® Mini-Cell electrophoresis tank (Invitrogen)

The inner chamber of the electrophoresis tank was filled with Tris-Glycine-SDS PAGE buffer (National Diagnostics; EC-870) and the outer compartment part filled with the same buffer. Protein samples were loaded onto the gel into individual wells, 20 μL of sample per well. Protein quantification was not performed since the samples used in this study were of equivalent protein content as they were obtained from wells with a similar number of cells. One well was loaded with molecular weight markers (Bio Rad: 1610375). Electrophoresis was performed at 150 V (constant voltage) for ~80 minutes until the bromophenol blue dye in the samples reached the bottom of the cassette.

Electrophoretic Transfer of Proteins onto Nitrocellulose Membrane

Once the electrophoresis was judged to be complete, the cassette was then broken apart and the gel carefully cut to size and placed in transfer buffer (National Diagnostics; EC-880). The gel was then transferred onto a nitrocellulose membrane using the Trans-blot Turbo Transfer system (Bio-Rad Laboratories) on a preprogramed setting for 30 minutes at up to 25V and 1A.

Antibody Incubations

The membrane was washed with tris-buffered saline, 0.1% tween 20 (TBST) then blocked with 2.5% BSA in TBST for 30 – 120 minutes on a shaker at room temperature. The membrane was then incubated with a *p*MLC antibody 1:2000 (Cell Signaling: 3675) in TBST, 2.5% BSA overnight at 4^{o}C on a shaker. The antibody solution was removed and the membrane washed washed 4 x 5 minutes on a shaker. The membrane was then incubated with an anti–rabbit IgG antibody coupled to HRP (Dako: P0448) at a 1:2000 dilution for 60 minutes on a shaker. The membrane was washed with TBST for 15 minutes followed by a further 4 x 5 minute washes on a shaker.

ECL Detection

The next steps were conducted in the dark room under safelight conditions. Enhanced chemiluminescence reagents (ECL, Biological Industries: 20-500-500A and 20-500-500B) were mixed and the membrane drained of TBST. The ECL reagents were poured onto the surface of the membrane for 3 minutes. The reagents were then drained from the membrane and it was placed between two plastic sheets and bubbles removed. The membrane was placed in a film cassette and X-ray film placed over the membrane followed by several exposure for 0.5 – 10 minutes. The films were developed and fixed using Kodak developer and fixer (Sigma: P7042 and Sigma: P7167). After each film had dried, it was scanned and band densities were analysed using Image Studio Lite software.

Further Quantification

Membranes were reprobed for actin and GAPDH as housekeeping genes. The membrane was washed with TBST for 5 min then blocked with 2.5% BSA in TBST for 30 minutes on a shaker. The membrane was then incubated with a GAPDH antibody 1:5000 (Cell Signaling: 2118) and an actin 1:5000 antibody (Sigma: A5228) in blocking solution for 1 hour on a shaker. The antibody solution was removed and the membrane washed with TBST. The membrane was then washed 4 x 5 minutes on a shaker. The membrane was incubated with anti-mouse HRP (Dako: P0447) diluted1:2000 in TBST/2.5% BSA for 60 minutes on a shaker. The membrane was washed with TBST and exposed to ECL reagents as described above.

Because actin and GAPDH are very abundant proteins and the ECL signals are very strong, the ECL reagents were then allowed to decay for ~20 min before being exposed to film. The membrane was placed in a film cassette and ECL film placed over the membrane followed by exposure for 0.5 – 5 minutes. The film was developed and scanned as described above.

Chapter 4: Biological Evaluation of Sydnone Analogues

After the successful development of a robust methodology for the preparation of 3,4-diarylsydnones and its application to synthesis of a number of fused combretastatin analogues, attention was turned to the evaluation of the efficacy of the compounds. The biological evaluation of the analogues required the development of number of assays to provide reliable data on vascular disruptive potential. Before beginning assay development, a positive control for vascular disruption was required. Therefore, in order to fully evaluate the vascular disruptive properties of the compounds, CA4P was synthesised.

4.1: Preparation of CA4P

Initially, a route to intermediate alkyne **60** using the Ohira-Bestmann variant of the Seyferth-Gilbert reaction was proposed (*scheme 26*). Silyl ether **59** was readily prepared from 3-hydroxyl-4-methoxybenzaldehyde, *tert*-butyldimethylsilyl chloride (TBSCl) and Hünig's base (DIPEA) in 98% yield. However, attempts to convert **59** to **60** *via* this methodology, led to conversions of less than 50% in a number of reactions. Unfortunately, the use of 3,4,5-trimethoxybenzaldehyde produced similar results.

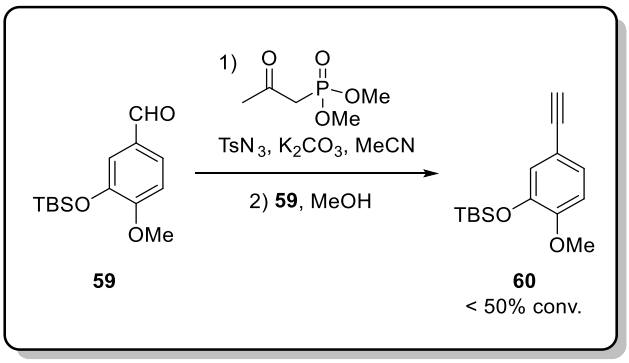

Scheme 26: Attempted preparation of 60 by Ohira-Bestmann reagent.

Employing an alternative strategy, alkyne **60** was prepared *via* Corey-Fuchs methodology. The reaction proceeded smoothly to yield **60**, in 79% yield, over two steps. Lara-Ochoa and co-worker have reported previously the copper-free Sonogashira coupling of the non-TBS-protected form of alkyne **60**, with 1-iodo-3,4,5-trimethoxybenzene in excellent yield.[72] Application of the reported conditions to **60** with 1-bromo-3,4,5-trimethoxybenzene resulted in the isolation of biaryl alkyne **61** in a yield of 95%. Conveniently, the silyl ether was cleaved under the reaction conditions to yield the free phenol. Conditions from the same authors described the selective reduction of alkyne **61** to CA4 with titanium(IV) tetra*iso*propoxide and *n*-butyl lithium (*n*BuLi). However, subjection of **61** to these conditions resulted in incomplete

conversion and an inseparable mixture of starting material and product. Deprotonation of the phenol with an extra equivalent of *n*BuLi, before addition of the titanium reagent and further *n*BuLi, resulted in complete conversion of the starting material and isolation of CA4 in 96% yield, >98:2 *Z*:*E*. The crude product was of high enough purity to be taken forward to the next step without further purification. CA4 was successfully phosphorylated with phosphorus oxychloride in dichloromethane. A "one pot" protocol, in which the ion exchange resin was added to the crude isolated phosphate monoester in water, resulted in product isolation in an 87% yield after recrystallisation from acetone. The purity of the product by HPLC was determined to be >99%. Therefore, CA4P was successfully synthesised in gram quantities, in a 63% yield over 6 steps (*scheme 27*).

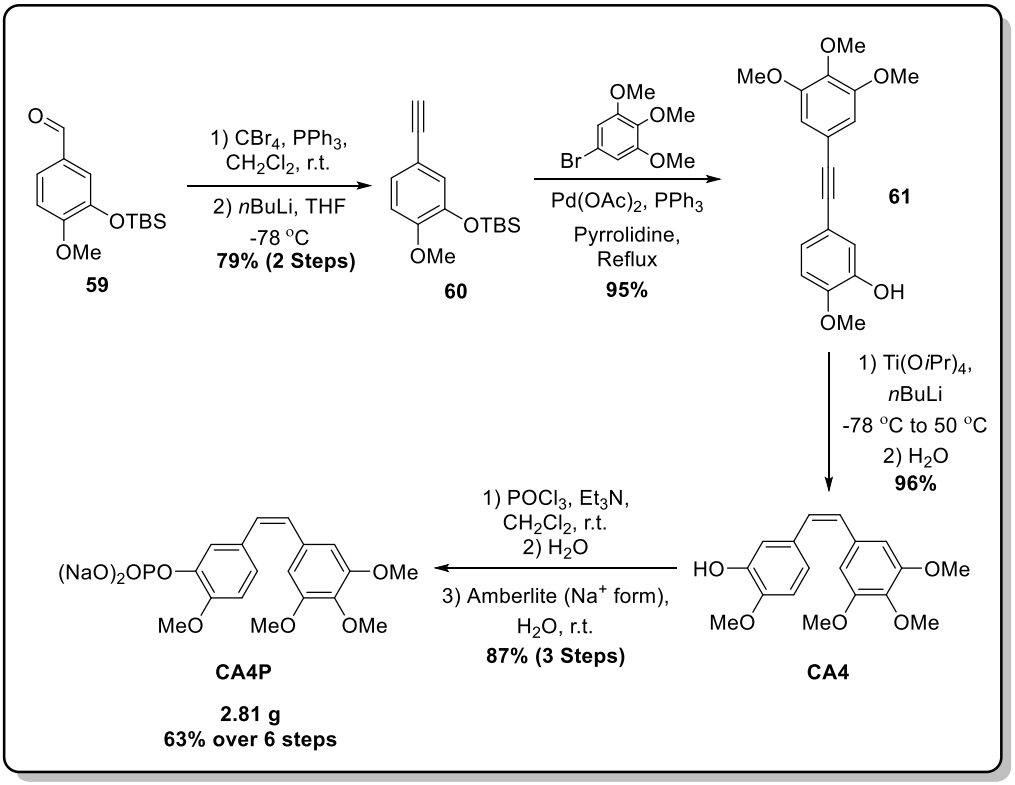

Scheme 27: Synthesis of CA4P.

4.2: Cell Proliferation Studies

Although a significant number of combretastatin analogues have been prepared over the years, a general method for assessing their efficacy is yet to be developed. A large number of reports focus on the direct activity of the compounds against cancerous cells.[64] Tozer and Kanthou *et al.* have previously shown that for CA4P vascular disruptive effects dominate, not direct targeting of cancerous cells.[63] Therefore, assays involving direct action on cancerous cells do not provide accurate data on the vascular disruptive capabilities of a compound. It was proposed that the primary target of VDAs, endothelial cells would provide a better insight into the activity of the compounds. The effect of vascular disrupting agents on the microtubule cytoskeleton and subsequent changes in endothelial cell morphology are thought to be integral to VDA therapeutic efficacy.[30,28] Therefore, human umbilical vein endothelial cells (HUVECs) were selected as the cell line for study, as they most closely resembled human blood vessels in culture. For the initial evaluation of the potential activity of the novel compounds, a rapid screening procedure was required. A convenient method for the assessment of activity was to study the effect that the compounds had on cell proliferation. Studies on proliferation were not necessarily the best probe of vascular disruptive potential - vascular disruption is effective on a much shorter time scale. However, they were useful as a blanket test of the effects of the compounds on cells, particularly of potential anti-mitotic effects. Crudely, it was assumed that the larger the effect a drug had on proliferation, the more potent its efficacy at targeting tubulin.

HUVECs were plated on 96 well plates and allowed to adhere for 24 hours. The cells were then treated with various concentrations of compound and incubated for 72 hours. A minimum of eight mechanical repeats were used for each concentration of drug. The cells were then fixed and stained with crystal violet solution, a marker for viable cells. The cells were lysed with acetic acid that released the dye into solution and the absorption at 590 nm was quantified. The absorption at 590 nm was proportional to the number of cells that survived treatment. By using a range of drug concentrations, it was possible to plot a growth curve and to calculate a GI_{50} value.

Initial screens provided some interesting insights into the relative activities of the compounds. Several *N*-(3,4,5-trimethoxyphenyl) (TMP) compounds had either low activity or were completely inactive in the assay (*table 9 entries 1-8*). However, only compounds containing the 3,4,5-trimethoxyphenyl moiety demonstrated interesting levels of activity (*entries 9-11 and entry 13*). Compounds without this unit demonstrated little or no activity (*entries 14-20*). Some interesting patterns were observed. For example, **26** was found to be

over one hundred times more potent than its structural isomer **22** (*entry 13 vs 1*) (*figure 15, A*). Similarly, direct CA4 analogue **58** exhibited a ten-fold increase in potency relative to its isomer **21** (*entry 11 vs 10*) (*figure 15, B*). This indicated that incorporation of the 3,4,5-trimethoxyphenyl group on the *C*4 position afforded the most potent compounds. This trend was further supported by 4-ethoxyphenyl analogues, with **32** exhibiting higher potency than **30** (*entry 12 vs 7*). These analogues were relatively inactive, which was in contrast to the findings of Romagnoli and Viola *et al.* who found the combination of a 4-ethoxyphenyl ring and TMP ring to be particularly potent.[80] Although not entirely unexpected, it was interesting to note that incorporation of a *meta*-hydroxyl group on the B ring did increase activity (*entry 10 vs 1 and 11 vs 13*) (*figure 15, C*). This finding is in contrast to the reports of Cushman and Hamel *et al.* who, in the case of stilbene analogues, reported that the *meta*-hydroxyl group was not necessary for activity.[68] Finally, the analogue of the Sanofi compound AVE 8062, **56**, exhibited slightly higher activity than the relevant CA4 analogue, **21** (*entry 9 vs 10*) (*figure 15, D*). To aid further investigations, the phosphate salt of the most active compound **58** was prepared using phosphorus oxychloride and ion exchange resin (**62**). In the screens it performed similarly to the parent compound (*entry 23 vs 11*). The slightly lower activity observed was likely due to the presence of small quantities of trisodium phosphate in the sample.

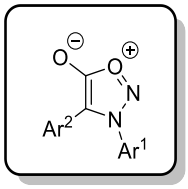

Entry	Ar^1	Ar^2	Compound	GI_{50}/μM
1	3,4,5-$MeOC_6H_2$	4-$MeOC_6H_4$	**22**	>20
2	3,4,5-$MeOC_6H_2$	2-$MeOC_6H_4$	**29**	>20
3	3,4,5-$MeOC_6H_2$	Ph	**24**	>20
4	3,4,5-$MeOC_6H_2$	4-MeC_6H_4	**34**	>20
5	3,4,5-$MeOC_6H_2$	3-$NO_2C_6H_4$	**53**	>20
6	3,4,5-$MeOC_6H_2$	2-Thiophenyl	**54**	>20
7	3,4,5-$MeOC_6H_2$	4-$EtOC_6H_4$	**30**	>4
8	3,4,5-$MeOC_6H_2$	2-ClC_6H_4	**55**	>20
9	3,4,5-$MeOC_6H_2$	3-H_2N-4-$MeOC_6H_3$	**56**	0.315
10	3,4,5-$MeOC_6H_2$	3-HO-4-$MeOC_6H_3$	**21**	0.526
11	3-HO-4-$MeOC_6H_3$	3,4,5-$MeOC_6H_2$	**58**	0.041
12	4-$EtOC_6H_4$	3,4,5-$MeOC_6H_2$	**32**	>1.5
13	4-$MeOC_6H_4$	3,4,5-$MeOC_6H_2$	**26**	0.336
14	4-$MeOC_6H_4$	4-$MeOC_6H_4$	**28**	>20
15	4-$MeOC_6H_4$	Ph	**27**	>2
16	4-$MeOC_6H_4$	2-Thiophenyl	**51**	>20
17	4-$MeOC_6H_4$	2-ClC_6H_4	**47**	>5
18	4-$MeOC_6H_4$	3-$NO_2C_6H_4$	**46**	>13
19	4-$EtOC_6H_4$	4-MeC_6H_4	**35**	>20
20	Ph	4-MeC_6H_4	**37**	>20
21	-	-	**CA4P**	0.008
22	-	-	**Colchicine**	0.025
23	3-[$(NaO)_2OPO$]-4-$MeOC_6H_3$	3,4,5-$MeOC_6H_2$	**62**	0.051

Table 9: Values for Growth Inhibition of HUVECs by Sydnone Analogues vs. CA4P and Colchicine.

Although a number of compounds demonstrated relatively potent effects, CA4P outperformed all sydnone analogues in the assay (*entry 21 vs 1-20*). Colchicine was also more potent (*entry 22*), but is unsuitable for use as a vascular disrupting agent. It was therefore

concluded that compounds demonstrating low nanomolar activity in the initial screening warranted further investigation.

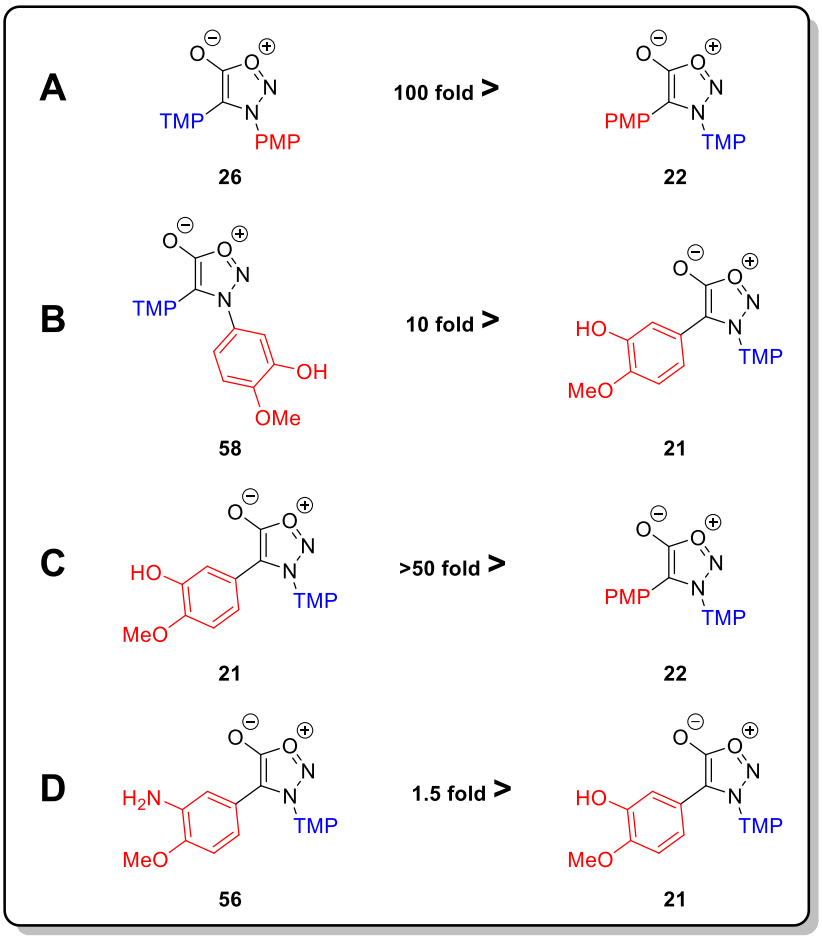

Figure 15: Key analogue comparisons.

4.3: Studies of Effects on the Cytoskeleton by Immunofluorescence

To confirm that the drug effects were microtubule-specific, drug-induced changes in the endothelial cell cytoskeleton and morphology were studied *via* immunofluorescence. The microtubule disruption associated with CA4 treatment is also accompanied by changes in cell shape and morphology brought about by the rapid remodelling of the actin cytoskeleton.[47] Therefore, endothelial cells in culture were stained for actin filaments using phalloidin and microtubules using an antibody to β–tubulin. The cells were treated with various concentrations of drug for 30 – 90 minutes before fixation, staining and imaging.

As a positive control, a limited dose response to a 30 minute CA4P treatment was conducted. During the interphase, polymers of α–tubulin and β-tubulin originate from the centrosome and radiate to the edge of the cell as tubular filaments, microtubules (*figure 16, A*). Along with actin and other cytoskeletal partners, microtubules control many cellular functions including; mitosis and cellular motility.[142] During the interphase, actin is mostly pericellular (*figure 16, B*). Upon treatment with 500 nM CA4P for 30 minutes, interphase microtubules became disrupted (*figure 16, C*) leading to changes in cell morphology. Disruption of microtubules led to the formation of actin stress fibres across the cells (*figure 16, D*). Halving the concentration to 250 nM resulted in similar effects to the higher dosage (*figure 16, E and F*). Lowering the concentration further to 100 nM resulted in less disruption of microtubules, with a higher proportion of intact microtubules visible (*figure 16, G*). Changes in cell morphology remained apparent and so did actin stress fibres (*figure 16, H*). A treatment of 50 nM CA4P had a much reduced effect on the cells, with a high proportion of microtubules remaining clearly intact (*chapter 5*). In comparison to the initial screens conducted, significantly higher concentrations of drug were required to observe effects in the immunofluorescence assays. This difference likely stemmed from the shorter timescale of these assays (30 min vs 72 h). It is therefore unsurprising that higher doses were required.

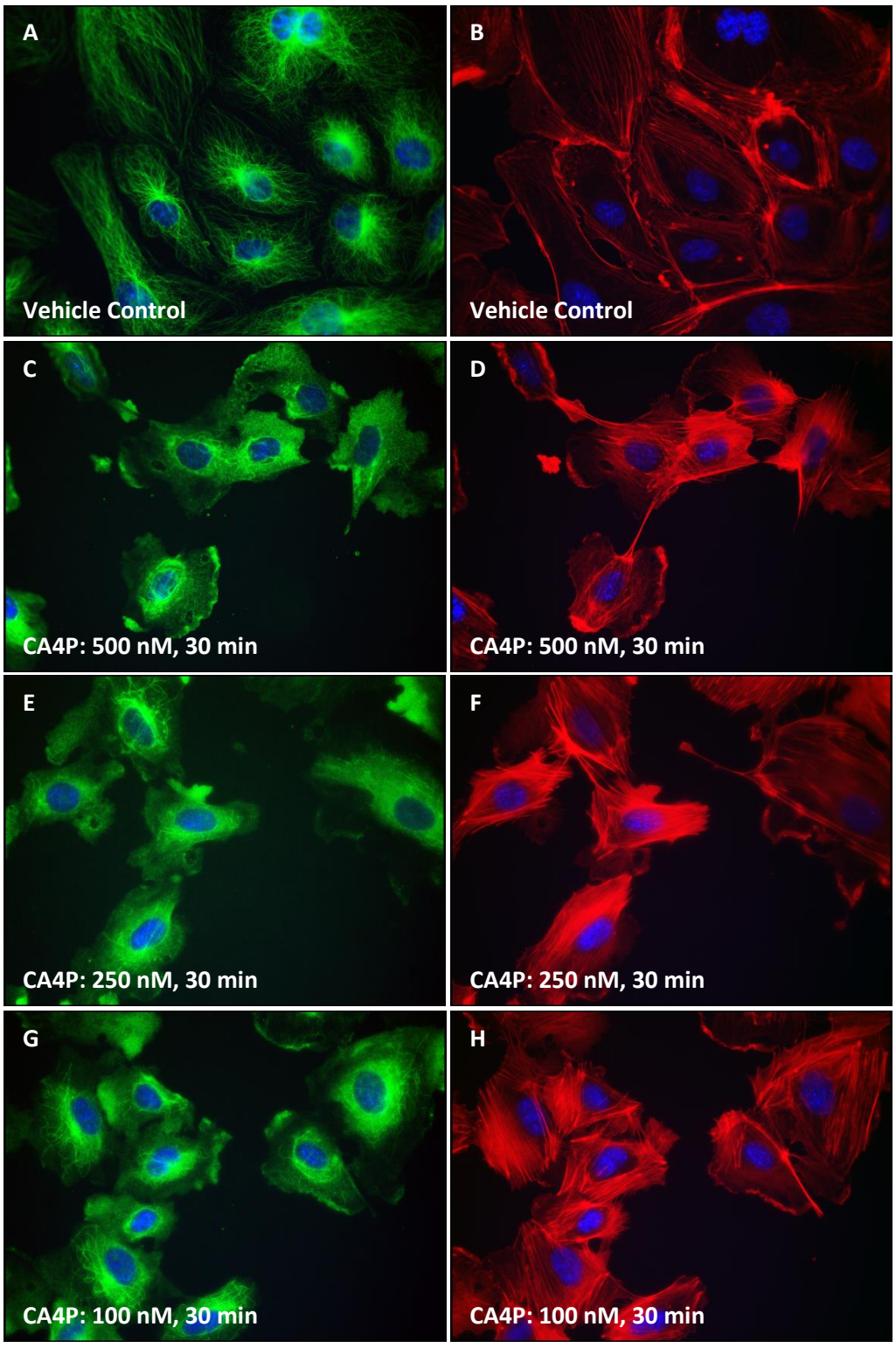

Figure 16: Effects of CA4P on HUVEC cytoskeletal structures. Cells were treated with a single dose of either vehicle (A, B), 500 nM CA4P (C, D), 250 nM CA4P (E, F) or 100 nM CA4P (G, H). Drug treatments were for 30 min. Cells were fixed and stained with an antibody to β-tubulin (A, C, E, G) and F-actin (B, D, F, H).

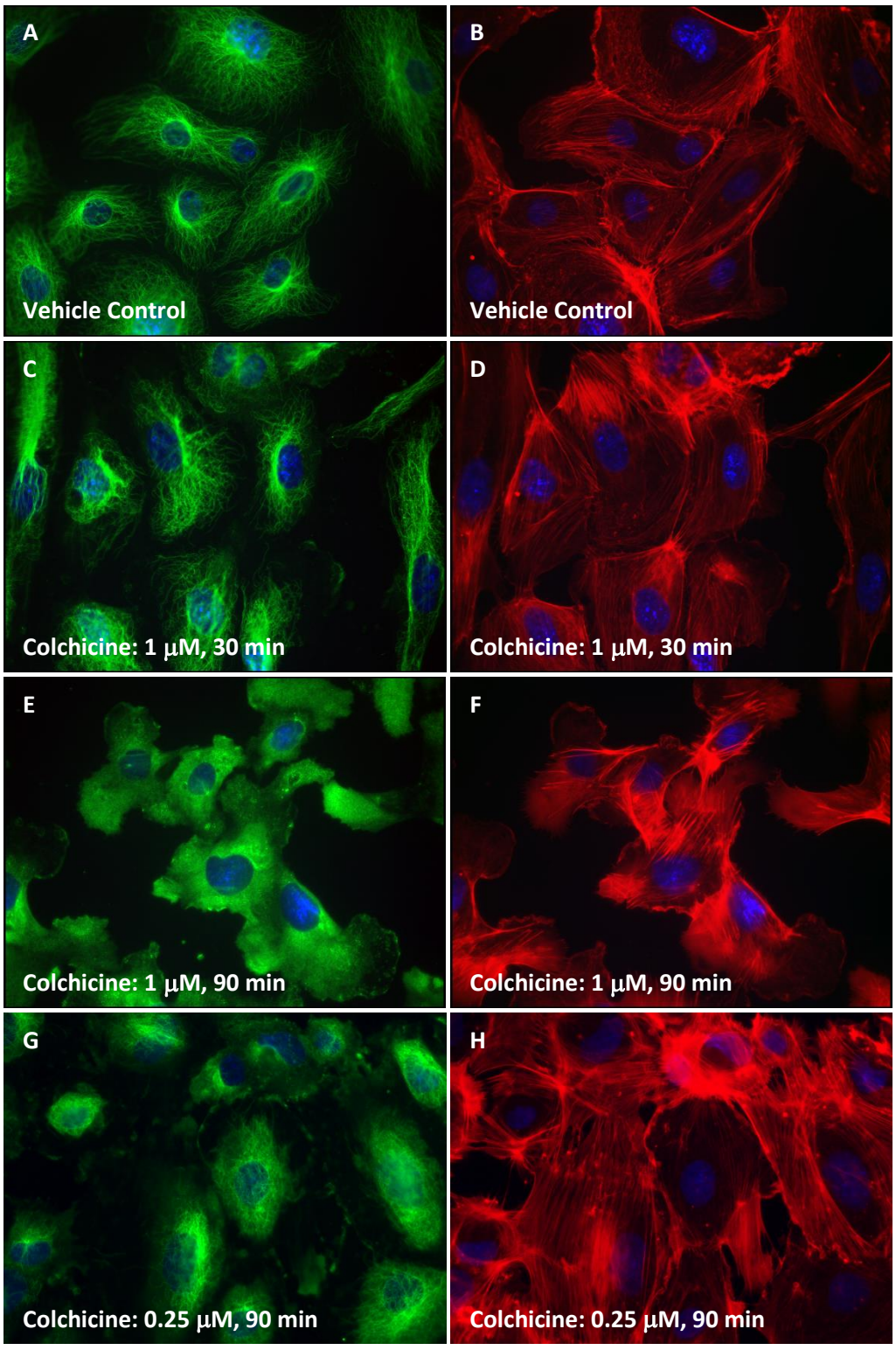

Figure 17: Effect of colchicine on cytoskeletal structures. Effects of colchicine on HUVEC cytoskeletal structures. Cells were treated with a single dose of either vehicle (A, B), 1 μM colchicine (C, D, E, F), 250 nM colchicine (G, H). Drug treatments were for 30 min (C, D) and 90 min (E, F, G, H). Cells were fixed and stained with an antibody to β-tubulin (A, C, E, G) and F-actin (B, D, F, H).

A further positive control was conducted with colchicine. Interestingly, colchicine appeared to be slower in action than CA4P. After a 30 minute treatment at 1 μM only a slight contraction of the cells was observed, with microtubules remaining intact (*figure 17, C and D*). A longer treatment time of 90 minutes yielded results that more closely resembled at 30 minute treatment with CA4P. Microtubules were disrupted and actin stress fibres were formed across the cells (*figure 17, E and F*). A lower dose of 250 nM for 90 minutes resulted in minor changes to cellular morphology and many microtubules remained intact (*figure 17, G and H*). These data indicated that colchicine was both less active and slower acting than CA4P. This could be indicative of a different mode of action.

Immunofluorescence studies focussed on five compounds; **22**, **26**, **21**, **58** and **56** (*figure 18*). All but **22** represented the most active compounds in the initial assay. **22** was used to assess whether a poor initial assay results were representative of minimal effects on cells. HUVECs were treated with each compound and incubated for thirty minutes prior to fixation. All fluorescence experiments were performed with both, vehicle treated and CA4P treated controls.

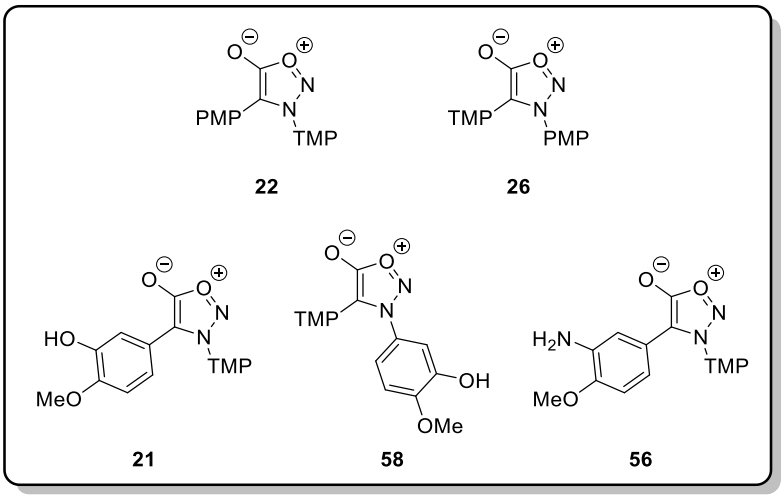

Figure 18: Sydnone analogues examined in immunofluorescence studies.

The first compound tested was **22**. As expected the compound showed negligible microtubule depolymerisation activity at a high dosage 10 μM (*figure 19, A*). The actin cytoskeleton also appeared intact and actin stress fibre formation was not evident (*figure 19, B*). This result provided evidence that compounds deemed inactive in the initial screens were indeed ineffective at inducing endothelial cell morphological changes.

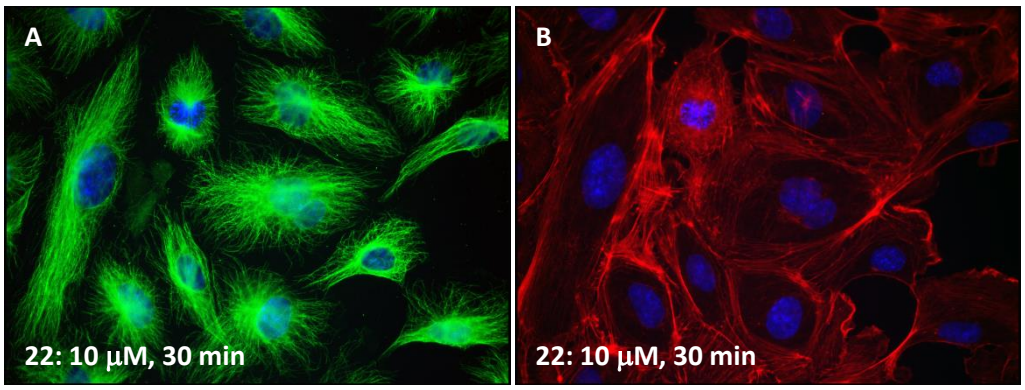

Figure 19: Effect of **22** on HUVEC cytoskeletal structures. Cells were treated with a single dose of 10 μM **22** (A, B). Drug treatments were for 30 min. Cells were fixed and stained with an antibody to β-tubulin (A) and F-actin (B).

Attention was then turned to the more active, structural isomer of **22**, **26**. In concurrence with the data from proliferation experiments, **26** was a much more effective drug. At 5 μM, **26** caused major disruption of the endothelial cell microtubules and instigated significant changes in the cell morphology and the formation of actin stress fibres (*figure 20, C and D*). However, lowering the concentration to 1 μM only resulted in the contraction of the cells, with evidence of only minor microtubule disruption (*figure 20, E and F*). These data provided further evidence of the gulf in activity between **26** and CA4P (336 nM vs 8 nM in initial screens).

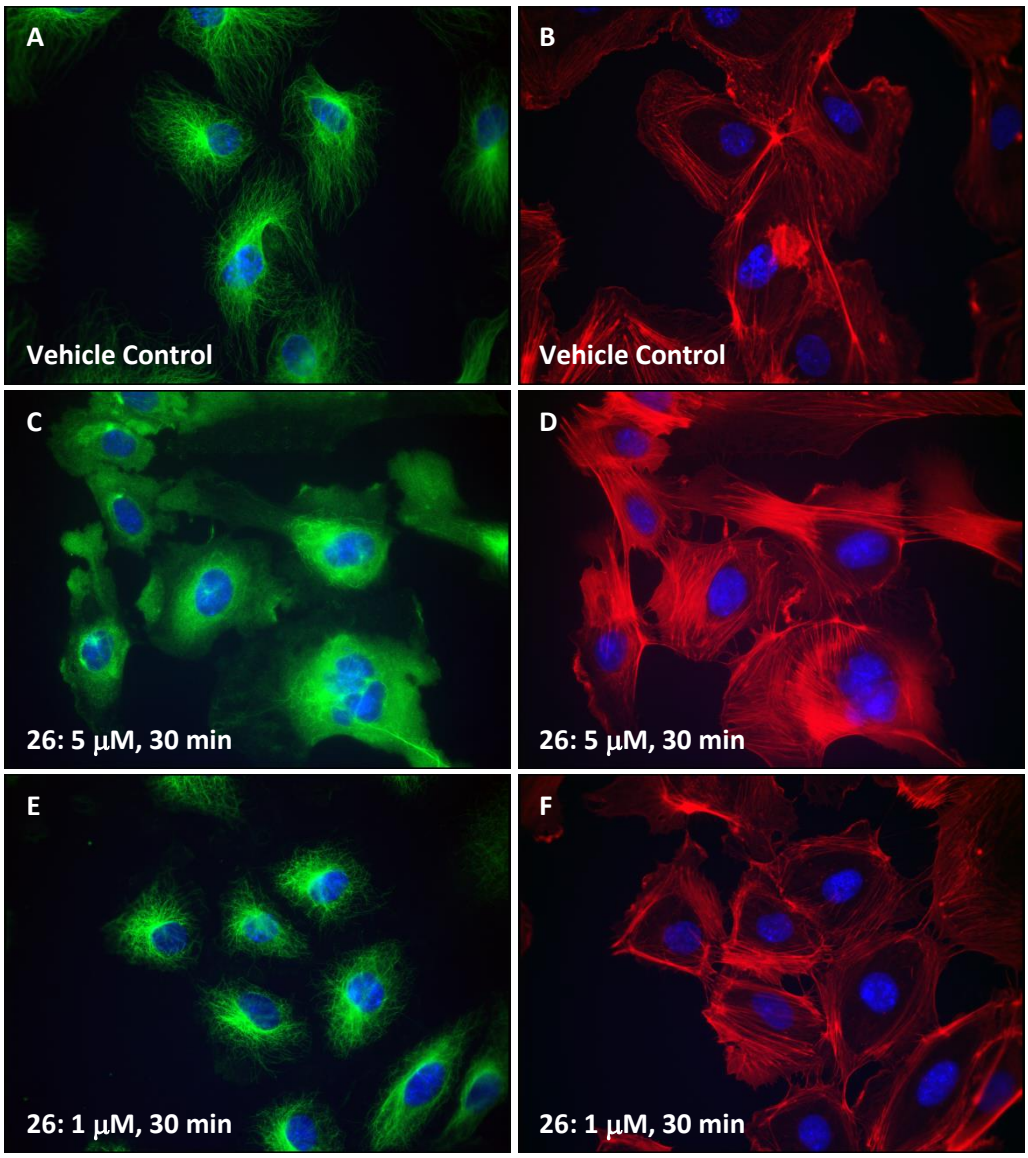

Figure 20: Effect of **26** on HUVEC cytoskeletal structures. Cells were treated with a single dose of either vehicle (A, B), 5 μM **26** (C, D) or 1 μM **26** (E, F). Drug treatments were for 30 min. Cells were fixed and stained with an antibody to β-tubulin (A, C, E) and F-actin (B, D, F).

Next, direct CA4 analogues, **21** and **58** were analysed. **21** was significantly less active than CA4P in initial screens (526 nM vs 8 nM) and this was echoed in the immunofluorescence assays. The result indicated that activity required a careful choice of bridging unit between the rings was required and when compared to **58**, the positioning of the rings on the linker was also important. At 5 μM, **21** initiated changes in cell morphology and the disruption of microtubules (*figure 21, C*). There was also the formation of actin stress fibres across the cells (*figure 21, D*). However there was also evidence of a number of microtubules remaining intact. Lowering the treatment to 1 μM only resulted in a slight contraction of the cells (*figure 21, E and F*).

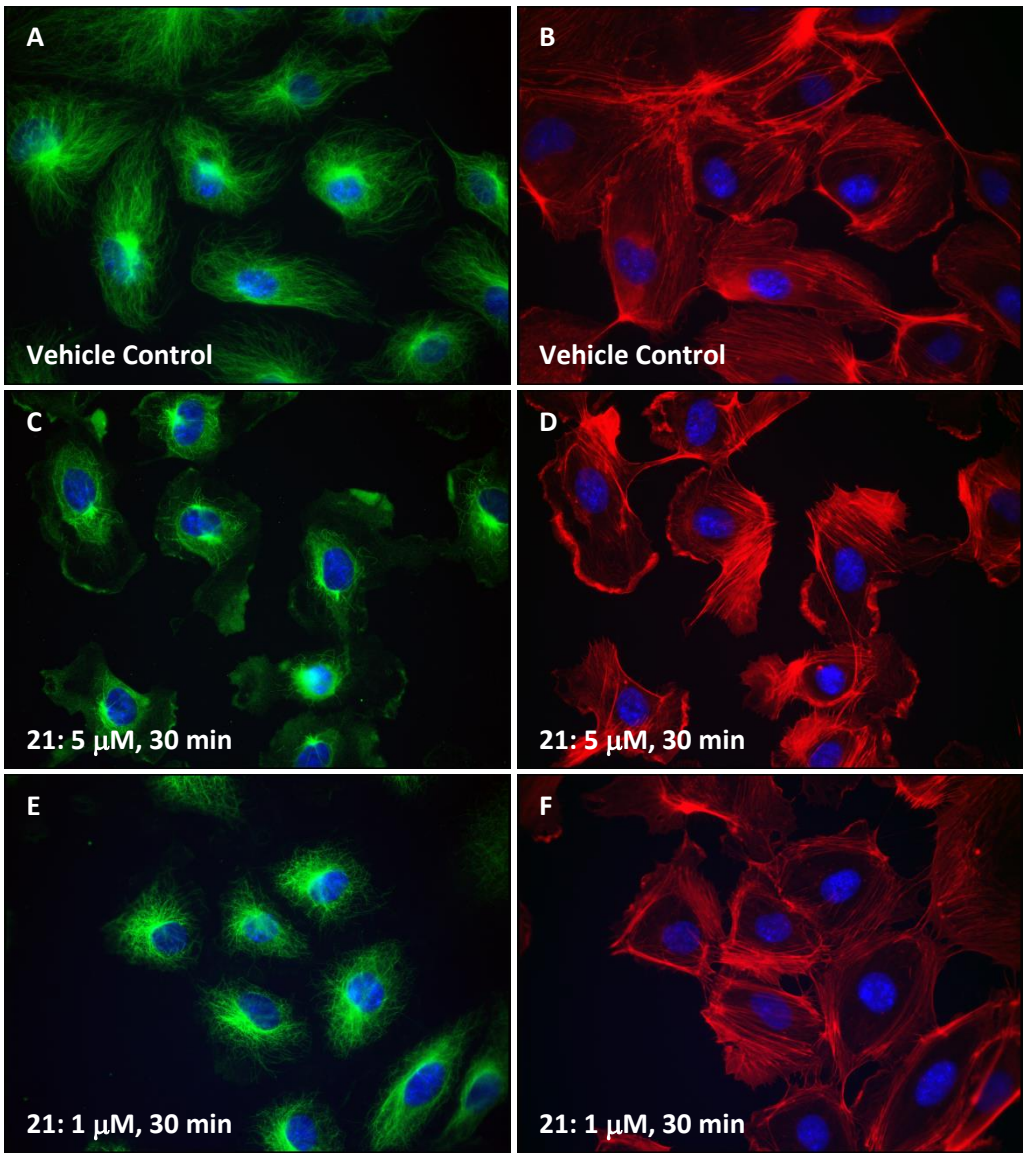

Figure 21: Effect of **21** on HUVEC cytoskeletal structures. Cells were treated with a single dose of either vehicle (A, B), 5 μM **21** (C, D) or 1 μM **21** (E, F). Drug treatments were for 30 min. Cells were fixed and stained with an antibody to β-tubulin (A, C, E) and F-actin (B, D, F).

58 was the most active analogue in the initial screens, it was hoped that this activity would be maintained in further screens. Satisfyingly, at 1 μM, **58** instigated similar levels of microtubule disruption and morphological changes to CA4P at the same concentration (*figure 22, C*). There was also clear formation of actin stress fibres (*figure 22, D*). These data were pleasing as they indicated that **58** was acting in a similar manner to CA4P, rather than colchicine. Reduction of the treatment concentration by a factor of two, to 500 nM, appeared similar to a 1 μM treatment (*figure 22, E and F*). A further halving of concentration to 250 nM resulted in changes in cellular morphology as well as actin stress fibre formation (*figure 22, G and H*). However, there was evidence of a number of microtubules avoiding disruption (*figure 22, G*). The level of disruption to microtubules was less significant than for CA4P at

the same concentration. Therefore, although **58** was less active than CA4P at 250 nM, they were both more effective at 500 nM and appeared to be equally active at this concentration. What's more, even as a greater number of microtubules remained intact, the changes in cell morphology continued to be quite profound. Therefore, it is possible that microtubules need not be fully disrupted for vascular disruption to occur *in vivo*.

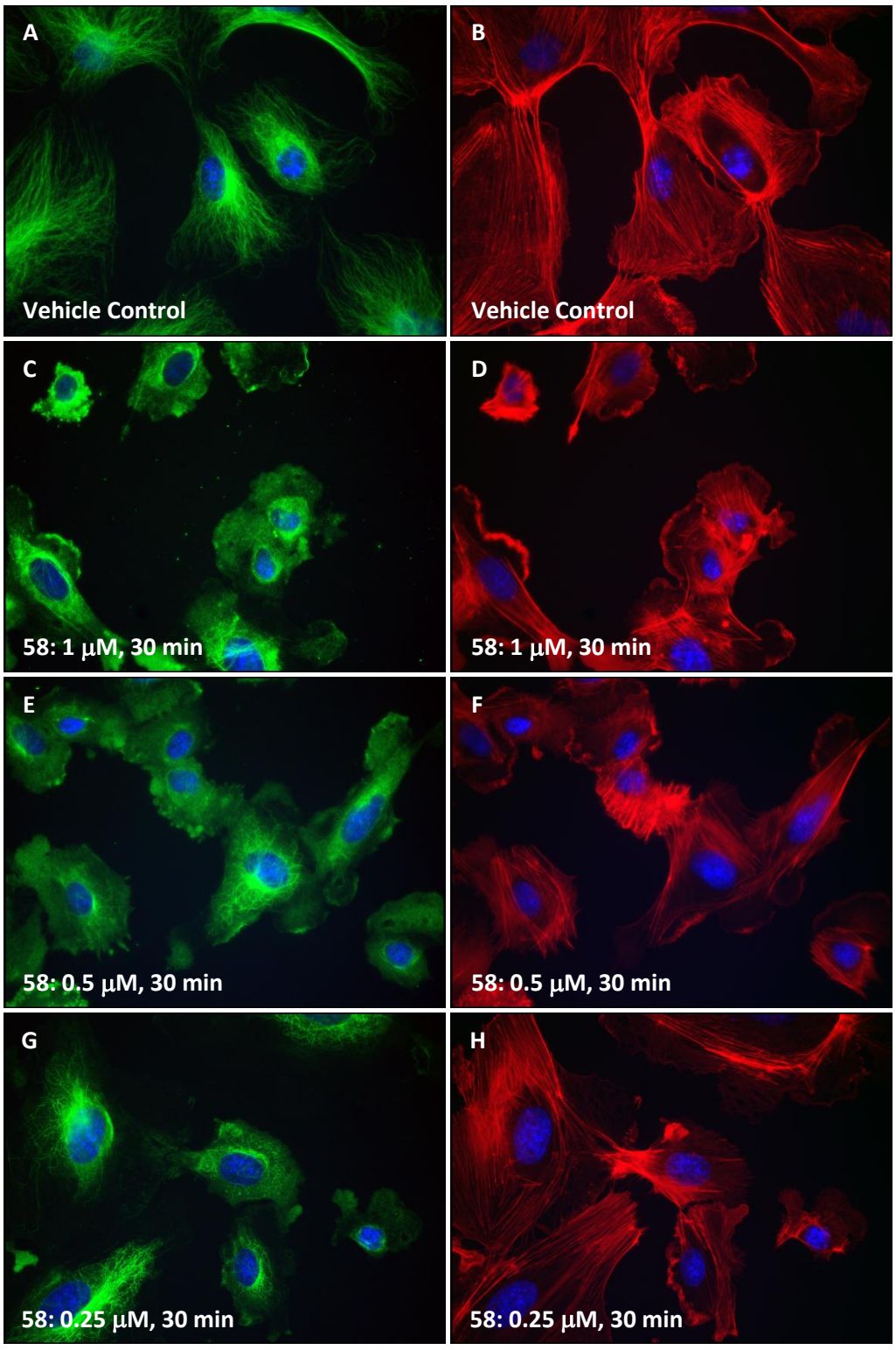

Figure 22: Effect of **58** on HUVEC cytoskeletal structures. Cells were treated with a single dose of either vehicle (A, B), 1 μM **58** (C, D), 500 nM **58** (E, F) or 250 nM **58** (G, H). Drug treatments were for 30 min. Cells were fixed and stained with an antibody to β-tubulin (A, C, E, G) and F-actin (B, D, F, H).

The final compound tested was **56**, a direct analogue of the Sanofi Aventis compound AVE 8062. The compound disrupted microtubules at a 5 μM dose and led to the formation of actin

stress fibres (*figure 23, A and B*). Similarly to **26**, which had a near identical GI_{50} to **56** in proliferation experiments (336 nM vs 315 nM), activity was severely diminished at a 1 μM treatment (*figure 23, C and D*). This result was particularly promising as **56** had the second highest activity of the compounds tested. In theory, **56** should also be the less active isomer. It is logical to assume that structural isomer **63**, with the 3,4,5-trimethoxyphenyl ring located on the sydnone *C*4 position (*figure 24*), should be more active according to early SAR data. Indeed, it can be inferred that because **56** was more active than **21**, **63** should be more active than **58**. Therefore, the preparation of **63** would be a logical starting point for future investigations in this area.

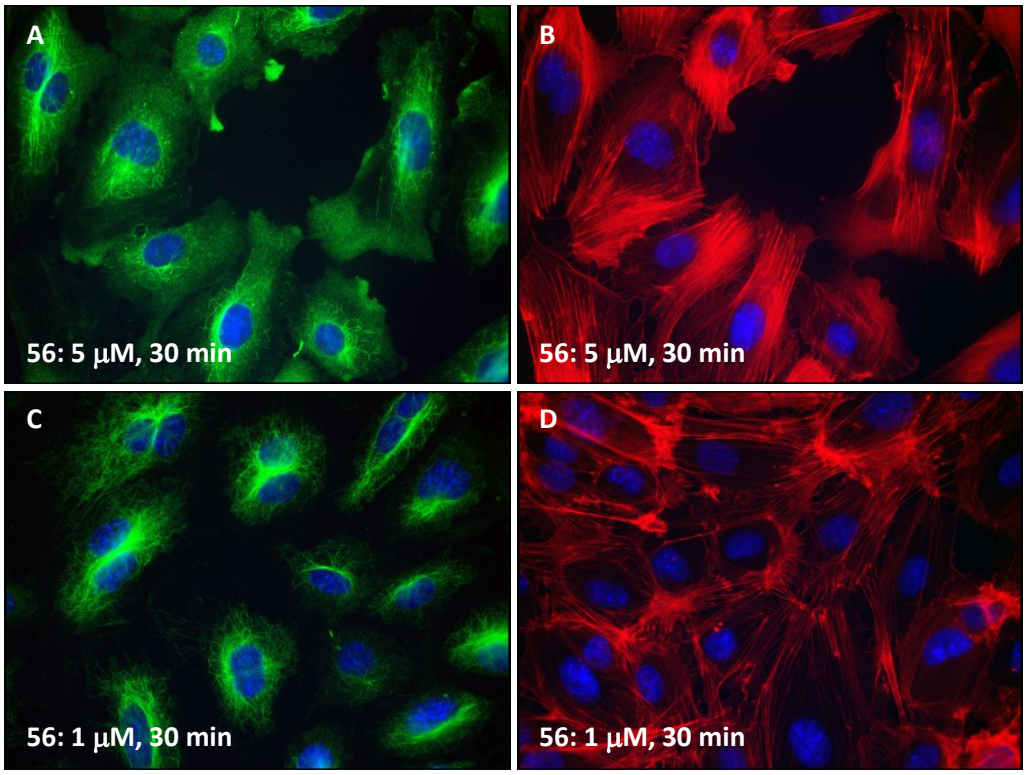

Figure 23: Effect of **56** on cytoskeletal structures. Cells were treated with a single dose of either 5 μM **56** (A, B) or 1 μM **56** (C, D). Drug treatments were for 30 min. Cells were fixed and stained with an antibody to β-tubulin (A, C) and F-actin (B, D).

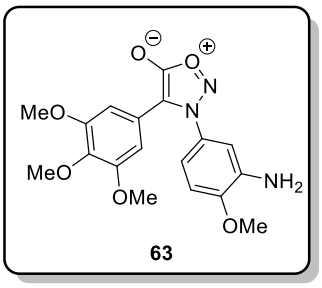

Figure 24: Priority target for 2nd generation compounds.

4.4: Studies on the Recovery of Cytoskeletal Structures after Drug Removal by Immunofluorescence

CA4P is thought to be a potent VDA at well below its maximum tolerated dose due to the reversibility of it's binding to tubulin.[143] Conversely, the high toxicity of colchicine is thought to be due to its pseudo-irreversible binding.[61] Therefore, an experiment was designed to probe these hypotheses and in turn determine whether **58** exhibited similar properties to CA4P or colchicine. The aim of the experiment was to test the reversibility of binding to tubulin using immunofluorescence. In theory, if the binding of a compound were reversible, then removing the drug from the cells after treatment and subsequent incubation would lead to recovery of the cells. The experiments were conducted in 8-well chamber slides as depicted in figure 25. Each experiment was conducted with an untreated control (A1/A2), a 30 minute drug treatment (B1/B2) and a treatment of 90 minutes – the full duration of the experiment (C1/C2). The final wells on the slide (D1/D2) were treated for 30 minutes before being washed three times with media. The cells were then incubated for 30 minutes before further washing with media and a further 30 minutes incubation. Both CA4P and colchicine were used a positive controls in the experiments.

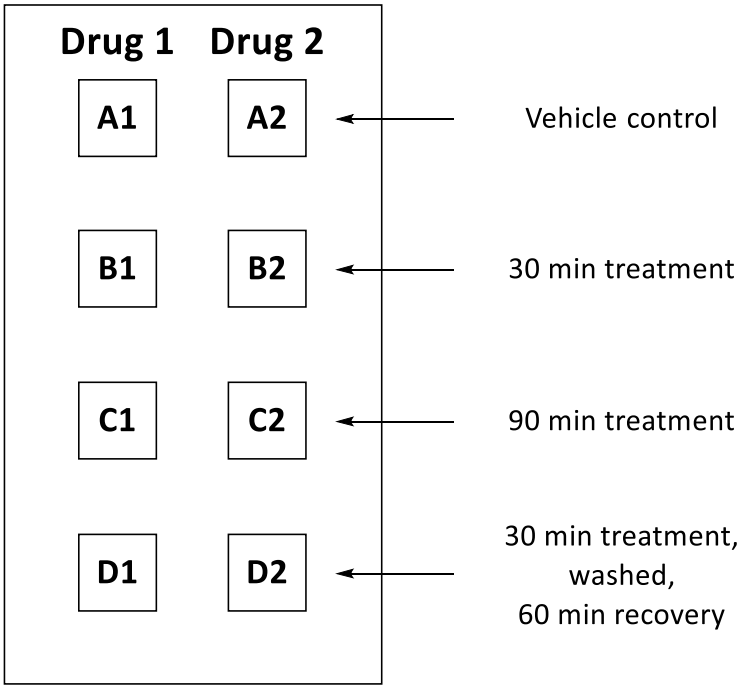

Figure 25: Typical experimental set up.

A ninety minute treatment (the duration of the experiment) of 1 μM CA4P resulted in microtubule disruption and changes in cell morphology (*figure 26, C and D*). In concurrence with the earlier treatment experiments (*vide infra*), a ninety minute treatment with 1 μM

colchicine resulted in disruption of the endothelial cell microtubules and had a profound effect on cellular morphology (*figure 26, E and F*). Similar results were observed for a ninety minute treatment with 1 μM **58** (*figure 26, G and H*). These data provided evidence that the effects lasted for the duration of the experiments.

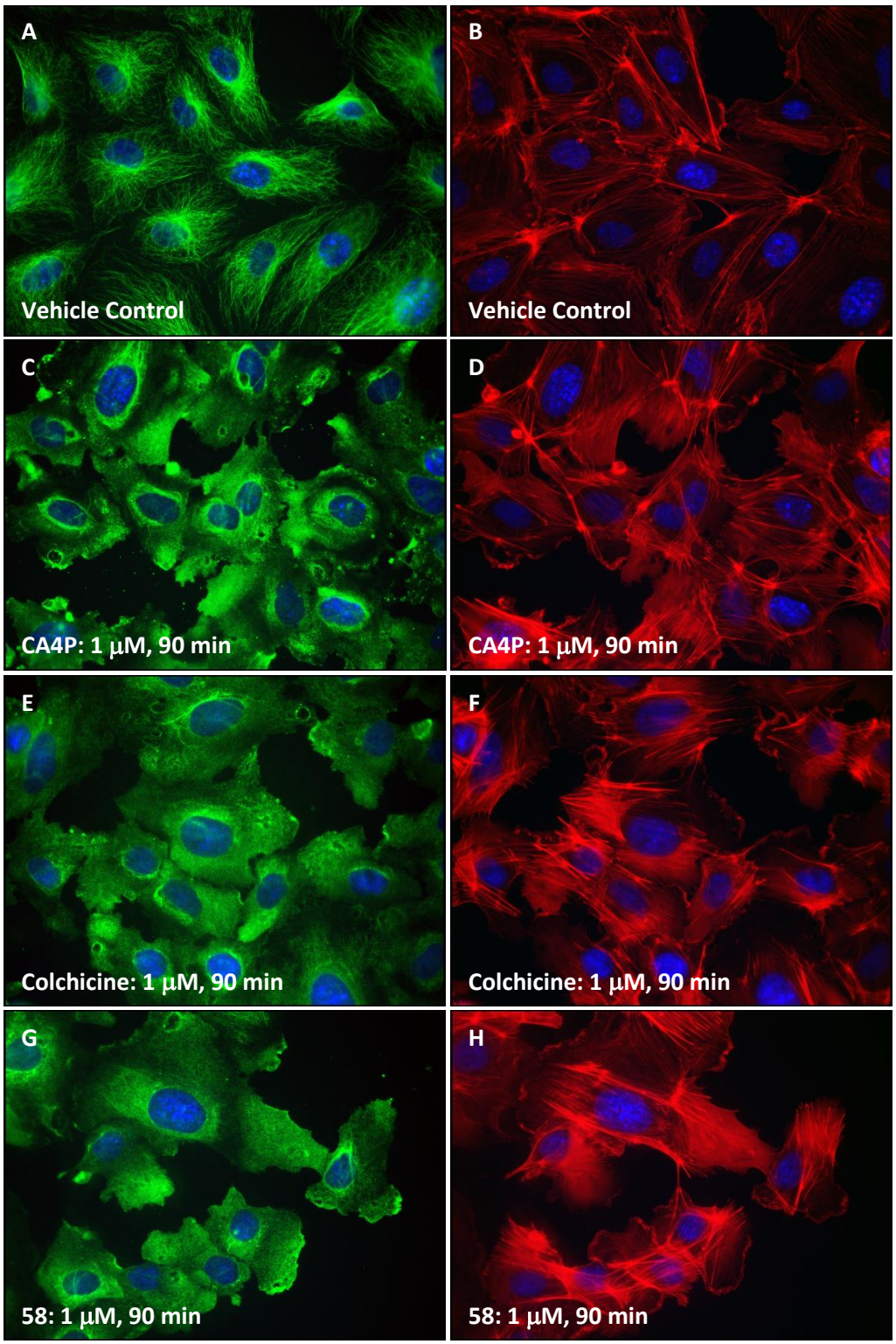

Figure 26: Cytoskeletal effects after 90 minute drug incubation. Cells were treated with a single dose of either vehicle control (A, B), 1 μM CA4P (C, D), 1 μM colchicine (E, F) or 1 μM **58** (G, H). Drug treatments were for 90 min. Cells were fixed and stained with an antibody to β-tubulin (A, C, E, G) and F-actin (B, D, F, H).

Pleasingly, cells which were washed and allowed sixty minutes incubation following a thirty minute treatment with CA4P showed significant signs of recovery. Microtubules were no

longer disrupted (*figure 27, A*) and actin stress fibres were reduced (*figure 27, B*). This was a clear indication that the binding of CA4P was indeed reversible. A particularly important finding was that a thirty minute treatment with 1 μM colchicine, followed by removal of the drug and sixty minutes recovery time led to results that resembled those of a ninety minute treatment (*figure 27, C and D*). These data had two implications; firstly, that the binding of colchicine was indeed pseudo-irreversible and secondly that its action was slower than that of CA4P. It is also interesting to note that this slower action was not due to a decreased rate of diffusion through the cell membrane. If it were the case, removal of the drug after thirty minutes would prevent microtubule disruption (*vide infra*).

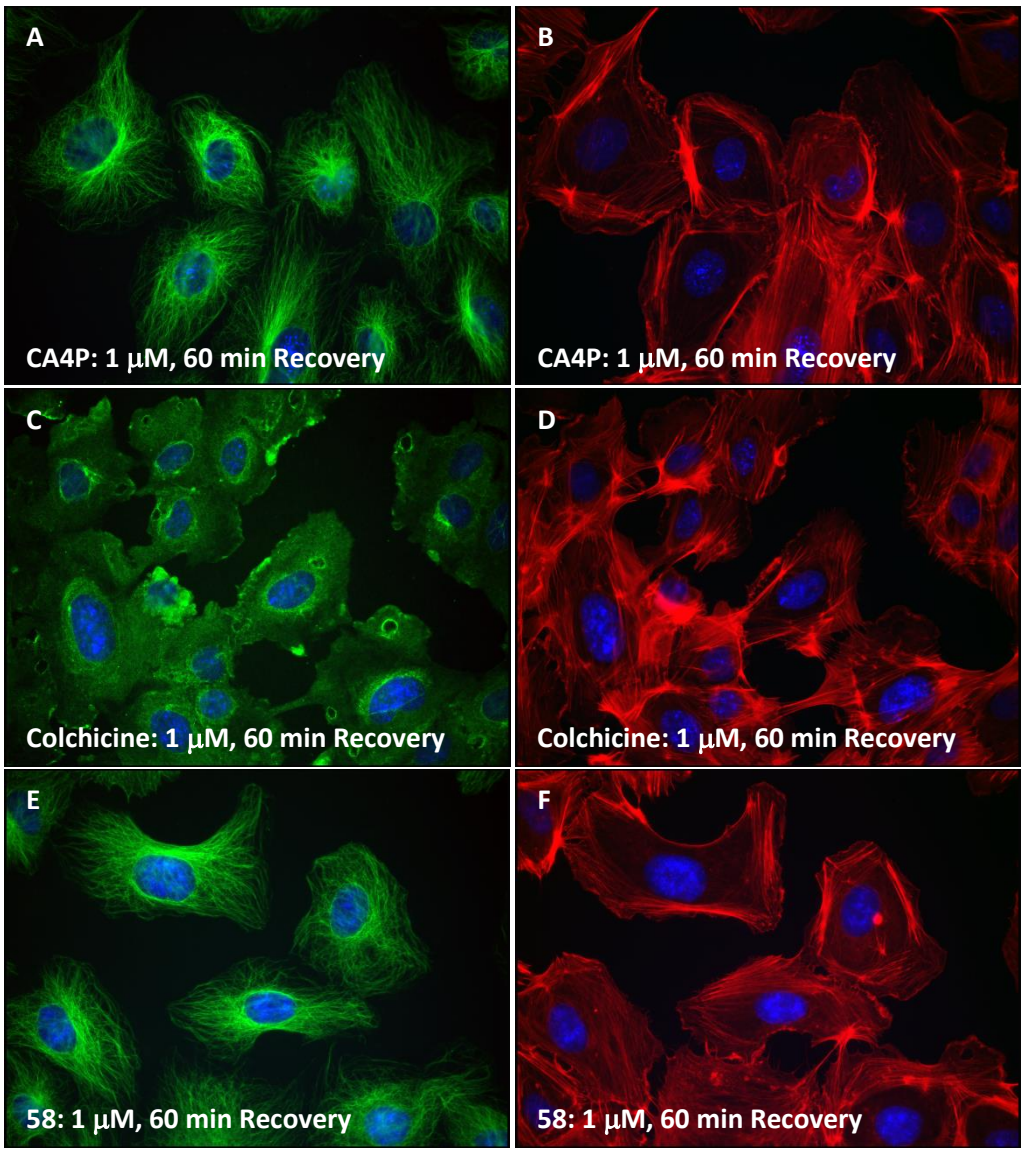

Figure 27: Recovery of cytoskeletal structures after drug removal. Cells were treated with a single dose of either 1 μM CA4P (A, B), 1 μM colchicine (C, D) or 1 μM **58** (E, F). Drug treatments were for 30 min. Cells were then washed with PBS (3x) and allowed to recover for 60 min. Cells were fixed and stained with an antibody to β-tubulin (A, C, E) and F-actin (B, D, F).

After demonstrating that there was a clear difference in the kinetics of binding for CA4P and colchicine, **58** was assessed in similar experiments. Pleasingly, allowing the cells sixty minutes incubation after a thirty minute treatment led to significant recovery of cytoskeletal structure (*figure 27, E and F*). This was indicative of reversible binding, similar to that of CA4P, and provided evidence of a similar mechanism of action. It also provided reasonable evidence that **58** would not suffer from the same toxicity profile as of colchicine. With the successful demonstration that both CA4P and **58** bind to tubulin reversibly and colchicine pseudo-irreversibly, an experiment was sought to quantify vascular disruptive-like properties.

4.5: Studies on Endothelial Cell Monolayer Permeability

Disruption of the endothelial cell monolayer is key to the activity of the VDAs.[47] Therefore, in an attempt to quantify this effect, HUVECs were grown on a permeable membrane into a confluent monolayer. The monolayer was then exposed to the drug for thirty minutes, followed by addition of a fluorescent dye to the top of the cells. The amount of fluorescent dye that passed through the monolayer into the well below could be used to quantify the level of monolayer disruption. The fluorescence emission in each well was normalised against the emission from a well in which the insert did not contain cells – the dye only had to pass through the membrane. The results presented are the average of three independent experiments.

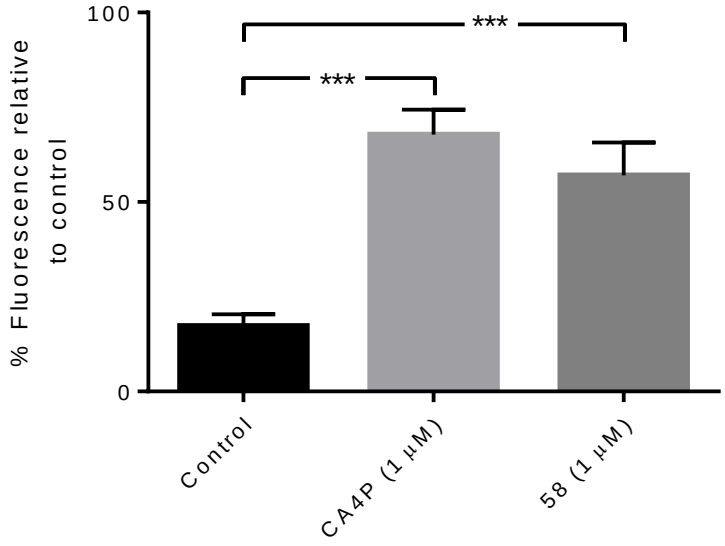

Chart 1: Drug-induced changes in endothelial monolayer permeability comparing CA4P and **58**. Confluent monolayers of cells grown on microporous filter inserts were treated with vehicle control, CA4P (1 μM, 30 min) or compound **58** (1 μM, 30 min). Drugs were removed and replaced with FITC –dextran for a further 30 min. The passage of FITC-dextran through the monolayer was quantified and expressed as a percentage of FITC that passed through a filter without cells. Results are a mean of 3 independent experiments ± SEM. Data were analysed by one way-Anova. ***$P < 0.001$ significant difference between control vehicle treated cells.

An untreated monolayer of HUVECs did indeed provide a barrier to the fluorescent dye, with only 17% relative to control passing through the monolayer (*chart 1*). A monolayer treated with 1 μM CA4P for thirty minutes prior to the addition of fluorescent dye became significantly more permeable. In this case, 68% of dye relative to control passed through the

monolayer, providing evidence that the monolayer was being disrupted. An unpaired t-test was carried out on the results and CA4P was shown to have significantly increased the amount of fluorescence passing through the cell monolayer. Pleasingly, treatment with 1 μM **58** also instigated a significant increase in fluorescence passing through the cell monolayer. For this treatment, 57% of fluorescence passed through the monolayer, indicating it was indeed perturbed. An unpaired t-test was also carried out to analyse the difference between a CA4P treatment and a **58** treatment. The difference between CA4P and **58** was found to not be significant. Therefore, at doses of 1 μM, CA4P and **58** instigated the same level of cell monolayer disruption.

4.6: Analysis of Signalling Pathway by Western Blot

CA4P induces microtubule disruption as well as changes in cell shape and morphology, which are attributed to the rapid remodelling of the actin cytoskeleton.[47,144] Previously, signalling pathways have been analysed and revealed that activation of the RhoA-GTPase signal pathway is involved in actin remodelling caused by CA4P.[47] RhoA causes stress fibre formation through polymerisation of actin and the phosphorylation of myosin light chain (MLC). This activity is dictated through the activation of serine/threonine Rho kinases (ROCKs). The activation of the RhoA-ROCK pathway by CA4P was confirmed by increases in MLC phosphorylation upon exposure to the drug.[47]

It was decided to investigate if **58** was activating the same signalling pathway as CA4P. To do this, phosphorylation of myosin light chain (MLC) was analysed by western blot. Western blots use gel electrophoresis to separate denatured proteins by length of polypeptide chain (somewhat like TLC separation). The proteins are then transferred to a membrane and stained with an antibody specific to that protein.[145,146] Therefore, by using a specific antibody to phosphorylated MLC (*p*MLC), it was possible to detect increases in the phosphorylation and use it as a marker for RhoA-ROCK signalling pathway activation. For the experiments, HUVECs were grown for 7 days without media change to reduce base levels of *p*MLC and then treated with various concentrations of **58** and CA4P and the results compared. Proteins that were proposed to be unnaffected by the presence of the drug compounds were used as a control for total sample protein isolated. The proteins selected were actin and glyceraldehyde-3-phosphate dehydrogenase (GAPDH). The results presented are the average of three independent experiments. Figure 28 shows a typical blot obtained. It is clear that pMLC was upregulated in the presence of both CA4P and **58**. To quantify the effect, blots were analysed with Image Studio™ Lite to determine the relative intensity of each band. The control signal was set as an intensity of one and all signals calculated relative to control. The results presented are the average of three independent experiments. The experiment confirmed that both CA4P and **58** significantly increased the phosphorylation of MLC relative to control (*chart 2*). This provided strong evidence that both compounds activated the same pathway and hence have the same mode of action.

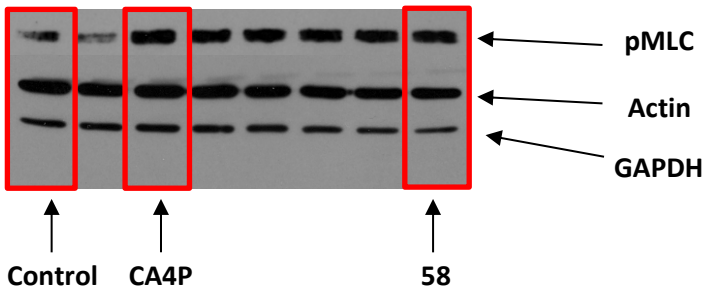

Figure 28

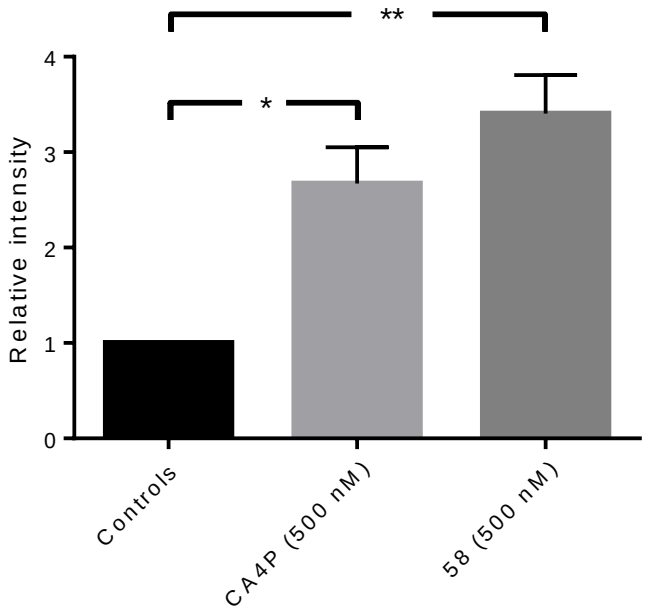

Chart 2: Study of drug-induced effects on phosphorylation of MLC by Western blot comparing CA4P and **58**. HUVECs were treated with increasing concentrations of CA4P or drug **58** for 15 minutes after which proteins were extracted and analysed for phosphorylation of Rho kinase target myosin light chain by western blotting using an antibody specific to the phosphorylated form of the protein. Immunoblots were reprobed with an antibody to actin to confirm equal loading. pMLC band intensities were analysed by ImageJ and results are were expressed as fold-increase over control cells treated with vehicle alone. Each column represents *the* mean of 3-4 independent cell culture experiments±SEM. Data were analysed by one way-Anova. *$P < 0.05$ significant difference between control vehicle treated cells. **$P < 0.01$ significant difference between control vehicle treated cells.

4.7: Studies of *in Vivo* Efficacy

It was next decided that the efficacy of **58** should be assessed *in vivo*. However, the compound was suffered from poor solubility in saline. Therefore, disodium phosphate compound **62** was used instead. All animal work was carried out by Mr. Matthew Fisher, who had obtained all necessary licenses and training for work with mice. An escalated maximum tolerated dose study was conducted in SCID (severe combined immunodeficiency) mice and **62** was found to have an MTD greater than 339 mg/kg (0.681 mmol/kg). With safe working limits established, SCID mice were implanted with 5 x 10^6 SW1222 (human colorectal adenocarcinoma) cells *via* subcutaneous injection. Tumours were allowed to 8 mm in diameter and then treated with either vehicle (50% Na_2CO_3/NaCl), CA4P (100 mg/kg, 0.227 mmol/kg) or a solution of **62** (339 mg/kg, 0.681 mmol/kg). A threefold higher dose of **62** was used due to the lower activity of the compound relative to CA4P *in vitro*. After 24 hours the animals were sacrificed and tumours removed and cut into sections. The sections were stained with hematoxylin and eosin (H & E) and the amount of necrosis scored by Chalkley grid method.[147] Scoring was conducted blind to avoid data bias. The results obtained exhibited variability within the CA4P group (*chart 3*). Disappointingly, **62** did not exhibit any tendency to increase tumour cell necrosis relative to control. It seems likely that compound was rapidly metabolised and did not reach the tumour blood vessels, otherwise some form of effect would likely have been observed. CA4P significantly increased necrosis relative to both control and **62** treated tumours.

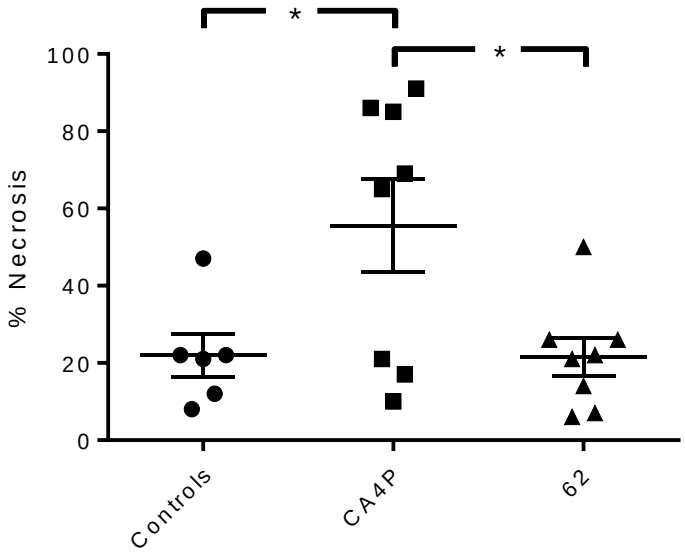

Chart 3: *In vivo* study of drug-induced effects on tumour cell necrosis comparing CA4P and **62**. Each point represents the combined data from a single tumour. 5 sections (cut at different tumour depths) were analysed per tumour using a x20 objective on a Nikon

Eclipse TS100 microscope. The total section was analysed and % necrosis calculated in each field from the relative number of points in a Chalkley eyepiece graticule co-incident with necrotic versus viable tumour tissue. Bars represent the mean±SEM of the combined data for each tumour. Data were analysed by one way-Anova. *$P < 0.05$ significant difference between control vehicle

Conclusion

Sydnones have rarely been used *in vivo* and their metabolically stability has not been extensively studied. It is likely that the sydnone-bridged combretastatin analogues do not have suitable pharmacokinetic or pharmacodynamics properties for use in a clinical setting.

In conclusion, sydnone analogues of CA4 have shown strong potential as vascular disrupting agents *in vitro*. The most potent compound, **58**, demonstrated potent activity at 500 nM in immunofluorescence assays. CA4P was more potent at lower concentrations in the same assay. Importantly, in an assay designed to test the vascular disrupting properties of the compounds, **58** showed similar characteristics to those of CA4P. It was also markedly different to the highly toxic, tubulin binding agent colchicine. Both **58** and CA4P significantly perturbed a confluent monolayer of cells and permeabalised the monolayer to macromolecules. Studies into the mechanism of action implicated that both CA4P and **58** to activate the RhoA-ROCK pathway and therefore have a similar mode of action. However, the phosphate prodrug of **58**, **62**, failed to have an effect on tumour cell necrosis when used *in vivo*. Therefore, the sydnone-bridged vascular disrupting agents are likely unsuitable molecules for further development.

Should future work be conducted in the area, it would need to focus on the metabolism of the compounds and the potential to improve PK/PD properties. From assay data it was postulated that the structural isomer of **56**, sydnone **63**, would be more active than the most active compound **58**. Therefore, in the event that metabolism and PK/PD did not appear problematic, **63** would represent the next logical lead compound for development.

Chapter 5: Synthesis of Pyrazole-Based Analogues of Combretastatin A4

Having successfully developed a synthetic method to access 3,4-diarylsydnones, and highlighted their interesting biological activities *in vitro*, attention was turned to the preparation of pyrazole-based analogues of CA4. Transferring the *cis*-1,2-diaryl structure from stilbenes to pyrazoles results in several potential targets. Specifically, in order to access all vicinal zones (*figure 29, I-III*), unique chemistries were required to access the desired compounds. Investigations began in the preparation 1,5-analogues.

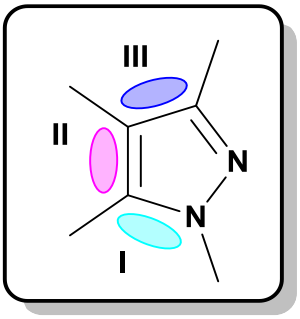

Figure 29: Pyrazole vicinal zones for analogue generation.

5.1: 1,5-Disubstituted Pyrazole-Based Analogues of CA4

1,5-Disubstituted pyrazole-based analogues were, in theory, available by the shortest synthetic route. It was envisioned that direct arylation of the sydnone, followed by cycloaddition with trimethylsilylacetylene and TBAF deprotection would furnish the target compounds (*scheme 28*). An advantage of this route was that the target analogues **64** and **65** could be synthesised from previously prepared sydnones **21** and **58** respectively.

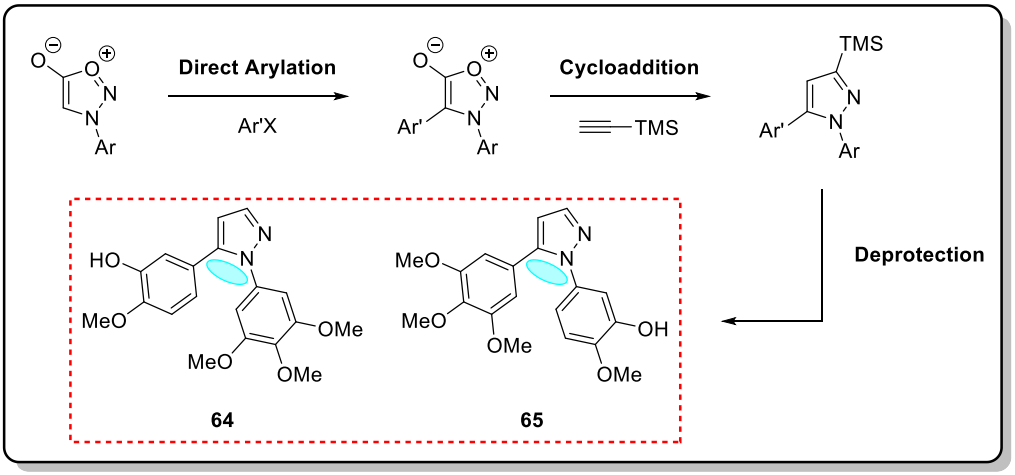

Scheme 28: Proposed route to 1,5-Disubstituted Pyrazoles.

Initial investigations focussed on the cycloaddition reaction. Model substrate **26** was subjected to various temperatures, equivalents of alkyne and concentrations (*table 10*). Interestingly, standard conditions using two equivalents of alkyne failed to afford more than trace product (*entry 1*). This was likely due to the relatively high volatility of trimethylsilylacetylene. Pleasingly, doubling the equivalents of alkyne led to successful cycloaddition and a quantitative yield of products **66a/b** (*entry 2*). Although inconsequential, the reaction was found to be highly regioselective (as judged by ^{1}H NMR), as expected from literature precedent.[101] The reactions were also found to be highly sensitive to concentration, with yields depreciating considerably at concentrations <1 M (*entries 3 and 4*). Unfortunately, attempts to increase scalability by conducting reactions under standard reflux apparatus led to only trace conversion of sydnone starting material.

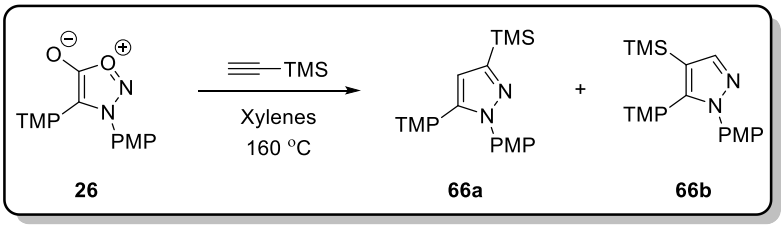

Entry	Eq. Alkyne	Concentration	Conditions	Result
1	2	1 M	Sealed Tube	<10% Conv.[a]
2	**4**	**1 M**	**Sealed Tube**	**100%[b] (95:5)[c]**
3	4	0.5 M	Sealed Tube	72%[b] (95:5)[c]
4	4	0.25 M	Sealed Tube	<10% Conv.[a]
5	4	1 M	Reflux	<10% Conv.[a]

a) As judged by ^{1}H NMR of the crude reaction mixture. b) Isolated yield of purified compound. c) Regioisomeric ratio as judged by ^{1}H NMR of the crude reaction mixture.

Table 10: Optimisation of cycloaddition.

To further probe the feasibility of the proposed route, the mixture of cycloadducts **66a** and **66b** were subjected to previously established conditions for removal of the trimethylsilyl group.[148] The regioisomeric mixture **66a** and **66b** was heated at reflux in 1 M tetrabutylammonium fluoride (TBAF) for 24 hours, which resulted in the isolation of **67** in good yield (*scheme 29*).

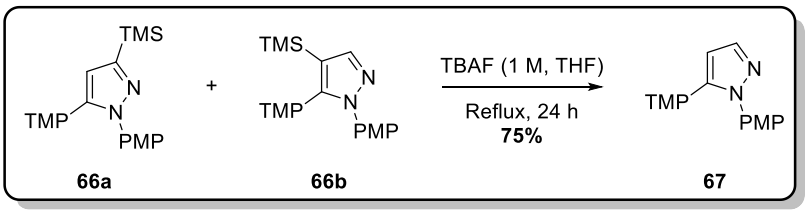

Scheme 29: Trial of TBAF-mediated trimethylsilyl group cleavage.

With proof of principle in hand, attention was turned to the preparation of combretastatin analogues **64** and **65**. Unfortunately sydnones **21** and **58** proved to be unreactive cycloaddition partners. It was postulated that the insolubility of the sydnones in xylenes was the source of the low reactivity. Pleasingly, TBS protection of the phenol **21** to generate **68** increased solubility and successfully afforded cycloaddition products **69a/b** and **69a/b** in high yield and regioselectivity (*scheme 30*).

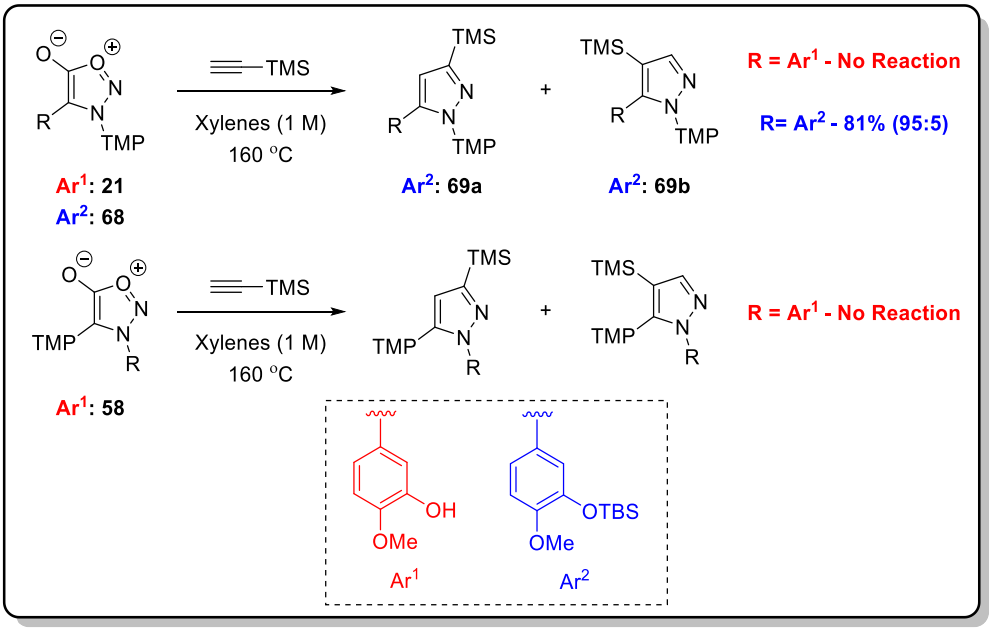

Scheme 30: Initial cycloaddition results.

It was proposed that the cycloadducts could undergo deprotection of both the TMS and TBS group during the TBAF deprotection conditions utilised previously. Therefore, the mixture of regioisomers **69a/b** were subjected to a refluxing solution of TBAF for 24 h. Disappointingly, although the reaction afforded the target pyrazole **64**, it was isolated in poor yield. Significant quantities of a similarly structured by-product were also isolated (*scheme 31*). The by-product was identified as fluoromethyl-substituted phenol **70**. Similar by-products were observed in the synthesis of the other pyrazole analogues.

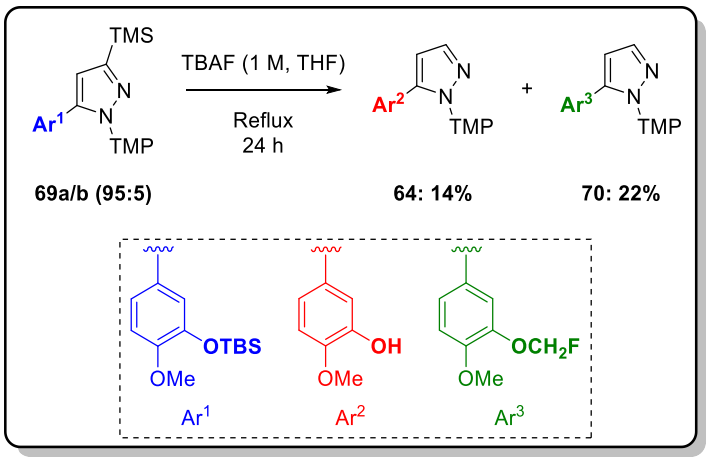

Scheme 31: Isolation of by-product **70**.

An interesting finding was that regioisomeric mixture of anilines **71a/b** did not suffer from the same issues when subjected to the reaction conditions and **72** was readily prepared in good yield (*scheme 32*).

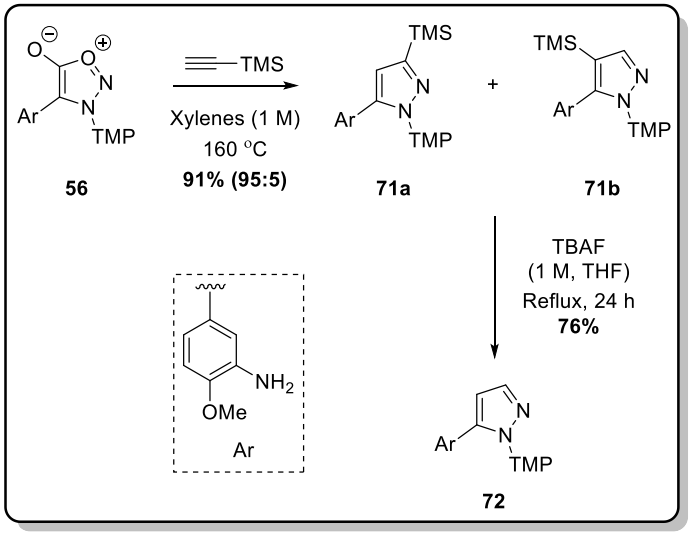

Scheme 32: Cycloaddition and silyl group removal with free aniline.

A strategy to overcome the problem of fluoromethylene incorporation was devised before investigations into their mechanism of formation. Accordingly, 3-bromo-4-methoxyphenol was protected as the benzyl ether (**73**) and subjected to directed arylation with 3,4,5-trimethoxyphenylsydnone (**19**) to afford 3,4-diarylsydnone **74** in moderate yield (*scheme 33*). Pleasingly, **74** underwent cycloaddition with trimethylsilylacetylene in excellent yield affording a regioisomeric mixture pyrazoles **75a/b** in a 9:1 ratio. The mixture of regioisomers readily underwent protodesilylation in refluxing TBAF to produce 1,5-diarylpyrazole **76** without any evidence of fluoromethyl ether by-product formation. Gratifyingly, standard hydrogenation conditions furnished CA4 analogue **64** in good yield.

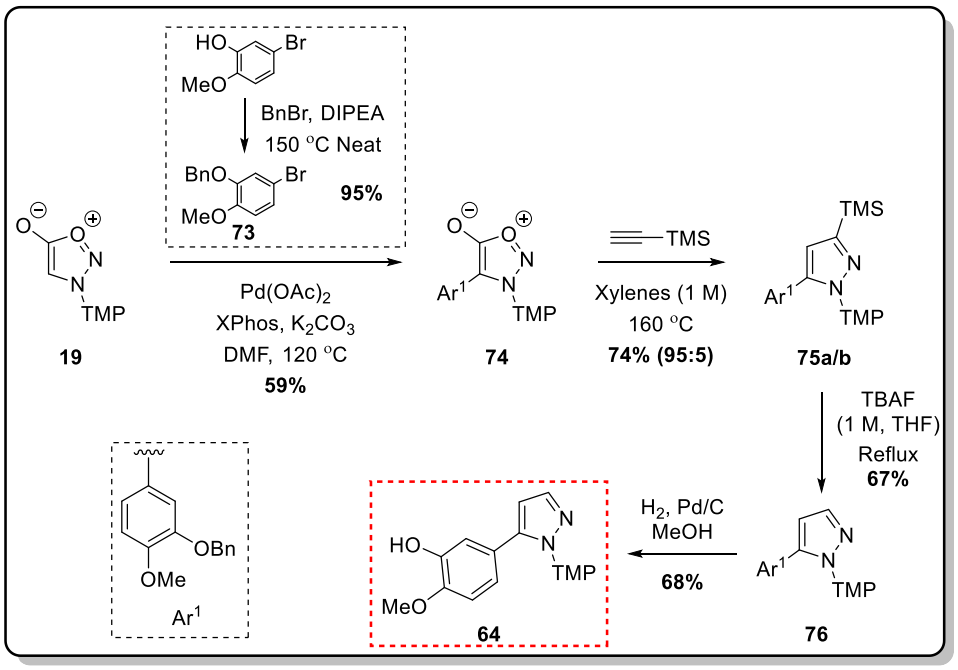

Scheme 33: Synthesis of **64**.

The preparation of pyrazole-based analogue **65** required some optimisation. Surprisingly, the benzyl protected phenol **77** was not stable to direct arylation conditions (*scheme 34*). It was found that benzyl protection had to be carried out after direct arylation (*scheme 35*). Cycloaddition of sydnone **78** proceeded in good yield and regioselectivity. TBAF deprotection afforded moderate yield of 1,5-disubstituted pyrazole **80**. The product was contaminated with a small amount of inseparable by-product. Fortunately, it was possible to isolate analogue **65**, cleanly, after benzyl deprotection.

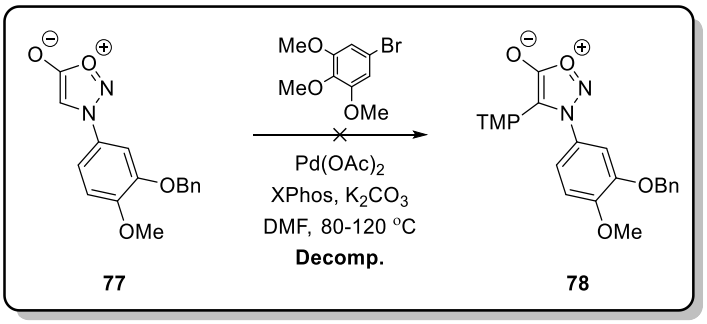

Scheme 34: Attempted direct arylation of **77**.

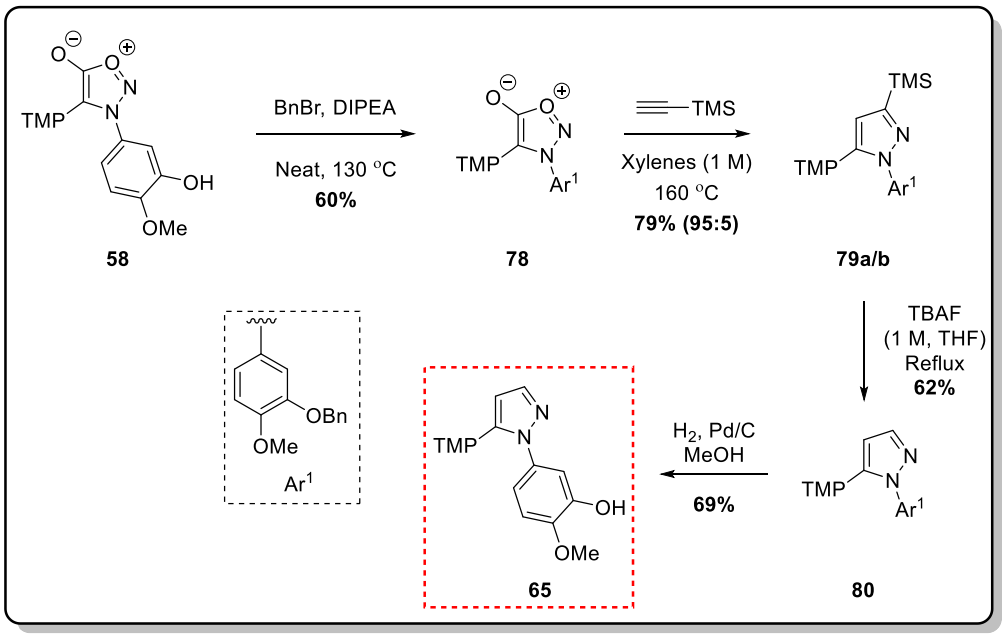

Scheme 35: Synthesis of **65**.

5.2: 4,5-Disubstituted Pyrazole-Based Analogues of CA4

The proposed route for the preparation of 4,5-pyrazole-based analogues of CA4P would begin with the direct arylation of *N*-methyl- and *N*-benzylsydnone (*scheme 36*). The resulting 4-substituted sydnones would then be subjected to cycloaddition with alkyne **81** to form pyrazole boronic esters. The trimethylsilyl group of the alkyne was required to direct the reaction towards the desired regioselectivity – with boronic ester incorporation on the pyrazole *C*4. The pyrazole boronic esters would then be subjected to Suzuki-Miyaura coupling conditions followed by deprotection of the trimethylsilyl group and, if present, the benzyl group to afford the target 4,5-pyrazole analogues. The route was potentially challenging for a number of reasons. Firstly, *N*-alkylsydnones have been identified as less reactive substrates in both the direct arylation of sydnones and alkyne cycloaddition reactions.[149,110] In particular, several studies from co-workers within the group had shown that the parent *N*-benzylsydnone often decomposed under cycloaddition conditions. Secondly, the key pyrazole boronic esters were predicted to be particularly challenging substrates for Suzuki-Miyaura coupling. Heterocyclic boronic esters are often difficult substrates[115] and in the proposed intermediates, the boronic ester environment is quite sterically hindered.

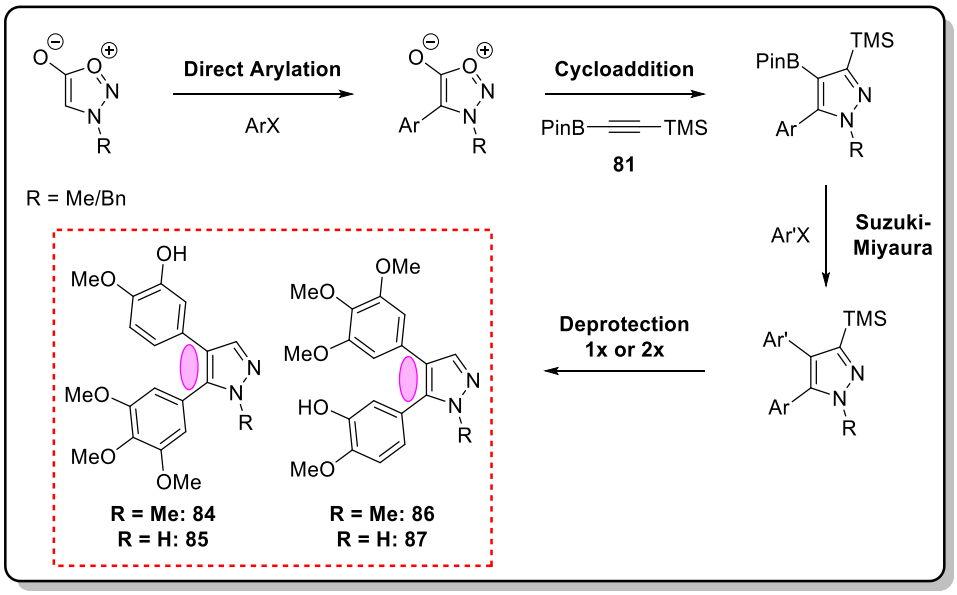

Scheme 36: Proposed route to 4,5-disubstituted pyrazoles.

Investigations were initially conducted in parallel with the preparation of 1,5-disubstituted analogues, however similar issues of fluoromethylation of the phenol began to arise. Therefore, the corresponding benzyl ethers were used and synthesis began with the successful direct arylation of *N*-methyl- and *N*-benzylsydnone with both 5-bromo-1,2,3-

trimethoxybenzene and benzyl protected phenol **73** to afford sydnones **86**, **87**, **88** and **89** in moderate to good yield (*scheme 37*).

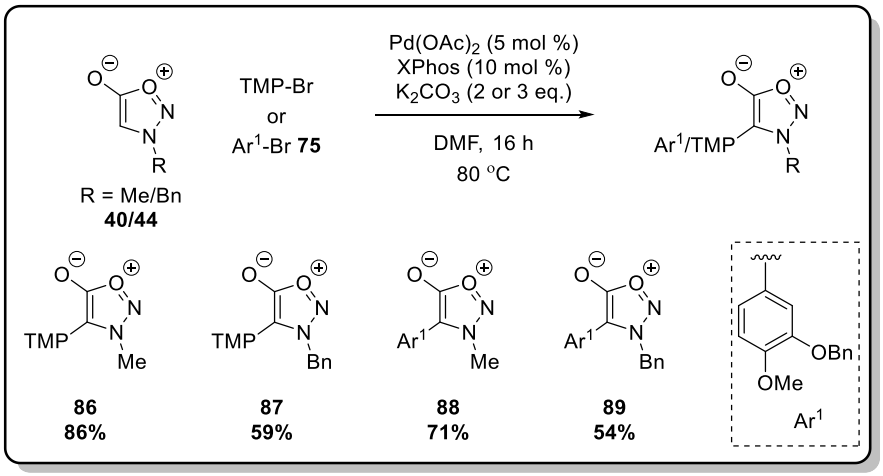

Scheme 37: Synthesis of cycloaddition precursors.

With ready access to scalable quantities of 4-substituted sydnones, work began on the cycloadditions of these substrates. Key alkyne **81** was readily prepared from trimethylsilylacetylene and isopropoxyboronic acid pinacol ester in acceptable yield on multigram scale (*scheme 38*). Gratifyingly, all substrates underwent cycloaddition with alkyne **81** after 48 h of heating at 180 °C, with only a single regioisomer observable. This was particularly pleasing as there are no reported examples of 4-aryl-substituted *N*-benzylsydnones undergoing cycloaddition to form pyrazoles. Indeed, reports of the cycloadditions of 4-substituted sydnones undergoing regioselective cycloaddition with disubstituted alkynes are scarce.[148,111] The products were often isolated with a minor contaminant of the corresponding protodeborylated pyrazole. This impurity was carried forward with a view to conducting the separation at a later stage.

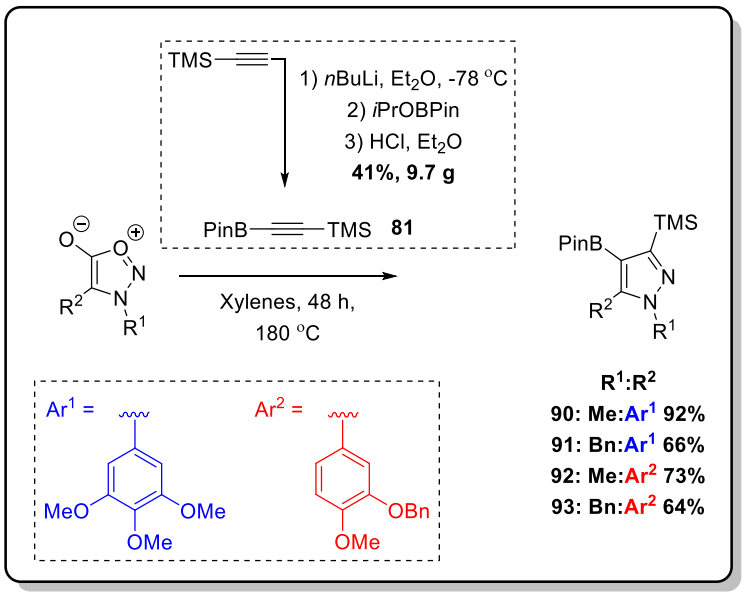

Scheme 38: Cycloadditions with alkynylboronate **81**.

With the target pyrazole boronic esters in hand, the utility of the compounds in Suzuki-Miyaura coupling was studied. Investigations on similar substrates (discussed later) had revealed a combination of the 2nd generation XPhos palladium precatalyst and sodium carbonate in 1,2-dimethoxyethane (DME)/water to be an effective coupling system. Pleasingly, application of the same system to pyrazoles **90**, **91**, **92** and **93** resulted in successful coupling (*scheme 39*).

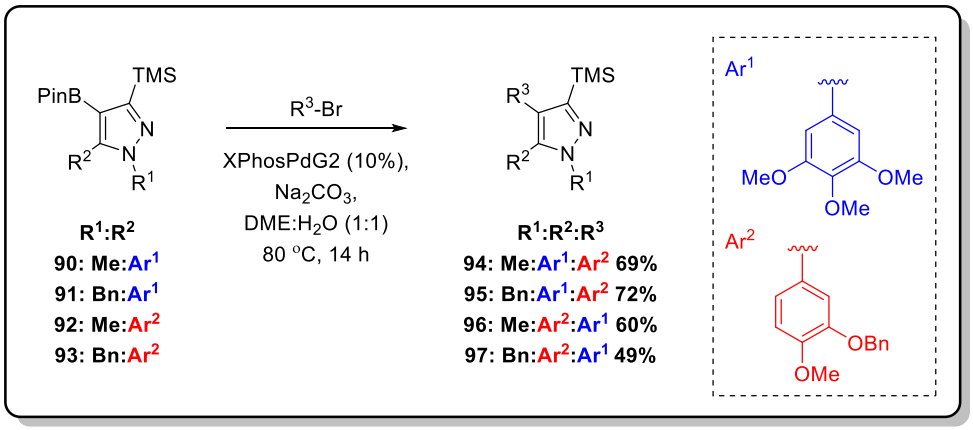

Scheme 39: Suzuki-Miyaura coupling of pyrazole boronic esters.

The four intermediates were subjected to TBAF in refluxing THF to remove the silyl group. Pleasingly, the four compounds reacted without issue to afford benzyl-protected drug precursors **98**, **99**, **100** and **101** in moderate yield (*scheme 40*). At this point the compounds were readily separated from the corresponding protodeborylation by-products.

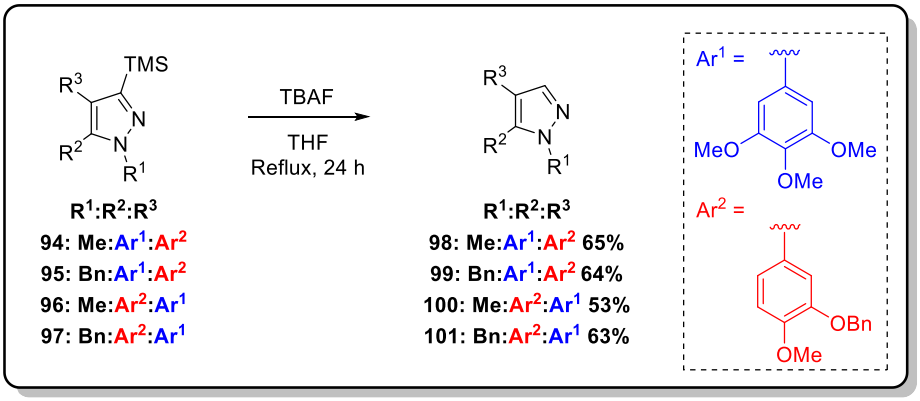

Scheme 40: TBAF-mediated trimethylsilyl group cleavage.

Hydrogenolysis of the benzyl-ether in *N*-methyl analogues **98** and **100** proceeded without incident (*scheme 41*). Hydrogenation of the *N*-benzyl pyrazoles **99** and **101** was particularly slow and resulted in the isolation of both the target *N-H* pyrazoles **83** and **85** as well as monodeprotected products **102** and **103**. The products were readily separable and were stored for subsequent biological activity studies.

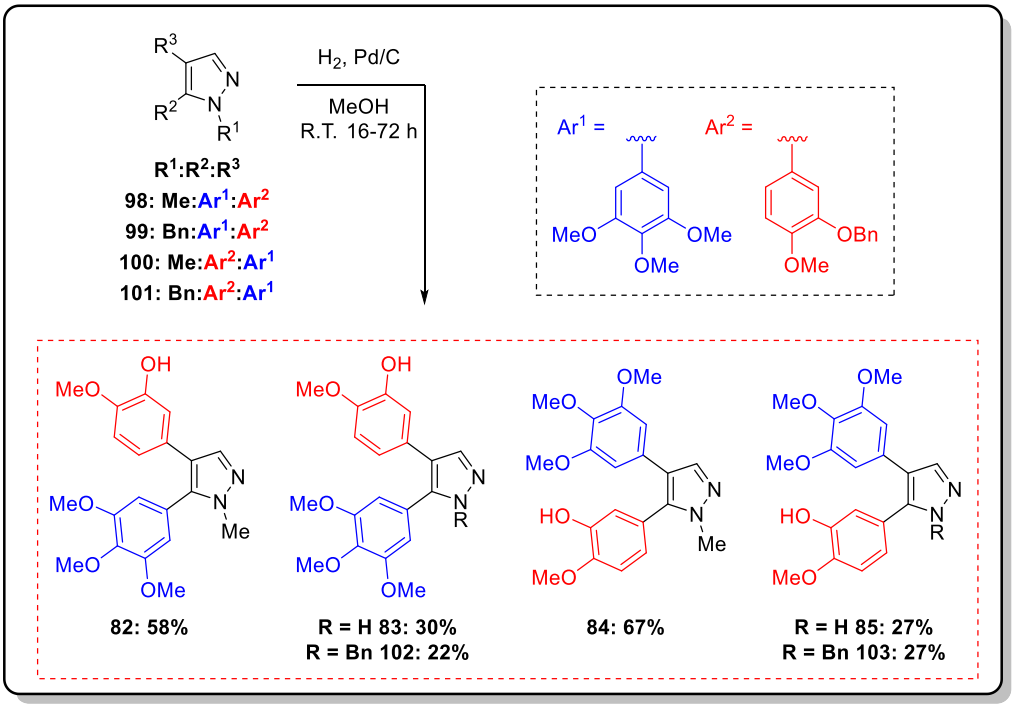

Scheme 41: Hydrogenolysis of benzyl alcohols and amines.

5.3: Investigations into Fluoromethylation

We next undertook investigations into the source of the intriguing mono-fluoromethylated compound **70**. The conditions required for the reaction are depicted in scheme 42. With regard to proposing a reasonable mechanism for this transformation, identification of the source of the methylene group was particularly puzzling. Nevertheless, the initial hypothesis was that the trimethylsilyl group could act as the C_1 source.

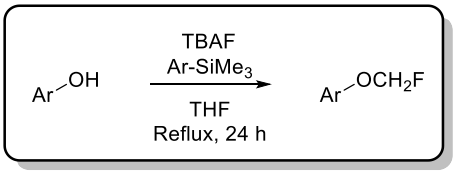

Scheme 42: Proposed general procedure.

4-Bromophenol was used as a model substrate for the initial investigations. Firstly, 4-bromophenol was heated with ten equivalents of TBAF in THF, but this resulted in the recovery of starting material (*scheme 43, A*). To test the importance of the trimethylsilyl group, 4-bromophenol was heated with TBAF in THF at reflux with trimethylsilylbenzene (*scheme 43, B*). However, this only resulted in the recovery of starting material. Next, in order to determine if the methoxy groups could be transferring the methylene unit, 4-bromophenol was heated in a mixture of TBAF in THF with 5-bromo-1,2,3-trimethoxybenzene (*scheme 43, C*). This only resulted in recovery of starting material. To examine if 4-bromophenol was simply a poor substrate for the reaction, phenol **64** was subjected to the same array of test reactions. In all cases starting material was recovered (*scheme 43, A-C*).

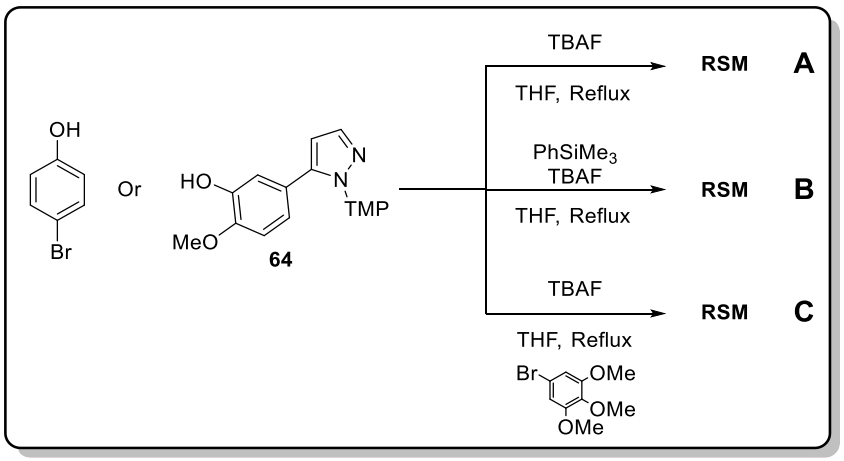

Scheme 43: Initial fluoromethylation trials.

Next, a surprising discovery was made. A new batch of **69a/b** did not deliver any of the fluoromethyl ether by-product when subjected to the previous set of conditions (*scheme 44*), with clean conversion to the silyl-cleaved pyrazole **64**.

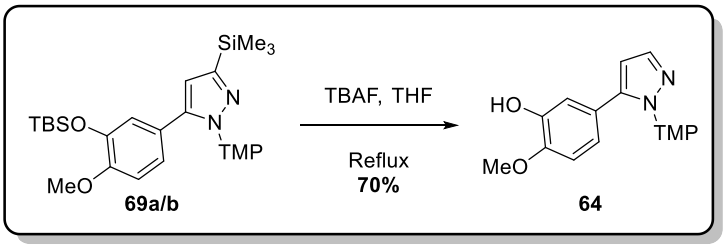

Scheme 44: Attempted repetition of original result.

Therefore, it became apparent that impurities within the starting material itself must have been causing the observed side reaction. Moreover, as this side reaction was observed over multiple substrates, it was proposed that a common impurity must be responsible. On reflection, it became apparent that some substrates had been transferred between vials as dichloromethane solutions. It was therefore proposed that dichloromethane was the likely source of the C_1 fragment. Indeed, heating 4-bromophenol with TBAF in THF and 20% dichloromethane resulted in complete conversion of starting material to fluoromethyl ether **104** as judged by ^{1}H NMR spectroscopy (*scheme 45*). Interestingly, a significant amount of acetal by-product **105** was also present in the crude material. Unfortunately, the compounds were not stable to silica, florisil^{TM} or alumina chromatography, with typically low yields obtained upon purification. The ratio of **104** to **105** also changed on chromatography, with acetal **105** often becoming the major product.

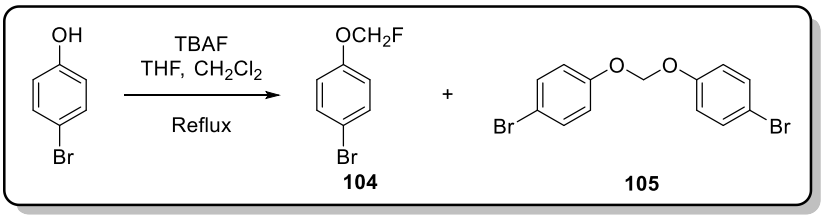

Scheme 45: CH_2Cl_2-doped reaction.

The relative instability of **104** compared to the original fluoromethylation product **70** was presumed to arise from the lack substitution *ortho* to the fluoromethyl ether. Steric interactions of an *ortho* substituent could help prevent acetal formation and therefore prevent it as a decomposition pathway. To probe the hypothesis, 3-hydroxy-4-methoxybenzaldehyde was subjected to the reaction conditions, resulting in *ca.* 60% conversion of starting material as judged by ^{1}H NMR spectroscopy. Fluoromethyl ether **106**

appeared stable to column chromatography and was isolated in 41% yield without evidence of acetal formation (*scheme 46*).

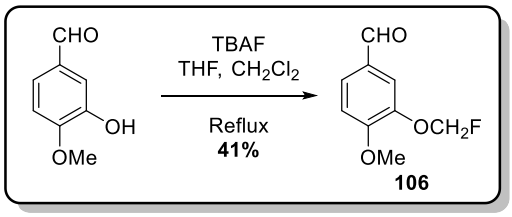

Scheme 46: Preparation of stable fluoromethylation product **106**.

Longer reaction times led to improved conversion, but resulted in mixtures of product, by-product and *Gem*-diol from aldehyde **106**. The reaction temperature was raised to 100 ^{o}C and conducted in a sealed tube, however this failed to improve conversion.

In order to gain further insight into the mechanism of the transformation, the nature of the alkylating agent was probed. 3-Hydroxy-4-methoxybenzaldehyde was subjected to the standard reaction conditions, but without TBAF and this led to quantitative recovery of starting material. There was no evidence for acetal, hydrate, or chloromethyl ether (*scheme 47*). This therefore implied the formation of a new intermediate was taking place that could act as an alkylating agent, and that dichloromethane was not sufficiently reactive.

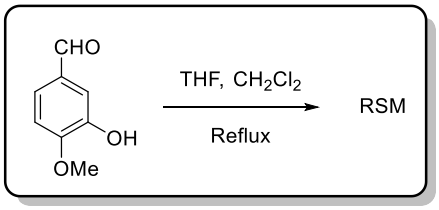

Scheme 47: Attempted chloromethylation in absence of TBAF.

A further possibility was the formation of a carbene during the reaction. Langlois had reported an interesting, isolated example of difluoromethylation *via* an interrupted Reimer-Tiemann reaction (*scheme 48*).[150] It was proposed that under the reaction conditions, dichloromethane could form a carbene *in situ* and react in a similar manner.

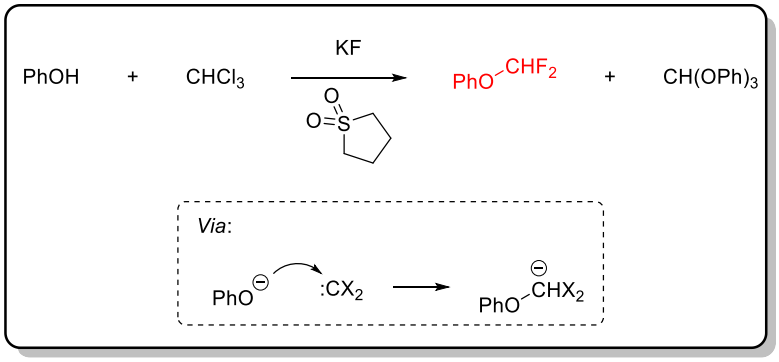

Scheme 48: Langlois interrupted Reimer-Tiemann reaction.

In order to assess the feasibility of a carbene-based mechanism, the reaction was conducted with deuterated dichloromethane in place of dichloromethane. If the reaction proceeded through a carbene, then loss of deuterium would be observed in the products. If the reaction proceeded *via* S_N2, complete deuterium incorporation was expected. The reaction resulted in >95% deuterium incorporation and the isolation of **107** in 31% yield (*scheme 49*), providing strong evidence that a carbene was not the reactive intermediate.

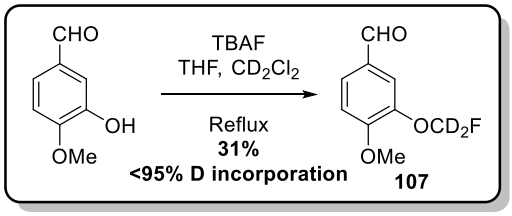

Scheme 49: Fluoromethylation with CD_2Cl_2.

Having conducted several experiments to-date, the working hypothesis for the formation of the difluoromethyl ethers is as follows. Under the conditions, a fluoride anion may be able to displace chloride from dichloromethane to generate CH_2ClF. Chlorofluoromethane has been shown to alkylate phenols,[151] and if generated in solution could act as the electrophile in a simple S_N2 reaction (*scheme 50*).

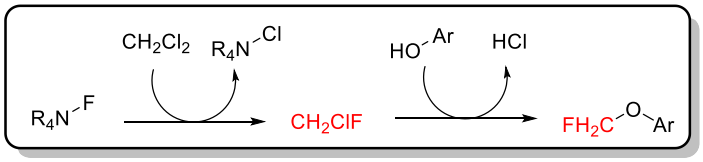

Scheme 50: Proposed mechanism of fluoromethylation.

5.4: 3,4-Disubstituted Pyrazole-Based Analogues of CA4

It was envisioned that 3,4-disubstituted pyrazole analogues could be prepared rapidly using chemistry previously developed within the group.[110] Parent sydnones could undergo highly regioselective cycloaddition with aryl-alkynylboronates to form pyrazole boronic esters, followed by Suzuki-Miyaura coupling to provide the 3,4-substituted analogues (*scheme 51*). Interestingly, deprotection of benzyl analogues **109** and **111** would provide a convergent route to pyrazoles **83** and **85** described in the 4,5-disubstituted analogue synthesis (*scheme 52*).

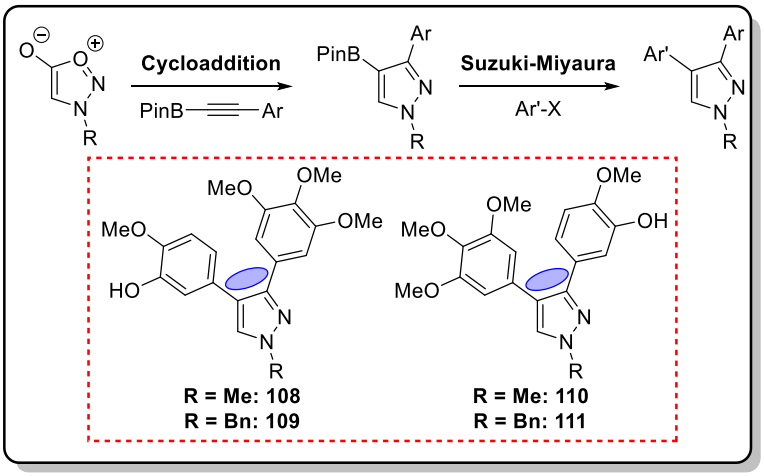

Scheme 51: Proposed route to 3,4-disubstituted pyrazoles.

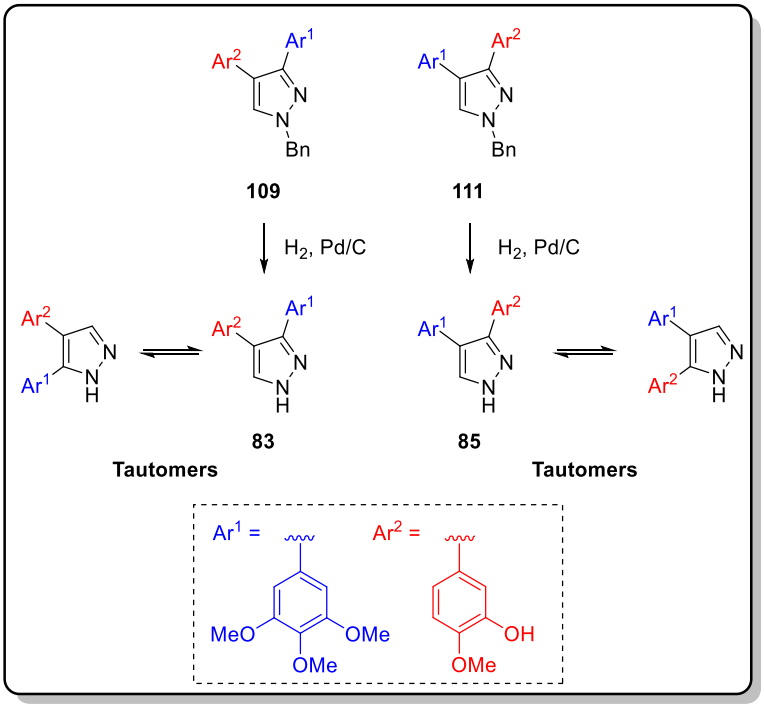

Scheme 52: Convergent route to analogues **83** and **85**.

Investigations began with the preparation of borylated alkyne **112** from 3,4,5-trimethoxyphenylacetylene. Deprotonation with *n*-butyllithium, followed by treatment with 2-isopropoxy-4,4,5,5-tetramethyl-1,3,2-dioxaborolane furnished the difficult to isolate, borylated alkyne, in poor yield (*scheme 53*). Nevertheless, alkyne **112** was subjected to cycloaddition conditions with *N*-methyl- and *N*-benzylsydnone. Unfortunately, the desired pyrazole boronic ester was never observed or isolated from the reactions. The only products isolated from the reactions were protodeborylated alkyne and the cycloadducts **113a/b** or **114a/b**, arising from cycloaddition with protodeboronated alkyne. Various attempts to form the pyrazole boronic ester using radical scavengers resulted in failure. Alkynylboronate **112** appeared to be incompatible with the reaction conditions, therefore a new strategy was developed, avoiding the use of electron rich alkynylboronates.

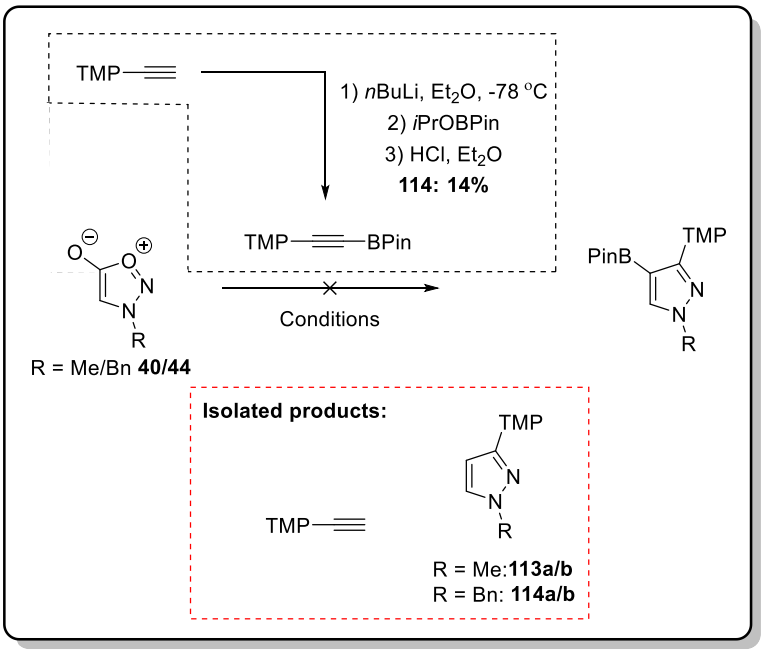

Scheme 53: Attempted cycloadditions with alkynylboronate **114**.

The new strategy sought to utilise the native regioselectivity of the sydnone cycloaddition with terminal alkynes, followed by the native reactivity of the pyrazole formed in reactions with electrophilic halogen sources (*scheme 54*). The intermediate 4-bromopyrazoles could then undergo Suzuki-Miyaura coupling to generate the desired CA4 analogues.

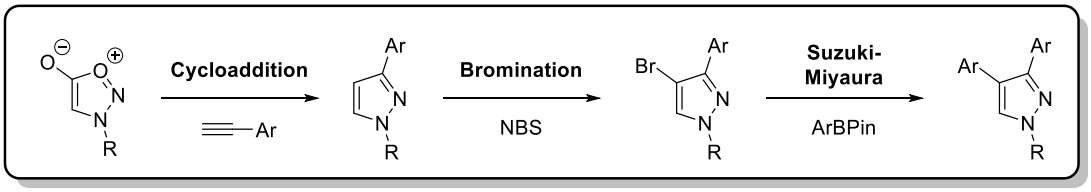

Scheme 54: Revised route to 3,4-disubstituted pyrazoles.

The new route began with the cycloadditions of *N*-methyl- and *N*-benzylsydnone with 3,4,5-trimethoxyphenylacetylene and TBS-ether **60**. The reactions proceeded smoothly in good yields and high regioselectivities (*scheme 55*). Next, electrophilic aromatic substitution with *N*-bromosuccinamide afforded 4-bromopyrazoles. The crude products were subjected to Suzuki-Miyaura coupling directly after basic workup. Pyrazoles **113a/b** and **114a/b**, bearing the 3,4,5-trimethoxyphenyl moiety in the 3-position were coupled with 3-hydroxy-4-methoxyphenylboronic acid pinacol ester, affording the target CA4 analogues **108** and **109** in good yield over 2 steps. *N*-benzyl analogue **109** was successfully transformed into free *N-H* pyrazole **83** *via* hydrogenation. Analysis of this sample and the compound formed *via* the 4,5-disubstituted analogue route confirmed that these pyrazoles were indeed the same. This was judged by inspection of individual spectra as well as those of mixed samples. In the case of pyrazoles **115** and **116**, bearing the TBS-ether-substituted phenyl ring, the boron coupling partner needed to be prepared. Attempts to isolate the 3,4,5-trimethoxyphenylboronic acid pinacol ester failed. The compound was observed in the crude reaction mixture, however attempts to purify the material were unsuccessful. Changing to the corresponding potassium trifluoroborate salt resulted in the successful isolation of the borylated compound in poor yield. Gratifyingly, a 3 step procedure of bromination, Suzuki-Miyaura coupling followed by silyl deprotection afforded in CA4 analogues **110** and **111** in synthetically useful yields. Finally *N*-benzyl analogue **111** was subjected the hydrogenation to form *N-H* pyrazole **85**. The reaction was conducted in H-Cube^{TM} which resulted in a good yield of 66%, a significant increase when compared to standard conditions.

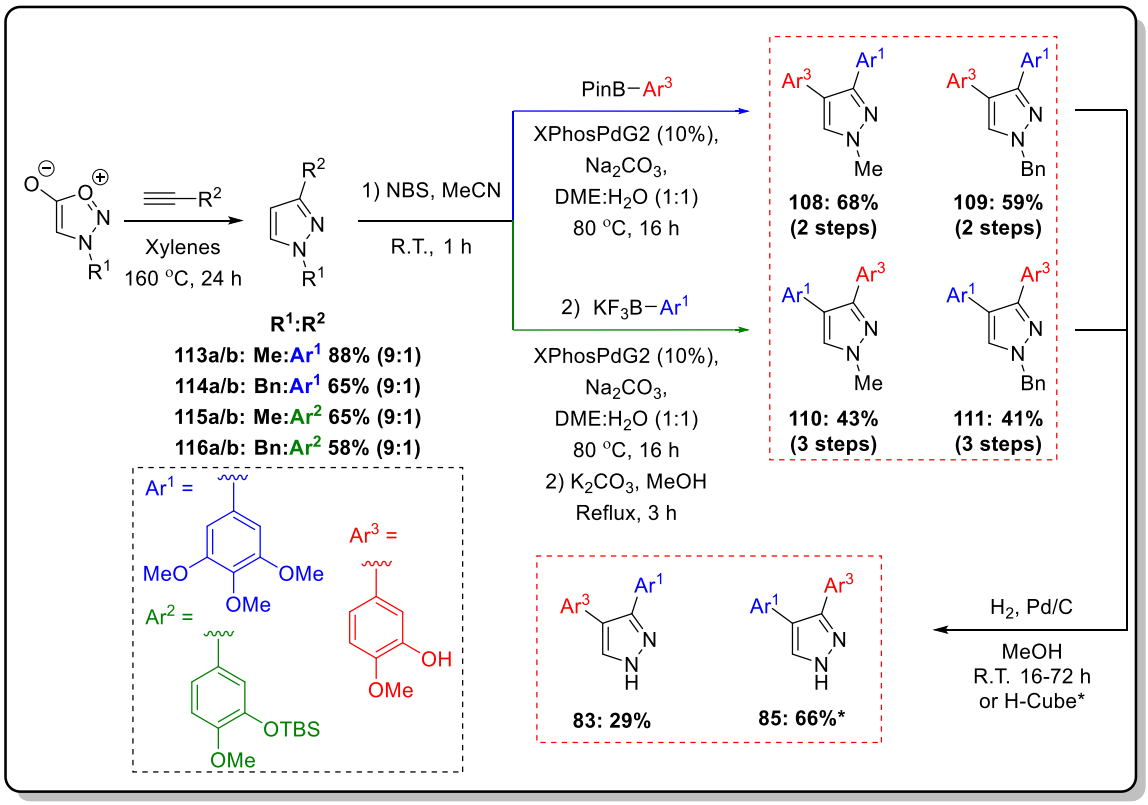

Scheme 55: Synthesis of 3,4-disubstituted pyrazole-based analogues of CA4.

In summary, modular routes for the preparation pyrazole-based CA4 analogues have been developed. Sydnones proved to be ideal precursors to the compounds, leading to the successful preparation of twelve direct pyrazole-based analogues of CA4 in a highly-regioselective manner (*figure 30*). An interesting monofluoromethylation reaction was also discovered and mechanistic insights obtained. The fluoromethylated products were found to be quite unstable, limiting the utility of the reaction. With the synthetic goal of the project achieved, attention turned to the biological evaluation of the compounds.

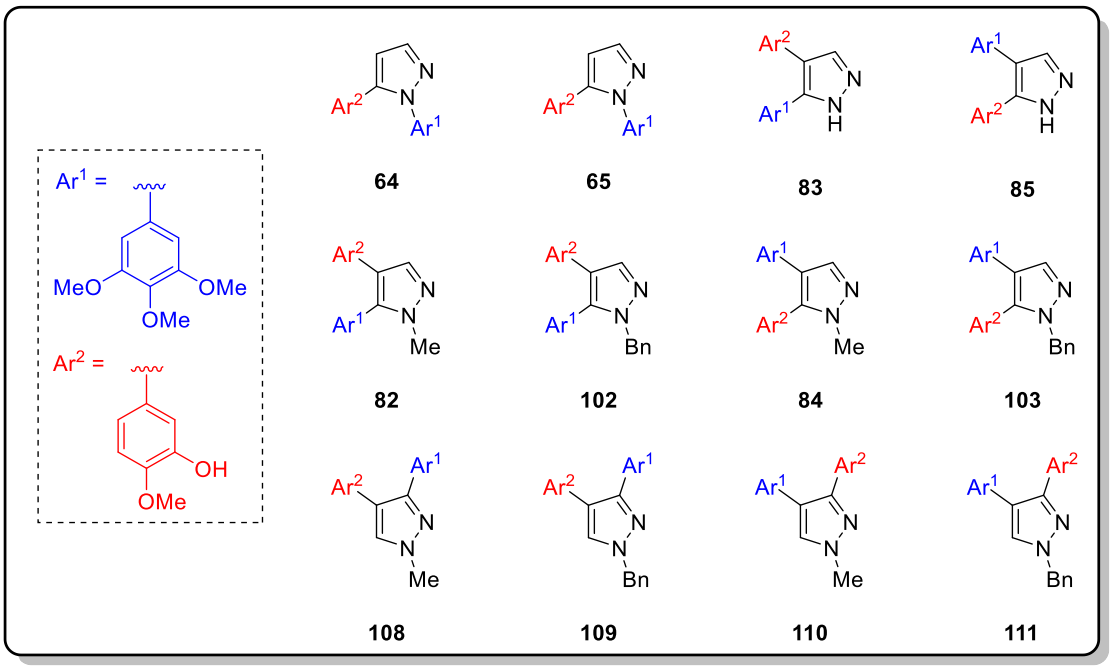

Figure 30: Pyrazole-based analogue library.

Chapter 6: Biological Evaluation of Pyrazole-Based Analogues of Combretastatin A4

With the synthetic goal of the project completed, attention turned to evaluation of the efficacy of the molecules as vascular disrupting agents. Due to the success of assays involving HUVECs with sydnone-based analogues of combretastatin A4, a similar approach to efficacy evaluation was carried out on the pyrazole-based analogues of CA4.

6.1: Cell Proliferation Studies

Similarly to studies on sydnones, initial screens focussed on the effect of the compounds on cell proliferation. The cells were treated with various concentrations of compound and incubated for 72 hours. The results were quite surprising, with activities ranging from 7 nM to >5 μM (*figure 31*). The activity range is particularly large when it is considered that all of the compounds screened were direct analogues of CA4, containing the same electron rich aromatic rings. Previous reports have stipulated that the olefinic linker of CA4 played a more structural than binding role,[64] yet such a stark range of activities appeared to contradict this hypothesis. Excitingly, the most active compound, **85** was equipotent to CA4P in the assay.

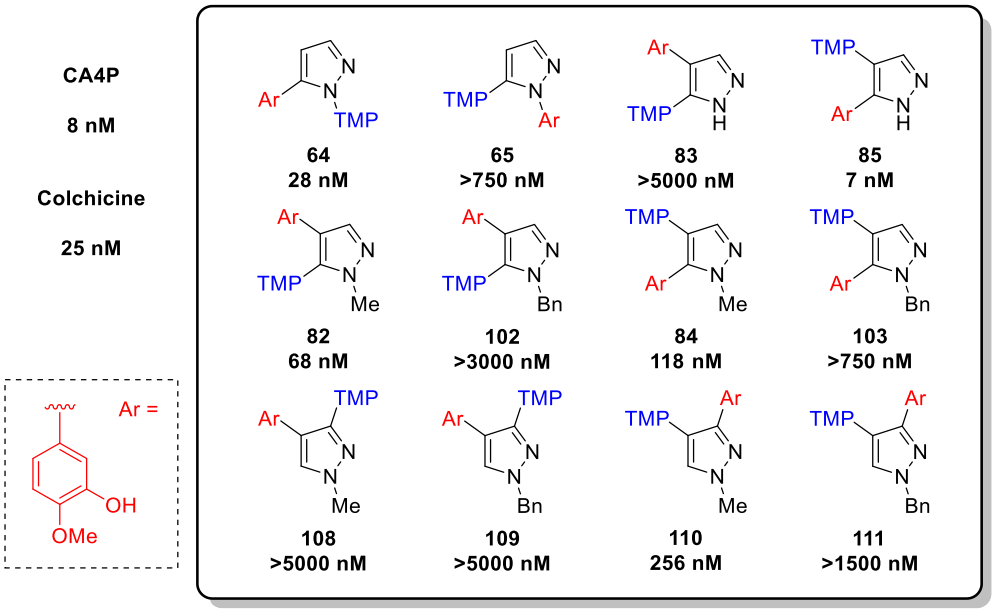

Figure 31: Values for growth inhibition of HUVECs by pyrazole analogues vs. CA4P and colchicine.

Initial analysis of the data gave some insights into possible structure activity relationships. Firstly, *N*-benzylpyrazoles exhibited lower activity than the corresponding *N*-methylpyrazoles (**103** vs **84** and **102** vs **82** etc.). Another interesting feature was that the most potent

compounds seemed to feature the phenolic ring in the *C*5 position of the pyrazole (**64**, **85** and **84**). In fact, in a number of cases merely swapping the aromatic rings around to locate the phenolic ring at the *C*5 position led to striking increases in activity (*figure 32 A and B*). The contrast in activity between **85** and **83** was particularly astounding (> 1000 fold). **85** was the most active compound of the series and **83** one of the least active. The only difference between the compounds was the *C*4/*C*5 substitution on the pyrazole core. A notable exception to the activity profile trend was **82**, which was almost twice as potent as its isomer **84** (*figure 32, C*). However, both compounds were reasonably potent, so the difference in activity was not quite as dramatic as other examples. **82** was the only example of a potent compound with the phenolic ring located at the pyrazole *C*4. Indeed the marked contrast in activity between **110** and **108** demonstrated that avoiding incorporation of the phenolic ring in the *C*4 position seemed to improve activity (*figure 32, D*).

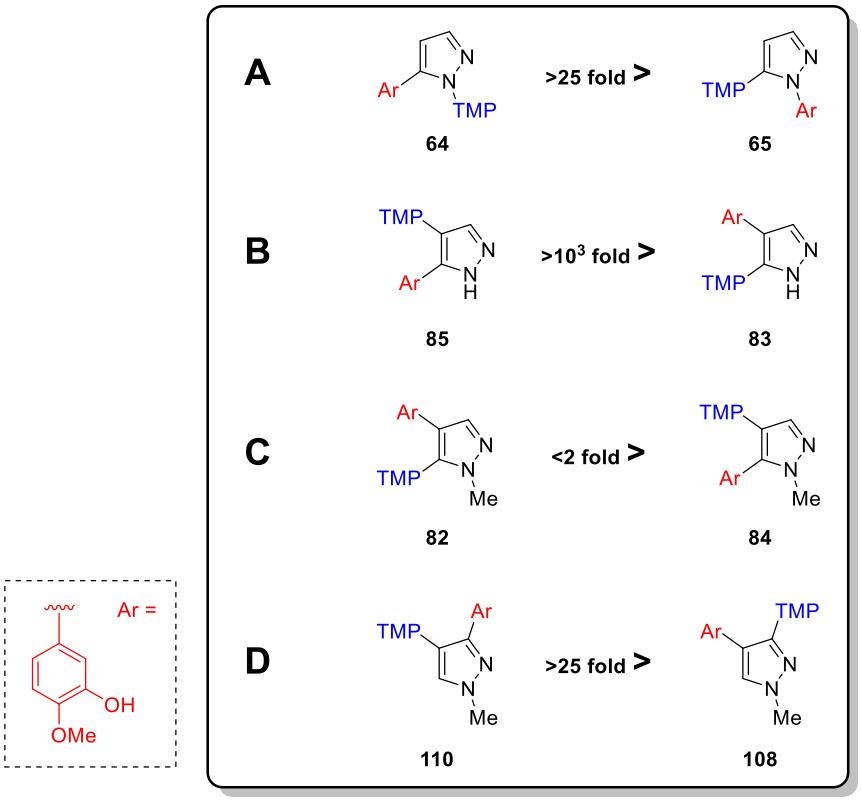

Figure 32: Key analogue comparisons.

With a number of compounds exhibiting low nanomolar activity identified, it was decided to focus further evaluation on the two most active – **85** and **64**, with GI_{50} values of 7 nM and 28 nM respectively (*figure 33*).

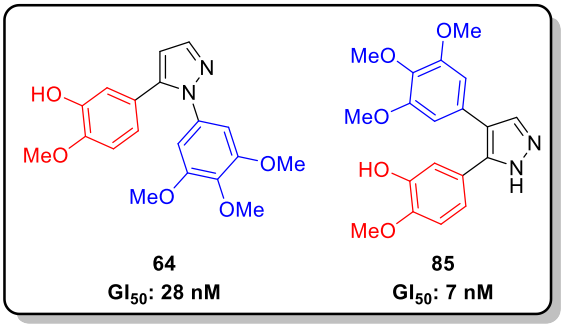

Figure 33: Most active pyrazole-based analogues.

6.2: Studies of Effects on the Cytoskeleton by Immunofluorescence

As with sydnone analogues, endothelial cells in culture were stained for actin filaments using phalloidin and microtubules using an antibody to β–tubulin. The cells were treated with various concentrations of drug for 30 minutes before fixation, staining, and imaging.

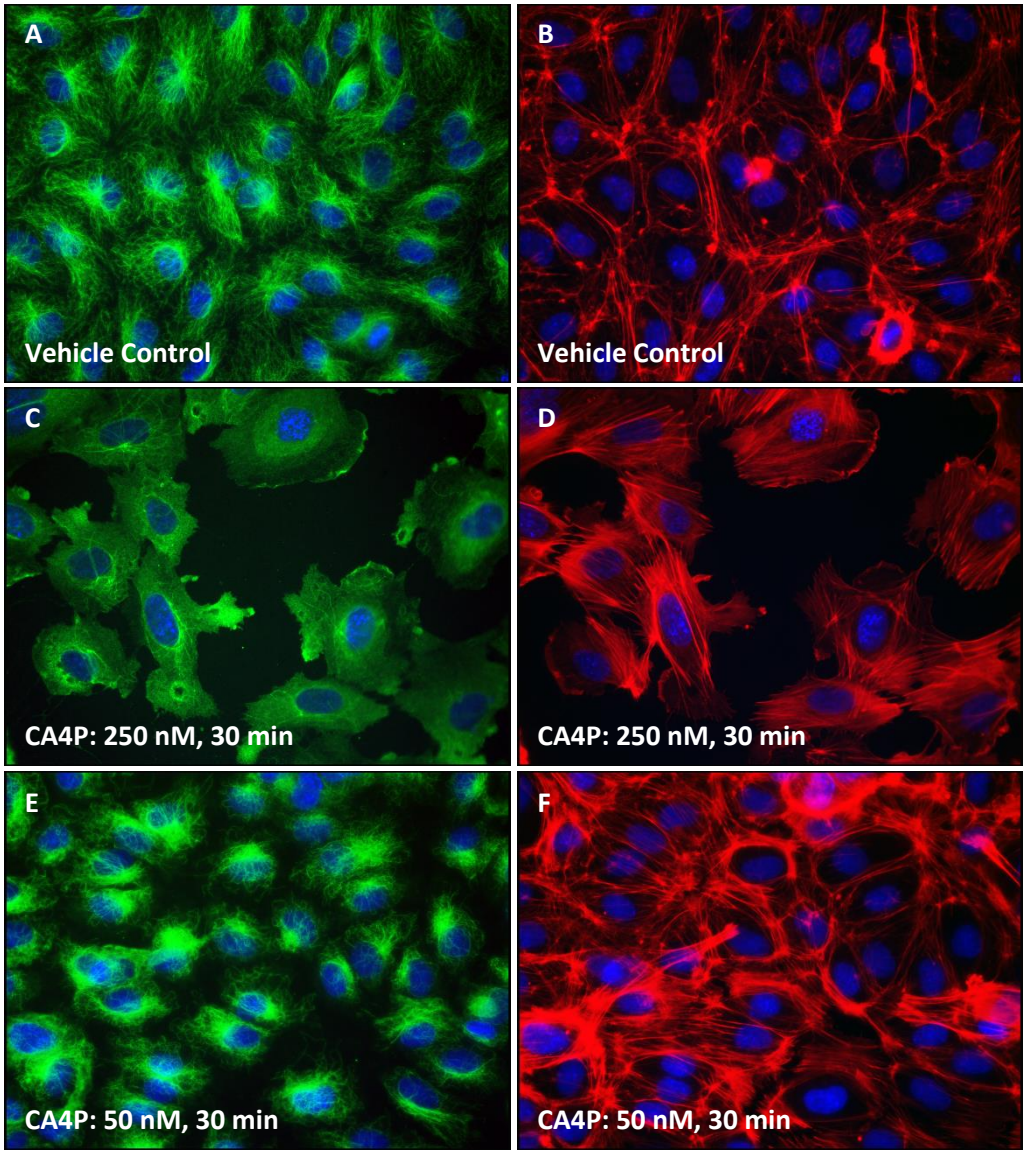

Figure 34: Effects of CA4P on HUVEC cytoskeletal structures. Cells were treated with a single dose of either vehicle (A, B), 250 nM CA4P (C, D) or 50 nM CA4P (E, F). Drug treatments were for 30 min. Cells were fixed and stained with an antibody to β-tubulin (A, C, E) and F-actin (B, D, F).

As previously shown, CA4P disrupted microtubules and instigated the formation of actin stress fibres at doses of 250 nM (*figure 34, C and D*). However, a lower dose of 50 nM led to marked reduction in activity, with many microtubules visibly intact (*figure 34, E and F*).

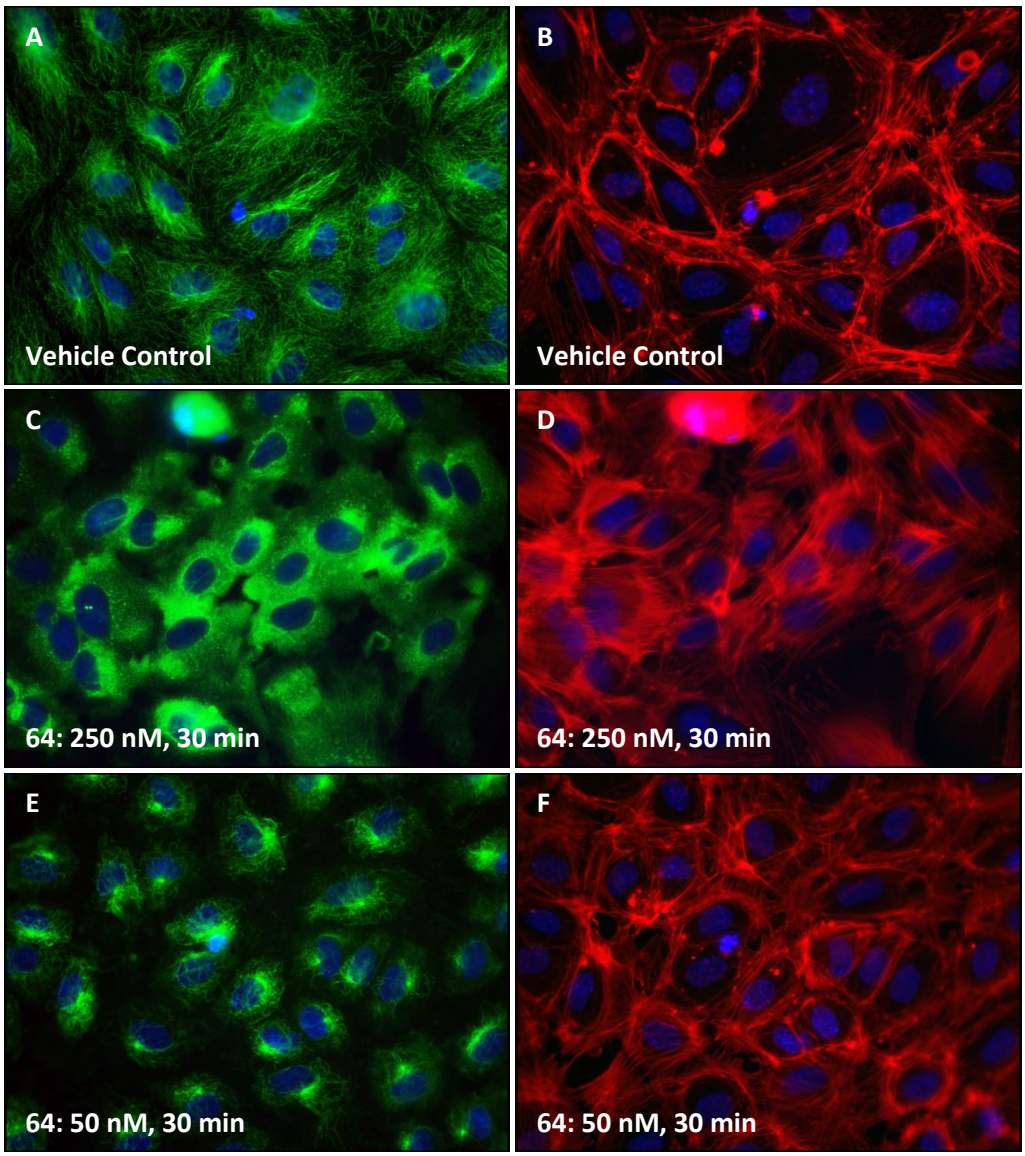

Figure 35: Effect of **64** on cytoskeletal structures. Cells were treated with a single dose of either vehicle (A, B), 250 nM **64** (C, D) or 50 nM **64** (E, F). Drug treatments were for 30 min. Cells were fixed and stained with an antibody to β-tubulin (A, C, E) and F-actin (B, D, F).

Similarly to CA4P, **64** induced changes in cell morphology and led to the formation of actin stress fibres at 250 nM (*figure 35, C and D*). The effects observed were less profound with a 50 nM dose. Many microtubules remained intact and cellular morphology was more closely maintained (*figure 35, E and F*).

Interestingly, **85** was effective at disrupting microtubules at concentrations of 250 nM (*figure 36, C and D*) and 50 nM (*figure 36, E and F*). Although more microtubules were intact at 50 nM, **85** was more active at this dose than both **64** and CA4P. Further reduction in concentration to 25 nM induced changes in cell morphology, but many microtubules remained intact (*figure 36, G and H*). Excitingly, **85** appeared to be slightly more active than CA4P in this assay, therefore further investigations into its mode of action were undertaken.

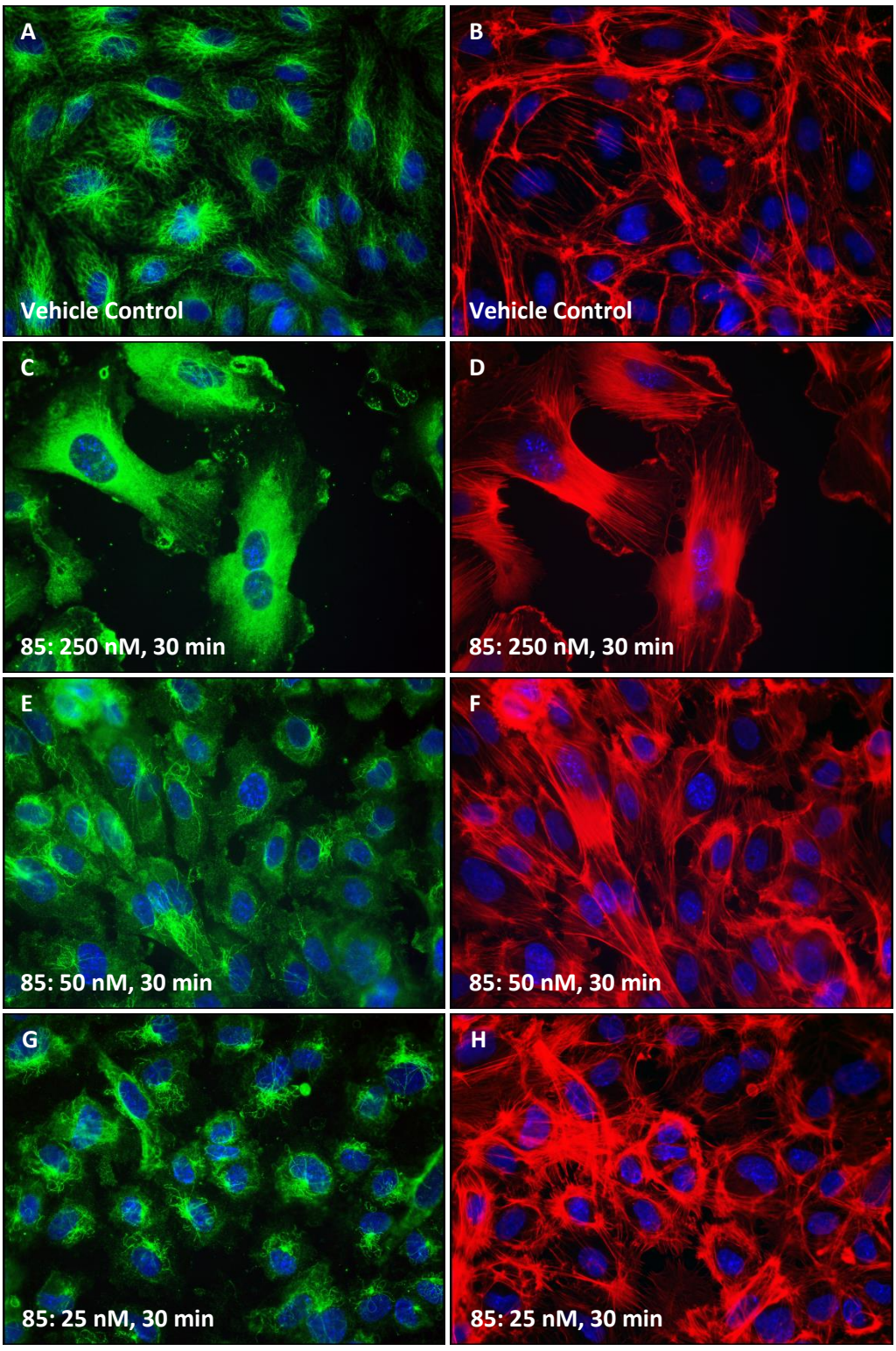

Figure 36: Effect of **85** on cytoskeletal structures. Cells were treated with a single dose of either vehicle (A, B), 250 nM **85** (C, D), 50 nM **85** (E, F) or 25 nM **85** (G, H). Drug treatments were for 30 min. Cells were fixed and stained with an antibody to β-tubulin (A, C, E, G) and F-actin (B, D, F, H).

6.3: Studies on the Recovery of Cytoskeletal Structures after Drug Removal by Immunofluorescence

The reversibility of binding to tubulin was probed for each compound using immunofluorescence. To confirm there was not a loss in efficacy over time, cells were treated with each drug at 250 nM for 90 minutes. As expected, there was no loss in efficacy for CA4P, **64** or **85** at this time point. Microtubules were disrupted, cell morphology altered, and actin stress fibres formed (*figure 37*).

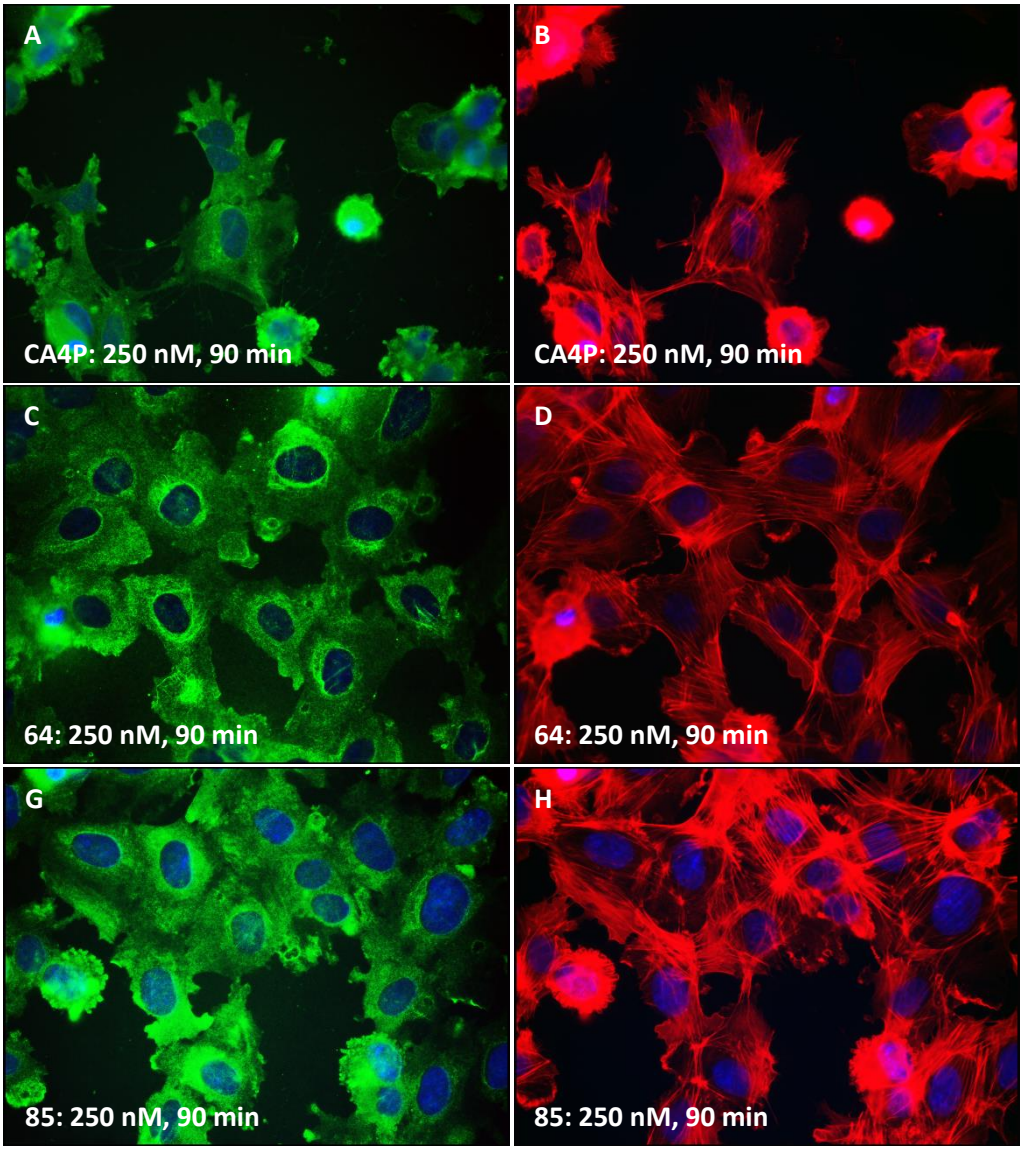

Figure 37: Cytoskeletal effects after 90 minute drug incubation. Cells were treated with a single dose of either 250 nM CA4P (A, B), 250 nM **64** (C, D) or 250 nM **85** (E, F). Drug treatments were for 90 min. Cells were fixed and stained with an antibody to β-tubulin (A, C, E, G) and F-actin (B, D, F, H).

Similarly to earlier work (*vide infra*), cells washed and incubated for 60 minutes after a 30 minute treatment of 250 nM CA4P showed significant signs of recovery. Microtubules reformed and there was a reduction of actin stress fibres (*figure 38, A and B*). Cells treated with 1 μM colchicine did not recover in this time (*figure 38, C and D*). Pleasingly, cells treated with **64** showed recovery of microtubules and a reduction in actin stress fibres (*figure 38, E and F*). Interestingly, cells treated with **85** had not fully recovered at this time point. Microtubules remained disrupted and actin stress fibres were visible across the cells (*figure 38, G and H*). However, on closer inspection microtubules were beginning to sprout from the centrosome, which indicated that the cells were beginning to recover. The recovery time required seemed to be longer.

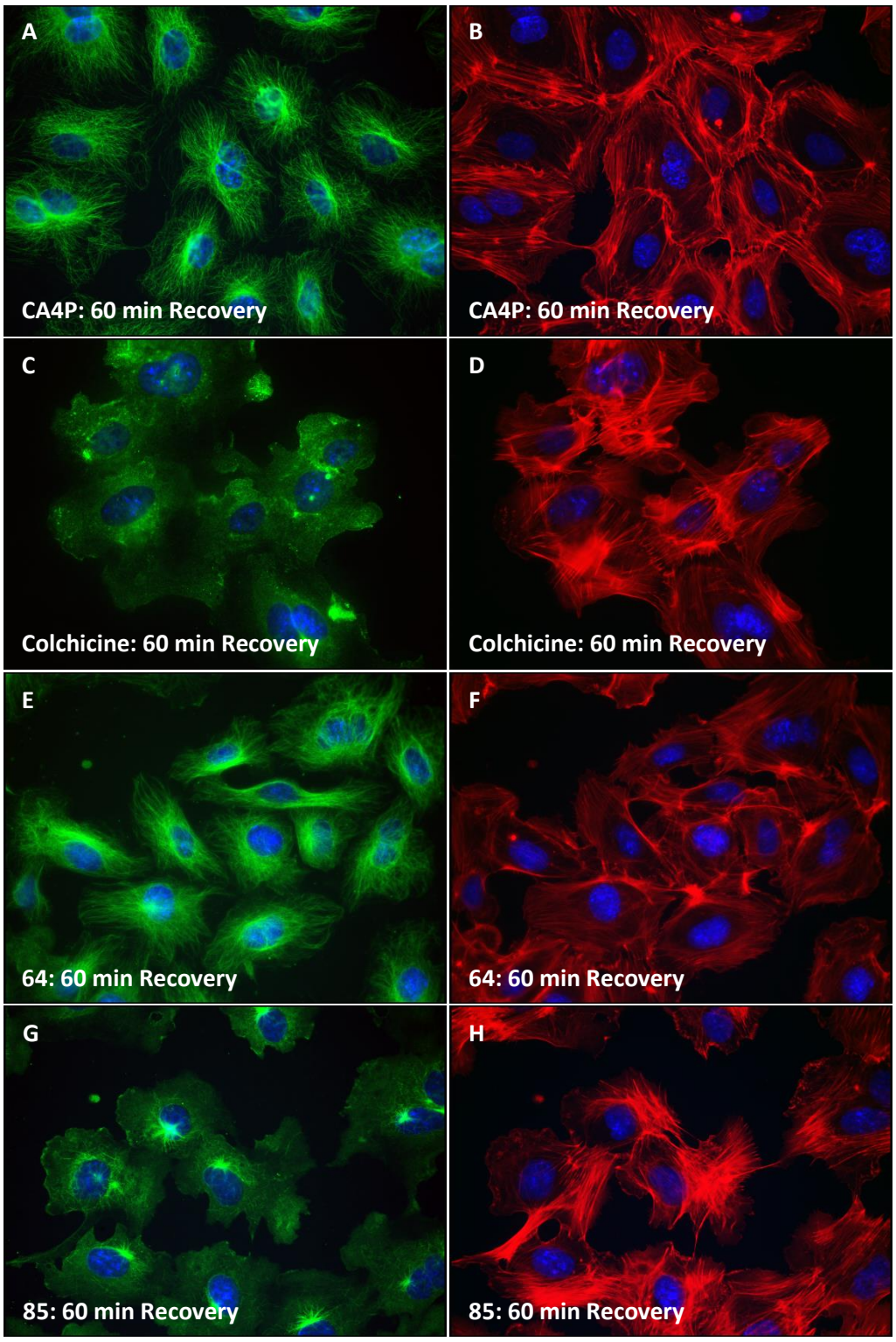

Figure 38: Recovery of cytoskeletal structures 60 min after drug removal. Cells were treated with a single dose of either 250 nM CA4P (A, B), 1 μM colchicine (C, D), 250 nM **64** (E, F) or 250 nM **85** (G, H). Drug treatments were for 30 min. Cells were then washed with PBS (3x) and allowed to recover for 60 min. Cells were fixed and stained with an antibody to β-tubulin (A, C, E, G) and F-actin (B, D, F, H).

To investigate if cells treated with **85** would recover, a longer incubation after removal of the drug was used. As a control, cells were treated with **85** for 150 minutes. The drug showed no loss in efficacy at this time point (*figure 39, A and B*). Pleasingly, when the cells were allowed 120 minutes incubation after removal of the drug, the cells showed significant signs of recovery (*figure 39, C and D*). Cells treated with colchicine followed by 120 minutes incubation after removal of the drug showed signs of microtubule disruption and actin stress fibres (*figure 39, E and F*). However, in some of the cells it appeared that microtubules were possibly beginning to reform. It was therefore possible that the delay in recovery of **85** compared to CA4P and **64** was a sign of potential toxicity. It was also possible that it was a sign of a wider therapeutic window for the drug. Either outcome would be very interesting. If slower recovery was an indication of toxicity, this assay would represent the first reliable *in vitro* assay for identifying the suitability of compounds as VDAs. Similarly, if it indicated a wider therapeutic window it would also be the first of its kind. However, to identify the significance of the result, it needed to be assessed in conjunction with *in vivo* data.

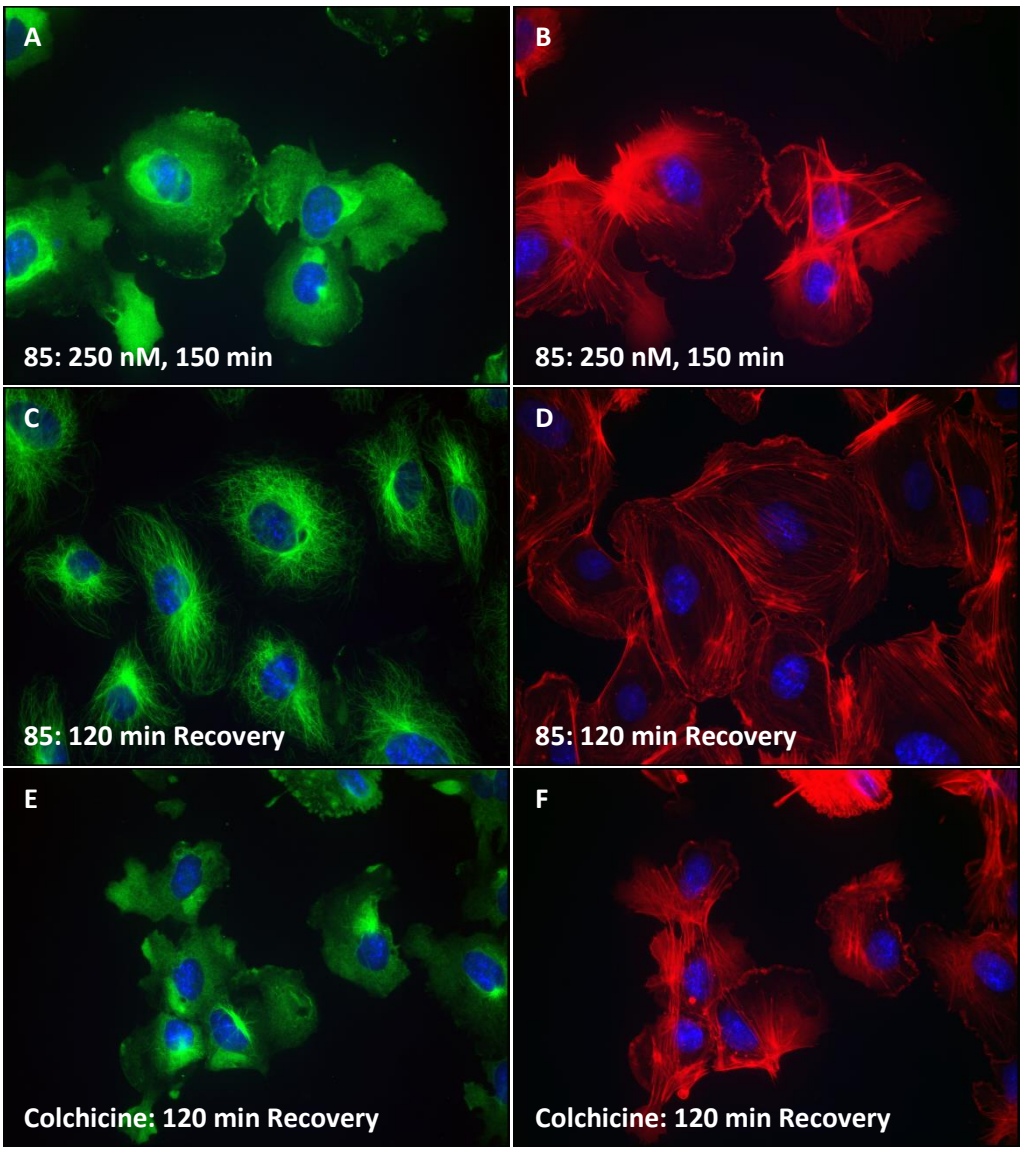

Figure 39: Recovery of cytoskeletal structures 120 minutes after drug removal. Cells were treated with a single dose of either 250 nM CA4P (A, B, C, D) or 1 μM colchicine (E, F). Drug treatments were for 30 min. Cells were then washed with PBS (3x) and allowed to recover for 120 min (C, D, E, F). Cells were fixed and stained with an antibody to β-tubulin (A, C, E) and F-actin (B, D, F).

6.4: Studies on Endothelial Cell Monolayer Permeability

As a further supplement to the data gather by immunofluorescence, the effects of **64** and **85** on endothelial monolayer permeability were studied by analysing the amount of fluorescent dye passing through a confluent monolayer of cells. Firstly, the results of a 1 μM dose of **64** on monolayer permeability were analysed. It was found that both CA4P (44% vs 5% fluorescence) and **64** (48% vs 5% fluorescence) instigated a significant increase in monolayer permeability relative to control (*chart 4*). There was no significant difference in the activities of the two drugs, meaning that they were equipotent at this dose.

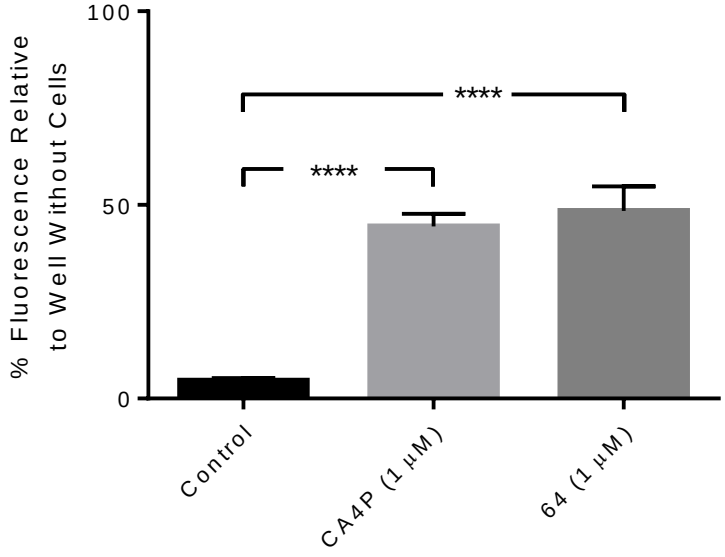

Chart 4: Drug-induced changes in endothelial monolayer permeability comparing CA4P and **64**. Confluent monolayers of cells grown on microporous filter inserts were treated with vehicle control, CA4P (1 μM, 30 min) or compound **64** (1 μM, 30 min). Drugs were removed and replaced with FITC –dextran for a further 30 min. The passage of FITC-dextran through the monolayer was quantified and expressed as a percentage of FITC that passed through a filter without cells. Results are a mean of 3 independent experiments ± SEM. Data were analysed by one-way Anova. ****, $P < 0.0001$ significant difference between control vehicle treated cells

Next, the activity of **85** was tested alongside CA4P. **85** maintained activity at 50 nM in immunofluorescence experiments whilst CA4P was considerably less active at the same dose. Therefore, it was decided to analyse the effect of a 50 nM dose of **85** and CA4P on endothelial cell monolayer permeability. A 50 nM dose of CA4P did not significantly increase permeability relative to control (*chart 5*), although there was a tendency towards increase. Interestingly, a 50 nM treatment of **85** significantly increased permeability relative to both control and

CA4P (69% vs 15% and 35% fluorescence). This provided further evidence that **85** was more active than CA4P *in vitro*.

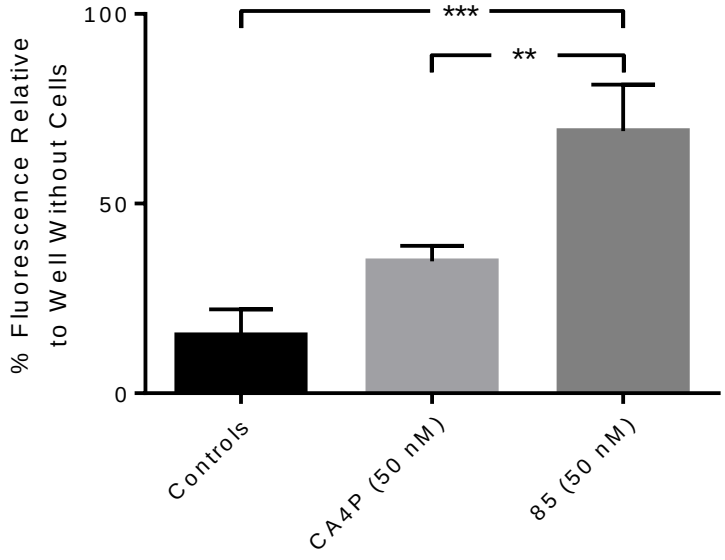

Chart 5: Drug-induced changes in endothelial monolayer permeability comparing CA4P and **85**. Confluent monolayers of cells grown on microporous filter inserts were treated with vehicle control, CA4P (50 nM, 30 min) or compound **85** (50 nM, 30 min). Drugs were removed and replaced with FITC –dextran for a further 30 min. The passage of FITC-dextran through the monolayer was quantified and expressed as a percentage of FITC that passed through a filter without cells. Results are a mean of 3 independent experiments mean of 3 independent cell culture experiments ± SEM. Data were analysed by one way-Anova. ***P* < 0.01 significant difference between control vehicle treated cells, ****P* < 0.001 significant difference between control vehicle treated cells.

6.5: Analysis of Signalling Pathway by Western Blot

With the intriguing results depicted in chart 5, attention was focused on **85** and the comparison of its activity with CA4P in assays linked to mode of action and vascular disruption. Previous studies had revealed that activation of the RhoA-GTPase signal pathway was involved in actin remodelling and monolayer disruption caused by CA4P.[35] Similarly to studies on sydnones, both **85** and CA4P induced effects on the phosphorylation of MLC in HUVECs were investigated. As shown in Figure 40, both compounds instigated significant increases in pMLC over a range of concentrations. This indicated that both compounds were acting *via* a similar pathway. Compound **85** induced significant phosphorylation of MLC at the lower tested concentration of 50 nM while CA4P was less active at this dose. To further confirm the involvement of ROCK in the induction of MLC phosphorylation by compound **85**, cells were treated with the specific ROCK inhibitor Y27632. Similar to what was previously published for CA4P,[47] the induction of MLC phosphorylation by compound **85** was abrogated by the Y27632. This confirmed the involvement of ROCK in the activation of MLC phosphorylation by compound **85** (*Figure 40 C*).

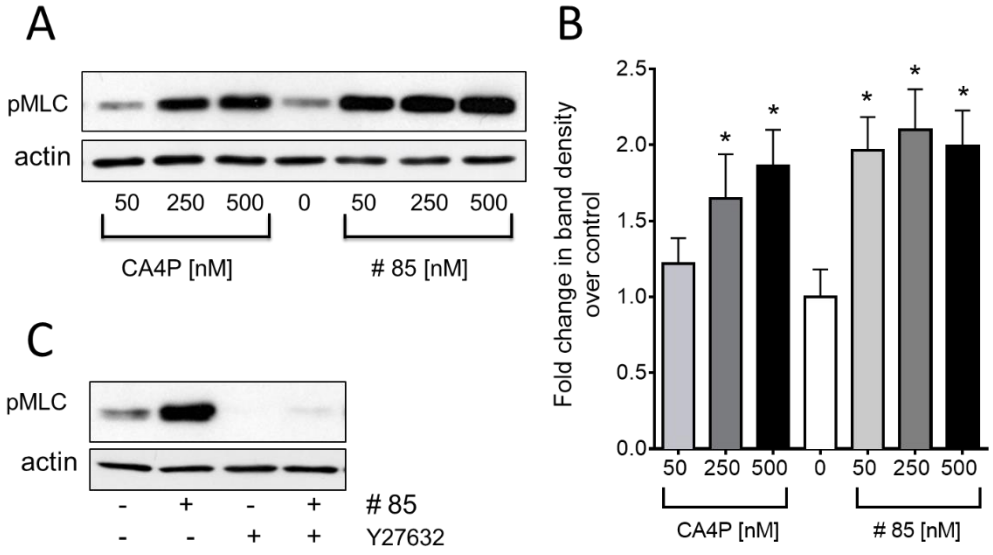

Figure 40. Drug-Induced induction of phosphorylation of Rho kinase target MLC. HUVECs were treated with increasing concentrations of CA4P or drug **85** for 15 minutes after which proteins were extracted and analysed for phosphorylation of Rho kinase target myosin light chain by western blotting using an antibody specific to the phosphorylated form of the protein (A). Immunoblots were reprobed with an antibody to actin to confirm equal loading. In B, pMLC band intensities were analysed by ImageJ and results are were expressed as fold-increase over control cells treated with vehicle alone. Each column represents the mean of 3-4 independent cell culture experiments±SEM. Data were analysed

by one way-Anova. *$P < 0.05$ significant difference between control vehicle treated cells. In C, HUVECs were incubated with Rho kinase inhibitor Y27632 (5 μM) for 5 minutes and then treated with 500 nM drug **85** for 15 minutes (B). Proteins were extracted and analysed for MLC phosphorylation as in A.

6.6: Studies of *in Vivo* Efficacy

Finally, the efficacy of **85** was assessed *in vivo*. As with the sydnone-based compound, all animal work was carried out by Mr. Matthew Fisher, who had obtained all necessary licenses and training for work with mice. The animals were implanted subcutaneously with SW1222 cells, similarly to the sydnone analogue. An escalated maximum tolerated dose study was conducted and **85** was found to have an MTD greater than 162 mg/kg (0.454 mmol/kg). With a safe threshold established, animals were treated with CA4P (100 mg/kg, 0.227 mmol/kg) or a solution of **85** (81 mg/kg, 0.227 mmol/kg) and necrosis levels in the tumours scored 24 hours post treatment by Chalkley grid method.[147] CA4P treated tumours instigated a significant increase in levels of necrosis. Tumours treated with **85** showed a tendency toward increased necrosis levels, however the results were not statistically significant (*chart 6*). CA4P appeared to exhibit greater variability in necrosis levels with multiple tumours showing no response upon treatment. Maximum response was higher for CA4P, but over one third of the treatment group failed to respond. In contrast, treatment with **85** resulted in much less variation, with 11% (a single tumour) failing to respond. It is of particular note that **85** appeared to be effective *in vivo* without further derivatisation for water solubility and successfully reached and had an effect on the tumours – a result supporting the hypothesis that pyrazole-based analogues of CA4 could not only be effective vascular disrupting agents, but also improve the PK/PD properties of CA4.

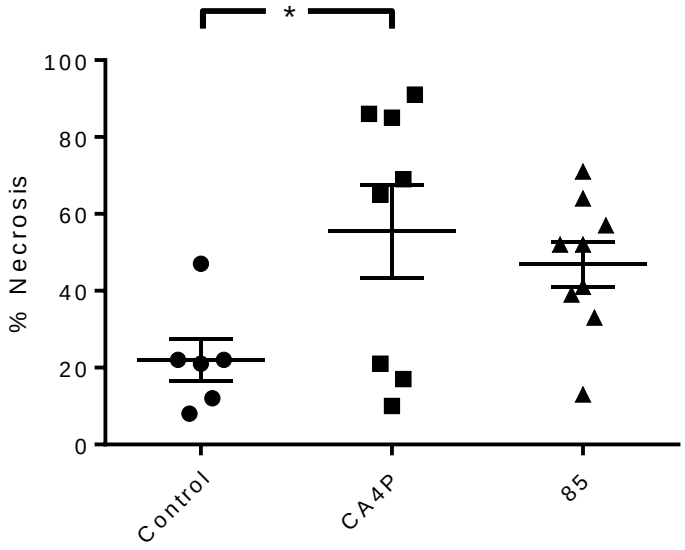

Chart 6: *In vivo* study of drug-induced effects on tumour cell necrosis comparing CA4P and **85**. Each point represents the combined data from a single tumour. 5 sections (cut at different tumour depths) were analysed per tumour using a x20 objective on a Nikon Eclipse TS100 microscope microscope. The total section was analysed and % necrosis

calculated in each field from the relative number of points in a Chalkley eyepiece graticule co-incident with necrotic versus viable tumour tissue. Bars represent the mean±SEM of the combined data for each tumour. Data were analysed by one way-Anova. *$P < 0.05$ significant difference between control vehicle

In conclusion, a number of pyrazole-based analogues of CA4 exhibited exciting activity *in vitro*. The most active compound, **85** was at least as potent as, or more active than CA4P in all *in vitro* assays conducted. Both CA4P and **85** were shown to disrupt microtubules and activate the same signalling pathway. At low doses, **85** significantly increased endothelial monolayer permeability relative to CA4P. **85** was shown to bind reversibly to tubulin and cells treated with the compound required more time to recover than from treatment with CA4P. Furthermore, the high *in vitro* activity observed was translated to *in vivo* activity. CA4P and **85** performed similarly well in the mouse model used, but only CA4P significantly increased tumour cell necrosis. Future studies should aim to further optimise the physical properties of the compound class. Further substitution of the pyrazole core could be examined and safety trials conducted.

Chapter 7: Directed Cycloaddition Reactions of Sydnones with Alkynyltrifluoroborate Salts

7.1: Introduction to Directed Cycloaddition Reactions

Although cycloaddition reactions of sydnones have been shown to be quite versatile in the preparation of novel pyrazole libraries, the reactions do present challenges. Typically, they require high temperatures over extended periods of time and a careful choice of substrate for high regioselectivity. Taran *et al.* have sought to address these issues by the use of copper catalysis with great success.[113,115] However, the reactions continue to be restricted to terminal alkynes and *N*-arylsydnones. An alternative approach to tackling the issues of high temperature and reaction time has been to utilise a Lewis acid-base complex-induced promotion of the process (*scheme 56*). A Lewis basic directing group can coordinate to a Lewis acidic handle on the alkyne partner to form the Lewis acid-base complex, which can then undergo cycloaddition. This strategy has a number of advantages; firstly it has the potential to lower the temperatures required for cycloaddition, secondly the reactions are regiospecific and finally, judicious choice of Lewis acidic handle opens possibilities for further product elaboration.

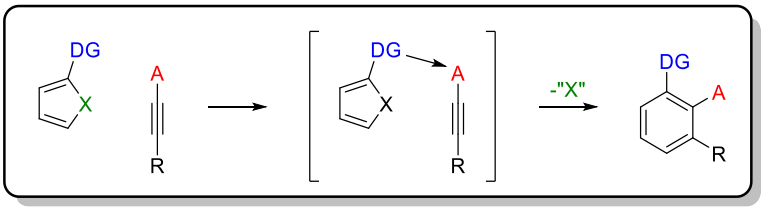

Scheme 56: General scheme for directed cycloaddition reactions.

Harrity *et al.* reported the first successful application of this principle with the cycloaddition of 1,2,4,5-tetrazines with *in situ* generated Lewis acidic alkynylboranes to form pyridazines (*scheme 57*).[152] Remarkably, reaction times and temperatures were reduced from 6 hours at 140 ^{o}C for the thermal reaction, to 10 minutes at room temperature when the directed cycloaddition strategy was employed (*scheme 57*). Alkynyltrifluoroborate salts, in the presence of trimethylsilylchloride, were employed for the *in situ* generation of the Lewis acidic cycloaddition partner.

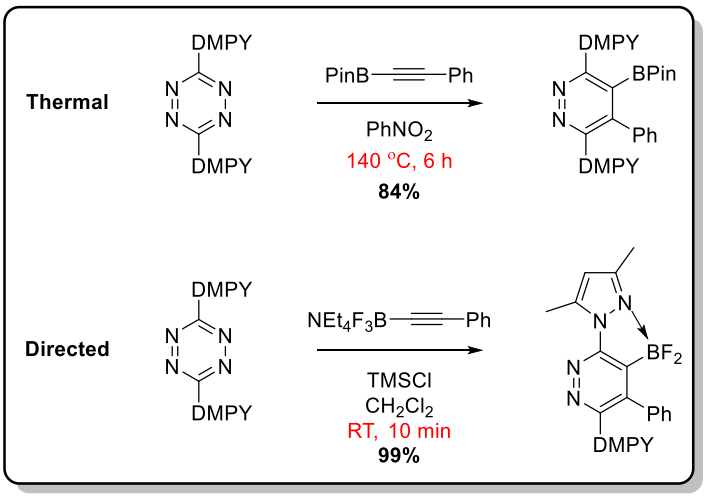

Scheme 57: Comparison of thermal cycloadditions of 1,2,4,5-tetrazines with directed cycloadditions.

Tetrazines are rather reactive dienes and so the chemistry was extended to less activated substrates by the successful application to 2-pyrones.[153] Typically, thermal cycloadditions of 2-pyrones require activating groups and temperatures of 170-180 °C. The reactions also suffer from variable levels of regiocontrol.[154] Under directed cycloaddition conditions the reactions were complete in 10 minutes at 40 °C with total regiocontrol (*scheme 58*). A variety of directing groups were compatible with the reaction conditions including thiazole and oxazole motifs. Perhaps the most attractive was the success of an amide directing group. However, esters were not effective as directing groups in the reactions.

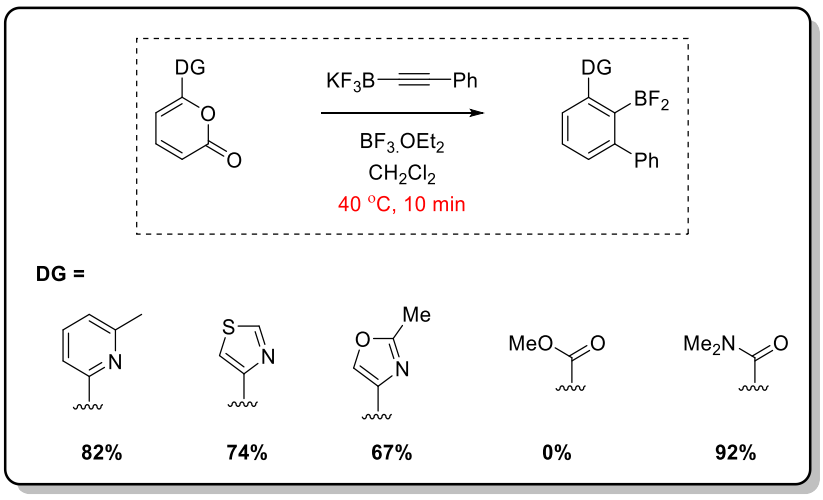

Scheme 58: Directed cycloaddition of 2-pyrones with alkynylboronates.

A particularly interesting finding was the isolation 3 different products during optimisation (*scheme 59*). Conducting the reaction at 0 °C resulted in the formation of the expected difluoroborane **118**, and the unusual fluoroalkynylborane **119** and dialkynylborane **120** in

2:1:1 ratio. Initial investigations into the formation of **119** and **120** found that they could not be formed from the difluoroborane and it was postulated that the compounds originated from competitive cycloadditions.

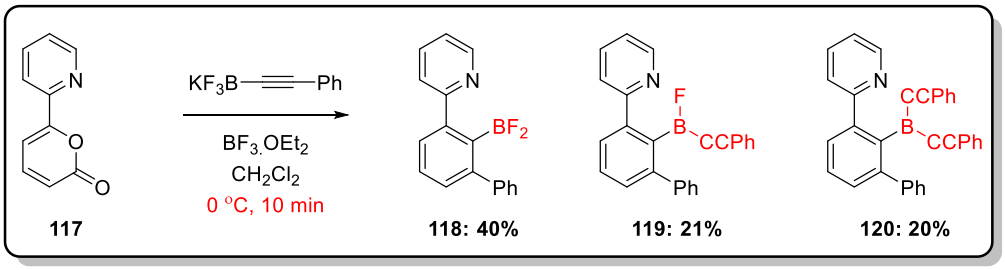

Scheme 59: Product distribution in 2-pyrone reactions at low temperature and short reaction times.

The unusual result prompted investigation into the mechanism of the reaction. Harrity and Meijer *et al.* undertook density functional theory (DFT) investigations as well as practical experiments.[155] The studies revealed a number of interesting subtleties in the reactions. Firstly, the formation of trisalkynylborane **123** is favoured under the reaction conditions and it was therefore likely that trisalkynylboranes were the 2π cycloaddition partners in the reactions (*scheme 60*). This implied that the initial cycloadduct in the reaction was dialkynylborane **124** and that this then underwent disproportionation to difluoroborane **125**. A further insight from DFT studies was that the reactions appeared to be asynchronous, with a build-up of negative charge on the carbon connected to the boron. This proceeded to initiate a nucleophilic attack at the pyrone *C*2, followed by completion of the formal cycloaddition. The large build-up of negative charge appears logical, as once coordinated to the directing group, the alkynylborane is formally a borate and therefore similar to an organometallic nucleophile in character.

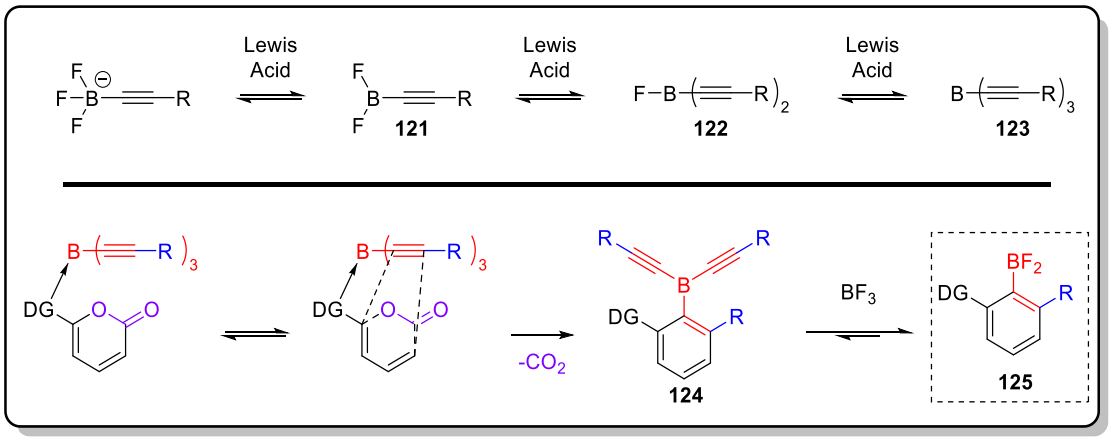

Scheme 60: Mechanism of directed cycloaddition of 2-pyrones.

In order to test the hypothesis, trisalkynylborane **125** was prepared *in situ* by the method described by Siebert *et al.*[156] then reacted with pyrone **117** to afford dialkynylborane **126** in 95% yield (*scheme 61*). Subjection of **126** to boron trifluoride in dichloromethane led to quantitative formation of difluoroborane **127**, supporting the hypothesis that trisalkynylboranes were the key reactive intermediates in the chemistry.

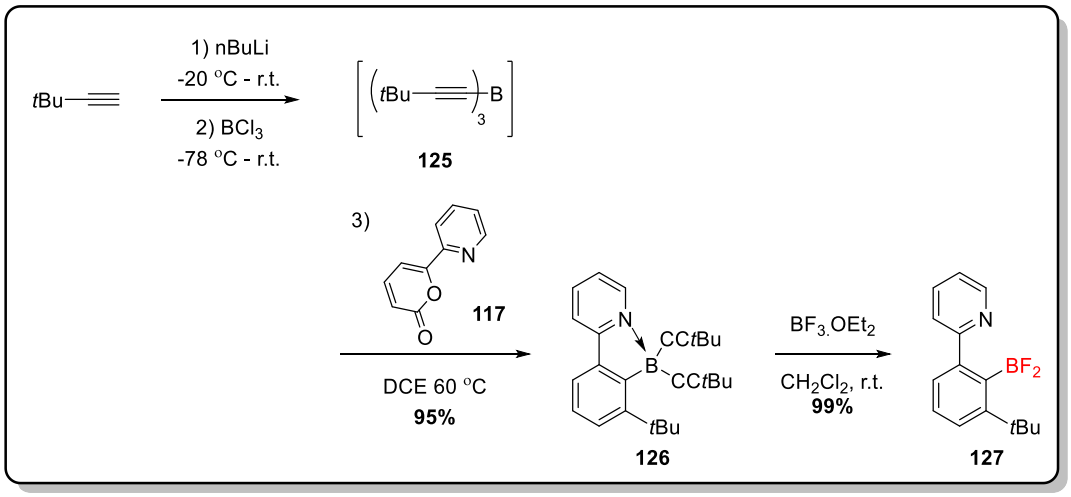

Scheme 61: Mechanistic evidence for disproportionation of products.

A further extension of the methodology was developed with the successful directed cycloaddition of alkynylaluminium reagents (*scheme 62*).[157] The arylaluminium reagents generated could not be isolated, but offered potential for further elaboration.

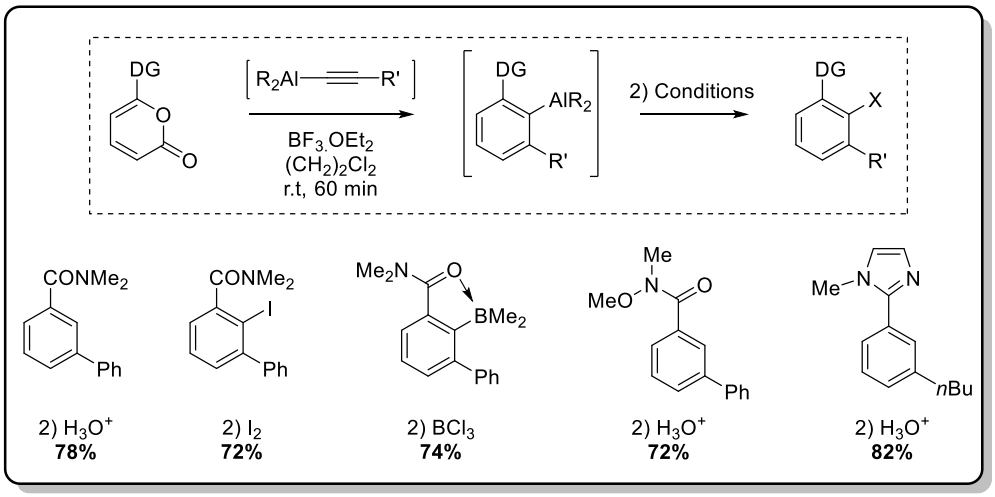

Scheme 62: Directed cycloaddition of 2-pyrones with alkynylaluminium reagents.

Very recently, the chemistry was applied to cycloadditions with 1,2,4-triazines.[158] Once again, significant enhancements in rate of reaction and a dramatic reduction in the temperatures required were observed (*scheme 63*).

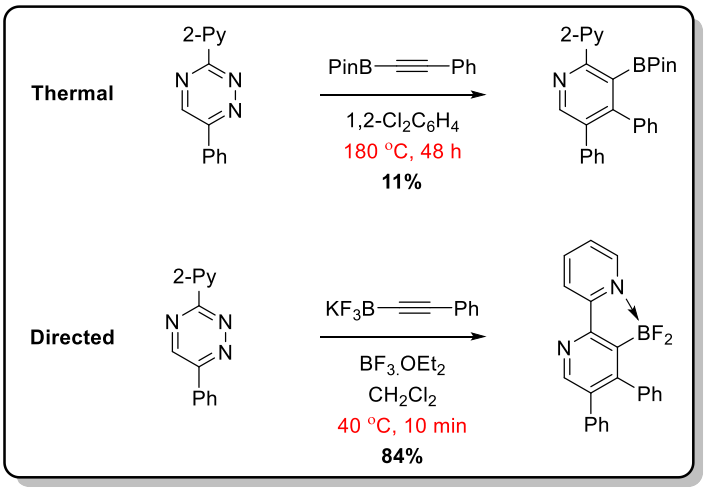

Scheme 63: Comparison of thermal cycloadditions of 1,2,4-triazines with directed cycloadditions.

7.2: Application of Directed Cycloaddition Reaction to Sydnones

Initial Results and Optimisation

With the previous success of directed cycloadditions with other substrates, application of the methodology to sydnones was attempted. The improved direct arylation methodology developed (*vide infra*) afforded access to scalable quantities of 4-(2-pyridyl)sydnones. Access to these sydnones was very difficult with previously developed methods, hence limiting attempts to extend directed cycloadditions to sydnones. The use of sydnones in this chemistry did present some significant challenges. 5-Membered rings had never been used before in directed cycloadditions. Furthermore, for the reaction to be successful, two nucleophilic components would need to react with one another (*scheme 64*). Nevertheless, work began with the preparation of model substrate 4-(2-pyridyl)-*N*-phenylsydnone **128**. Standard direct arylation conditions furnished sydnone **128** in quantitative yield on gram scale (*scheme 65*).

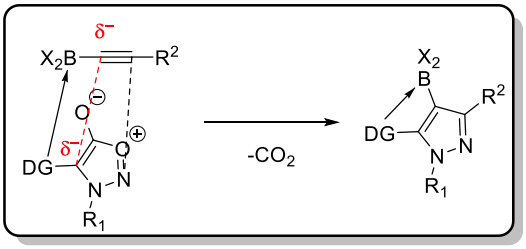

Scheme 64: A possible inherent problem in reactivity.

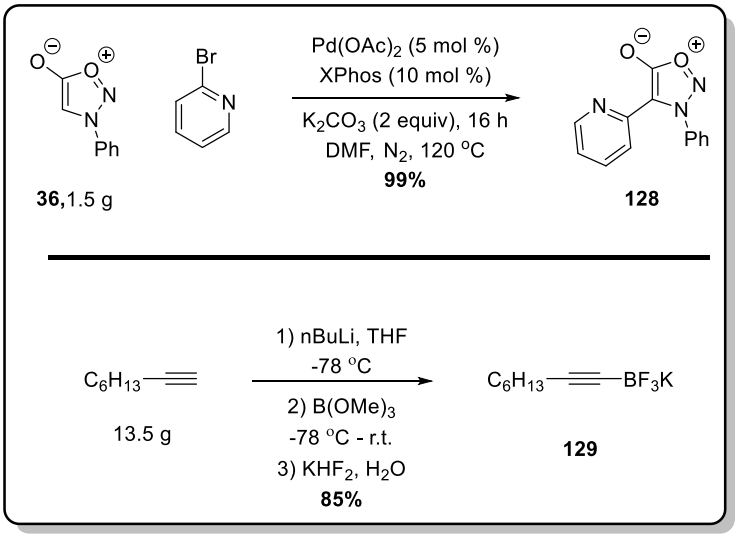

Scheme 65: Multigram scale starting material synthesis.

Alkynyltrifluoroborate **129** was prepared on multigram scale using previously established methods (*scheme 65*).[159] With access to large quantities of both model substrates, work

began to establish optimal reaction conditions. Application of optimal reaction conditions for 2-pyrones to sydnone **128** and alkyne **129** led to a highly surprising result. The reaction was monitored by TLC analysis and immediately a new, highly fluorescent blue spot appeared. Between 2 – 3 hours the relative intensity of this spot and the spot corresponding to sydnone **128** appeared unchanged. After work-up, the expected difluoroborane product **130** was not observed - the crude ^{1}H NMR spectrum only contained signals corresponding to dialkynylborane **131** and sydnone **128** in a roughly 3:1 mixture (*scheme 66*). Intrigued by this result, attempts were made to optimise toward **131** (*table 10*). It is important to note the stoichiometry of the reaction is 3:1 in terms of alkyne:sydnone (*scheme 67*). Therefore, three equivalents of alkyne and three equivalents of Lewis acid form one theoretical equivalent of trisalkynylborane. Conversely to previous examples, where the product could undergo disproportionation to the difluoroborane, the amount of alkyne available for reaction was limited solely to the theoretical equivalents of trisalkynylborane. With this detail in mind, optimisation began by increasing the reaction temperature to 60 °C, but this did not improve conversion (*entry 2*). Interestingly, reduction in temperature to 25 °C also had negligible impact (*entry 3*). Next, stoichiometry of boron trifluoride was reduced to 1.1 equivalents and the reaction left for 16 hours. This resulted in negligible alteration of conversion (*entry 4*). This indicated that the theoretical equivalents of trisalkynylborane were indeed important. To further probe this theory, alkyne loading was increased to 4 and 5 equivalents whilst maintaining boron trifluoride at 1.1 equivalents. These experiments afforded similar results to 3 equivalents of alkyne (*entries 5 and 6*). These results appeared to rule out decomposition of some of the alkyne starting material resulting in lower yields. Increasing the amount of alkyne and boron trifluoride to four equivalents each resulted in an increase in conversion, providing further evidence that theoretical equivalents of trisalkynylborane were important (*entry 7*). Excitingly, further increase to 5 equivalents of alkyne and Lewis acid afforded full conversion and an isolated yield of 100% in only 30 minutes (*entry 8*). An increase to six equivalents yielded a similar result (*entry 9*). Reducing equivalents of boron trifluoride to two slowed down the reaction, but quantitative yield was achieved in two hours (*entry 11*). The reaction was scalable to 5 mmol and also afforded **131** quantitative yield.

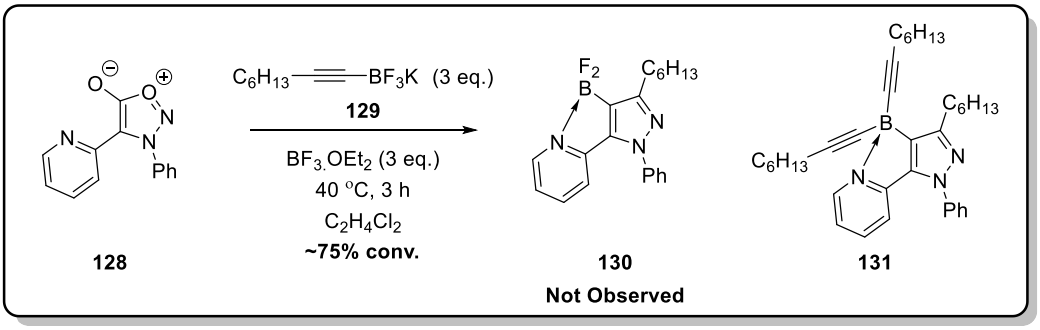

Scheme 66: Application of 2-pyrone standard conditions to sydnones.

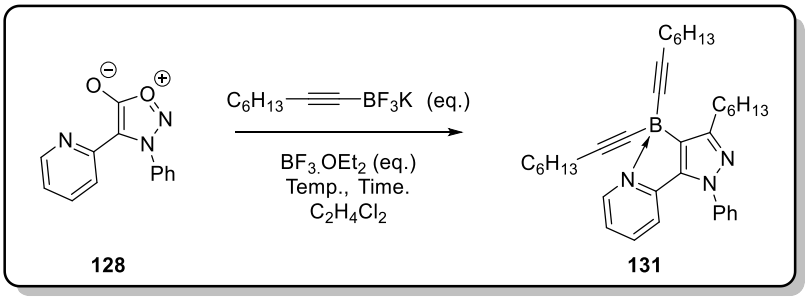

Entry	Eq. Alkyne	Eq. $BF_3.OEt_2$	Theoretical Eq. Borane	Temp. (°C)	Time (h)	Ratio[a]
1	3	3	1	40	3	75:25
2	3	3	1	60	3	70:30
3	3	3	1	25	3	70:30
4	3	1.1	1	25	16	65:35
5	4	1.1	1.1	25	16	65:35
6	5	1.1	1.1	25	16	65:35
7	4	4	1.3	25	3	85:15
8	5	5	1.7	25	0.5	100:0 (100%)[b]
9	6	6	2	25	0.5	100:0 (99%)[b]
10	5	2	1.7	25	3	100:0 (100%)[b]
11	**5**	**2**	**1.7**	**25**	**2**	**100:0 (100%)[b]**
12	5	2	1.7	25	1	90:10

a) Ratio of product:starting material in the crude reaction mixture as judged by ^{1}H NMR. b) Isolated yield of purified material.

Table 10: Optimisation of reaction conditions.

A particularly interesting observation can be made about the reactions with one theoretical equivalent of trisalkynylborane. If one considers the reaction conversion (*table 10, entries 1-6*), it is apparent that average conversion is roughly 67%. It was proposed that this could be indicative of a stoichiometry of $^2/_3$. However, this appears to contradict the proposed mechanism and also the stoichiometry proposed in scheme 67. Inevitably, the isolation of dialkynylboranes as the only reaction products was a key factor in the observed conversions and different reaction requirements to other substrates. The reasons for the isolation of

dialkynylboranes as the sole products is discussed later. Critically, if the product disproportionation from the dialkynylborane to the difluoroborane were not possible, stoichiometry of the reaction would be solely dependent on the amount of trisalkynylborane available to react (3:1 stoichiometry). Alternatively, if the dialkynylborane was the thermodynamic product, the stoichiometry of alkyne to product would also be 3:1. Therefore, the difference in isolated products, linked to a variation in kinetics or thermodynamics of the sydnone system, has instilled different stoichiometric constraints on the directed cycloaddition. However, although this has provided a basis for different reaction stoichiometry, it cannot alone explain the observed conversions. The implications of these observations and mechanistic studies are discussed later.

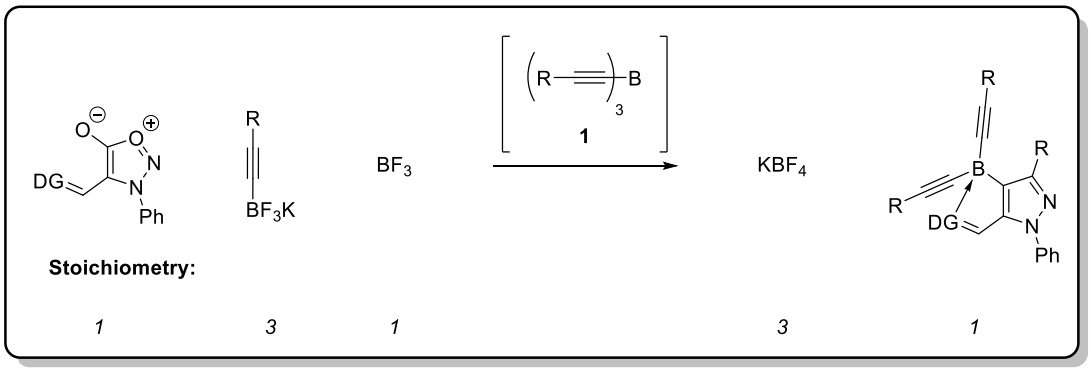

Scheme 67: Reaction stoichiometry.

7.3: Investigation of Reaction Scope and Further Functionalisation

With optimum reaction conditions in hand, work began on the preparation of substrates for a reaction scope. Firstly, compounds that would probe the effect of directing group were prepared. Direct arylation provided a range of 2-pyridyl substrates (**132** – **137**) and 4-thiazole **138** in good yields (*scheme 68*). Unfortunately, 4-oxazole **139** and imidazoles, **140** and **141**, could not be prepared by this methodology. Sydnone starting material was recovered in the unsuccessful cases, but no trace of aryl bromide was recovered.

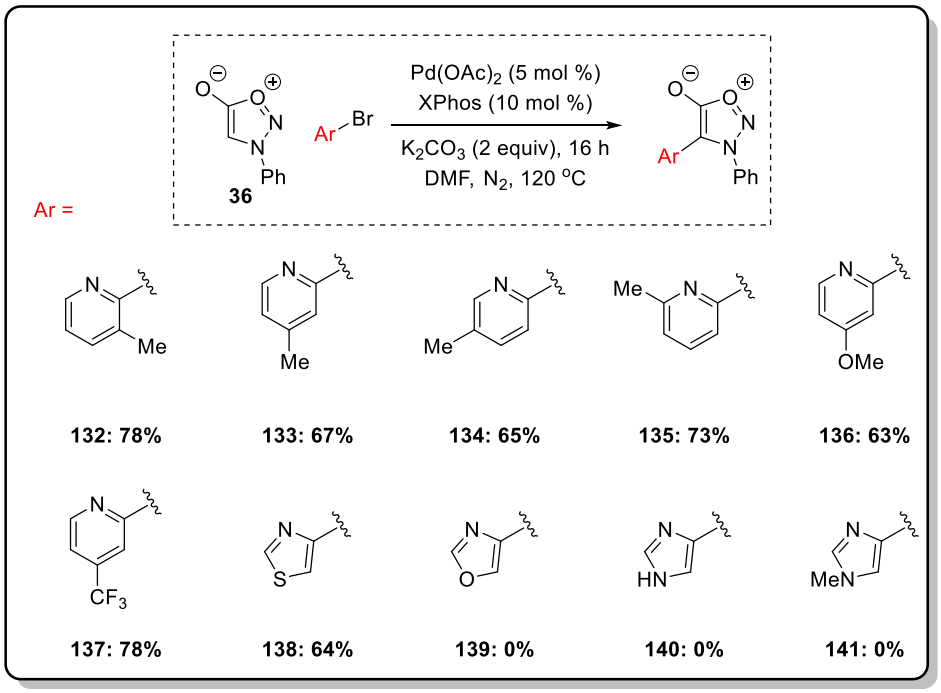

Scheme 68: Synthesis of starting materials containing heteroaryl directing groups.

In an attempt to expand from heteroaryl directing groups, further substrates were prepared. Carboxylic acid **142** was prepared by the reaction of lithiated sydnone with solid carbon dioxide (*scheme 69*). Concurrent screens within the group had shown carboxylic acids and carboxylate salts to be unsuccessful directing groups. Amides had been successful directing groups for previous substrates in directed cycloadditions,[155] hence, Weinreb amide **143** was prepared from acid **142**. Harrity *et al.* recently reported the use of further acid derivatives, oxazolines, as directing groups in *C-H* amidation.[124] It was therefore proposed that oxazolines could also act as directing groups for directed cycloaddition chemistry. Oxazoline **145** was also prepared from acid **143**, by amidation followed Appel-like cyclisation. The 6-membered oxazine variant was also targeted for synthesis. Oxazine **147** was also prepared from acid **142**, by amidation followed dehydrative cyclisation. Alternative cyclisation strategies were attempted, but failed to afford the target material in improved yield (*scheme 70*). The major

product isolated in the reactions was chloride-substituted amide **148**. Exhaustive attempts were made to cyclise amide **148**, however formation of oxazine **147** was never observed in any of the reactions attempted. This indicated that chloride **148** was not an intermediate in the formation of oxazine **147**, but a stable, competitive by-product.

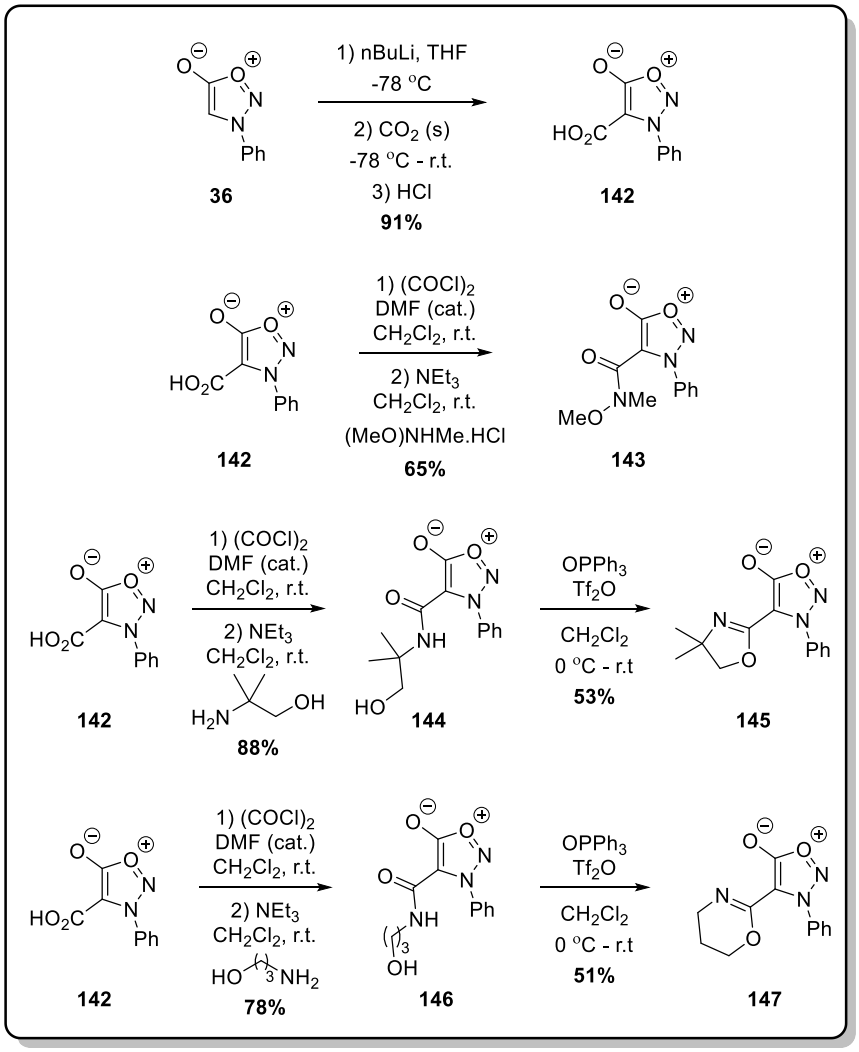

Scheme 69: Synthesis of starting materials containing alternative directing groups.

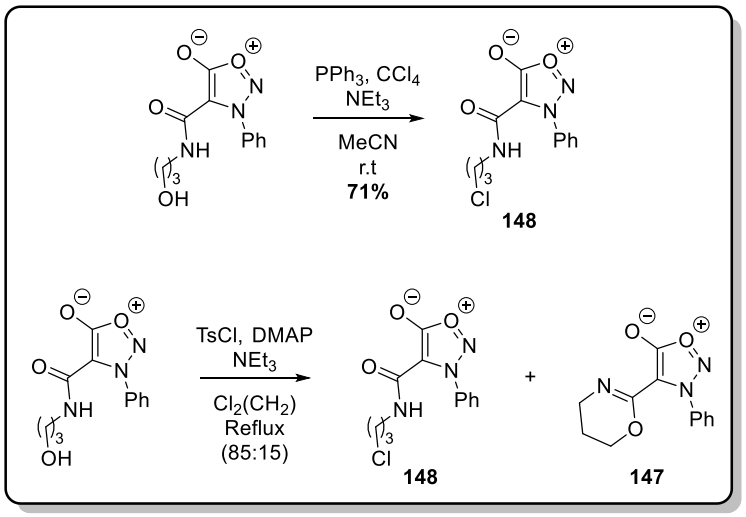

Scheme 70: Attempted alternative cyclisation strategy.

With a reasonable number of substrates containing a variety of directing groups in hand, attention was turned to their reactivity in the directed cycloaddition reactions. Pleasingly, substitution at all positions of the pyridine was well tolerated (*scheme 71,* **149** *to* **154**). Use of an electron donating methoxy group afforded quantitative yield of **153**. As expected, incorporation of a trifluoromethyl substituent *para* to the nitrogen retarded the reaction somewhat and led to a slightly lower isolated yield of **154**. Disappointingly, 5-membered heterocycles appeared unreactive to the directed cycloaddition. 4-Thiazole substrate **138** only exhibited trace reactivity at elevated temperatures of 40 ^{o}C. This result was particularly disappointing as 5-membered heterocycles had been shown to be competent directing groups for both tetrazines and 2-pyrones.[152,153] The lack of reactivity with sydnones can perhaps be explained by the strain associated with the transition state required to access the cycloadduct intermediate **159** (*scheme 72*). The intermediate consists of five fused rings. In the case of the cycloadduct **159**, four of the five fused rings are 5-membered rings. The ideal bond angles in a 5-membered are 108^{o}, whereas in a 6-membered ring they are 120^{o}. A higher number of small internal angles increases strain in the fused system. Therefore, the more 5-membered rings in the fused system, the more strain the system experiences. Changing from a 5-membered to a 6-membered directing group changes the form of the cycloadduct to only having three of the five fused rings as 5-membered rings **160**. This system readily undergoes directed cycloaddition. Conversely to **159**, thiazole was a successful directing group in the 2-pyrone cycloadditions. The cycloadduct **161** arising from this cycloaddition contains only two 5-membered rings in the fused system.

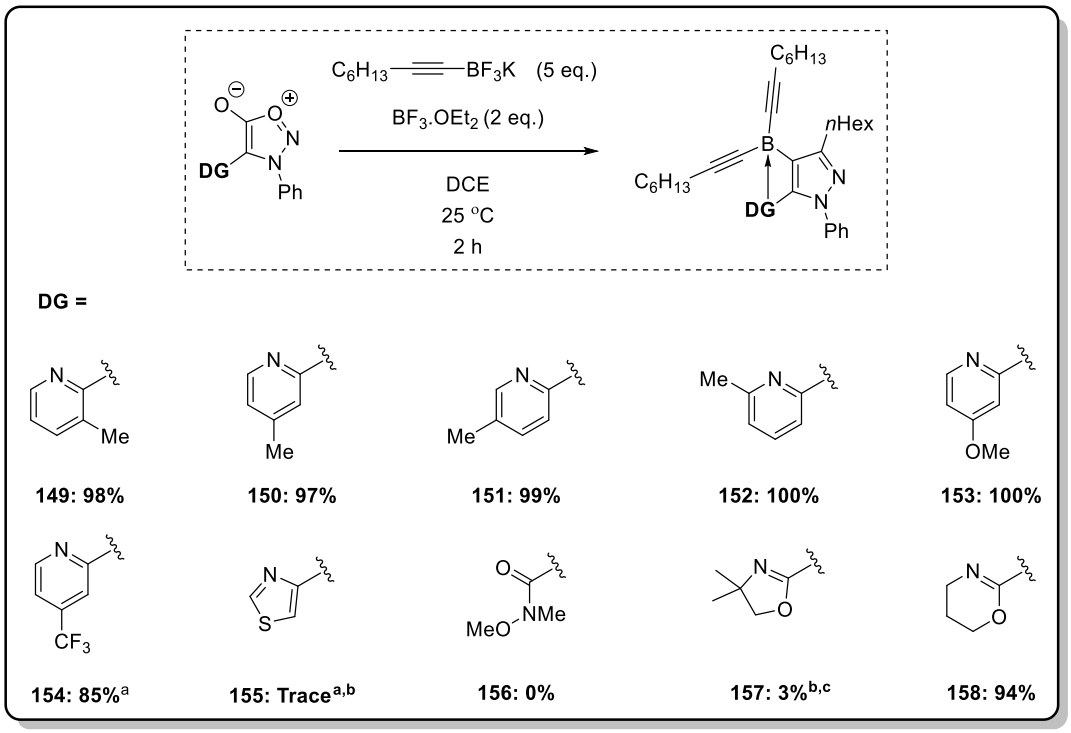

Scheme 71: Scope of directing groups in directed cycloaddition.

Unfortunately, Weinreb amide **143** did not facilitate cycloaddition. An extensive screen of amides was conducted within the group and all examples afforded similarly poor results. Oxazoline **145** a resulted in an extremely low yield of the corresponding boronic acid **157**. An interesting subtlety in this case was that the crude reaction mixture did not display any evidence of the product **157** as judged by ^{1}H NMR. The final product was therefore being formed during chromatographic purification. An extremely positive outcome came with the success of oxazine to form **158**, demonstrating that it was possible to utilise non-aromatic directing groups. When compared with oxazoline **157**, this result provided further evidence for 5-membered ring directing groups being problematic in the reaction system.

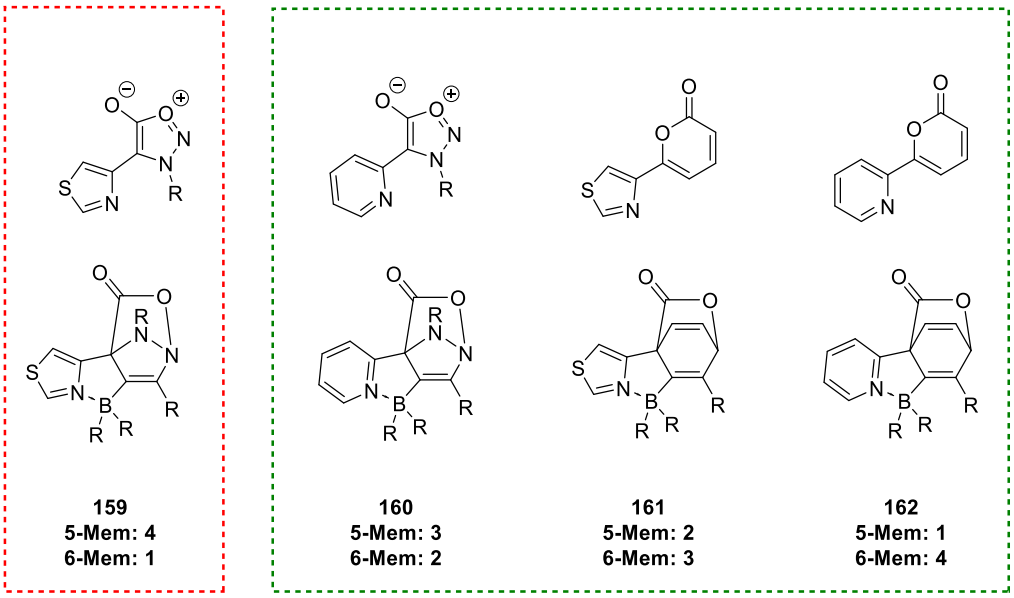

Scheme 72: Structure of cycloadducts of various substrates. Green box: successful in reaction. Red box: unsuccessful in reaction.

After the directing groups were screened, it was decided to examine the scope with respect the *N*-substituent of the sydnone and the scope with respect to the alkyne. Firstly, a small selection of sydnones were prepared bearing various groups on the *N*3 position (*scheme 73*). Good yields were achieved for the preparation of 4-(2-pyridyl)-*N*-(4-$MeOC_6H_4$)sydnone **163** and 4-(2-pyridyl)-*N*-(4-FC_6H_4)sydnone **164**. A slightly diminished yield of *N*-methyl substrate **165** was obtained from the direct arylation reaction and unusually low yield was also obtained of *N*-benzylsydnone **165**. Attempted optimisation for improved yields was met without success, but significant quantities of starting sydnone were recovered in all cases. Although *N*-benzylsydnone has often been the least reactive partner in direct arylation reactions, in most cases at least moderate yields were obtained (*vide infra*). In this case, *N*-benzylsydnone and 2-bromopyridine appeared to be mismatched as coupling partners. In spite of low yields in the starting material synthesis, enough material was isolated to examine the reactivity of the substrates in directed cycloadditions.

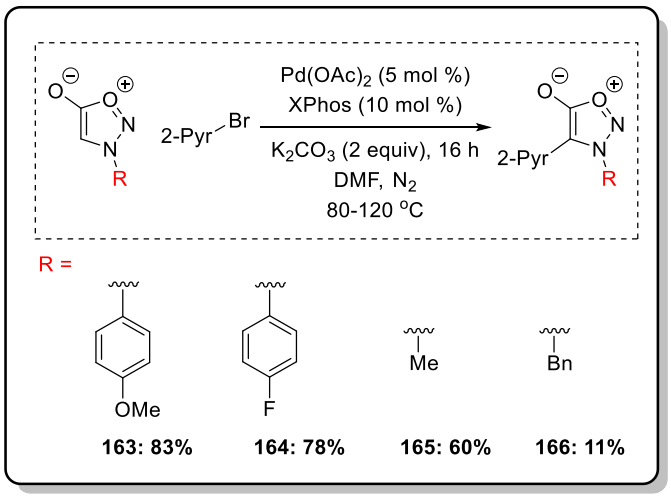

Scheme 73: Synthesis of starting materials containing different nitrogen substituents.

N-Arylsydnones **163** and **164** reacted smoothly under the optimised cycloaddition conditions, furnishing the corresponding pyrazoles **167** and **168** in excellent yields (*scheme 74*). *N*-Alkylsydnones **165** and **166** were slower to react and afforded the corresponding products in slightly diminished yields. *N*-Methylpyrazole **169** was particularly prone to protodeboronation and required rapid elution during purification to avoid product degradation. Turning attention to the scope of the alkyne, both phenylacetylene- and acetylene-derived trifluoroborates were suitable substrates. However, the terminal alkyne afforded lower yields. Increasing the number of alkyne equivalents used led to a small improvement in yield. Unfortunately, ynone derived trifluoroborates underwent rapid protodeboronation under the reaction conditions and were therefore unsuitable substrates. Pleasingly, crystals of pyrazole **171** were successfully grown from dimethylformamide and the structure successfully solved by X-ray crystallographic analysis (*figure 41*, hydrogen atoms omitted for clarity). The structure unambiguously confirmed the regiochemistry of the product, as well as highlighting the bond between the pyridine nitrogen and the boron. The latter having a tetrahedral arrangement. ^{11}B NMR spectroscopy had indicated the presence of the *B*-*N* bond, however the crystal structure offered more convincing evidence.

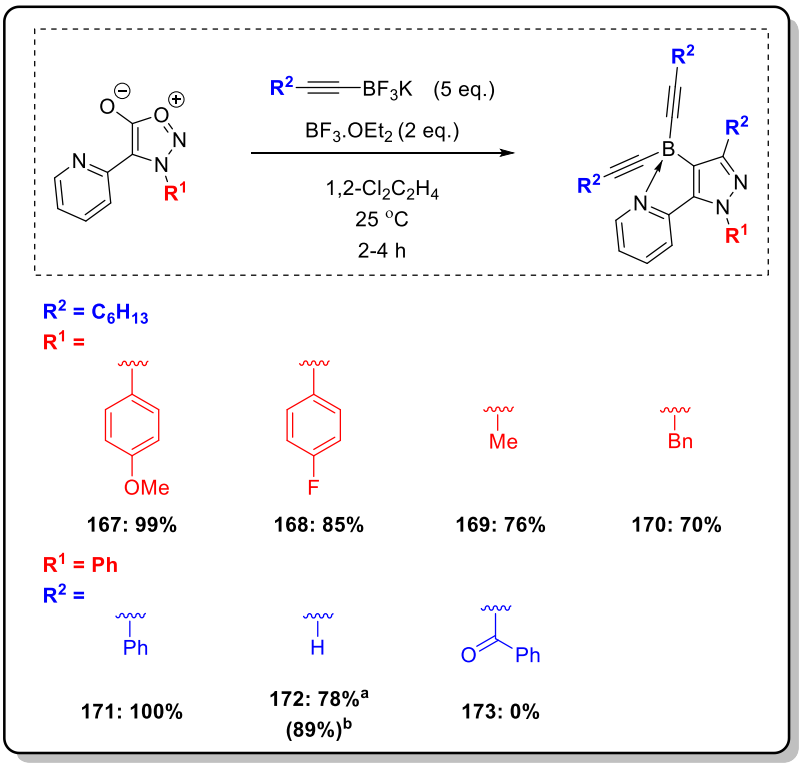

Scheme 74: Scope of *N*-substituent and alkynyltrifluoroborate.

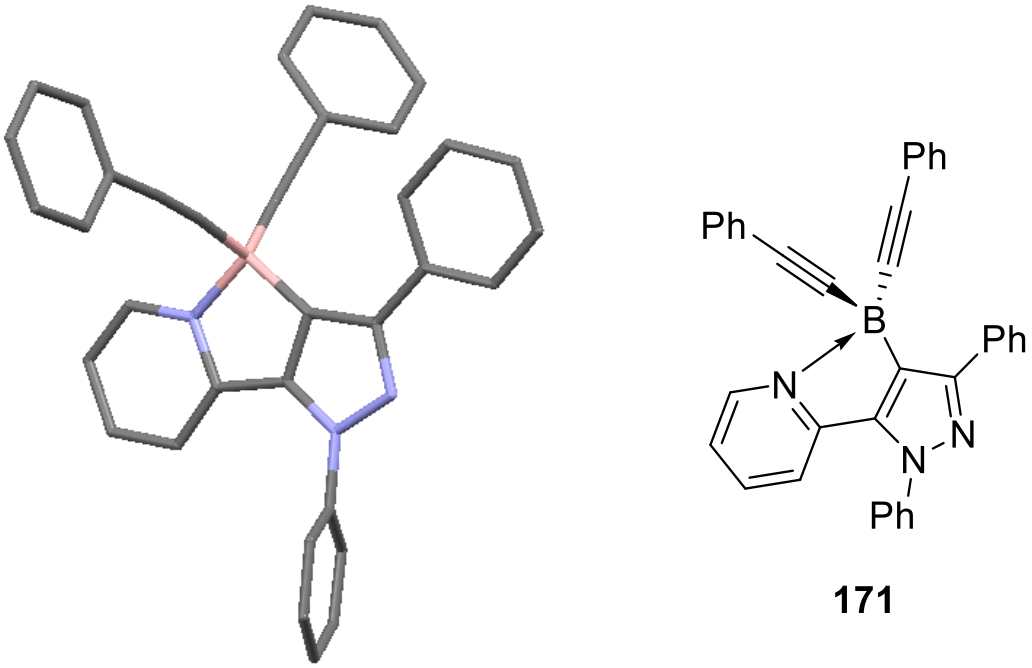

Figure 41: X-Ray crystal structure of **171**.

With the completion of a respectable substrate scope, attention was turned to the investigation of other reactivities. Dialkynylboranes had only previously been isolated as minor products and the reactivity of this unusual boron motif had not been investigated.

Firstly, conditions for protodeboronation were sought. Although often an unwanted side reaction, protodeboronation was successfully achieved in excellent yield using sodium carbonate in water:tetrahydrofuran at reflux (*scheme 75*). More interesting was the successful oxidation of the dialkynylborane. Gentle heating of **131** with hydrogen peroxide afforded aromatic alcohol **175** in very good yield. Dialkynylborane **131** was successfully transformed into the more conventional pinacol ester **176** in excellent yield when subjected to pinacol and caesium carbonate in tetrahydrofuran. Interestingly, on 50 mg scale sodium carbonate successfully promoted this reaction, however only trace reactivity was observed at 500 mg scale. Caesium carbonate promoted reaction both on small and larger scales, presumably due to its higher solubility in tetrahydrofuran. Arguably the most important reaction of organoboranes is Suzuki-Miyaura cross coupling. The reaction required some optimisation but, cross coupling was successfully achieved in the presence of 2nd generation XPhos palladium precatalyst and sodium carbonate in a mixture of 1:1 water:1,2-dimethoxyethane.

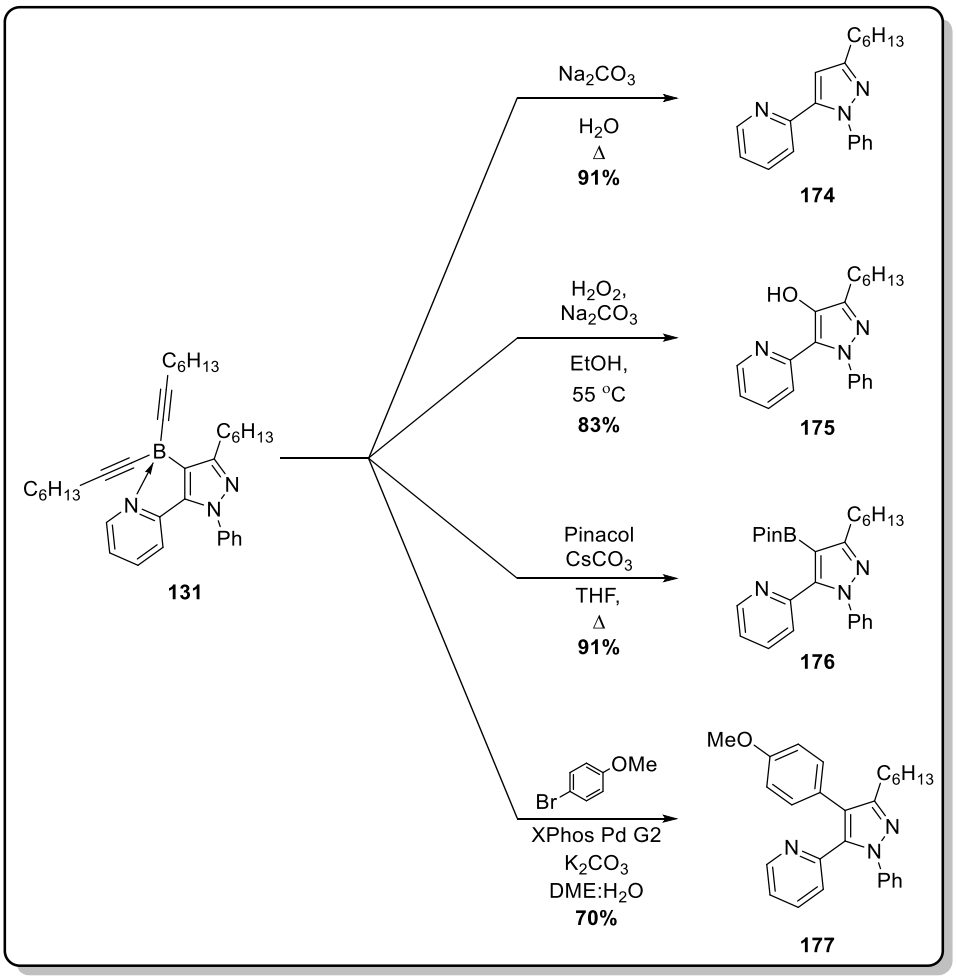

Scheme 75: Further functionalisation of dialkynylborane.

In an attempt to broaden the versatility of the chemistry, it was decided to probe the feasibility of hydrolysis of the oxazine motif. The model substrate for investigation was prepared *via* gram scale directed cycloaddition of **147**, followed by subjection of the crude isolated material to Suzuki-Miyaura coupling (*scheme 76*). This produced significant quantities of pyrazole **178** in 70% yield (9:1 product:protodeboronated product) over 2 steps.

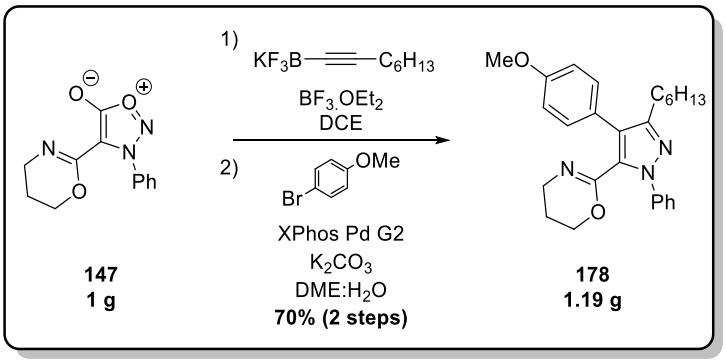

Scheme 76: Preparation of oxazine **178**.

6-Membered oxazines are less common in the literature than their 5-membered oxazoline counterparts. Nevertheless, there are various reports on the deprotection of oxazolines. Most common is acid mediated cleavage to the carboxylic acid,[160,161] therefore investigations began with this as the start point. Initially, encouraging results were obtained in refluxing hydrochloric acid. Chloride-substituted amide **179** was formed in moderate yield after 2 hours in refluxing 6 M hydrochloric acid (*scheme 77*). Subjection of amide **179** to the same conditions for 16 hours resulted recovery of starting material, with some loss of material to decomposition. Unfortunately, subjection of oxazine **178** to refluxing concentrated hydrochloric acid resulted in decomposition. A concern was raised when these results were compared to initial attempts at formation of oxazine bearing sydnone **147** (*vide infra*). Chloride-substituted amide by-product **148** was isolated in a number of cases, indicating it could be a thermodynamic sink. In order to eliminate the possibility of forming the chloride-substituted amide **179**, acid deprotection using H_2SO_4 according to Yu's protocol was attempted.[162] Unfortunately, the reaction mixture only showed evidence of decomposition and starting material (*scheme 77*). It appeared that the secondary amides were stable compounds and harsh conditions would be needed to cleave them to carboxylic acids, which would most likely destroy the pyrazole. Therefore, efforts were made to devise conditions that would avoid formation of the secondary amide.

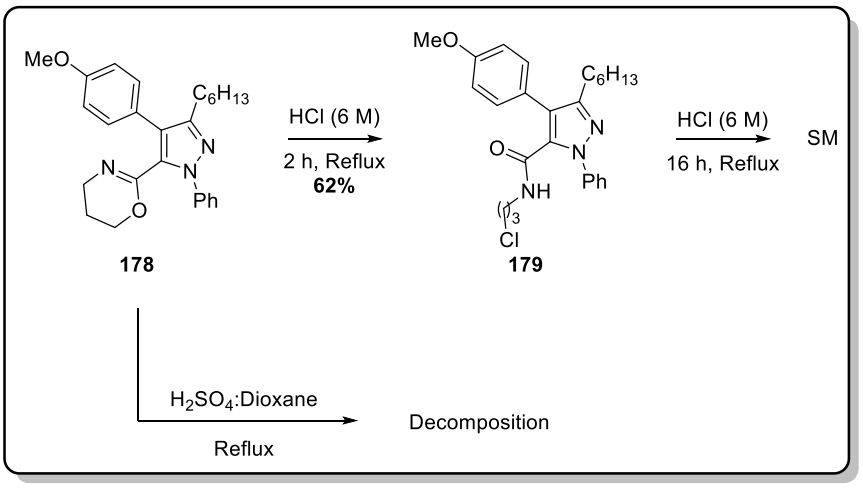

Scheme 77: Acid-mediated cleavage of oxazine.

Meyers and co-worker had previously shown that oxazolines could be reduced with sodium borohydride to the aminal.[163] Unfortunately, employing these conditions only resulted in recovery of starting material. The use of more reactive lithium aluminium hydride also failed to reduce the oxazine, with isolation of mostly starting material and some amide. Another common method for the deprotection of oxazolines is reaction with an electrophile followed by reaction with a base. In particular, methyl iodide has been commonly employed.[164] Unfortunately, only a poor yield of amide **180** was isolated from the reaction (*scheme 78*).

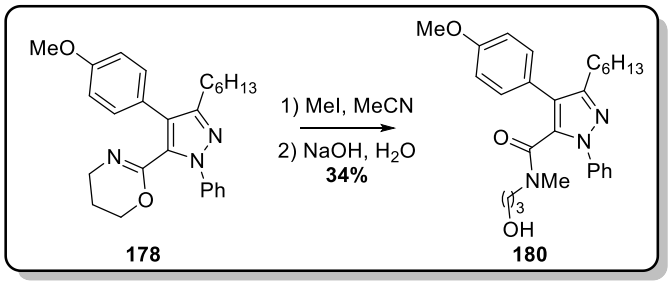

Scheme 78: Methylation/hydrolysis of oxazine.

Pittman Jr. *et al.* recently reported the use of a similar methodology using for the cleavage of oxazolines.[165] By using acyl chlorides as the electrophiles, the oxazoline could be opened to the imide. It was hoped that the imide intermediate would be more reactive to hydrolysis than the amide. Initial attempts to apply this method focussed on a “one pot” protocol. Whereby, the bulky pivaloyl chloride was used as the electrophile, followed by refluxing in sodium hydroxide (*scheme 79*). Unfortunately, this strategy only afforded amide **179** in moderate yield and recovery of starting material. As a note, during the first step of the reaction the reaction solvent evaporated.

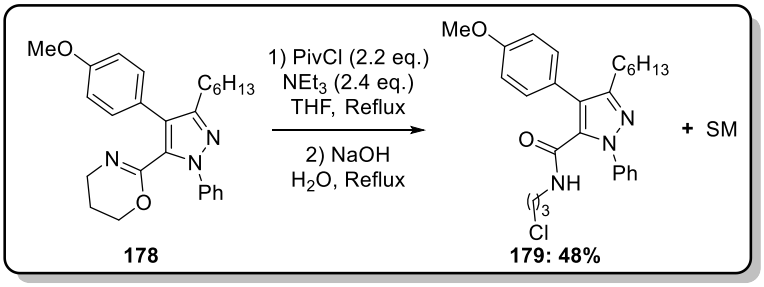

Scheme 79: Pivaloyl chloride activation/opening of oxazine.

It was therefore decided to isolate the imide before hydrolysis. A small screening of conditions was conducted (*table 11*). Initially, conditions were kept the same as for the one pot procedure resulting in excellent mass recovery, but an essentially 1:1:1 mixture of imide, amide and oxazine (*entry 1*). Again, the solvent evaporated in this instance. Interestingly, when the conditions were repeated but the solvent did not evaporate, only trace reactivity was observed (*entry 2*). Increasing the equivalents of pivaloyl chloride and base resulted in 24% yield of imide **181** (*entry 3*). Reaction with further increased equivalents of acid chloride and base as a neat mixture resulted in an improved yield of 35% (*entry 4*).

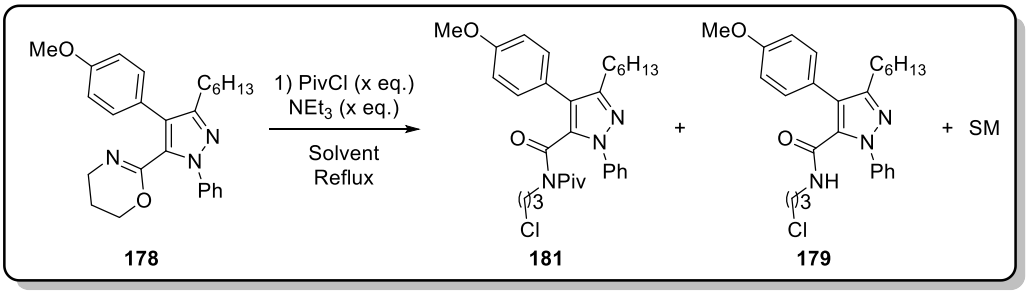

Entry	Eq. PivCl	Eq. NEt_3	Solvent	Imide 181[a]	Amide 179[a]	SM 178[a]
1	2.2	2.4	THF (Evaporated)	29%	27%	28%
2	2.2	2.4	THF	Trace	x	90%
3	5	5.5	THF	24%	Trace	60%
4	10	11	None	35%	x	39%

a) Isolated yields of purified material.

Table 11: Initial optimisation of formation of imide **181**.

Before further optimisation was carried out on the formation of imide **181**, proof of principle was sought for hydrolysis of the imide. Initial attempts with DIBAL-H were unsuccessful and only resulted in recovery of starting material. Surprisingly, use of lithium aluminium hydride resulted in solely reduction of the pivaloyl unit of the imide to afford amide **179** in 55% yield (*scheme 80*). The preferential reduction of such a bulky group over the target carbonyl

indicated that formation of any product other than the amide would be incredibly difficult. Therefore, it was decided to abandon the oxazine deprotection strategy.

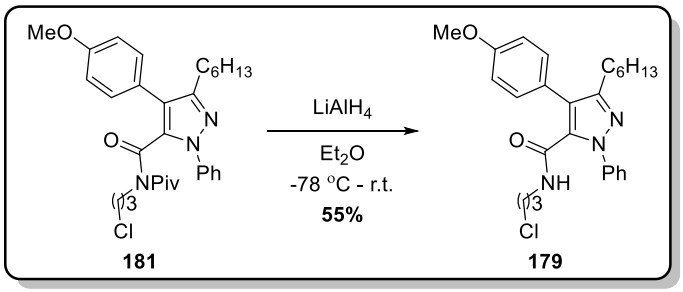

Scheme 80: Reduction of **181** with lithium aluminium hydride.

7.4: Mechanistic Studies and Investigations into Unusual Reaction Features

General Reactivity

When comparing directed cycloadditions of sydnones with previous directed cycloaddition substrates, three reaction features of the sydnone system were distinct:

- The requirement of five equivalents of alkyne for complete conversion
- The lack of reactivity of directing groups that were previously successful with 2-pyrones/triazines
- The isolation of dialkynylboranes as the only reaction products

Such stark differences in reactivity and product distribution indicated that the generally accepted mechanism for the reaction with 2-pyrones depicted above in scheme 60 was not valid for the reaction with sydnones. In other words, there were extra mechanistic components/constraints in the sydnone reactions that resulted in fundamental differences in reactivity. Firstly, the relative structural properties of the various starting materials and products were considered (*figure 42*). The most apparent structural difference is the ring size of the sydnone, which as mentioned earlier could possibly lead to extra strain in the cycloadducts. A further difference is the presence of Lewis basic groups (in addition to the directing group) in both the starting material and product from sydnone cycloadditions. In the previous substrates, only the triazine also contains extra Lewis basic groups in both the starting material and product. Extra Lewis basic groups could potentially bind to boron and either lead to stable complexes or sequester reactive Lewis acid intermediates. With key structural differences in mind, attempts were made to elucidate the source of reactivity differences.

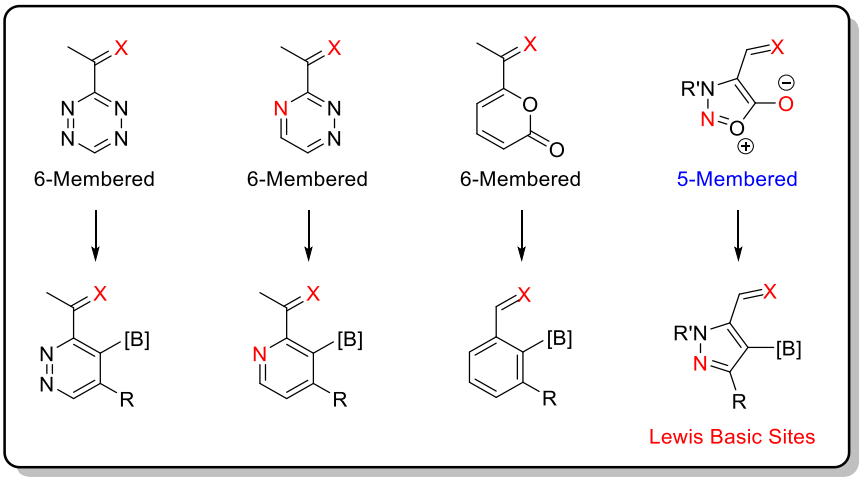

Figure 42: Directed cycloaddition substrate comparison.

In the sydnone system, both the exocyclic oxygen and *N*2 can potentially act as a Lewis base. Sutton *et al.* have previously calculated the net charges of a sydnone, pyridine and pyrazole using molecular orbital calculations (*figure 43*).[166] Interestingly, these data showed a significant amount of negative charge to be located on the exocyclic oxygen. It is therefore logical that the exocyclic oxygen could compete for Lewis acid with the directing group. It also follows that the pyrazole, when formed, could also compete for Lewis acid.

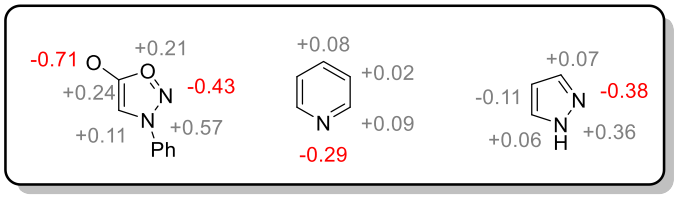

Figure 43: Calculated net charges of *N*-phenylsydnone, pyridine and pyrazole.

A particularly interesting report by Bregadze *et al.* detailed the formation of boron pincer complex **183** from azomethine **182** bearing a phenol (*scheme 81, A*).[167] Carbonyls were also shown to act in a similar manner to the azomethine. Very recently, Liu *et al.* reported difluoroborane pincer complexes derived from bipyridyl **184** containing an amine (*scheme 81, B*).[168] Pincer complex **185** was formed simply from treatment of **184** with $BF_3.OEt_2$ and NEt_3. The pincer portion of the molecule bears a striking resemblance to 4-pyridylsydnones and the reaction conditions were also similar. It was proposed that the sydnone bearing a directing group could form a similar complex with the trisalkynylborane resulting in the loss of acetylide. This type of reactivity could result in the observed conversions, but only if the acetylide lost could not regenerate an alkynylborane species. Furthermore, if certain pincer complexes were particularly stable, their formation could potentially explain substrates that fail to undergo cycloaddition e.g. amide **143**.

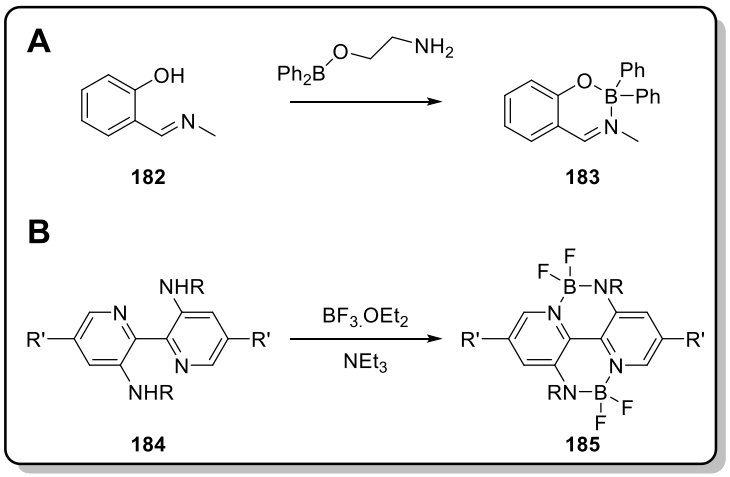

Scheme 81: Boron pincer complexes prepared by Bregadze and Liu.

A revised mechanism is proposed in scheme 82. After formation of trisalkynylborane, the stable, cationic pincer complex **187** is formed with the loss of acetylide. Disproportionation of **187** with BF_3 leads to the formation of **188** and dialkynylfluoroborane. Dialkynylfluoroborane is known to be short-lived and can undergo disproportionation to trisalkynylborane and BF_3.[155] Trisalkynylborane can then open the pincer complex **188** to afford cycloaddition precursor **189**. It is interesting to note that in this case, the Lewis acidic boron coordination to the exocyclic oxygen could further activate the sydnone to cycloaddition. Harrity *et al.* recently demonstrated Lewis acidic activation of sydnones with copper triflate.[116] Directed cycloaddition would then afford **190** with the loss of CO_2 and the liberated borenium cation quenched with the acetylide counter ion to form alkynyldifluoroborane. It is likely that the pyrazole *N*2 would rapidly form a stable Lewis acid/base complex with any available Lewis acid, which could have further implications in the reaction system (*vide infra*).

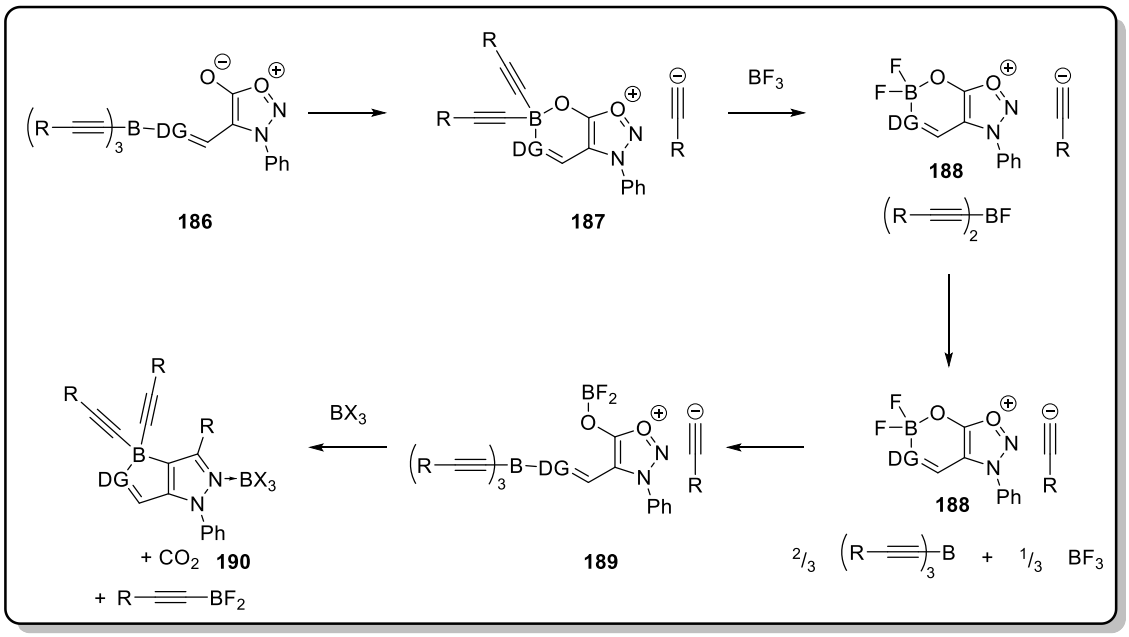

Scheme 82: Revised mechanistic proposal.

With a new mechanistic proposal in hand, attempts were made to find evidence for reaction intermediates. Because of the complexity of the system and the numerous possibilities of isomeric species, it was decided to identify potential intermediates by mass spectroscopy. Boron has a characteristic isotope pattern and fluorine has a single stable isotope, thus mass ions containing boron would be readily identifiable. Three substrates with different reactivities in directed cycloadditions were chosen for analysis by mass spectroscopy; **128**, **145** and **143** (*scheme 83*). A model reaction was devised using $BF_3.OEt_2$ without alkynyltrifluoroborate. It was proposed that boron trifluoride would model the reactivity of reactive borane species in the reaction, without instigating cycloaddition on reactive substrates. Interestingly, subjection of reactive substrate **128** gave rise to mass ions corresponding to addition of BF_2 and B_2F_6. These were tentatively assigned as pincer complex **191** and double bound substrate **192**. Importantly, it confirmed that either the sydnone exocyclic oxygen or *N*2 could compete for Lewis acid and also provided suggestive evidence for the proposed pincer complexes. Subjection of **145** to boron trifluoride also gave rise to mass ions corresponding to addition of B_2F_6, tentatively assigned as **193**. However, no pincer complex was observed in this case. Unreactive substrate **143** gave rise to a mass ion corresponding to addition of BF_2. This was tentatively assigned as pincer complex **194**, and provided further evidence for these intermediates. Alternatively, the boron could be coordinated between the amidomethoxy group and the carbonyl. However, analogous experiments within the laboratory on the *N*,*N*-dimethylamide variant of **143** also showed a mass ion corresponding to the proposed pincer complex. Interestingly, when Weinreb amide **143** was subjected to standard directed cycloaddition reaction conditions and the mixture

analysed by mass spectroscopy, the same mass ion was observed. This indicated it could be a stable compound that prevents cycloaddition occurring.

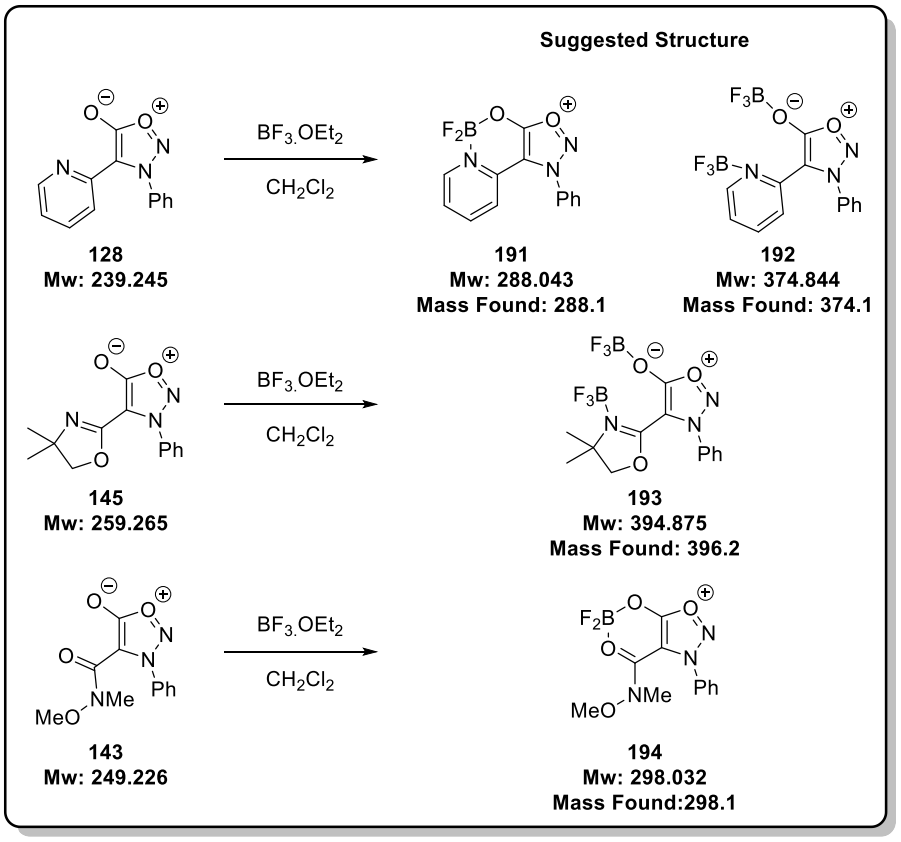

Scheme 83: Structures indicated by mass spectroscopy.

The current hypothesis for the stark contrast observed in directing group reactivity for the directed cycloaddition of sydnones is that the formation pincer complexes and their subsequent opening with further Lewis acid is fundamental to reaction progress. In the case of amide directing groups, the pincer complex is formed and is particularly stable and cannot be opened by further Lewis acid, resulting in the isolation of starting material after workup.

Reaction Stoichiometry

As depicted above in table 10, reaction with a single theoretical equivalent of trisalkynylborane resulted in conversions of roughly $^2/_3$. If only stoichiometry were considered, the most apparent source of $^2/_3$ conversion would be the loss of a single alkynyltrifluoroborate equivalent. Such a loss could formally be classed as loss of an acetylide from the trisalkynylborane (as proposed above in scheme 82). If the acetylide lost could not regenerate an alkynylborane species, the theoretical equivalents of trisalkynylborane would drop to 0.67. However, such a loss is unlikely to result in the observed conversions for two reasons; firstly, any acetylide generated would likely react with a Lewis acidic boron species to regenerate an alkynylborane. Secondly, the reaction would formally only require a single extra equivalent of alkynyltrifluoroborate (four in total) for complete conversion and two extra equivalents were required. It was proposed that other factors were contributing to lower than expected conversions. Hence, it was proposed that the nature of the pyrazole product must play a role. Once the pyrazole product is formed it contains a Lewis basic nitrogen that could bind to and sequester trisalkynylborane. It is feasible that once enough product is formed it could bind the remaining trisalkynylborane.

A rather simplified control experiment was undertaken to assess the competition in binding between a pyrazole and pyridine. A 1:1 molar ratio of *N*-phenylpyrazole and 2-phenylpyridine was subjected to a single equivalent of $BF_3.OEt_2$ and the mixture analysed by ^{1}H NMR. The spectrum contained 4 compounds in a roughly 1:1:1:1 ratio. Two compounds were identified as unreacted *N*-phenylpyrazole and 2-phenylpyridine. The two remaining compounds were assigned as the corresponding boron trifluoride adducts of the two starting materials. This indicated that the pyrazole nitrogen could indeed compete as a Lewis base with pyridine. Therefore, it is believed that the requirement for extra equivalents of alkynyltrifluoroborate stems from competitive binding of trisalkynylborane to pyrazole product.

Investigations into the Formation of Difluoroboranes

Having only previously been isolated as minor products in the directed cycloadditions of 2-pyrones, the formation of dialkynylboranes as major products in directed cycloadditions of sydnones was a particularly unusual feature of the reactions. In the case of the 2-pyrone chemistry, dialkynylborane cycloadducts had been shown to react with BF_3, BCl_3 and BBr_3 to form difluoro- dichloro- and dibromoboranes respectively. Indeed, this type of reactivity resulted in dihaloboranes constituting the major isolated products from 2-pyrone directed cycloadditions.[155] The fact that pyrazoles were always isolated as dialkynylboranes indicated that this chemistry was not viable on pyrazole dialkynylboranes. Nevertheless, attempts were made to convert pyrazole **131** to the corresponding dihaloboranes. Firstly, **131** was resubjected to the standard reaction conditions, leading to recovery of starting material. Next, **131** was subjected to 5 equivalents of Lewis acid at 25 °C (*scheme 84*). Boron trifluoride failed to convert the dialkynylborane, with starting material recovered. Subjection to boron trichloride resulted in some protodeboronation of the starting material, but dihaloborane was not observed. Boron tribromide resulted in full consumption of starting material, but only protodeboronated product **174** and apparent alkyne polymerisation products were observed in the crude reaction material.

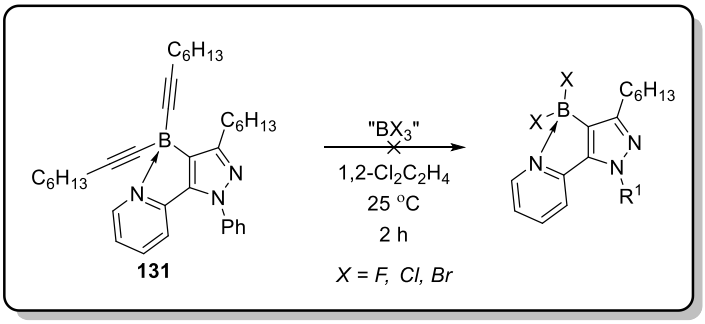

Scheme 84: Reaction of **131** with trihaloboranes.

With boron trichloride and boron tribromide resulting in the formation of protodeboronated by-product, attempts were made to use boron trifluoride at higher temperature. Unfortunately, heating at 40 °C resulted in 36% isolated yield of the protodeboronated by-product. As a final strategy for the direct transformation of dialkynylborane **131** to the corresponding difluoroborane, **130** was treated with KHF_2. However, this only resulted recovery of starting material contaminated with product arising from protodeboronation.

To further probe the unexpected lack of reactivity, NMR experiments were undertaken. In order to supplement density functional theory (DFT) calculations being conducted by collaborators, the model substrate used in calculations, dialkynylborane **171**, was examined

in further studies. Various equivalents of boron trifluoride were added to dialkynylborane **171** in CD_2Cl_2 and the reaction monitored by ^{1}H-, ^{19}F- and ^{11}B NMR spectroscopy. Unfortunately, it was not possible to identify the product formed with absolute certainty. Addition of one equivalent of BF_3 resulted a net downfield shift of signals in ^{1}H NMR (*spectrum 1*). Addition for further BF_3 resulted in a further downfield shifts. This indicated that there was an interaction between BF_3 and the starting material and further BF_3 possibly had further interaction. Product aggregation could also not be ruled out. When a single equivalent of BF_3 was added, the ^{19}F NMR spectrum contained single signal that was downfield shifted from $BF_3.OEt_2$ (*spectrum 2*). Logically, it was concluded that this signal arose from coordination of BF_3 to the pyrazole nitrogen forming **195** (*figure 44*). Addition of five equivalents of BF_3 resulted in the formation of a similar signal, with a possible second signal underneath. It was hypothesised that the second signal could arise from the formation of a double adduct such as **196**. However, ^{11}B NMR appeared to contradict **196** as a possibility. A single equivalent of BF_3 resulted in a new signal upfield shifted from $BF_3.OEt_2$ (*spectrum 3*). The signal corresponding to the dialkynylborane did not shift indicating its environment had not changed. Five equivalents of BF_3 resulted in a relatively broad signal arising from BF_3. Importantly, the dialkynylborane was again unchanged, seemingly indicating that **195** was not the product. A control experiment using *N*-phenylpyrazole and boron trifluoride afforded a product with similar fluorine and boron signals as compared to those observed in the NMR experiment with **171**. These signals were assigned to boron trifluoride coordination to the pyrazole *N*2 in both products. The observed product was therefore tentatively assigned **195** (*figure 44*). It was hypothesised that this product was an energetic sink and thus prevented disproportionation to the difluoroborane.

^{1}H NMR

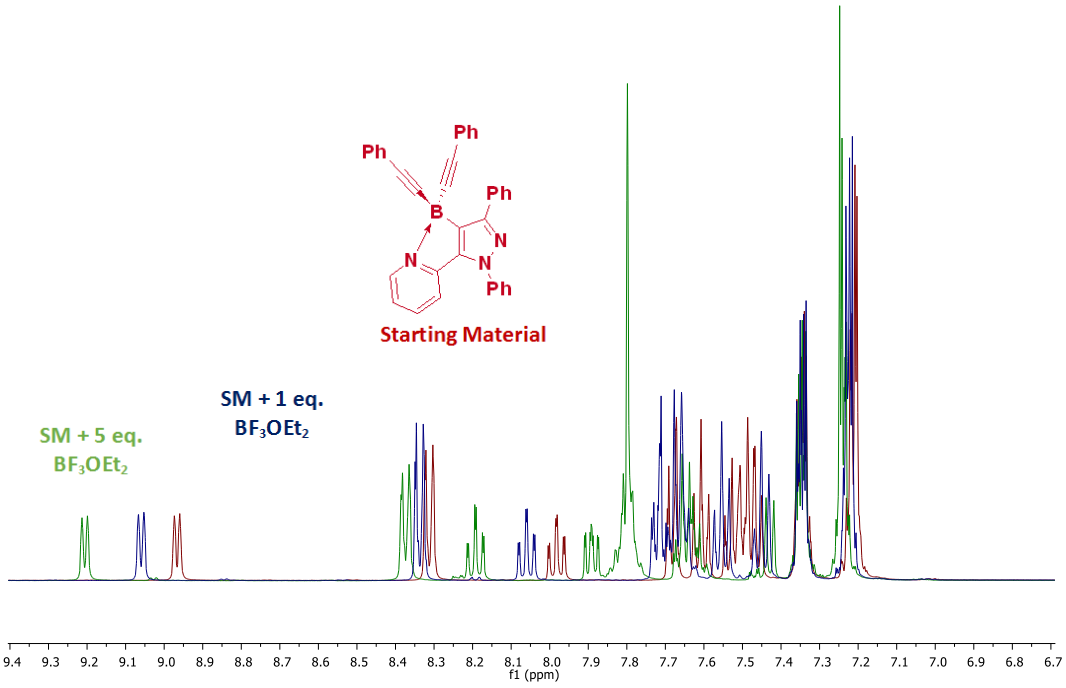

Spectrum 1: Overlay ^{1}H NMR spectra of **171** (red), 1 equivalent of $BF_3.OEt_2$ with **171** (blue) and 5 equivalents of $BF_3.OEt_2$ with **171** (green).

^{19}F NMR

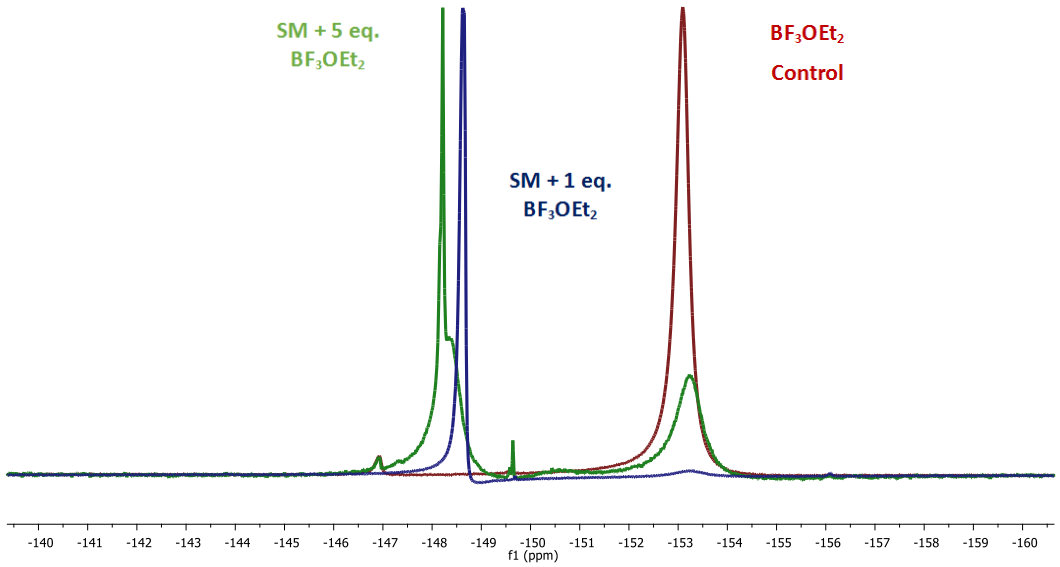

Spectrum 2: Overlay ^{19}F NMR spectra of $BF_3.OEt_2$ (red), 1 equivalent of $BF_3.OEt_2$ with **171** (blue) and 5 equivalents of $BF_3.OEt_2$ with **171** (green).

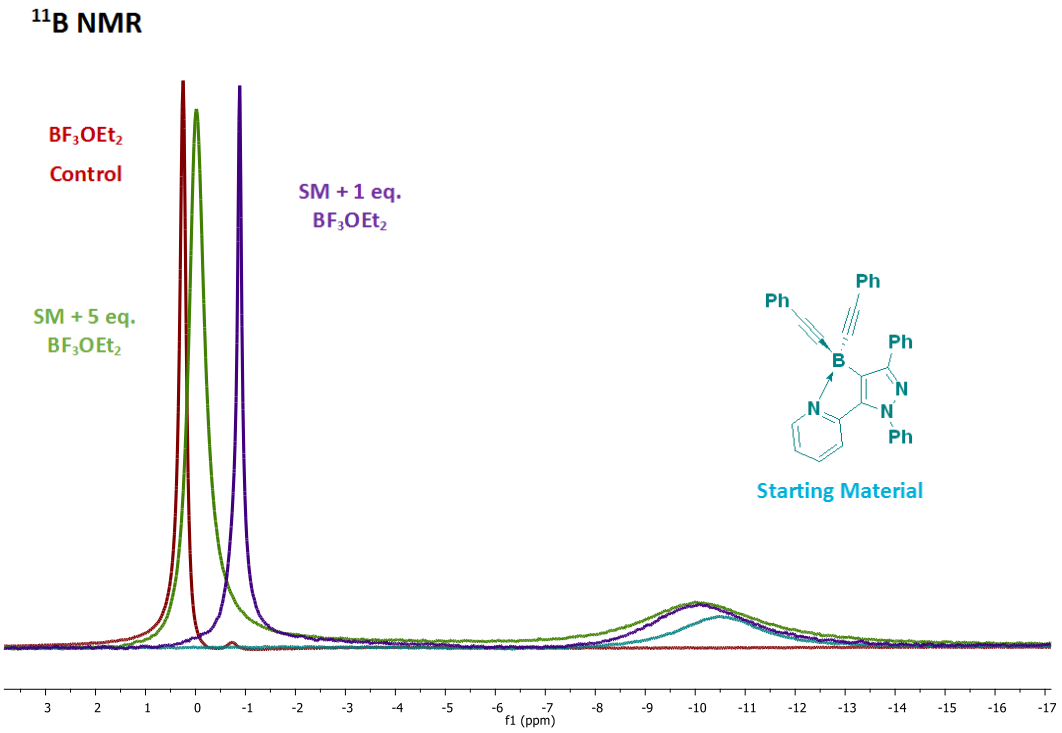

Spectrum 3: Overlay ^{11}B NMR spectra of $BF_3.OEt_2$ (red), **171** (blue), 1 equivalent of $BF_3.OEt_2$ with **171** (purple) and 5 equivalents of $BF_3.OEt_2$ with **171** (green).

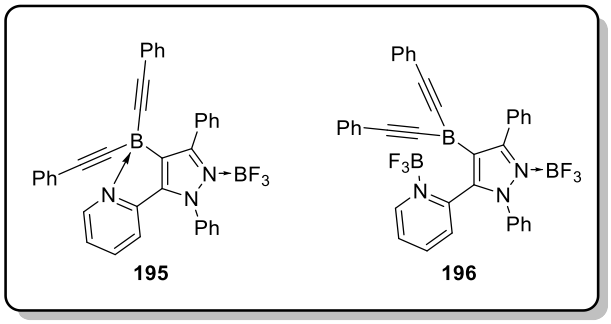

Figure 44: Potential structures observed in NMR experiments.

Attempts to observe the compound formed from the reaction of **171** with boron trifluoride by mass spectroscopy were met with limited success. Only mass ions corresponding to **171** and protodeborylation were readily identifiable. An unusual high mass ion was observed at m/z 917. This was tentatively assigned as dimer **197**, where an acetylide anion has been lost from one of the monomer constituents and is presumably a counter ion to the complex. It was not clear how such a structure could readily revert to starting material upon aqueous work up. The structure would also likely have quite distinct ^{11}B NMR shifts compared to the starting material. However, the boron signal is not shifted under any of the conditions analysed. Therefore, **197** is not believed to be a significant structure in the chemistry of **171**.

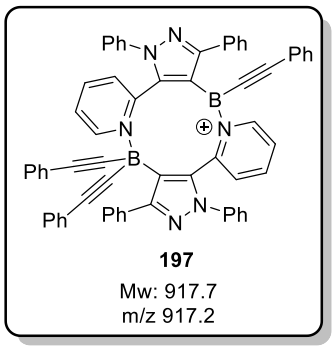

Figure 45: Tentative assignment of mass ion 917.

In conclusion, directed cycloaddition methodology was successfully extended to sydnones. Reaction temperatures were reduced from 180 °C to 25 °C, reaction times reduced from 48 h to 2 h, and the yields obtained were typically high. Conversely to previous examples, the only observed products were dialkynylboranes rather than difluoroboranes. It is believed that as soon as the dialkynylborane pyrazole is formed, it binds to further Lewis acid and generates a highly stable complex which is dissociated on work up. It is this highly stable complex that prevents disproportionation to the difluoroborane. All attempts to generate the difluoroborane from either the dialkynylborane or by separate means were unsuccessful. However, dialkynylboranes were successfully transformed into other functional groups in classical boron chemistry. In comparison to other substrates, only a limited number of directing groups were found to be compatible with the reaction. Directing group ring size appeared to be a critical factor in reactivity. Amides were unsuccessful directing groups, possibly due to the formation of stable pincer complexes which were observed by mass spectroscopy. Attempts to broaden the utility of the chemistry by transforming the oxazine directing group into a carbonyl compound failed to come to fruition. Future work in the area will likely focus on application of the system to further heterocycles (e.g. münchnones or *iso*sydnones). Further work on understanding the equilibria and kinetics involved in the reactions and how the different substrate systems affect them is also warranted.

Chapter 8: Future Work

Sydnone-based vascular disrupting agents

Due to the lack of success of the lead compound, 58, in vivo, sydnone-based vascular disrupting agents appeared to be less promising than their pyrazole counterparts. Before further analogues are synthesised, a comprehensive study of in vivo compound stability should be undertaken. If the compounds are stable to physiological conditions, the priority target would be **63**, as mentioned earlier. It would also be interesting to look at the activity of **198** and **199**, where the 3,4,5-trimethoxyphenyl ring has been altered (*figure 46*).

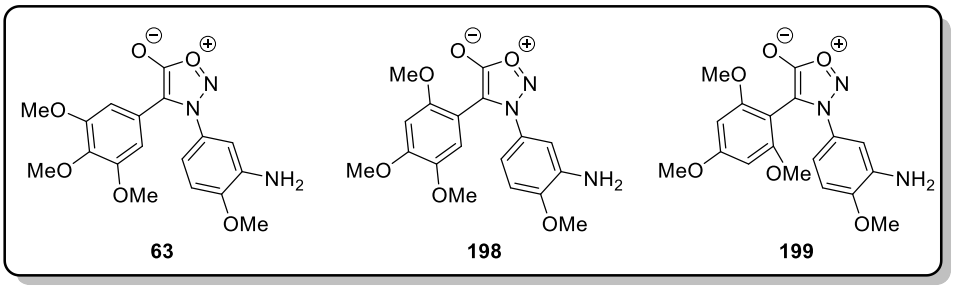

Figure 46: Priority targets for sydnone-based vascular disrupting agents.

Pyrazole-based vascular disrupting agents

The success of pyrazole **85** both *in vitro* and *in vivo* has highlighted pyrazole-based analogues of CA4 as an interesting avenue of medicinal chemistry research. The lead compound should be subjected to DMPK studies to further assess its suitability as a drug candidate. If necessary, prodrug forms could be prepared. Logically, the priority of further synthetic targets should be focussed around the successful structure of **85**. Some priority targets for 2nd generation compound synthesis are depicted in figure 47.

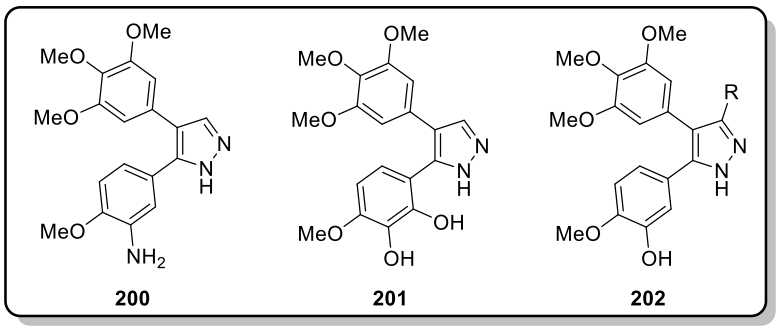

Figure 47: Priority targets for pyrazole-based vascular disrupting agents.

Fluoromethylation

In spite of the limited utility of monofluoromethyl ethers, the formation of fluoromethylating reagents from other readily available materials remains an interesting prospect. Therefore, further research in this area is warranted. In terms of monofluoromethylation, instability issues could possibly be overcome by the use of carbon nucleophiles (*scheme 85*). Potentially enolates or enolate equivalents could react with *in situ* generated chlorofluoromethane to afford fluoromethylated carbonyl compounds such as **203**. These could be prone to elimination, but would then offer an interesting method to access α,β-unsaturated carbonyl compounds.

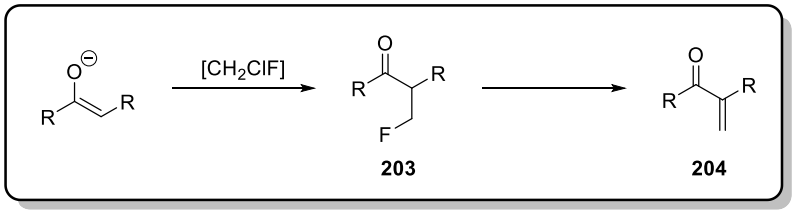

Scheme 85: Alternative nucleophile for monofluoromethylation.

An alternative, potentially more synthetically useful avenue of research, would be to extend the methodology to difluoro- and trifluoromethylation (*scheme 86*). Trace reactivity was observed in difluoromethylation test reactions using chloroform. If this could be optimised it would represent a useful synthetic tool. The reaction could potentially be improved through use of additives such as metal cations to drive salt formation or triphenylphosphine to help remove halogens from the starting material.

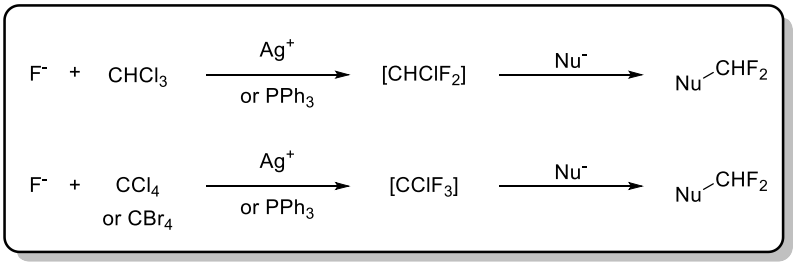

Scheme 86: Methods for difluoro- and trifluoromethylation.

Directed cycloadditions

After directed cycloaddition methodology was successfully applied to sydnones, other similar classes of compounds could also be good substrates. For example, *iso*sydnones could allow the use of amide directing groups. Pincer complex formation would not be possible due to the different positioning of the exocyclic oxygen (*scheme 87*). Compared to their sydnone

counterparts, the chemistry of *iso*sydnones is not well established and the synthesis of the substrates could prove challenging.

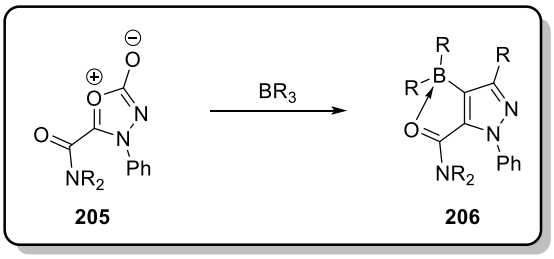

Scheme 87: Directed cycloaddition with *iso*sydnones.

Another related class of compounds are münchnones. In contrast to sydnones, münchnones have two possible locations for the directing group, *C*2 or *C*4. Münchnones bearing a directing group at the *C*4, such as **207** (*scheme 88*) might be expected to have similar limitations to sydnones in directed cycloaddition chemistry. However, münchnones bearing a directing group at *C*2, such as **209**, could be expected to have enhanced reactivity. However, münchnones can be unstable and are often formed *in situ* for reaction. Therefore, accessing the starting materials for directed cycloaddition could be problematic.

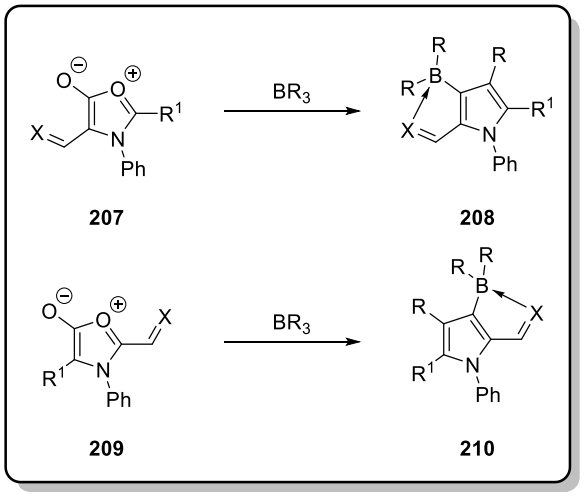

Scheme 87: Directed cycloaddition with münchnones.

Chapter 9: Experimental

9.1: General Procedures and Equipment

^{1}H NMR spectra were recorded on a Bruker AVIII HD 400 (400 MHz), Bruker AVI 400 (400 MHz), or DPX-400 (400 MHz) supported by an Aspect 3000 data system. Chemical shifts are reported in parts per million (ppm) from tetramethylsilane with the residual protic solvent resonance as the internal standard ($CHCl_3$: δ 7.26, DMSO: δ 2.50). Data are reported as follows: chemical shift, integration, multiplicity (s = singlet, d = doublet, t = triplet, q = quartet, m = multiplet, br = broad), coupling constants (Hz), assignments. ^{13}C NMR spectra were recorded on a Bruker AVIII HD 400 (100.6 MHz), Bruker AVI 400 (100.6 MHz), or DPX-400 (100.6 MHz) with complete proton decoupling. Chemical shifts are reported in ppm from tetramethylsilane with the solvent as the internal reference ($CDCl_3$: δ 77.16, DMSO: δ 39.52).

High-resolution mass spectra (HRMS), recorded for accurate mass analysis, were performed on electrospray mode (TOF ES^+). Infrared (IR) spectra were recorded on a Perkin Elmer Paragon 100 FTIR spectrophotometer, ν_{max} in cm^{-1}. Samples were recorded as thin films using sodium chloride plates, as a dichloromethane solution or as solids using a solid probe. Bands were characterised as broad (br), strong (s), medium (m), and weak (w). All solvents and reagents were purified using standard laboratory techniques according to methods published in "Purification of Laboratory Chemicals" by Armarego and Perrin (Pergamon Press, 2009).[169] Flash chromatography was performed on silica gel (BDH Silica Gel 60 43-60). Thin layer chromatography (TLC) was performed on aluminium backed plates pre-coated with silica (0.2 mm, Merck DC-alufolien Kieselgel 60 F254) which were developed using standard visualising agents: ultraviolet (UV) light or potassium permanganate.

General Procedure A: Preparation of Amino Esters:

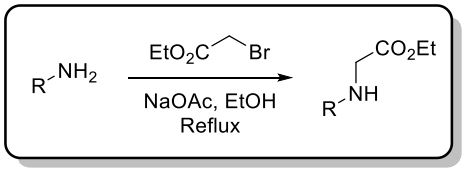

To a suspension of the amine/aniline (1 eq.) and sodium acetate (2 eq.) in ethanol (0.5 – 1.0 M) was added ethyl bromoacetate (1.0 eq.) and the mixture heated at reflux for 4 hours. The solvent was removed *in vacuo*, followed by the addition of CH_2Cl_2 and filtration and concentration of the filtrate. Flash silica chromatography (gradient starting with 100% 40-60 petroleum ether and ending with 50% ethyl acetate in 40-60 petroleum ether) afforded the title amino esters.

General Procedure B: Preparation of Amino Acids:

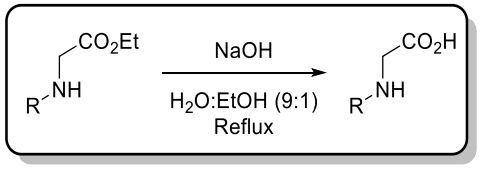

To a suspension of the amino ester (1 eq.) in water:ethanol (9:1, 0.3 M) was added sodium hydroxide (1.5 eq.) and the mixture heated at reflux for 90 minutes. The reaction was allowed to cool to RT before acidification with concentrated hydrochloric acid to pH 4-6, leading to product precipitation. The solid was isolated and dried *in vacuo*. Alternatively, if precipitation was not observed, the mixture was extracted with ethyl acetate, dried over $MgSO_4$ and the solvent removed *in vacuo*. The products could be further purified by recrystallization from ethanol.

General Procedure C: Preparation of Sydnones:

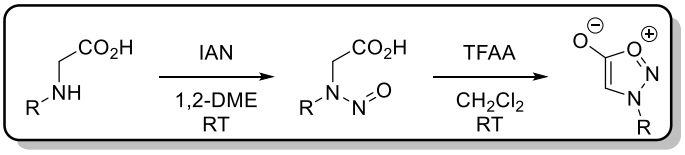

To a suspension of amino acid (1 eq.) in 1,2-dimethoxyethane (1,2-DME) (0.25 M) was added isopentyl nitrite (IAN) (1.1 eq.) and the reaction stirred for 3-4 hours. The mixture was concentrated *in vacuo* (*note: waterbath temperature should not exceed 30 ^{o}C to prevent decomposition*) followed by the addition of petroleum ether:diethyl ether (15:1) to provide the crude product as a solid or oil. The liquor was then decanted and the remaining material dried *in vacuo* (**Caution**: ***nitrosamine intermediates are highly toxic and suspected carcinogens***). The crude material was suspended in CH_2Cl_2 (0.25 M) under nitrogen without further purification. Trifluoroacetic anhydride (TFAA) (1.5 eq.) was carefully added at 0 °C and the reaction allowed to warm to RT and stirred for 90 minutes. Water was added and trifluoroacetic acid (TFA) by-product was carefully quenched with sodium bicarbonate and extracted with CH_2Cl_2. The combined organic layers were dried over $MgSO_4$ and volatiles removed *in vacuo* affording the target sydnones. The compounds could be further purified by recrystallisation from ethanol.

General Procedure D: Synthesis of 3,4-Diarylsydnones using Triphenylphosphine as a Ligand:

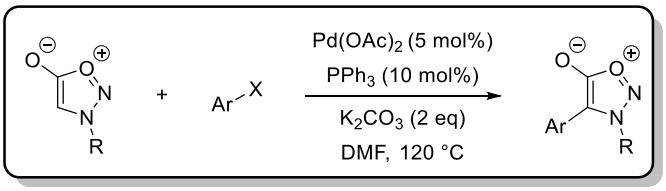

A mixture of sydnone (1 eq.), aryl halide (1.5 eq.), palladium acetate (5 mol %), triphenylphosphine (10 mol %) and potassium carbonate (2-3 eq.) in DMF (0.25 – 0.5 M) under an atmosphere of nitrogen was heated at 80 - 120 °C for 14 hours before the reaction was allowed to cool to ambient temperature and water was added. The resulting mixture was extracted with ethyl acetate:40-60 petroleum ether (9:1) and the combined organic layers dried over $MgSO_4$ and concentrated *in vacuo*. Flash silica chromatography (eluting solvent 20%-100% ethyl acetate in 40-60 petroleum ether) afforded the target 3,4-diarylsydnones. The compounds can be further purified by recrystallisation from ethanol or dichloromethane/petrol.

General Procedure E: Synthesis of 3,4-Diarylsydnones using Tributylphosphine as a Ligand:

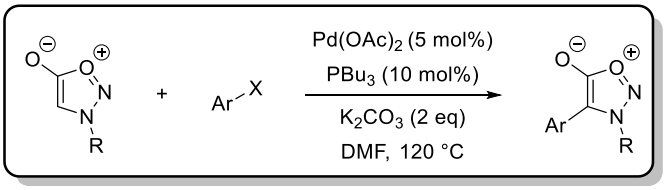

A mixture of sydnone (1 eq.), aryl halide (1.5 eq.), palladium acetate (5 mol %), tributylphosphine (50 mol %) and potassium carbonate (2-3 eq.) in DMF (0.25 – 0.5 M) under an atmosphere of nitrogen was heated at 80 - 120 °C for 14 hours before the reaction was allowed to cool to ambient temperature and water was added. The resulting mixture was extracted with ethyl acetate:40-60 petroleum ether (9:1) and the combined organic layers dried over $MgSO_4$ and concentrated *in vacuo*. Flash silica chromatography (eluting solvent 20%-100% ethyl acetate in 40-60 petroleum ether) afforded the target 3,4-diarylsydnones. The compounds can be further purified by recrystallisation from ethanol or dichloromethane/petrol.

General Procedure F: Preparation of 3,4-Diarylsydnones using XPhos as a Ligand:

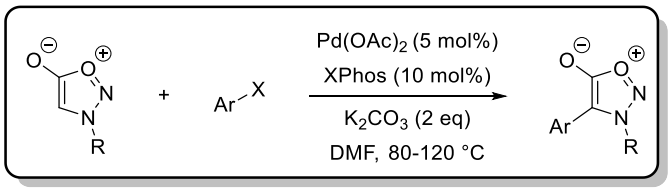

A mixture of sydnone (1 eq.), aryl halide (1.5 eq.), palladium acetate (5 mol %), XPhos (10 mol %) and potassium carbonate (2-3 eq.) in DMF (0.25 – 0.5 M) under an atmosphere of nitrogen was heated at 80 - 120 °C for 14 hours before the reaction was allowed to cool to ambient temperature and water was added. The resulting mixture was extracted with ethyl acetate:40-60 petroleum ether (9:1) and the combined organic layers dried over $MgSO_4$ and concentrated *in vacuo*. Flash silica chromatography (eluting solvent 20%-100% ethyl acetate in 40-60 petroleum ether) afforded the target 3,4-diarylsydnones. The compounds could be further purified by recrystallisation from ethanol or dichloromethane/petrol.

General Procedure G: Cycloadditions of Sydnones with Terminal Alkynes:

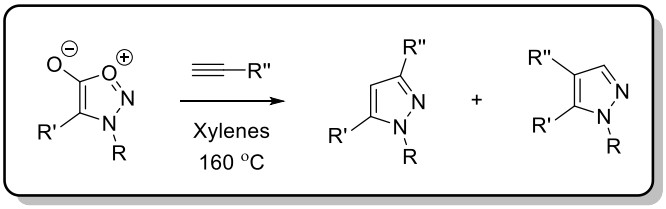

A Schlenk tube was charged with sydnone (1 eq.), alkyne (2-4 eq.) and xylenes (1 M). The tube was then sealed and heated at 160 °C for 24 hours. The mixture was allowed to cool to ambient temperature and loaded onto a short plug of silica and washed with 40-60 petroleum ether before elution with ethyl acetate. Volatiles were removed *in vacuo* and the crude residue purified by flash silica chromatography (gradient starting with 100% 40-60 petroleum ether and ending with 40% ethyl acetate in 40-60 petroleum ether) affording the target 1,3,5-trisubstituted pyrazoles as major products.

General Procedure H: Trimethylsilyl Group Cleavage:

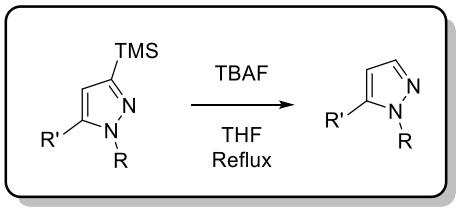

A flask equipped with a reflux condenser was charged with pyrazole (1 eq.), and TBAF (10 eq. 1 M solution in THF) and heated at reflux under an inert atmosphere of nitrogen for 24 hours. The mixture was allowed to cool to ambient temperature, poured into water, neutralised with $NaHCO_3$ and extracted with ethyl acetate. The combined organic layers were dried over $MgSO_4$ and concentrated *in vacuo*. Flash silica chromatography (gradient starting with 100% 40-60 petroleum ether and ending with 60% ethyl acetate in 40-60 petroleum ether) afforded the target desilated pyrazoles.

General Procedure I: Benzyl Deprotection:

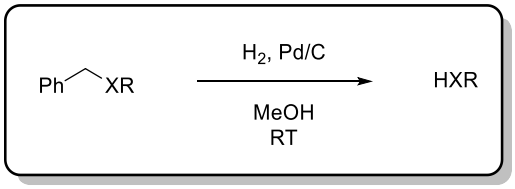

A flask was charged with pyrazole and Pd/C (10% wt./wt., 100 mg/mmol) and methanol (0.1 M). The flask was flushed with H_2 (balloon) and stirred for 24-72 hours. The mixture was filtered through celite™ and concentrated *in vacuo*. Flash silica chromatography (gradient starting with 100% 40-60 petroleum ether and ending with 100% ethyl acetate in 40-60 petroleum ether) afforded the target pyrazoles.

General Procedure J: Thermal Cycloaddition of Sydnones with Alkynylboronates:

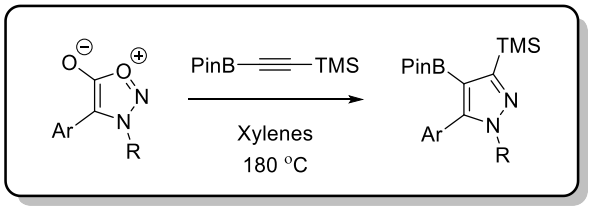

A Schlenk tube was charged with sydnone (1 eq.), alkyne (2 eq.) and xylenes (1 M). The tube was then sealed and heated at 180 °C for 48 hours. The mixture was allowed to cool to ambient temperature and loaded onto a short plug of silica and washed with 40-60 petroleum ether before elution with ethyl acetate. Volatiles were removed *in vacuo* and the crude residue purified by flash silica chromatography (gradient starting with 100% 40-60 petroleum ether and ending with 40% ethyl acetate in 40-60 petroleum ether) affording the target pyrazole boronic esters.

General Procedure K: Suzuki-Miyaura Coupling of Pyrazole Boronic Acid Derivatives:

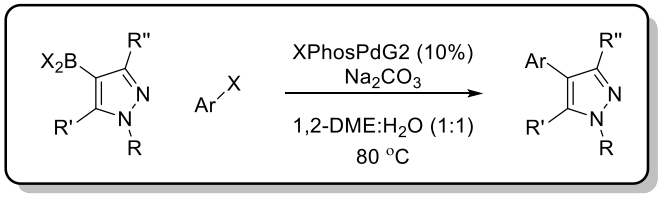

A flask equipped with a reflux condenser was charged with pyrazole boronic ester (1 eq.), XPhosPdG2 (0.1 eq.), sodium carbonate (2 eq.) and degassed 1,2-dimethoxyethane:water (1:1, 0.1 M) and heated at 80 °C under an inert atmosphere of nitrogen for 14 hours. The mixture was allowed to cool to ambient temperature, poured into water and extracted with ethyl acetate. The combined organic layers were dried over $MgSO_4$ and concentrated *in vacuo*. Flash silica chromatography (gradient starting with 100% 40-60 petroleum ether and ending with 40% ethyl acetate in 40-60 petroleum ether) afforded the target cross-coupled pyrazoles as an inseparable mixture of the target material and the product arising from protodeboronation. Only characterisation for the target material is reported.

General Procedure L: Bromination and Subsequent Suzuki-Miyaura Coupling of Pyrazoles:

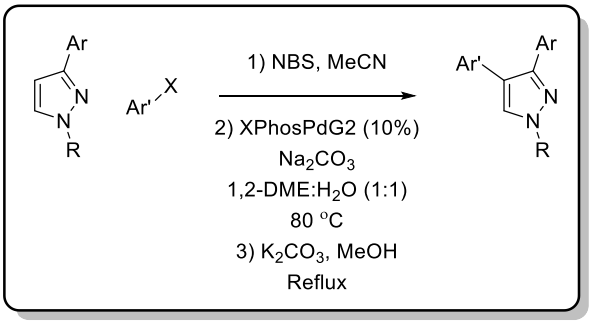

i) To a flask containing pyrazole was added a solution of *N*-bromosuccinamide (1 eq.) in acetonitrile (0.2 M). The resulting mixture was stirred for one hour at ambient temperature, before being poured into water. The mixture was extracted with ethyl acetate and the combined organic layers washed with aqueous sodium hydroxide (1 M). The organic layer was dried over $MgSO_4$, filtered and volatiles removed *in vacuo*. The crude material was concentrated into a flask. The flask was then charged with aryl boronate (1.5 eq.), XPhosPdG2 (10 mol %), sodium carbonate (2-3.5 eq.) and thoroughly degassed 1,2-dimethoxyethane:water (1:1, 0.1 M). The mixture was heated at 80 ^{o}C for 14 hours, cooled to ambient temperature, poured into water and extracted with ethyl acetate. The combined organic layers were dried over $MgSO_4$, filtered and volatiles removed *in vacuo*. Flash silica chromatography (gradient starting with 100% 40-60 petroleum ether and ending with 100% ethyl acetate in 40-60 petroleum ether) afforded the target pyrazoles.

ii) In cases where the products obtained were the TBS-protected phenols, the crude Suzuki-Miyaura product was subjected to potassium carbonate (3 eq.) in refluxing methanol for 3 hours, before the mixture was poured into water and extracted with ethyl acetate. The organic layers were dried over $MgSO_4$, filtered and volatiles removed *in vacuo*, followed by purification.

General Procedure M: Preparation of Alkynyltrifluoroborates:

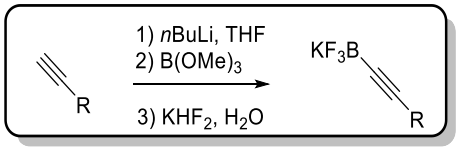

To a solution of alkyne (1 eq.) in THF (0.5 M) at -78 °C was slowly added *n*-BuLi (~2.5 M, 1 eq.) and the reaction stirred for 1 h at -78 °C. Trimethylborate (1.5 eq.) was added slowly and the reaction stirred for 1 h at -78 °C. The reaction was allowed to warm to -20 °C and stirred for a further hour. A solution of potassium hydrogen difluoride (6 eq.) in water (90% v/v) was added at -20 °C and the mixture allowed to warm to ambient temperature and stirred for a further 2 h. Volatiles were removed *in vacuo* and the resulting solid was triturated in boiling acetone and volatiles removed *in vacuo*. The resulting solid was dissolved in minimum boiling acetone, allowed to cool to ambient temperature and product precipitated with diethyl ether. The resulting alkynyltrifluoroborate salts were isolated by filtration affording.

General Procedure N: Directed Cycloadditions of Sydnones:

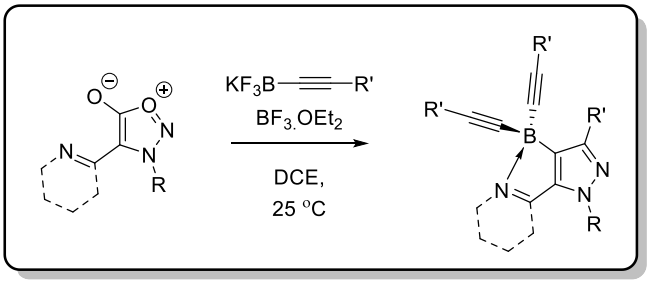

To a suspension of sydnone (1 eq.) and alkynyl potassium trifluoroborate (5 eq.) in dichloroethane (0.2 M) under an atmosphere of nitrogen at 25 °C was added a solution of $BF_3.OEt_2$ (2-5 eq.) in dichloroethane (0.4 M). The reaction was stirred for 2-4 hours at 25 °C before brine was added. The resulting mixture was extracted with dichloromethane and the combined organic layers dried over $MgSO_4$, filtered through a short pad of Celite™ and concentrated *in vacuo*. When required, flash silica chromatography (gradient starting with 100% 40-60 petroleum ether and ending with 40% ethyl acetate in 40-60 petroleum ether) afforded the target pyrazoles.

9.2: Experimental and Spectroscopic Data

N-(3,4,5-Trimethoxyphenyl)glycine ethyl ester:

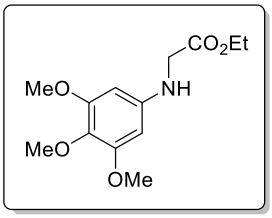

Following general procedure A using 3,4,5-trimethoxyaniline (10.0 g, 54.6 mmol), ethylbromoacetate (9.12 g, 54.6 mmol) and sodium acetate (8.96 g, 109 mmol), ethyl *N*-(3,4,5-trimethoxyphenyl)glycine ethyl ester was isolated as a colourless solid (12.1 g, 82%).

M.p.: 73-75 °C; ^{1}H NMR (400 MHz, $CDCl_3$): δ 1.30 (3H, t, *J* = 7.0 Hz), 3.75 (3H, s), 3.82 (6H, s), 3.88 (2H, s), 4.25 (2H, q, *J* = 7.0 Hz), 5.84 (2H, s); ^{13}C NMR (101 MHz, $CDCl_3$): δ 14.4, 46.5, 56.1, 61.2, 61.5, 90.8, 130.8, 144.0, 154.1, 171.2; FTIR: ν_{max} 3374 (m), 2979 (w), 2937 (w), 1727 (s), 1012 (s); HRMS calculated for $C_{13}H_{20}NO_5$ (ES^+)($+H^+$): 270.1341. Found: 270.1331.

N-(4-Methoxyphenyl)glycine ethyl ester:[170]

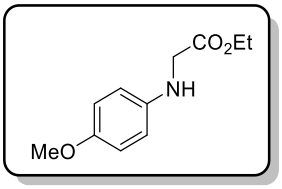

Following general procedure A using *p*-anisidine (10.0 g, 81.2 mmol), ethylbromoacetate (13.7 g, 81.2 mmol) and sodium acetate (13.3 g, 162 mmol), *N*-(4-methoxyphenyl)glycine ethyl ester was isolated as a white solid (9.04 g, 53%).

M.p.: 42-43 °C (lit. [170] 43 °C); ^{1}H NMR (400 MHz, $CDCl_3$): δ 1.29 (3H, t, *J* = 7.0 Hz), 3.74 (3H, s), 3.86 (2H, s), 4.23 (2H, q, *J* = 7.0 Hz), 6.59 (2H, d, *J* = 9.0 Hz), 6.79 (2H, d, *J* = 9.0 Hz), ^{13}C NMR (101 MHz, $CDCl_3$): δ 14.3, 47.0, 55.9, 61.4, 114.5, 115.1, 141.4, 152.8, 171.5.

N-(4-Ethoxyphenyl)glycine ethyl ester:[171]

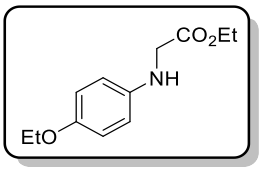

Following general procedure A using *p*-phenetidine (10.0 g, 72.9 mmol), ethylbromoacetate (12.2 g, 72.9 mmol) and sodium acetate (12.0 g, 146 mmol), *N*-(4-ethoxyphenyl)glycine ethyl ester was isolated as a tan solid (10.2 g, 62%).

M.p.: 93-94 °C; ^{1}H NMR (400 MHz, $CDCl_3$): δ 1.29 (3H, t, *J* = 7.0 Hz), 1.37 (3H, t, *J* = 7.0 Hz), 3.86 (2H, s), 3.95 (2H, q, *J* = 7.0 Hz), 4.23 (2H, q, *J* = 7.0 Hz), 6.58 (2H, d, *J* = 9.0 Hz), 6.79 (2H, d, *J* = 9.0 Hz); ^{13}C NMR (101 MHz, $CDCl_3$): δ 14.3, 15.1, 47.0, 61.4, 64.2, 114.6, 115.2, 115.9, 123.8, 141.4, 152.1, 171.6; FTIR: ν_{max} 3378 (w), 2977 (w), 1736 (s), 1012 (s); HRMS calculated for $C_{12}H_{18}NO_3$ (ES^+)($+H^+$): 224.1287. Found: 224.1291.

N-(3-Hydroxy-4-methoxyphenyl)glycine ethyl ester:

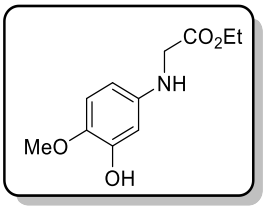

Following general procedure A using 5-amino-2-methoxyphenol (2.0 g, 14.4 mmol), ethylbromoacetate (2.40 g, 14.4 mmol) and sodium acetate (2.36 g, 28.7 mmol), ethyl *N*-(3-hydroxy-4-methoxyphenyl)glycine ethyl ester was isolated as an orange oil (2.80 g, yield 87 %).

^{1}H NMR (400 MHz, $CDCl_3$): δ 1.27 (3H, t, *J* = 7.0 Hz), 3.79 (3H, s), 3.83 (2H, s), 4.22 (2H, q, *J* = 7.0 Hz), 4.80 (1H, br), 6.10 (1H, dd, *J* = 3.0, 8.5 Hz), 6.29 (1H, d, *J* = 3.0 Hz), 6.71 (1H, d, *J* = 8.5 Hz); ^{13}C NMR (101 MHz, $CDCl_3$): δ 14.3, 46.6, 56.8, 61.0, 101.1, 104.1, 112.4, 139.8, 142.3, 146.7, 171.4; FTIR: ν_{max} 3400 (br), 2982 (m), 2837 (w), 1737 (s), 1025 (s), 945 (w); HRMS calculated for $C_{11}H_{16}NO_4$ (ES^+)($+H^+$): 226.1079. Found: 226.1071.

N-(3,4,5-Trimethoxyphenyl)glycine:

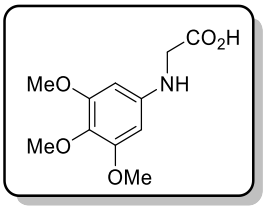

Following general procedure B using *N*-(3,4,5-trimethoxyphenyl)glycine ethyl ester (12.1 g, 44.9 mmol) and sodium hydroxide (3.60 g, 89.8 mmol), *N*-(3,4,5-trimethoxyphenyl)glycine was isolated as orange crystals (9.9 g, 91% yield).

M.p.: 111-114 °C; ^{1}H NMR (400 MHz, $CDCl_3$): δ 3.76 (3H, s), 3.82 (6H, s), 3.96 (2H, s), 5.86 (2H, s). ^{13}C NMR (101 MHz, $CDCl_3$): δ 46.3, 56.2, 61.2, 91.1, 131.2, 143.5, 154.2, 175.3; FTIR: ν_{max} 3400 (w), 2945 (w), 2837 (w), 1730 (s), 997 (s); HRMS calculated for $C_{11}H_{15}NO_5$ (ES^+)($+H^+$): 242.1028. Found: 242.1017.

N-(4-Methoxyphenyl)glycine:[172]

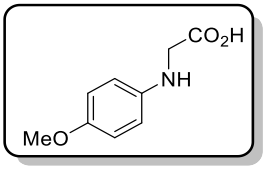

Following general procedure B using *N*-(4-methoxyphenyl)glycine ethyl ester (9.0 g, 43 mmol) and sodium hydroxide (3.4 g, 86 mmol), *N*-(4-methoxyphenyl)glycine was isolated as a colourless solid (5.2 g, 67%).

M.p.: 139-142 °C (lit.[172] 142 °C); ^{1}H NMR (400 MHz, DMSO-d_6): δ 3.63 (3H, s), 3.72 (2H, s), 6.50 (2H, d, *J* = 9.0 Hz), 6.71 (2H, d, *J* = 9.0 Hz), 8.89 (1H, br); ^{13}C NMR (101 MHz, DMSO-d_6): δ 45.4, 55.3, 113.1, 114.5, 142.3, 150.9, 172.9.

N-(4-Ethoxyphenyl)glycine:[173]

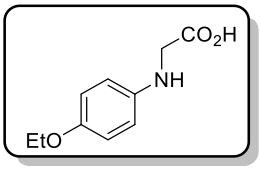

Following general procedure B using *N*-(4-ethoxyphenyl)glycine ethyl ester (10.1 g, 45.2 mmol) and sodium hydroxide (3.62 g, 90.2 mmol), *N*-(4-ethoxyphenyl)glycine was isolated as a brown solid (3.8 g, 43%).

M.p.: 141 °C (lit.[173] 159-162 °C, dec.); ^{1}H NMR (400 MHz, DMSO-d_6): δ 1.26 (3H, t, *J* = 7.0 Hz), 3.72 (2H, s), 3.87 (2H, q, *J* = 7.0 Hz), 6.49 (2H, d, *J* = 9.0 Hz), 6.70 (2H, d, *J* = 9.0 Hz); ^{13}C NMR (101 MHz, DMSO-d_6): δ 15.0, 45.6, 63.4, 113.3, 115.4, 142.4, 150.3, 173.1.

N-(4-Fluorophenyl)glycine:[174]

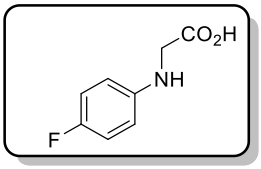

A flask was charged with 4-fluoroaniline (10 g, 90 mmol), methylbromoacetate (15.1 g, 99 mmol), Hünig's base (14 g, 108 mmol) and DMF (100 mL) and heated at 60 °C for 16 h. The resulting mixture was allowed to cool to RT, poured into water and extracted with ethyl acetate. The combined organic layers were dried over $MgSO_4$ and the solvent removed *in vacuo*. The resulting crude orange solid and sodium hydroxide (5.4 g, 135 mmol) were suspended in water:ethanol (150 mL, 9:1) and heated at reflux for 90 min. The reaction mixture was allowed to cool to RT and acidified to pH 4 with concentrated hydrochloric acid resulting in precipitation of the crude product as a tan solid. The solid was thoroughly dried in vacuum oven affording *N*-(4-Fluorophenyl)glycine as a tan solid (6.6 g, 43%).

M.p.: 136-138 °C; (lit.[174] 138 °C) ^{1}H NMR (400 MHz, DMSO-d_6): δ 6.52-6.58 (2H, m), 6.92 (2H, t, *J* = 9.0 Hz); ^{13}C NMR (101 MHz, DMSO-d_6): δ 45.3, 113.1 (d, *J* = 7.5 Hz), 115.4 (d, *J* = 22.0 Hz), 145.1, 154.7 (d, *J* = 231.0 Hz), 172.9; ^{19}F NMR (235 MHz, DMSO-d_6): δ -129.31 (tt, *J* = 9.0, 4.5 Hz).

N-(3-Hydroxy-4-methoxyphenyl)glycine:

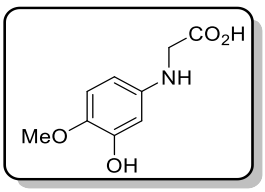

Following general procedure B using ethyl 2-((3-hydroxy-4-methoxyphenyl)amino)acetic acid (2.80 g, 12.4 mmol) and sodium hydroxide (0.75 g, 18.7 mmol), *N*-(3-hydroxy-4-methoxyphenyl)glycine was isolated as a colourless solid (0.97 g, 40%).

M.p.: >330 °C; ^{1}H NMR (400 MHz, DMSO-d_6): δ 3.62 (3H, s), 3.65 (2H, s), 5.91 (1H, dd, *J* = 2.5 Hz, 8.5 Hz), 6.08 (1H, d, *J* = 2.5 Hz), 6.66 (1H, d, *J* = 8.5 Hz), 8.65 (1H, s); ^{13}C NMR (101 MHz, DMSO-d_6): δ 45.4, 56.9, 101.3, 102.4, 114.9, 139.5, 143.5, 147.6, 173.0; HRMS calculated for $C_9H_{12}NO_4$ (ES^+)($-H^+$): 198.0766. Found: 198.0758.

N-(3,4,5-Trimethoxyphenyl)sydnone, **19**:

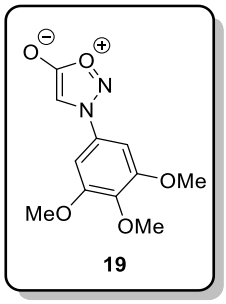

19

Following general procedure C using *N*-(3,4,5-trimethoxyphenyl)glycine (4.37 g, 18.1 mmol), IAN (2.12 g, 18.1 mmol) and TFAA (5.70 g, 27.2 mmol), sydnone **19** was isolated as orange crystals (4.05 g, 89%).

M.p.: 179-182 °C; ^{1}H NMR (400 MHz, $CDCl_3$): δ 3.90 (3H, s), 3.93 (6H, s), 6.75 (1H, s), 6.93 (2H, s); ^{13}C NMR (101 MHz, $CDCl_3$): δ 56.8, 61.2, 94.1, 99.2, 130.4, 141.3, 154.3, 169.0; FTIR: ν_{max} 3136 (w), 2944 (w), 1752 (s), 1604 (s), 1241 (s), 1126 (s), 999 (s); HRMS calculated for $C_{11}H_{13}N_2O_5$ (ES^+)($+H^+$): 253.0824. Found: 253.0817.

N-(4-Methoxyphenyl)sydnone, **25**:[175]

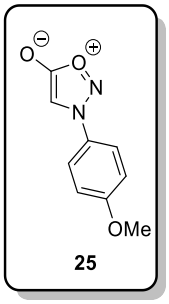

25

Following general procedure C using *N*-(4-methoxyphenyl)glycine (3.44 g, 19.0 mmol), IAN (2.23 g, 19.0 mmol) and TFAA (5.99 g, 28.5 mmol), sydnone **25** was isolated as orange crystals (3.13 g, 86%).

M.p.: 126 °C (dec.) (lit.[175] 126 °C); ^{1}H NMR (400 MHz, $CDCl_3$): δ 3.88 (3H, s), 6.68 (1H, s), 7.06 (2H, d, *J* = 9.0 Hz), 7.64 (2H, d, *J* = 9.0 Hz); ^{13}C NMR (101 MHz, DMSO-d_6): δ 55.9, 93.5, 115.3, 122.7, 127.8, 162.5, 169.2.

N-(4-Ethoxyphenyl)sydnone, **31**:[173]

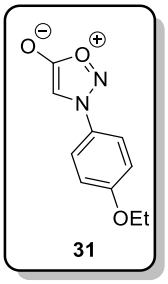

31

Following general procedure C using *N*-(4-ethoxyphenyl)glycine (2.51 g, 12.9 mmol), IAN (1.51 g, 12.9 mmol) and TFAA (4.06 g, 19.4 mmol), sydnone **31** was isolated as orange crystals (1.93 g, 73%).

M.p.: 125-126 °C (lit.[173] 127-128 dec.); ^{1}H NMR (400 MHz, $CDCl_3$) δ 1.46 (3H, t, *J* = 7.0 Hz), 4.11 (2H, q, *J* = 7.0 Hz), 6.66 (1H, s), 7.05 (2H, d, *J* = 9.0 Hz), 7.63 (2H, d, *J* = 9.0 Hz); ^{13}C NMR (101 MHz, $CDCl_3$): δ 14.7, 64.2, 93.5, 115.8, 122.8, 127.7, 162.1, 169.3.

N-Phenylsydnone, **36**:[173]

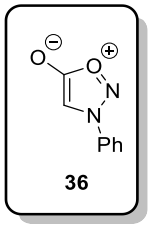

36

Following general procedure C using *N*-phenylglycine (15 g, 99 mmol), IAN (12.8 g, 109 mmol) and TFAA (31.0 g, 149 mmol), sydnone **36** was isolated as tan crystals (10.9 g, 68%).

M.p.: 130 °C (lit.[173] 134-136 dec.); ^{1}H NMR (400 MHz, $CDCl_3$) δ 6.78 (1H, s), 7.58 – 7.76 (5H, m); ^{13}C NMR (101 MHz, $CDCl_3$): δ 93.8, 121.4, 130.4, 132.6, 134.9, 169.1.

N-(4-Fluorophenyl)sydnone, **38**:[174]

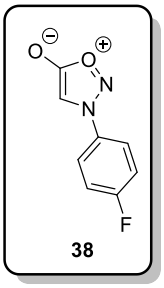

38

Following general procedure D using *N*-(4-fluorophenyl)glycine (6.55 g, 38.7 mmol), IAN (4.53 g, 38.7 mmol) and TFAA (12.2 g, 58.1 mmol), sydnone **38** was isolated as orange crystals and recrystallised from dichloromethane (3.94 g, 57%).

M.p.: 152 °C (lit.[174] 154 °C); ^{1}H NMR (400 MHz, DMSO-d_6) δ 7.49 – 7.57 (2H, m), 7.75 (1H, s), 7.95 – 8.02 (2H, m); ^{13}C NMR (101 MHz, DMSO-d_6): δ 95.1, 117.2 (d, *J* = 24 Hz), 124.2 (d, *J* = 10 Hz), 131.0, 163.8 (d, *J* = 251 Hz), 168.5 (s); ^{19}F NMR (235 MHz, DMSO-d_6): δ -107.4 - -107.5 (m).

N-Methylsydnone, **40**:[175]

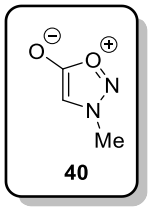

40

Following general procedure D using *N*-(methyl)glycine (10.0 g, 112 mmol), IAN (13.2 g, 112 mmol) and TFAA (35.3 g, 168.3 mmol), sydnone **40** was isolated as a colourless amorphous solid (726 mg, 6%).

^{1}H NMR (400 MHz, $CDCl_3$) δ 4.05 (3H, s), 6.34 (1H, s); ^{13}C NMR (101 MHz, $CDCl_3$): δ 39.5, 95.9, 169.4.

N-Ethylsydnone, **42**:[173]

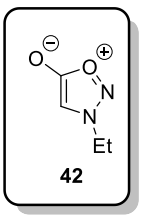

42

N-Ethylglycine (19.7 g, 191 mmol) was suspended in water (150 mL) at 0 °C and concentrated hydrochloric acid (30 mL) was added. Sodium nitrite (13.2 g, 191 mmol) in water (50 mL) was

added over the course of 30 minutes at 0 °C. The reaction was stirred for a further hour at 0 °C. The reaction mixture was extracted with ethyl acetate and the organic phase dried over $MgSO_4$ and the volatiles removed *in vacuo*, affording the crude nitrosamine intermediate as a yellow oil (6.5 g, 26%). The oil was dissolved in CH_2Cl_2 at 0 °C and TFAA (7.0 ml, 50 mmol) was carefully added. The reaction was stirred for 90 minutes at room temperature, water was added and TFA by-product was carefully quenched with $NaHCO_3$ followed by extraction with CH_2Cl_2. The organic phase was dried over $MgSO_4$ and the volatiles removed *in vacuo*, affording sydnone **42** as an orange oil (2.75 g, 13% over 2 steps).

^{1}H NMR (400 MHz, $CDCl_3$) δ 1.62 (3H, t, *J* = 7.5 Hz), 4.32 (2H, q, *J* = 7.5 Hz), 6.33 (1H, s); ^{13}C NMR (101 MHz, $CDCl_3$): δ 14.1, 48.9, 94.3, 169.5.

N-Benzylsydnone, **44**:[176]

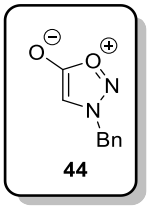

44

Following general procedure D using *N*-benzylglycine hydrochloride (15.0 g, 74.4 mmol), IAN (8.71 g, 74.4 mmol), and TFAA (23.4 g, 112 mmol), sydnone **44** was isolated a colourless solid and recrystallised from ethanol (6.62 g, 51%).

M.p.: 66-67 °C (dec.) (lit.[176] 66-67 °C); ^{1}H NMR (400 MHz, $CDCl_3$): δ 5.35 (2H, s), δ 6.25 (1H, s), δ 7.3-7.46 (5H, m); ^{13}C NMR (101 MHz, $CDCl_3$): δ 57.2, 94.8, 128.7, 129.5, 130.0, 130.6, 169.24.

N-(3-Hydroxy-4-methoxyphenyl)sydnone, **57**:

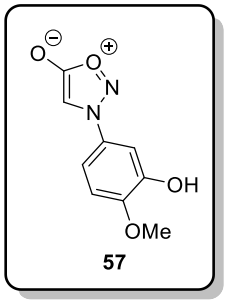

57

Following general procedure C using *N*-(3-Hydroxy-4-methoxyphenyl)glycine (0.97 g, 4.9 mmol), IAN (0.58 g, 4.9 mmol) and TFAA (1.56 g, 7.41 mmol), sydnone **57** was isolated as a brown solid (0.29 g, 28%).

M.p.: 205-209 °C (dec.); ^{1}H NMR (400 MHz, DMSO): δ 3.87 (3H, s), 7.18 (1H, d, *J* = 9.0 Hz), 7.30 (1H, d, *J* = 2.5 Hz), 7.36 (1H, dd, *J* = 2.5, 9.0 Hz), 7.66 (1H, s), 9.99 (1H, s). ^{13}C NMR (101 MHz, DMSO): δ 56.0, 94.3, 108.1, 112.2, 112.5, 127.4, 147.4, 150.8, 168.5; FTIR: ν_{max} 3248 (br), 2924 (w), 1755 (s), 1720 (s), 1517 (s), 1285 (s), 1031 (m); HRMS calculated for $C_9H_9N_2O_4$ (ES^+)($+H^+$): 209.0562. Found: 209.0553.

4-Bromo-*N*-(3,4,5-trimethoxyphenyl)sydnone, **20**:

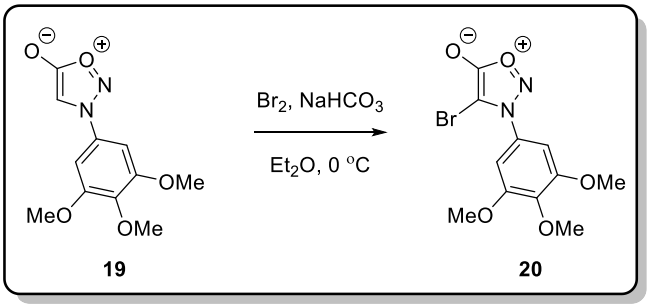

To a suspension of sydnone **19** (100 mg, 0.397 mmol) and sodium hydrogen carbonate (134 mg, 1.60 mmol) in Et_2O (4 mL) at 0 °C was added bromine (192 mg, 1.20 mmol) sydnone **20** was isolated as a colourless solid (71 mg, 53%).

M.p.: 110-115 °C (dec.); ^{1}H NMR (400 MHz, $CDCl_3$): δ 3.93 (6H, s), 3.95 (3H, s), 6.81 (2H, s); ^{13}C NMR (101 MHz, $CDCl_3$): δ 56.8, 61.3, 84.2, 91.6, 102.5, 129.1, 141.3, 154.1, 165.7; FTIR: ν_{max} 1777 (s), 1603 (s), 1506 (s), 1463 (s), 1415 (s) 1230 (s), 1129 (s), 984 (s), 819 (s); HRMS calculated for $C_{11}H_{12}N_2O_5{}^{79}Br$ (ES^+)($+H^+$): 330.9930. Found: 330.9923.

Attempted Suzuki-Miyaura Coupling of **20**:

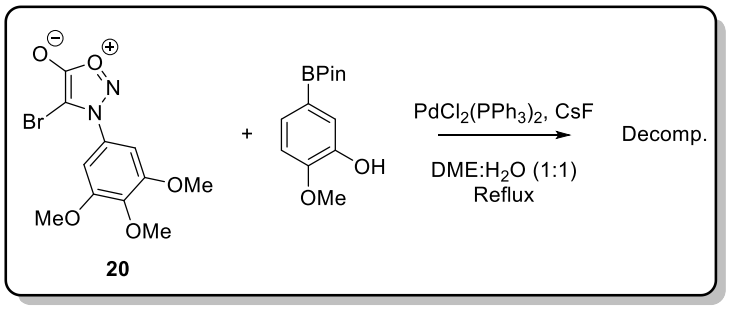

A flask equipped with condenser was charged with sydnone **20** (200 mg, 0.604 mmol), 3-hydroxy-4-methoxyphenylboronic acid pinacol ester (228 mg, 0.912 mmol), $PdCl_2(PPh_3)_2$ (21 mg, 0.030 mmol), caesium fluoride (275 mg, 1.81 mmol) and 1,2-DME:H_2O (6 mL, 1:1) and heated at reflux for 14 h. The mixture was allowed to cool to ambient temperature, poured into water and extracted with ethyl acetate. The combined organic layers were dried over $MgSO_4$ and volatiles removed *in vacuo* resulting in a mixture of unidentifiable products.

4-(4-Methoxyphenyl)-*N*-(3,4,5-trimethoxyphenyl)sydnone, **22** and 4-phenyl-*N*-(3,4,5-trimethoxyphenyl)sydnone, **24**:

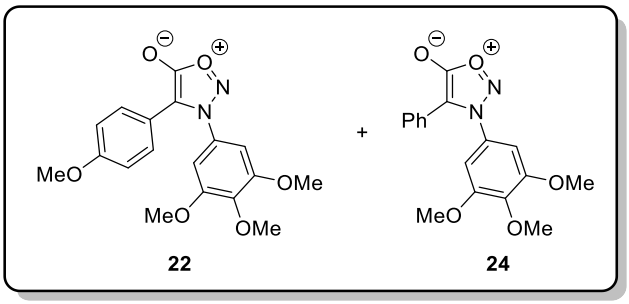

Following general procedure D using sydnone **19** (150 mg, 0.595 mmol) and 4-bromoanisole (166 mg, 0.879 mmol), a mixture of 3,4-diarylsydnone **22** and by-product **24** was isolated. Flash silica chromatography (eluting solvent 40% ethyl acetate in 40-60 petroleum ether) afforded 3,4-diarylsydnone **22** as an orange solid (117 mg, 55%) and by-product **24** as tan solid (33 mg, 17%).

22: M.p.: 165-167 °C (dec.); ^{1}H NMR (400 MHz, $CDCl_3$): δ 3.78 (6H, s), 3.79 (3H, s), 3.92 (3H, s), 6.67 (2H, s), 6.85 (2H, d, *J* = 9.0 Hz), 7.29 (2H, d, *J* = 9.0 Hz); ^{13}C NMR (101 MHz, $CDCl_3$): δ 55.4, 56.6, 61.2, 102.5, 108.0, 114.3, 116.8, 128.9, 129.9, 140.6, 154.1, 159.9, 167.2; FTIR: ν_{max} 2945 (w), 1723 (m), 1604 (s), 1232 (s), 1121 (s), 1019 (s), 987 (s); HRMS calculated for $C_{18}H_{19}N_2O_6$ (ES^+)($+H^+$): 359.1243. Found: 359.1226.

24: M.p.: 146-147 °C (dec.); ^{1}H NMR (400 MHz, $CDCl_3$): δ 3.77 (6H, s), 3.93 (3H, s), 6.69 (2H, s), 7.28-7.39 (5H, m); ^{13}C NMR (101 MHz, $CDCl_3$): δ 56.6, 61.3, 102.4, 107.8, 124.6, 127.4, 128.8, 128.9, 129.9, 140.8, 154.1, 167.1; FTIR: ν_{max} 2945 (w), 1746 (s), 1603 (s), 1232 (s), 1125 (s), 977 (s); HRMS calculated for $C_{18}H_{19}N_2O_6$ (ES^+)($+H^+$): 329.1137. Found: 329.1125.

4-(3,4,5-Trimethoxyphenyl)-*N*-(4-methoxyphenyl)sydnone **26**:

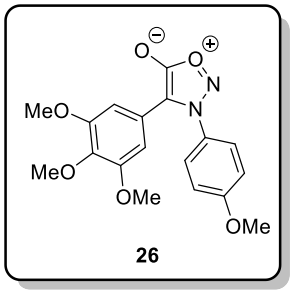

Following general procedure D using sydnone **25** (150 mg, 0.781 mmol) and 5-bromo-1,2,3-trimethoxybenzene (289 mg, 1.17 mmol), **26** was isolated as a yellow solid (138 mg, 49%).

M.p.: 155-157 °C (dec.); ^{1}H NMR (400 MHz, $CDCl_3$): δ 3.65 (6H, s), 3.82 (3H, s), 3.89 (3H, s), 6.55 (2H, s), 7.06 (2H, d, *J* = 9.0 Hz), 7.44 (2H, d, *J* = 9.0 Hz); ^{13}C NMR (101 MHz, $CDCl_3$): δ 56.0, 56.1, 61.1, 104.2, 107.9, 115.3, 120.0, 126.6, 127.5, 138.5, 153.4, 162.3, 167.1. FTIR: ν_{max} 3116 (w), 3091 (w), 2944 (w), 2841 (w), 1729 (s), 1578 (s), 1125 (s), 991 (m); HRMS calculated for $C_{18}H_{19}N_2O_6$ (ES^+)($+H^+$): 359.1243. Found: 359.1239.

4-Phenyl-*N*-(3,4,5-trimethoxyphenyl)sydnone, **24**:

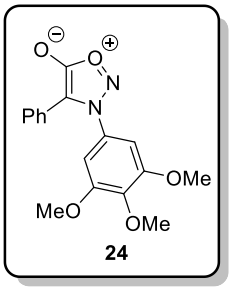

24

Following general procedure D using sydnone **19** (150 mg, 0.595 mmol) and bromobenzene (140 mg, 0.886 mmol), 3,4-diarylsydnone **24** was isolated as a tan solid (119 mg, 61%).

See above for characterisation data.

4-(3-Hydroxy-4-methoxyphenyl)-*N*-(3,4,5-trimethoxyphenyl)sydnone **21**:

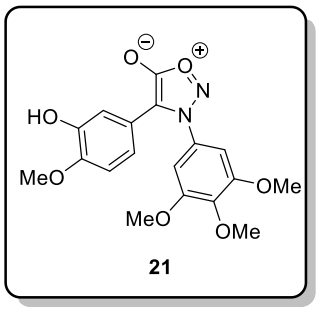

21

Following general procedure D using sydnone **19** (822 mg, 3.26 mmol) and (5-bromo-2-methoxyphenoxy)(tert-butyl)dimethylsilane (1.60 g, 4.89 mmol). Flash alumina chromatography (eluting solvent 2% methanol in dichloromethane) afforded **21** as a yellow solid (128 mg, 11%).

M.p.: 237-239 °C (dec.); ^{1}H NMR (400 MHz, DMSO-d_6): δ 3.73 (9H, s), 3.76 (3H, s), 6.71 (1H, dd, *J* = 8.5, 2.0 Hz), 6.88 (1H, d, *J* = 2.0 Hz), 6.91 (1H, d, *J* = 8.5 Hz), 7.13 (2H, s), 9.28 (1H,s); ^{13}C NMR (101 MHz, DMSO-d_6): δ 55.5, 56.5, 60.4, 103.9, 108.1, 112.0, 114.1, 117.0, 118.5, 129.9, 139.8, 146.3, 148.1, 153.5, 166.2; FTIR: ν_{max} 3415 (br), 3062 (w), 2947 (w), 1718 (s), 1605 (m), 1243 (s), 1125 (s), 1014 (s), 949 (m); HRMS calculated for $C_{18}H_{19}N_2O_7$ (ES^+)($+H^+$): 375.1192. Found: 375.1192.

3,4-Bis(4-methoxyphenyl)sydnone, **28**[177] and 4-phenyl-*N*-(4-methoxyphenyl)sydnone, **27**:[177]

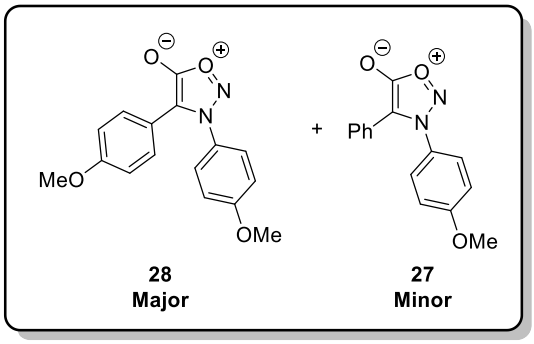

Following general procedure D using sydnone **25** (100 mg, 0.521 mmol) and 4-bromoanisole (146 mg, 0.781 mmol), a mixture of 3,4-diarylsydnone **28** and by-product **27** was isolated. Flash silica chromatography (eluting solvent 40% ethyl acetate in 40-60 petroleum ether) afforded **28** as a tan solid (45 mg, 29%) and by-product **27** as tan solid (13 mg, 9%).

28: M.p.: 136-137 °C (dec.) (lit.[177] 139–140 °C); ^{1}H NMR (400 MHz, $CDCl_3$) δ 3.78 (3H, s), 3.89 (3H, s), 6.82 (2H, d, *J* = 9.0 Hz), 7.02 (2H, d, *J* = 9.0 Hz), 7.24 (2H, d, *J* = 9.0 Hz), 7.39 (2H, d, *J* = 9.0 Hz); ^{13}C NMR (101 MHz, $CDCl_3$) δ 55.4, 55.9, 108.0, 114.4, 115.2, 117.0, 126.3, 127.4, 129.0, 159.8, 162.1, 167.4.

27: M.p.: 106-107 °C (dec.) (lit.[177] 122-123 °C); ^{1}H NMR (400 MHz, $CDCl_3$) δ 3.89 (3H, s), 7.02 (2H, d, *J* = 9.0 Hz), 7.30 (5H, s), 7.39 (2H, d, *J* = 9.0 Hz); ^{13}C NMR (101 MHz, $CDCl_3$) δ 55.9, 107.8, 115.3, 124.8, 126.3, 127.4, 127.5, 128.7, 128.9, 162.2, 167.3.

4-(2-Methoxyphenyl)-*N*-(3,4,5-trimethoxyphenyl)sydnone, **29**:

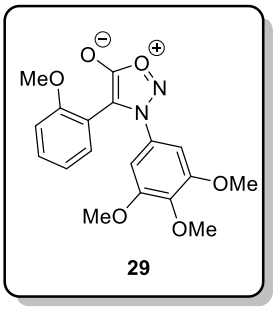

Following general procedure D using sydnone **19** (150 mg, 0.595 mmol) and 2-bromoanisole (166 mg, 0.888 mmol), 3,4-diarylsydnone **29** was isolated as a yellow solid (148 mg, 70%).

M.p.: 180-181 °C (dec.); ^{1}H NMR (400 MHz, $CDCl_3$): δ 3.40 (3H, s), 3.66 (6H, s), 3.84 (3H, s), 6.60 (2H, s), 6.78 (1H, dd, *J* = 8.5, 1.5 Hz), 7.03 (1H, td, *J* = 7.5, 1.0 Hz), 7.36 (1H, ddd, *J* = 8.5, 7.5, 1.5 Hz), 7.44 (1H, dd, *J* = 7.5, 1.5 Hz). ^{13}C NMR (101 MHz, $CDCl_3$): δ 55.1, 56.4, 61.2, 100.6, 105.3, 111.3, 114.0, 121.4, 131.3, 131.4, 131.7, 140.2, 153.6, 156.9, 167.8; FTIR: ν_{max} 2941

(b), 2837 (s), 1731 (s), 1607 (m), 1238 (s), 1120 (s), HRMS calculated for $C_{18}H_{19}N_2O_6$ (ES^+)($+H^+$): 359.1243. Found: 359.1226.

3,4-Bis(4-methoxyphenyl)sydnone, **28**:

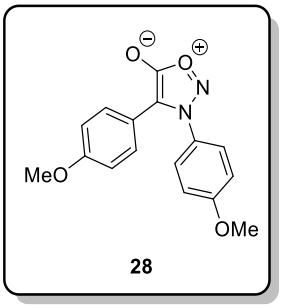

28

Following general procedure E using sydnone **25** (100 mg, 0.520 mmol) and 4-bromosydnone (146 mg, 0.781 mmol), 3,4-diarylsydnone **28** was isolated as a tan solid (77 mg, 50%).

See characterisation data above.

4-(4-Ethoxyphenyl)-*N*-(3,4,5-trimethoxyphenyl)sydnone, **30**:

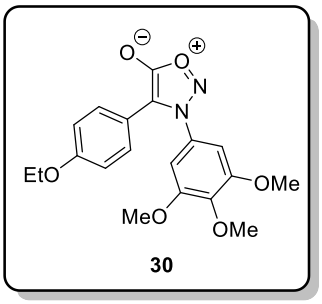

30

Following general procedure E using sydnone **19** (150 mg, 0.595 mmol) and 4-bromophenetole (181 mg, 0.900 mmol), 3,4-diarylsydnone **30** was isolated as a tan solid (23 mg, 10%).

M.p.: 143-144 °C (dec.); ^{1}H NMR (400 MHz, $CDCl_3$) δ 1.40 (3H, t, *J* = 7.0 Hz), 3.78 (6H, s), 3.92 (3H, s), 4.01 (2H, q, *J* = 7.0 Hz), 6.67 (2H, s), 6.83 (2H, d, *J* = 9.0 Hz), 7.27 (2H, d, *J* = 9.0 Hz); ^{13}C NMR (101 MHz, $CDCl_3$) δ 14.8, 56.7, 61.3, 63.7, 102.5, 108.2, 114.9, 116.7, 129.0, 130.1, 140.7, 154.2, 159.4, 167.3; FTIR: ν_{max} 2985 (w), 2941 (w), 1749 (s), 1600 (m), 1231 (s), 1125 (s), 999 (m), 978 cm^{-1} (s); HRMS calculated for $C_{19}H_{21}N_2O_6$ (ES^+)($+H^+$): 373.1400. Found: 373.1408.

3,4-Bis(4-methoxyphenyl)sydnone (with 4-bromoanisole), **28**:[177]

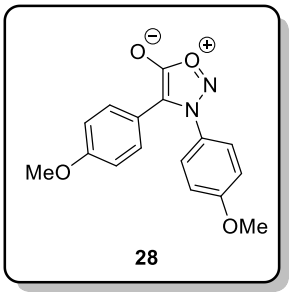

28

Following general procedure F using sydnone **25** (100 mg, 0.521 mmol) and 4-bromoanisole (146 mg, 0.782 mmol), 3,4-diarylsydnone **28** was isolated as a tan solid (134 mg, 86%).

See characterisation data above.

3,4-Bis(4-methoxyphenyl)sydnone (with 4-chloroanisole), **28**:[177]

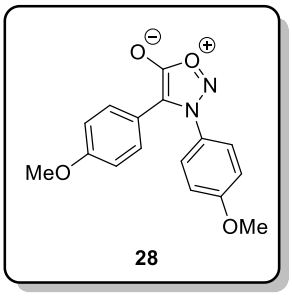

28

Following general procedure F using sydnone **25** (103 mg, 0.536 mmol) and 4-chloroanisole (115 mg, 0.807 mmol), 3,4-diarylsydnone **28** was isolated as a tan solid (127 mg, 79%).

See characterisation data above.

3,4-Bis(4-methoxyphenyl)sydnone, **28** (5 mmol scale):[177]

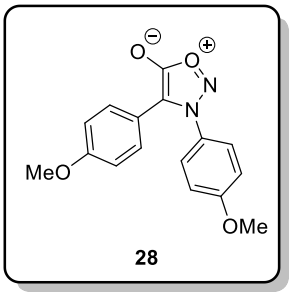

28

Following general procedure F using sydnone **25** (1.00 g, 5.21 mmol) and 4-chloroanisole (0.99 g 7.8 mmol), 3,4-diarylsydnone **28** was isolated as a tan solid (1.51 g, 97%).

See characterisation data above.

4-(4-Tolyl)-*N*-(4-methoxyphenyl)sydnone, **33**:

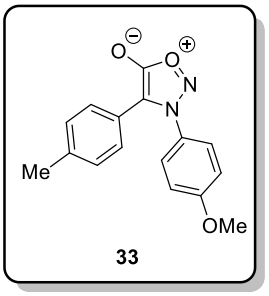

33

Following general procedure F using sydnone **25** (99 mg, 0.52 mmol) and 1-chloro-4-methylbenzene (98 mg, 0.77 mmol), 3,4-diarylsydnone **33** was isolated as tan crystals (121 mg, 83%).

M.p.: 106 °C (dec.); ^{1}H NMR (400 MHz, $CDCl_3$) δ 2.30 (3H, s), 3.88 (3H, s), 7.02 (2H, d, *J* = 9.0 Hz), 7.09 (2H, d, *J* = 8.0 Hz), 7.18 (2H, d, *J* = 8.0 Hz), 7.38 (2H, d, *J* = 9.0 Hz); ^{13}C NMR (101 MHz, $CDCl_3$) δ 21.4, 55.9, 108.0, 115.2, 121.8, 126.3, 127.4, 127.5, 129.5, 138.9, 162.1, 167.3; FTIR: ν_{max} 3076 (w), 2840 (w), 1736 (s), 1110 (s), 1002 (w), 968 (m); HRMS calculated for $C_{16}H_{15}N_2O_3$ (ES^+)($+H^+$): 283.1083. Found: 283.1085.

4-(4-Tolyl)-*N*-(3,4,5-trimethoxyphenyl)sydnone, **34**:

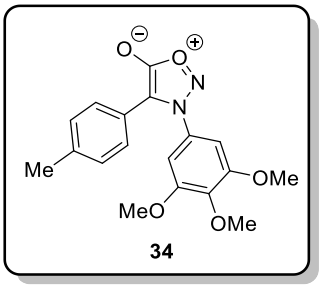

34

Following general procedure F using sydnone **19** (151 mg, 0.599 mmol) and 1-chloro-4-methylbenzene (114 mg, 0.901 mmol), 3,4-diarylsydnone **34** was isolated as colourless crystals (196 mg, 96%).

M.p.: 140-141 °C (dec.); ^{1}H NMR (400 MHz, $CDCl_3$) δ 2.31 (3H, s), 3.75 (6H, s), 3.91 (3H, s), 6.67 (2H, s), 7.10 (2H, d, *J* = 8.0 Hz), 7.22 (2H, d, *J* = 8.0 Hz); ^{13}C NMR (101 MHz, $CDCl_3$) δ 21.4, 56.6, 61.2, 102.5, 108.0, 121.7, 127.3, 129.5, 130.0, 139.0, 140.7, 154.1, 167.1; FTIR: ν_{max} 2942 (w), 2840 (w), 1749 (s), 1128 (s), 984 (m); HRMS calculated for $C_{18}H_{19}N_2O_5$ (ES^+)($+H^+$): 343.1294. Found: 343.1283.

4-(4-Tolyl)-*N*-(4-ethoxyphenyl)sydnone, **35**:

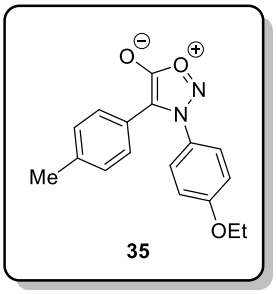

35

Following general procedure F using sydnone **31** (127 mg, 0.616 mmol) and 1-chloro-4-methylbenzene (117 mg, 0.924 mmol), 3,4-diarylsydnone **35** was isolated as a tan solid (140 mg, 77%).

M.p.: 123-124 °C (dec.); ^{1}H NMR (400 MHz, $CDCl_3$) δ 1.45 (3H, t, *J* = 7.0 Hz), 2.29 (3H, s), 4.09 (2H, q, *J* = 7.0 Hz), 6.99 (2H, d, *J* = 9.0 Hz), 7.08 (2H, d, *J* = 8.0 Hz), 7.18 (2H, d, *J* = 8.0 Hz), 7.35 (2H, d, *J* = 9.0 Hz); ^{13}C NMR (101 MHz, $CDCl_3$) δ 14.7, 21.4, 64.3, 108.0, 115.6, 121.9, 126.2, 127.2, 127.3 129.5, 138.8, 161.5, 167.3; FTIR: ν_{max} 2981 (w), 2934 (w), 1737 (s), 1115 (m), 1041 (m), 1002 (m); HRMS calculated for $C_{17}H_{17}N_2O_3$ (ES^+)($+H^+$): 297.1239. Found: 297.1249.

4-(4-Tolyl)-*N*-phenylsydnone, **37**:[101]

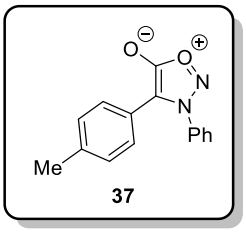

37

Following general procedure F using sydnone **36** (102 mg, 0.629 mmol) and 1-chloro-4-methylbenzene (119 mg, 0.940 mmol), 3,4-diarylsydnone **37** was isolated as a tan solid (131 mg, 83%).

M.p.: 134-136 °C (dec.) (Lit[101] 141-143 °C) ^{1}H NMR (400 MHz, $CDCl_3$) δ 2.30 (3H, s), 7.08 (2H, d, *J* = 8.0 Hz), 7.16 (2H, d, *J* = 8.0 Hz), 7.47 (2H, d, *J* = 7.5 Hz), 7.57 (2H, t, *J* = 7.5 Hz), 7.60-7.70 (1H, m); ^{13}C NMR (101 MHz, $CDCl_3$) δ 21.4, 108.2, 121.6, 125.0, 127.4, 129.5, 130.2, 132.1, 134.8, 139.0, 167.3.

4-(4-Tolyl)-*N*-(4-fluorophenyl)sydnone, **39**:

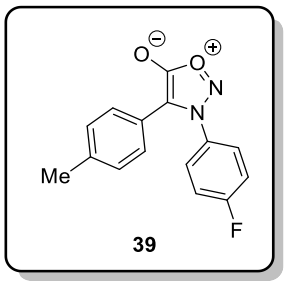

39

Following general procedure F using sydnone **38** (100 mg, 0.555 mmol) and 1-chloro-4-methylbenzene (105 mg, 0.830 mmol), 3,4-diarylsydnone **39** was isolated as an orange solid (102 mg, 68%). *Note: Product was unstable in solutions of dichloromethane and chloroform.*

M.p.: 150-151 °C ; ^{1}H NMR (400 MHz, $CDCl_3$) δ 2.32 (3H, s), 7.12 (2H, d, *J* = 8.0 Hz), 7.17 (2H, d, *J* = 8.0 Hz), 7.22-7.30 (2H, m), 7.46-7.54 (2H, m); ^{13}C NMR (101 MHz, $CDCl_3$) δ 21.4, 108.3, 117.5 (d, *J* = 24.0 Hz), 121.3, 127.2 (d, *J* = 9.0 Hz), 128.6 (d, *J* = 223.0 Hz), 130.8 (d, *J* = 3.0 Hz), 139.3, 163.0, 165.5, 167.1; ^{19}F NMR (376 MHz, $CDCl_3$) δ -107.3 - -107.4 (m); FTIR: ν_{max} 3080 (w), 2158 (w), 1738 (s), 1507 (s), 1234 (s), 1006 (m); HRMS calculated for $C_{15}H_{12}N_2O_2F$ (ES^+)($+H^+$): 271.0883. Found: 271.0891.

4-(4-Tolyl)-*N*-(methyl)sydnone, **41**:

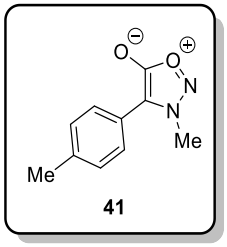

41

Following general procedure F at 80 °C using sydnone **40** (129 mg, 1.29 mmol) and 1-chloro-4-methylbenzene (245 mg, 1.94 mmol), 3,4-arylated sydnone **41** was isolated as a colourless crystals (164 mg, 67%).

M.p.: 98-99 °C; ^{1}H NMR (400 MHz, $CDCl_3$) δ 2.40 (3H, s), 4.11 (3H, s), 7.30 (2H, d, *J* = 8.0 Hz), 7.46 (2H, d, *J* = 8.0 Hz); ^{13}C NMR (101 MHz, $CDCl_3$) δ 21.4, 38.9, 108.2, 121.4, 127.6, 129.9, 139.5, 167.4; FTIR: ν_{max} 3024 (w), 2924 (w), 1719 (s), 1536 (m), 1445 (m), 1311 (m), 1087 (m), 986 (s); HRMS calculated for $C_{10}H_{11}N_2O_2$ (ES^+)($+H^+$): 191.0821. Found: 191.0813.

4-(4-Tolyl)-*N*-(ethyl)sydnone, **43**:

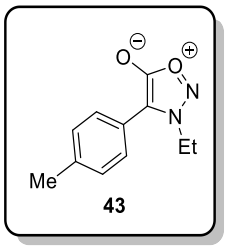

Following general procedure F at 80 °C using sydnone **42** (104 mg, 0.911 mmol) and 1-chloro-4-methylbenzene (173 mg, 1.37 mmol), 3,4-arylated sydnone **43** was isolated as a colourless solid (134 mg, 72%). *Note: product was not stable and began to decompose after isolation.*

M.p.: 165-167 °C; ^{1}H NMR (400 MHz, $CDCl_3$) δ 1.53-1.59 (3H, m), 2.40 (3H, s), 4.46 (2H, q, *J* = 7.5 Hz), 7.30 (2H, d, *J* = 8.0 Hz), 7.41 (2H, d, *J* = 8.0 Hz); ^{13}C NMR (101 MHz, $CDCl_3$) δ 13.8, 21.4, 47.6, 107.2, 121.5, 128.0, 130.0, 139.3, 167.7; FTIR: ν_{max} 2820 (b), 2537 (b), 1668 (s), 1611 (m), 1417 (m), 1283 (s), 960 (m) 945 (s); HRMS calculated for $C_{11}H_{13}N_2O_2$ (ES^+)($+H^+$): 205.0977. Found: 205.0981.

4-(4-Tolyl)-*N*-(benzyl)sydnone, **45**:

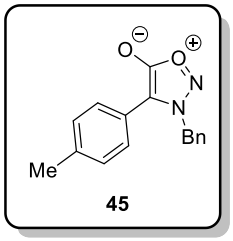

Following general procedure F at 80 °C using sydnone **44** (100 mg, 0.568 mmol) and 1-chloro-4-methylbenzene (107 mg, 0.845 mmol), arylated sydnone **45** was isolated as a yellow solid (93 mg, 61%).

M.p.: 81 °C; ^{1}H NMR (400 MHz, $CDCl_3$) δ 2.36 (3H, s), 5.49 (2H, s), 7.14-7.19 (2H, m), 7.21 (2H, d, *J* = 8.0 Hz), 7.27 (2H, d, *J* = 8.0 Hz), 7.31-7.40 (3H, m); ^{13}C NMR (101 MHz, $CDCl_3$) δ 21.5, 55.3, 108.1, 121.3, 127.7, 128.5, 129.4, 129.5, 130.0, 131.6, 139.8, 167.7; FTIR: ν_{max} 3039 (w), 2994 (w), 2958 (w), 1724 (s), 991 (s), 960 (m); HRMS calculated for $C_{16}H_{15}N_2O_2$ (ES^+)($+H^+$): 267.1134. Found: 267.1143.

4-Phenyl-*N*-(4-methoxyphenyl)sydnone, **27**:[177]

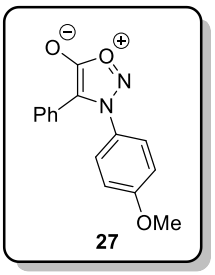

27

Following general procedure F using sydnone **25** (105 mg, 0.547 mmol) and chlorobenzene (92 mg, 0.82 mmol), 3,4-diarylsydnone **27** was isolated as a pink solid (122 mg, 83%).

See characterisation data above.

4-(3-Nitrophenyl)-*N*-(4-methoxyphenyl)sydnone, **46**:[177]

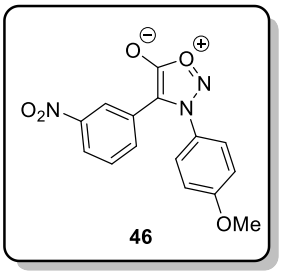

46

Following general procedure F using sydnone **25** (104 mg, 0.542 mmol) and 1-chloro-3-nitrobenzene (128 mg, 0.812 mmol), 3,4-diarylsydnone **46** was isolated as a yellow solid (144 mg, 85%).

M.p.: 152-153 °C (dec.); ^{1}H NMR (400 MHz, $CDCl_3$) δ 3.92 (3H, s), 7.09 (2H, d, *J* = 9.0 Hz), 7.43 (2H, d, *J* = 9.0 Hz), 7.50 (1H, t, *J* = 8.0 Hz), 7.75 (1H, d, *J* = 8.0 Hz), 8.02-8.12 (2H, m); ^{13}C NMR (101 MHz, d_6-DMSO) δ 56.9, 106.5, 115.4, 121.2, 122.8, 126.5, 126.6, 127.1, 130.2, 132.8, 147.6, 161.9, 166.2.

4-(2-Chlorophenyl)-*N*-(4-methoxyphenyl)sydnone, **47**:

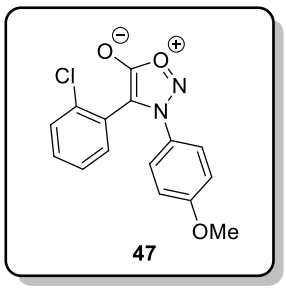

47

Following general procedure F using sydnone **25** (102 mg, 0.531 mmol) and 1,2-dichlorobenzene (117 mg, 0.796 mmol), 3,4-diarylsydnone **47** was isolated as an orange oil (151 mg, 94%).

^{1}H NMR (400 MHz, $CDCl_3$) δ 3.82 (3H, s), 6.91 (2H, d, *J* = 9.0 Hz), 7.27-7.40 (6H, m); ^{13}C NMR (101 MHz, $CDCl_3$) δ 55.8, 105.8, 115.0, 120.4, 124.0, 125.2, 127.5, 130.4, 131.5, 133.0, 135.4, 162.0, 167.2; FTIR: ν_{max} 3066 (w), 2936 (w), 2843 (w), 1757 (s), 1743 (s), 1028 (m), 1002 (m); HRMS calculated for $C_{15}H_{12}N_2O_3Cl^{35}$ (ES^+)($+H^+$): 303.0536. Found: 303.0524.

4-(3-Chlorophenyl)-*N*-(4-methoxyphenyl)sydnone, **48**:

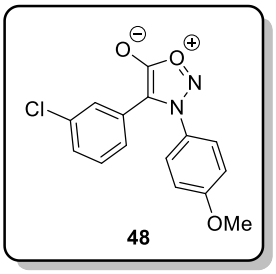

48

Following general procedure F using sydnone **25** (100 mg, 0.521 mmol) and 1,3-dichlorobenzene (115 mg, 0.782 mmol), 3,4-diarylsydnone **48** was isolated as a yellow solid (125 mg, 79%).

M.p.: 118 °C (dec.); ^{1}H NMR (400 MHz, $CDCl_3$) δ 3.90 (3H, s), 7.05 (2H, d, *J* = 9.0 Hz), 7.10 (1H, dt, *J* = 7.5, 1.5 Hz), 7.20 (1H, t, *J* = 7.5 Hz), 7.24 (1H, dt, *J* = 8.0, 1.5 Hz), 7.36-7.42 (3H, m); ^{13}C NMR (101 MHz, $CDCl_3$) δ 56.0, 106.4, 115.5, 125.2, 126.2, 126.5, 127.0, 127.1, 128.7, 130.0, 134.9, 162.4, 166.9; FTIR: ν_{max} 3078 (w), 2937 (w), 2842 (w), 1749 (s), 1735 (s), 1125 (s), 1028 (m); HRMS calculated for $C_{15}H_{12}N_2O_3Cl^{35}$ (ES^+)($+H^+$): 303.0536. Found: 303.0535.

4-(4-Aminophenyl)-*N*-(4-methoxyphenyl)sydnone, **49**:

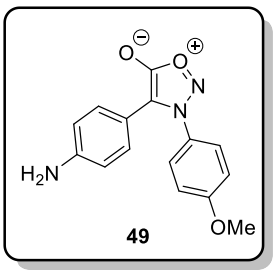

49

Following general procedure F using sydnone **25** (100 mg, 0.521 mmol) and 4-chloroaniline (99 mg, 0.779 mmol), 3,4-diarylsydnone **49** was isolated as a yellow solid (33 mg, 22%).

M.p.: 158 °C; ^{1}H NMR (400 MHz, $CDCl_3$) δ 3.85 (2H, s), 3.88 (3H, s), 6.56 (2H, d, *J* = 9.0 Hz), 7.00 (2H, d, *J* = 9.0 Hz), 7.08 (2H, d, *J* = 9.0 Hz), 7.38 (2H, d, *J* = 9.0 Hz); ^{13}C NMR (101 MHz, $CDCl_3$) δ 55.9, 108.7, 114.2, 115.0, 115.2, 126.3, 127.6, 129.0, 147.1, 162.0, 167.5; FTIR: ν_{max} 3461 (w), 3359 (m), 3232 (w), 1732 (s), 1607 (m), 1249 (s), 1182 (m); HRMS calculated for $C_{15}H_{14}N_3O_3$ (ES^+)($+H^+$): 284.1035. Found: 284.1045.

4-(Thiophen-2-yl)-*N*-(4-methoxyphenyl)sydnone, **51**:

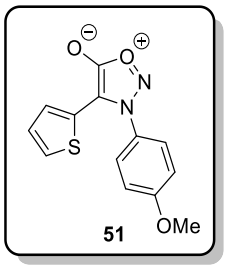

51

Following general procedure F using sydnone **25** (101 mg, 0.526 mmol) and 2-chlorothiophene (93 mg, 0.78 mmol), 3,4-diarylsydnone **51** was isolated orange crystals (128 mg, 89%).

M.p.: 129 °C; ^{1}H NMR (400 MHz, $CDCl_3$) δ 3.93 (3H, s), 6.98 (1H, dt, *J* = 5.0, 4.0 Hz), 7.11 (2H, d, *J* = 9.0 Hz), 7.23 (1H, dd, *J* = 5.0, 1.0 Hz), 7.33 (1H, dd, *J* = 4.0, 1.0 Hz), 7.46 (2H, d, *J* = 9.0 Hz); ^{13}C NMR (101 MHz, $CDCl_3$) δ 57.0, 106.6, 115.4, 125.8, 126.1, 126.2, 126.4, 127.3, 127.5, 162.8, 165.9; FTIR: ν_{max} 3080 (w), 2941 (w), 2840 (w), 1756 (s), 1735 (s), 1176 (m), 1017 (s), 991 (m); HRMS calculated for $C_{13}H_{11}N_2O_2S$ (ES^+)($+H^+$): 275.0490. Found: 275.0503.

4-(4-Pyridyl)-*N*-(4-methoxyphenyl)sydnone, **52**:

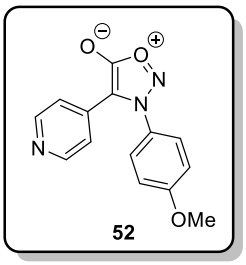

52

Following general procedure F using sydnone **25** (100 mg, 0.521 mmol), 4-chloropyridine hydrogen chloride (119 mg, 0.780 mmol) and potassium carbonate (252 mg, 1.82 mmol), 3,4-diarylsydnone **52** was isolated pink crystals (109 mg, 78%).

M.p.: 108-110 °C; ^{1}H NMR (400 MHz, $CDCl_3$) δ 3.92 (3H, s), 7.09 (2H, d, *J* = 9.0 Hz), 7.20 (2H, br d, *J* = 9.0 Hz), 7.42 (2H, d, *J* = 9.0 Hz), 8.50 (2H, br); ^{13}C NMR (101 MHz, $CDCl_3$) δ 56.0, 105.0, 115.7, 119.9, 126.3, 126.9, 132.5, 150.2, 162.8, 166.4; FTIR: ν_{max} 2934 (w), 2841 (w), 1742 (s), 1596 (m), 1510 (s), 1258 (s), 1026 (m); HRMS calculated for $C_{14}H_{12}N_3O_3$ (ES^+)($+H^+$): 270.0879. Found: 270.0871.

4-(4-Aminophenyl)-*N*-(4-methoxyphenyl)sydnone, **49**: (using 4-bromoaniline)

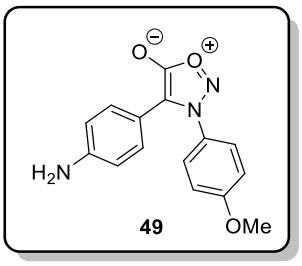

49

Following general procedure F using sydnone **25** (100 mg, 0.521 mmol) and 4-bromoaniline (134 mg, 0.779 mmol), 3,4-diarylsydnone **49** was isolated as an yellow solid (137 mg, 93%).

See characterisation data above.

4-(4-Hydroxyphenyl)-*N*-(4-methoxyphenyl)sydnone, **50**: (using 4-bromophenol)

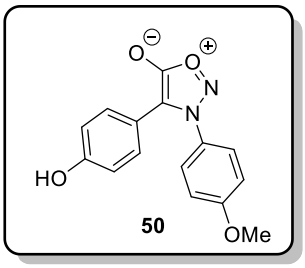

50

Following general procedure F using sydnone **25** (100 mg, 0.521 mmol) and 4-bromophenol (135 mg, 0.780 mmol), 3,4-diarylsydnone **50** was isolated as a tan solid (86 mg, 58%).

M.p.: 212-214 °C; ^{1}H NMR (400 MHz, $CDCl_3$) δ 3.89 (3H, s), 5.08 (1H, br), 6.76 (2H, d, *J* = 9.0 Hz), 7.02 (2H, d, *J* = 9.0 Hz), 7.19 (2H, d, *J* = 9.0 Hz), 7.39 (2H, d, *J* = 9.0 Hz); ^{13}C NMR (101 MHz, DMSO- d_6) δ 55.8, 108.5, 115.1, 115.5, 117.6, 127.0, 129.2, 132.0, 157.9, 161.5, 166.5; FTIR: ν_{max} 3254(br), 1710 (s), 1603 (m), 1513 (s), 1249 (s), 1171 (s), 1026 (m), 998 (m), 834 (s); HRMS calculated for $C_{15}H_{13}N_2O_4$ (ES^+)($+H^+$): 285.0875. Found: 285.0873.

4-(4-Methoxyphenyl)-*N*-(3,4,5-trimethoxyphenyl)sydnone, **22**:

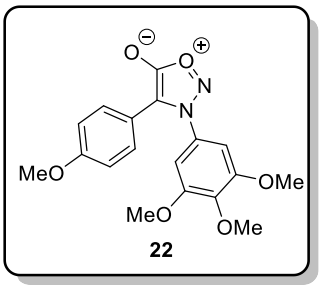

Following general procedure F using sydnone **19** (114 mg, 0.452 mmol) and 4-bromoanisole (97 mg, 0.68 mmol), 3,4-diarylsydnone **22** was isolated as yellow crystals (119 mg, 73%).

See characterisation data above.

4-(2-Methoxyphenyl)-*N*-(3,4,5-trimethoxyphenyl)sydnone, **29**:

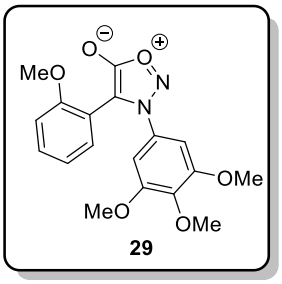

Following general procedure F using sydnone **19** (200 mg, 0.792 mmol) and 2-bromoanisole (223 mg, 1.19 mmol), 3,4-diarylsydnone **29** was isolated as a yellow solid (202 mg, 71%).

See characterisation data above.

4-Phenyl-*N*-(3,4,5-trimethoxyphenyl)sydnone, **24**:

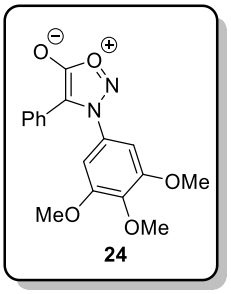

Following general procedure F using sydnone **19** (99 mg, 0.39 mmol) and chlorobenzene (66 mg, 0.59 mmol), 3,4-diarylsydnone **24** was isolated as a tan solid (124 mg, 81%).

See above for characterisation data.

4-(3-Nitrophenyl)-*N*-(3,4,5-trimethoxyphenyl)sydnone, **53**:

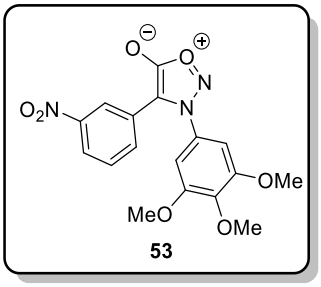

53

Following general procedure F using sydnone **19** (103 mg, 0.408 mmol) and 1-chloro-3-nitrobenzene (96 mg, 0.61 mmol), 3,4-diarylsydnone **53** was isolated as orange crystals (137 mg, 90%).

M.p.: 148-149 °C; ^{1}H NMR (400 MHz, $CDCl_3$) δ 3.82 (6H, s), 3.95 (3H, s), 6.71 (2H, s), 7.52 (1H, td, *J* = 8.0, 1.0 Hz), 7.76-7.82 (1H, m), 8.08-8.15 (2H, m); ^{13}C NMR (101 MHz, $CDCl_3$) δ 56.8, 61.4, 102.6, 105.6, 121.1, 123.0, 126.5, 129.2, 129.9, 132.0, 141.5, 148.3, 154.6, 166.4; FTIR: ν_{max} 1748 (s), 1731 (s), 1605 (m), 1535 (s), 1352 (s), 1265 (s), 1230 (s), 1126 (s), 987 (m); HRMS calculated for $C_{17}H_{16}N_3O_7$ (ES^+)($+H^+$): 374.0988. Found: 374.0990.

4-(Thiophen-2-yl)-*N*-(3,4,5-trimethoxyphenyl)sydnone, **54**:

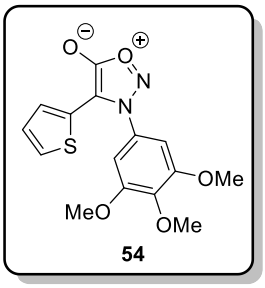

54

Following general procedure F using sydnone **19** (103 mg, 0.410 mmol) and 2-chlorothiophene (73 mg, 0.62 mmol), 3,4-diarylsydnone **54** was isolated as yellow crystals (111 mg, 81%).

M.p.: 173-174 °C; ^{1}H NMR (400 MHz, $CDCl_3$) δ 3.86 (6H, s), 3.96 (3H, s), 6.76 (2H, s), 7.00 (1H, dt, *J* = 5.0, 4.0 Hz), 7.26 (1H, dd, *J* = 5.0, 1.0 Hz), 7.39 (1H, dd, *J* = 4.0, 1.0 Hz); ^{13}C NMR (101 MHz, $CDCl_3$) δ 56.7, 61.4, 103.5, 106.5, 125.6, 126.2, 126.7, 127.5, 128.7, 141.3, 154.3, 165.7; FTIR: ν_{max} 3094 (w), 2943 (w), 2835 (w), 1746 (s), 1605 (m), 1235 (s), 1127 (s), 998 (w); HRMS calculated for $C_{15}H_{15}N_2O_5S$ (ES^+)($+H^+$): 335.0702. Found: 335.0704.

4-(4-Ethoxyphenyl)-*N*-(3,4,5-trimethoxyphenyl)sydnone**, 30**:

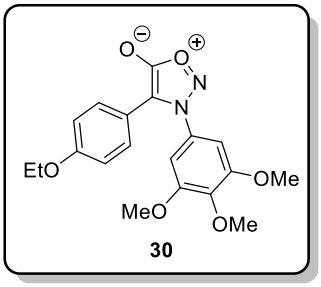

30

Following general procedure F using sydnone **19** (200 mg, 0.792 mmol) and 4-bromophenetole (239 mg, 1.19 mmol), 3,4-diarylsydnone **30** was isolated as a tan solid (272 mg, 92%).

See above for characterisation data.

4-(2-Chlorophenyl)-*N*-(3,4,5-trimethoxyphenyl)sydnone **55**:

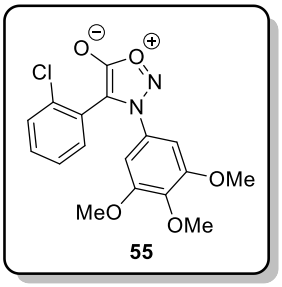

55

Following general procedure F using sydnone **19** (101 mg, 0.399 mmol) and 1,2-dichlorobenzene (88 mg, 0.60 mmol), **55** was isolated as a colourless solid (105 mg, 73%).

M.p.: 135-136 °C; ^{1}H NMR (400 MHz, $CDCl_3$) δ 3.67 (6H, s), 3.85 (3H, s), 6.59 (2H, s), 7.29-7.45 (4H, m); ^{13}C NMR (101 MHz, $CDCl_3$) δ 56.4, 61.2, 101.2, 105.7, 124.3, 127.6, 129.9, 130.3, 131.7, 132.9, 135.7, 140.6, 153.7, 167.0; FTIR: ν_{max} 3058 (w), 2943 (w), 1757 (s), 1608 (m), 1234 (m), 1130 (s), 1049 (w), 988 (m); HRMS calculated for $C_{17}H_{16}Cl^{35}N_2O_5$ (ES^+)($+H^+$): 363.0748. Found: 363.0736.

4-(3-Amino-4-methoxyphenyl)-*N*-(3,4,5-trimethoxyphenyl)sydnone **56**:

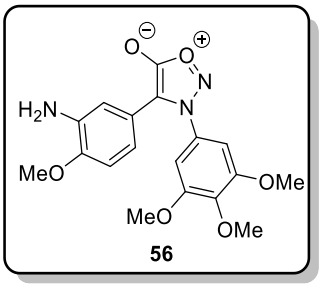

56

Following general procedure F using sydnone **19** (100 mg, 0.396 mmol) and 5-bromo-2-methoxyaniline (120 mg, 0.595 mmol), **56** was isolated as an orange solid (135 mg, 91%).

M.p.: 173-174 °C; ^{1}H NMR (400 MHz, $CDCl_3$) δ 3.77 (6H, s), 3.80 (3H, s), 3.83 (2H, s), 3.90 (3H, s), 6.52 (1H, dd, *J* = 8.5, 2.0 Hz), 6.64 (1H, d, *J* = 8.5 Hz), 6.68 (2H, s), 6.85 (1H, d, *J* = 2.0 Hz); ^{13}C NMR (101 MHz, $CDCl_3$) δ 55.6, 56.6, 61.2, 102.5, 108.4, 110.2, 113.4, 117.1, 118.1, 130.1, 136.6, 140.5, 147.7, 154.0, 167.2; FTIR: ν_{max} 3471 (w), 3367 (w), 2941 (w), 2838 (w), 1732 (s), 1606 (m), 1224 (s), 1127 (s); HRMS calculated for $C_{18}H_{20}N_3O_6$ (ES^+)($+H^+$): 374.1352. Found: 374.1353.

4-(3-Hydroxy-4-methoxyphenyl)-*N*-(3,4,5-trimethoxyphenyl)sydnone **21**:

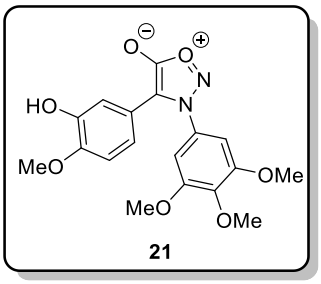

Following general procedure F using sydnone **19** (500 mg, 1.98 mmol) and 5-bromo-2-methoxyphenol (604 mg, 2.97 mmol). Flash silica chromatography (eluting solvent 10%-30% ethyl acetate in dichloromethane) afforded **21** as a yellow solid (599 mg, 81%).

See above for characterisation data.

4-(3,4,5-Trimethoxyphenyl)-*N*-(3-hydroxy-4-methoxyphenyl)sydnone **58**:

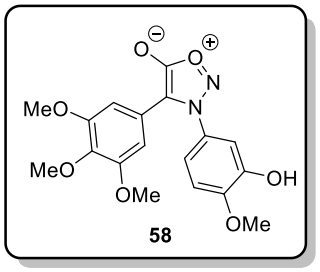

Following general procedure F using sydnone **57** (473 mg, 2.27 mmol) and 5-bromo-1,2,3-trimethoxybenzene (842 mg, 3.41 mmol), **58** was islolated as a colourless solid (402 mg, 47%).

M.p.: 196-197 °C; ^{1}H NMR (400 MHz, $CDCl_3$) δ 3.67 (6H, s), 3.83 (3H, s), 4.00 (3H, s), 5.94 (1H, s), 6.59 (2H, s), 6.92-7.05 (2H, m), 7.09 (1H, s); ^{13}C NMR (101 MHz, $CDCl_3$) δ 56.1, 56.5, 61.0, 104.7, 108.0, 111.0, 111.7, 117.2, 119.9, 127.8, 138.5, 147.0, 149.5, 153.3, 167.2; FTIR: ν_{max}

3295 (br), 3082 (w), 2940 (w), 2836 (w), 1710 (s), 1600 (w), 1581 (m), 1509 (s), 1229 (s), 1125 (s) 1014 (m), 998 (m); HRMS calculated for $C_{18}H_{19}N_2O_7$ (ES^+)($+H^+$): 375.1192. Found: 375.1181.

4-(3,4,5-Trimethoxyphenyl)-*N*-(4-ethoxyphenyl)sydnone, **32**:

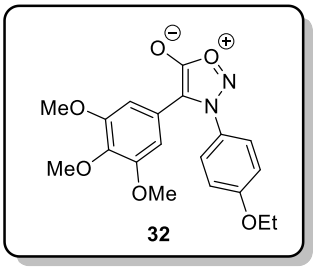

32

Following general procedure F using sydnone **31** (102 mg, 0.494 mmol) and 5-bromo-1,2,3-trimethoxybenzene (149 mg, 0.741 mmol), **32** was isolated as colourless crystals (140 mg, 76%).

M.p.: 129-130 °C (dec.); ^{1}H NMR (400 MHz, $CDCl_3$) δ 1.45 (3H, t, *J* = 7.0 Hz), 3.63 (6H, s), 3.80 (3H, s), 4.09 (2H, q, *J* = 7.0 Hz), 6.54 (2H, s), 7.03 (2H, d, *J* = 9.0 Hz), 7.41 (2H, d, *J* = 9.0 Hz); ^{13}C NMR (101 MHz, $CDCl_3$) δ 14.7, 56.0, 60.8, 64.4, 104.6, 107.8, 115.7, 120.0, 126.2, 127.1, 138.4, 153.3, 161.6, 166.8; FTIR: ν_{max} 2984 (w), 2937 (w), 2834 (w), 1743 (s), 1583 (m), 1250 (m), 1126 (s), 1046 (w), 1002 (w); HRMS calculated for $C_{19}H_{21}N_2O_6$ (ES^+)($+H^+$): 373.1400. Found: 373.1411.

4-(3,4,5-Trimethoxyphenyl)-*N*-(4-methoxyphenyl)sydnone **26**:

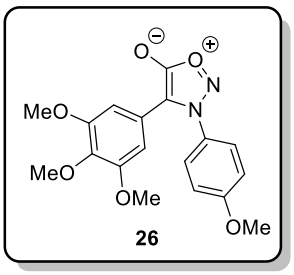

26

Following general procedure F using sydnone **26** (100 mg, 0.521 mmol) and 5-bromo-1,2,3-trimethoxybenzene (193 mg, 0.781 mmol), **26** was isolated as a yellow solid (132 mg, 71%).

See above for characterisation data.

3-((*Tert*-butyldimethylsilyl)oxy)-4-methoxybenzaldehyde **59**:[178]

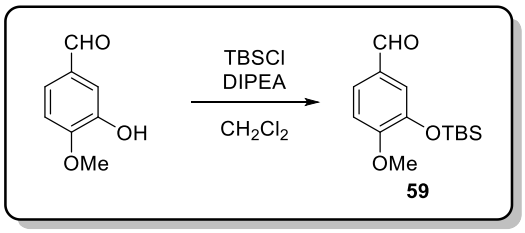

To a solution of 3-hydroxyl-4-methoxybenzaldehyde (10.0 g, 65.7 mmol) and TBSCl (12.0 g, 79.6 mmol) in CH_2Cl_2 (150 mL), under an atmosphere of nitrogen, was added DIPEA (17.1 g, 132 mmol) and the reaction stirred at room temperature for 14 hours. Aqueous NH_4Cl was added and the mixture extracted with CH_2Cl_2. The organic phase was dried over $MgSO_4$ and the volatiles were removed *in vacuo.* Flash silica chromatography (eluting solvent 10% ethyl acetate in 40-60 petroleum ether) afforded **59** as a colourless oil (17.2 g, 98%).

^{1}H NMR (400 MHz, $CDCl_3$) δ 0.17 (6H, s), 1.00 (9H, s), 3.90 (3H, s), 6.95 (1H, d, *J* = 8.5 Hz), 7.37 (1H, d, *J* = 2.0 Hz), 7.48 (1H, dd, *J* = 8.5, 2.0 Hz), 9.82 (1H, s); ^{13}C NMR (101 MHz, $CDCl_3$) δ -4.5, -3.5, 25.8, 55.7, 111.3, 120.2, 126.4, 130.3, 145.7, 156.7, 191.0.

Tert-butyl(5-(2,2-dibromovinyl)-2-methoxyphenoxy)dimethylsilane:[179]

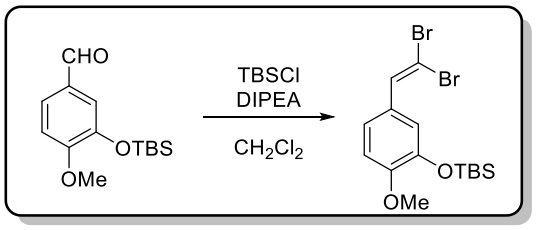

To a solution of **59** (10.4 g, 39.0 mmol) and triphenylphosphine (22.9 g, 78.1 mmol) in CH_2Cl_2 (100 mL), at 0 ^{o}C, under an atmosphere of nitrogen, was added carbon tetrabromide (14.2 g, 42.9 mmol) in CH_2Cl_2 (100 mL) dropwise. The mixture was allowed to warm to room temperature and stirred for 2 hours. Water was added and the reaction mixture extracted with CH_2Cl_2. The organic phase was dried over $MgSO_4$ and volatiles were removed *in vacuo*. Cold diethyl ether was added to the crude material, followed by filtration and removal of volatiles *in vacuo*. Flash silica chromatography (eluting solvent 10% ethyl acetate in 40-60 petroleum ether) afforded *tert*-butyl(5-(2,2-dibromovinyl)-2-methoxyphenoxy) dimethylsilane as an orange oil (14.9 g, 91%). N.B. the product contained small amounts of triphenylphosphine oxide and was characterised by ^{1}H NMR spectroscopy only.

^{1}H NMR (400 MHz, $CDCl_3$) δ 0.16 (6H, s), 1.00 (9H, s), 3.82 (3H, s), 6.82 (1H, d, *J* = 8.5 Hz), 7.09 (1H, dd, *J* = 8.5, 2.0 Hz), 7.18 (1H, d, *J* = 2.0 Hz), 7.35 (1H, s); ^{13}C NMR (101 MHz, $CDCl_3$) δ -4.5. 18.6, 25.8, 55.6, 87.1, 111.7, 120.8, 122.9, 128.1, 136.4, 144.8, 151.5.

Tert-butyl(5-ethynyl-2-methoxyphenoxy)dimethylsilane, **60:**[179]

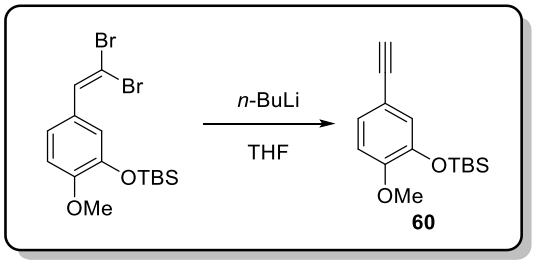

To a solution of *tert*-butyl(5-(2,2-dibromovinyl)-2-methoxyphenoxy)dimethylsilane (14.8 g, 35.3 mmol) in THF (150 mL) at -78 °C was added *n*BuLi (~2.5 M in hexane) (35 mL, 64.0 mmol). The reaction was stirred for one hour at -78 °C before warming to room temperature. Aqueous NH_4Cl was added and extracted with ethyl acetate, the organic phase was dried over $MgSO_4$ and volatiles removed *in vacuo*. Flash silica chromatography (eluting solvent 20% ethyl acetate in 40-60 petroleum ether) afforded **60** as an orange oil (8.05 g, 87%) and was characterised by ^{1}H NMR spectroscopy only.

^{1}H NMR (400 MHz, $CDCl_3$) δ 0.15 (6H, s), 0.99 (9H, s), 2.97 (1H, s) 3.81 (3H, s), 6.77 (1H, d, *J* = 8.5 Hz), 6.98 (1H, d, *J* = 2.0 Hz), 7.09 (1H, dd, *J* = 8.5, 2.0 Hz) ; ^{13}C NMR (101 MHz, $CDCl_3$) δ -4.5. 18.6, 25.8, 55.6, 72.8, 81.4, 111.9, 114.1, 124.8, 127.1, 144.9, 152.6.

2-Methoxy-5-((3,4,5-trimethoxyphenyl)ethynyl)phenol, **61**:[72]

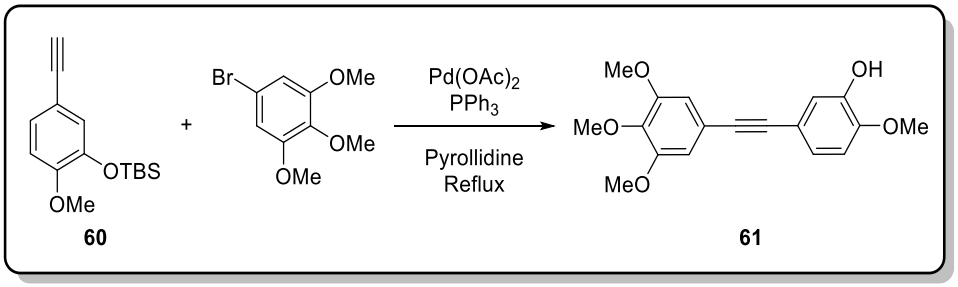

A solution of **60** (8.05 g, 30.7 mmol), 1-bromo-3,4,5-trimethoxybenzene (5.05 g, 20.5 mmol), palladium acetate (0.09 g, 0.4 mmol) and triphenylphosphine (0.24 g, 0.8 mmol) in pyrollidine (60 mL) was heated at reflux for one hour. Aqueous NH_4Cl was added and the reaction mixture extracted with ethyl acetate. The organic phase was washed with aqueous HCl, dried over $MgSO_4$ and volatiles removed *in vacuo*. Flash silica chromatography (eluting solvent 40%

ethyl acetate in 40-60 petroleum ether) afforded **61** as orange crystals (6.10 g, 95%). M.p. 97-99 °C (lit.[72] 97 °C);

^{1}H NMR (400 MHz, $CDCl_3$) δ 3.87 (3H, s), 3.88 (6H, s), 3.92 (3H, s), 5.62 (1H, s,), 6.75 (2H, s), 6.82 (1H, d, *J* = 8.5 Hz), 7.06 (1H, dd, *J* = 8.5, 2.0 Hz), 7.09 (1H, d, *J* = 2.0 Hz); ^{13}C NMR (101 MHz, $CDCl_3$) δ 55.2, 56.0, 61.0, 88.0, 88.5, 108.7, 110.6, 116.0, 117.6, 118.6, 124.3, 138.6, 145.4, 147.1, 153.1.

Combretastatin A-4:[72]

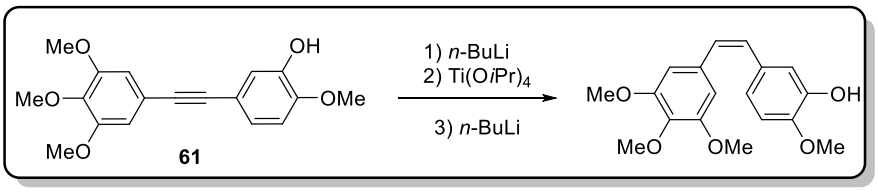

To a solution of **61** (2.39 g, 7.62 mmol) in THF (75 mL) at -78 °C was added *n*BuLi (~2.4 M in hexane) (3.2 mL, 7.7 mmol) and the reaction mixture stirred for five minutes. Titanium(IV) tetraisopropoxide (4.3 mL, 15 mmol) was added, followed by the careful addition of *n*BuLi (~2.4 M in hexane) (13 mL, 31 mmol). The reaction was warmed to 50 °C for one hour, followed by addition of aqueous NH_4Cl and extraction with ethyl acetate. The organic phase was dried over $MgSO_4$ and the volatiles removed *in vacuo*, affording CA4 (2.32 g, 96%) as a brown oil and was characterised by ^{1}H NMR spectroscopy only before immediate further reaction.

^{1}H NMR (250 MHz, $CDCl_3$) δ 3.70 (6H, s), 3.84 (3H, s), 3.87 (3H, s), 5.50 (1H, s), 6.41 (1H, d, *J* = 12 Hz), 6.48 (1H, d, *J* = 12 Hz), 6.53 (2H, s), 6.68-6.84 (2H, m), 6.92 (1H, d, *J* = 2.0 Hz).

Combretastatin A-4-phosphate:[180]

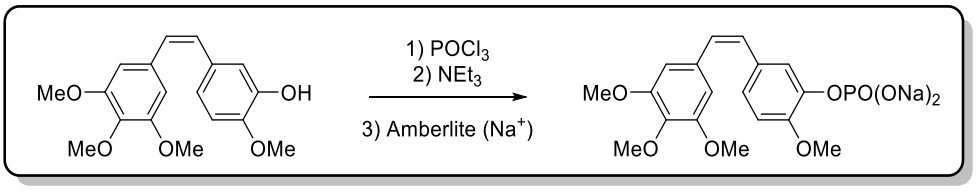

To a solution of phosphorus oxychloride (6.8 g, 44 mmol) in CH_2Cl_2 (100 mL) was added CA4 (2.32 g, 7.33 mmol) in CH_2Cl_2 (10 mL) dropwise and the reaction stirred for one hour at room temperature. Triethylamine (1.78 g, 17.6 mmol) was added and the reaction stirred at room temperature for 14 hours. Water was added and the reaction mixture extracted with CH_2Cl_2. Volatiles were removed *in vacuo*, and the crude material dissolved in a minimum of acetonitrile. Amberlite IR-120 Na^+ form (2 g) in water was added and the reaction stirred at

room temperature for 16 hours. The reaction was filtered and the solvent removed *in vacuo*. The crude material was recrystallised from acetone affording CA4P (2.81 g, 87%) as a colourless solid.

M.p. 188-191 °C (dec.) (Lit.[181] 190-195 °C dec.); ^{1}H NMR (400 MHz, D_2O) δ 3.54 (6H, s), 3.61 (3H, s), 3.69 (3H, s), 6.37-6.56 (4H, m), 6.82 (1H, d, *J* = 8.5 Hz), 6.89 (1H, d, *J* = 8.5 Hz), 7.07 (1H, s); ^{13}C NMR (101 MHz, DMSO-d_6) δ 55.6, 55.7, 60.1, 106.0, 112.2, 121.2, 121.9, 128.5, 129.0, 129.5, 132.3, 136.6, 143.0, 149.4 (d, *J* = 6.5 Hz), 152.5; ^{31}P NMR (101 MHz, D_2O) δ -3.83; HRMS calculated for $C_{18}H_{21}O_8P$ (acid form) (ES^+)($+H^+$): 397.1052. Found: 397.1046.

4-(3,4,5-Trimethoxyphenyl)-*N*-(3-*O*-phosphate[sodium salt]-4-methoxyphenyl)sydnone, **62**:

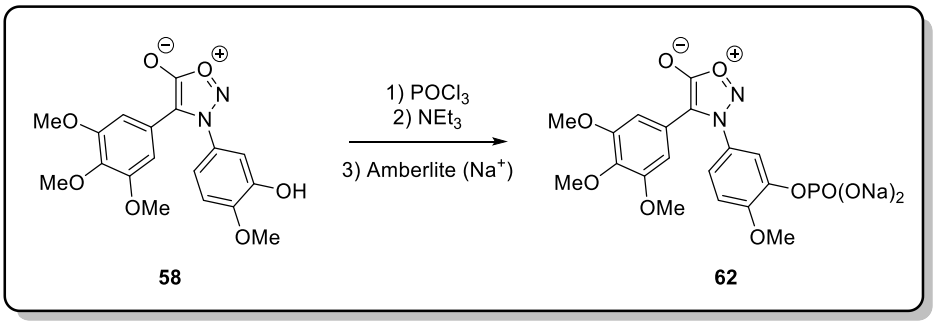

58 **62**

To a suspension of **58** (73 mg, 0.20 mmol) in CH_2Cl_2 (1 mL) was added a solution of phosphorus oxychloride (179 mg, 1.17 mmol) in CH_2Cl_2 (1 mL) dropwise and the reaction stirred for one hour at room temperature. Triethylamine (47 mg, 0.47 mmol) was added and the reaction stirred at room temperature for 16 hours. Water was added and the reaction mixture extracted with CH_2Cl_2. Volatiles were removed *in vacuo*, and the crude material dissolved in a minimum of acetonitrile. Amberlite IR-120 Na^+ form (200 mg) in water was added and the reaction stirred at room temperature for 16 hours. The mixture was filtered and volatiles removed *in vacuo*. The resulting solid was recrystallized from acetone affording **62** as a yellow solid (78 mg, 80%). N.B. the compound was contaminated with a small amount of inseparable trisodium phosphate.

^{1}H NMR (400 MHz, D_2O) δ 3.69 (6H, s), 3.78 (3H, s), 3.94 (3H, s), 6.63 (2H, s), 7.24 (1H, d, *J* = 9.0 Hz), 7.32 (1H, app d, *J* = 9.0 Hz), 7.52 (1H, app s); ^{13}C NMR (101 MHz, D_2O) δ 56.0, 56.3, 60.9, 105.6, 109.5, 113.2, 118.0, 119.6, 121.7, 125.8, 137.4, 141.8 (d, *J* = 7.0 Hz), 152.6, 153.7 (d, *J* = 5.0 Hz), 168.8; ^{31}P NMR (162 MHz, D_2O) δ -4.32; FTIR: ν_{max} 3397 (br), 2949 (w), 1732 (s), 1580 (m), 1509 (s), 1283 (m), 1122 (s), 1109 (s), 946 (s); HRMS calculated for $C_{18}H_{17}N_2Na_2O_{10}P$ (TOF ES^+)($+H^+$): 499.0494. Found: 499.0473.

1-(4-Methoxyphenyl)-3-(trimethylsilyl)-5-(3,4,5-trimethoxyphenyl)-pyrazole, **66a** and 1-(4-methoxyphenyl)-4-(trimethylsilyl)-5-(3,4,5-trimethoxyphenyl)-pyrazole **66b**:

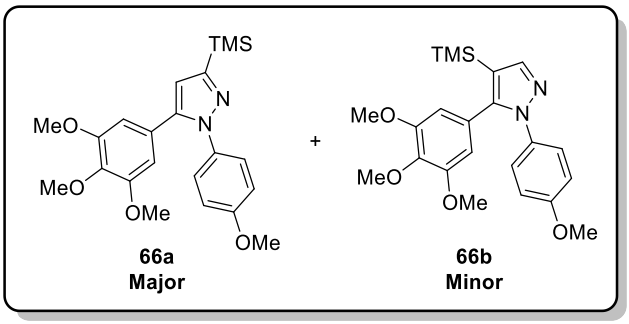

Following general procedure G using sydnone **26** (200 mg, 0.558 mmol) and trimethylsilylacetylene (219 mg, 2.23 mmol) in xylenes (0.56 mL), an inseparable mixture of pyrazole **66a** and **66b** was isolated as a brown oil (230 mg, 100%, 95:5).

^{1}H NMR (400 MHz, $CDCl_3$) δ 0.36 (9H, s), 3.67 (6H, s), 3.80 (3H, s), 3.84 (3H, s), 6.41 (2H, s), 6.57 (1H, s), 6.87 (2H, d, *J* = 9.0 Hz), 7.26 (2H, d, *J* = 9.0 Hz); ^{13}C NMR (101 MHz, $CDCl_3$) δ -0.8, 55.7, 56.1, 61.1, 106.1, 113.3, 114.2, 126.3, 127.1, 133.8, 137.8, 143.1, 153.1, 153.6, 159.0; FTIR: ν_{max} 2955 (w), 2835 (w), 1584 (m), 1514 (s), 1244 (s), 1125 (s); HRMS (ESI-TOF) *m/z* $[M+H]^+$ calculated for $C_{22}H_{29}N_2O_4Si$: 413.1897. Found: 413.1905.

1-(4-Methoxyphenyl)-3-(trimethylsilyl)-5-(3,4,5-trimethoxyphenyl)-pyrazole, **66a** and 1-(4-methoxyphenyl)-4-(trimethylsilyl)-5-(3,4,5-trimethoxyphenyl)-pyrazole **66b**:

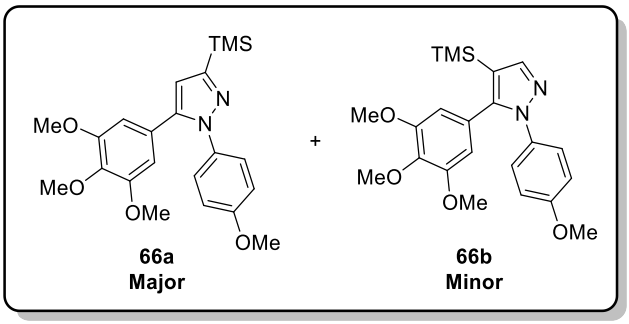

Sydnone **26** (100 mg, 0.279 mmol) and trimethylsilylacetylene (110 mg, 1.12 mmol) in xylenes (0.56 mL), an inseparable mixture of pyrazole **66a** and **66b** was isolated as a brown oil (83 mg, 72%, 95:5).

See above for characterisation data.

1-(4-Methoxyphenyl)-5-(3,4,5-trimethoxyphenyl)-pyrazole, **67**:

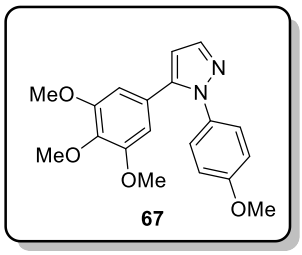

67

Following general procedure H using a mixture of pyrazoles **66a** and **66b** (222 mg, 0.539 mmol, 95:5) and and TBAF in THF (5.4 mL, 5.4 mmol), pyrazole **67** was isolated as an orange solid (137 mg, 75%).

M.p.: 92-94 °C; ^{1}H NMR (400 MHz, $CDCl_3$) δ 3.66 (6H, s), 3.80 (3H, s), 3.84 (3H, s), 6.41 (2H, s), 6.47 (1H, d, *J* = 2.0 Hz), 6.87 (2H, d, *J* = 9.0 Hz), 7.23 (2H, d, *J* = 9.0 Hz), 7.67 (1H, d, *J* = 2.0 Hz); ^{13}C NMR (101 MHz, $CDCl_3$) δ 55.6, 56.1, 61.0, 106.1, 106.9, 114.1, 126.0, 126.9, 133.5, 138.0, 140.0, 142.9, 153.1, 159.0; FTIR: ν_{max} 2931 (w), 2835 (w), 1586 (m), 1514 (s), 1415 (m), 1241 (s), 1121 (s), 1002 (m), 835 (s); HRMS (ESI-TOF) *m/z* $[M+H]^+$ calculated for $C_{19}H_{21}N_2O_4$: 341.1501. Found: 341.1504.

4-(3-[(*Tert*-butyldimethylsilyl)oxy]-4-methoxyphenyl)-*N*-(3,4,5-trimethoxyphenyl)sydnone, **68**:

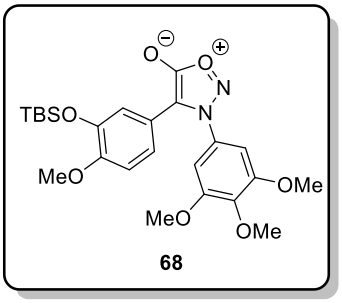

68

To a solution of sydnone **21** (200 mg, 0.535 mmol) and TBSCl (161 mg, 1.07 mmol) in DMF (2 mL), under an atmosphere of nitrogen, was added DIPEA (138 mg, 1.07 mmol) and the reaction stirred at room temperature for 14 hours. Aqueous NH_4Cl was added and the mixture extracted with ethyl acetate. The organic phase was dried over $MgSO_4$ and the volatiles were removed *in vacuo.* Flash silica chromatography (gradient 100% 40-60 petroleum ether to 40% ethyl acetate) afforded **68** as an orange solid (211 mg, 81%).

M.p.: 97-98 °C; ^{1}H NMR (400 MHz, $CDCl_3$) δ 0.03 (6H, s), 0.90 (9H, s), 3.79 (6H, s), 3.80 (3H, s), 3.91 (3H, s), 6.67 (1H, d, *J* = 2.5 Hz), 6.68 (2H, s), 6.82 (1H, d, *J* = 8.5 Hz), 7.18 (1H, dd, *J* = 8.5, 2.5 Hz); ^{13}C NMR (101 MHz, $CDCl_3$) δ -4.7, 18.4, 25.7, 55.6, 56.6, 61.2, 102.6, 108.1, 112.2,

117.1, 119.7, 121.6, 130.1, 140.7, 145.1, 151.8, 154.2, 167.1; FTIR: ν_{max} 2933 (w), 1729 (m), 1606 (m), 1460 (m), 1225 (s), 1125 (s), 1015 (m), 999 (m), 946 (m), 837 (s); HRMS (ESI-TOF) *m/z* $[M+H]^+$ calculated for $C_{24}H_{33}N_2O_7Si$: 489.2057. Found: 489.2081.

1-(3,4,5-Trimethoxyphenyl)-3-(trimethylsilyl)-5-(3-[(*tert*-butyldimethylsilyl)oxy]-4-methoxyphenyl)-pyrazole, **69a** and 1-(3,4,5-trimethoxyphenyl)-4-(trimethylsilyl)-5-(3-[(*tert*-butyldimethylsilyl)oxy]-4-methoxyphenyl) -pyrazole, **69b**:

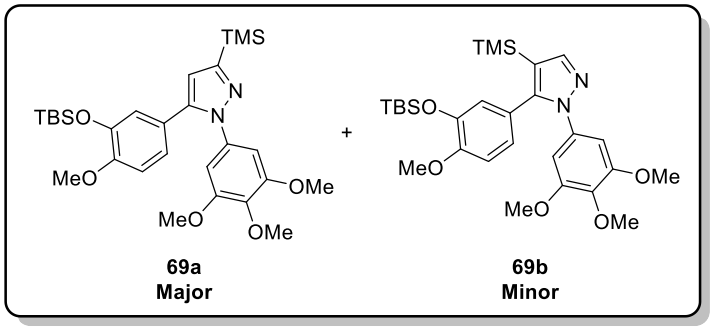

Following general procedure G using sydnone **68** (150 mg, 0.307 mmol) and trimethylsilylacetylene (121 mg, 1.23 mmol), an inseparable mixture of pyrazole **69a** and **69b** was isolated as a clear oil (136 mg, 82%, 95:5).

^{1}H NMR (400 MHz, $CDCl_3$) δ 0.01 (6H, s), 0.35 (9H, s), 0.90 (9H, s), 3.70 (6H, s), 3.79 (3H, s), 3.81 (3H, s), 6.52 (1H, s), 6.54 (2H, s), 6.68 (1H, d, *J* = 2.0 Hz), 6.79 (1H, d, *J* = 8.5 Hz), 6.87 (1H, dd, *J* = 8.5, 2.0 Hz); ^{13}C NMR (101 MHz, $CDCl_3$) δ -4.8, -0.9, 18.4, 25.7, 55.6, 56.1, 61.0, 103.3, 111.8, 113.4, 121.4, 122.4, 123.6, 136.2, 137.2, 143.0, 144.8, 151.1, 153.2, 153.7; FTIR: ν_{max} 2954 (w), 2930 (w), 2857 (w), 1598 (m), 1496 (m), 1463 (m), 1415 (m), 1229 (s), 1127 (s), 1007 (m), 979 (m) 980 (m), 937 (m); HRMS (ESI-TOF) *m/z* $[M+H]^+$ calculated for $C_{28}H_{43}N_2O_5Si_2$: 543.2711. Found: 543.2728.

1-(3,4,5-Trimethoxyphenyl)-5-(3-hydroxy-4-methoxyphenyl)-pyrazole, **64** and 1-(3,4,5-trimethoxyphenyl)-5-(3-fluoromethoxy-4-methoxyphenyl)-pyrazole, **70**:

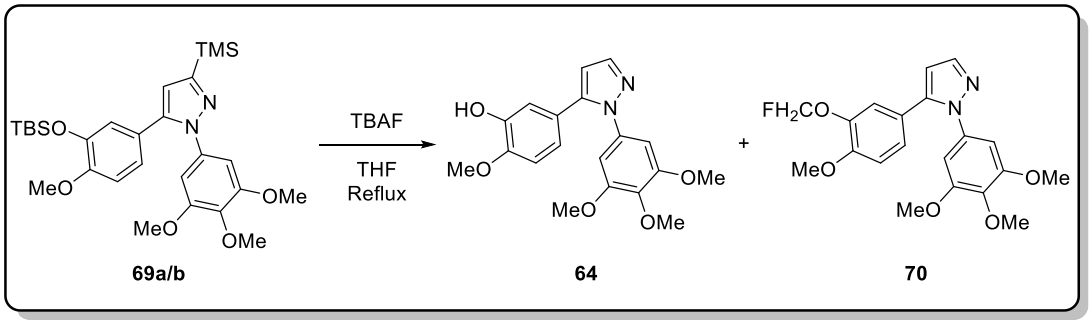

Following general procedure H using a mixture of pyrazoles **69a** and **69b** (131 mg, 0.241 mmol, 95:5) and TBAF in THF (2.4 mL, 2.4 mmol), pyrazole **64** was isolated as a colourless solid (12 mg, 14%) and pyrazole **70** was isolated as a clear oil (21 mg, 22%).

64: M.p.: 102-103 °C; ^{1}H NMR (400 MHz, $CDCl_3$) δ 3.68 (6H, s), 3.83 (3H, s), 3.86 (3H, s), 5.99 (1H, br), 6.42 (1H, d, *J* = 2.0 Hz), 6.53 (2H, s), 6.69 (1H, dd, *J* = 8.5, 2.0 Hz), 6.76 (1H, d, *J* = 8.5, Hz), 6.87 (1H, d, *J* = 2.0, Hz), 7.65 (1H, d, *J* = 2.0 Hz); ^{13}C NMR (101 MHz, $CDCl_3$) δ 56.0, 56.2, 61.1, 102.9, 107.9, 110.6, 115.2, 121.0, 123.8, 135.9, 137.2, 140.1, 142.9, 145.6, 146.8, 153.1; FTIR: ν_{max} 3133 (br), 2933 (w), 2840 (w), 1601 (m), 1499 (s), 1458 (m), 1420 (m), 1272 (m), 1232 (s), 1118 (s), 1010 (m), 1002 (m), 933 (m); HRMS (ESI-TOF) *m/z* $[M+H]^+$ calculated for $C_{19}H_{21}N_2O_5$: 357.1445. Found: 357.1446.

70: ^{1}H NMR (400 MHz, $CDCl_3$) δ 3.71 (6H, s), 3.84 (3H, s), 3.88 (3H, s), 5.58 (2H, d, *J* = 54.5 Hz), 6.48 (1H, d, *J* = 2.0 Hz), 6.53 (2H, s), 6.88 (1H, d, *J* = 8.5 Hz), 7.01 (1H, dd, *J* = 8.5, 2.0 Hz), 7.03-7.05 (1H, m), 7.69 (1H, d, *J* = 2.0 Hz); ^{13}C NMR (101 MHz, $CDCl_3$) δ 56.2, 56.3, 61.1, 101.4 (d, J = 220.5 Hz), 103.2, 107.3, 112.1, 118.3, 123.4, 125.0, 135.8, 137.5, 140.2, 142.3, 145.4, 149.9, 153.3; ^{19}F NMR (377 MHz, $CDCl_3$) δ -149.1 (t, *J* = 54 Hz); FTIR: ν_{max} 2933 (w), 2838 (w), 1598 (m), 1505 (s), 1455 (m), 1417 (m), 1229 (s), 1119 (s), 1002 (m), 972 (m); HRMS (ESI-TOF) *m/z* $[M+H]^+$ calculated for $C_{20}H_{22}N_2O_5F$: 389.1513. Found: 389.1499.

1-(3,4,5-Trimethoxyphenyl)-3-(trimethylsilyl)-5-(3-amino-4-methoxyphenyl)-pyrazole, **71a** and 1-(3,4,5-trimethoxyphenyl)-4-(trimethylsilyl)-5-(3-amino-4-methoxyphenyl)-pyrazole, **71b**:

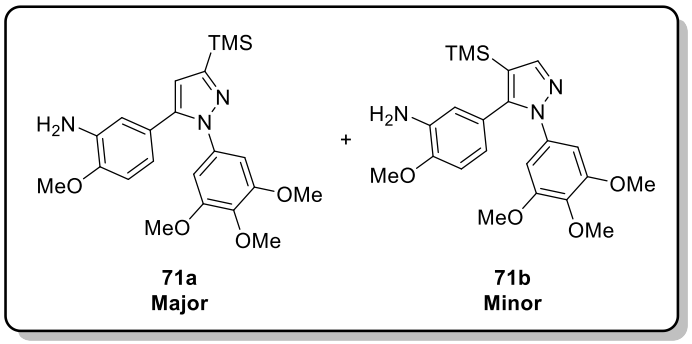

71a **Major** **71b** **Minor**

Following general procedure G using sydnone **56** (150 mg, 0.402 mmol) and trimethylsilylacetylene (158 mg, 1.61 mmol), an inseparable mixture of pyrazole **71a** and **71b** was isolated as a brown oil (156 mg, 91%, 95:5).

^{1}H NMR (400 MHz, $CDCl_3$) δ 0.35 (9H, s), 3.69 (6H, s), 3.81 (3H, s), 3.81 (3H, s), 6.50 (1H, s), 6.53-6.58 (3H, m), 6.62 (1H, d, *J* = 2.0 Hz), 6.67 (1H, d, *J* = 8.5 Hz); ^{13}C NMR (101 MHz, $CDCl_3$)

δ -0.9, 55.6, 56.1, 61.0, 103.2, 110.1, 113.5, 115.1, 119.1, 123.7, 136.1, 136.3, 137.1, 143.4, 147.2, 153.1, 153.6; FTIR: ν_{max} 3465 (br), 3372 (br), 2955 (w), 2836 (w), 1598 (m), 1505 (s), 1455 (m), 1418 (m), 1228 (s), 1125 (s), 980 (m), 835 (s); HRMS (ESI-TOF) *m/z* $[M+H]^+$ calculated for $C_{22}H_{30}N_3O_4Si$: 428.2006. Found: 428.2023.

1-(3,4,5-Trimethoxyphenyl)- 5-(3-amino-4-methoxyphenyl)-pyrazole, **72**:

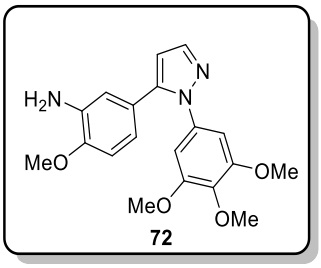

72

Following general procedure H using a mixture of pyrazoles **71a** and **71b** (156 mg, 0.365 mmol) and TBAF in THF (3.7 mL, 3.7 mmol), pyrazole **72** was isolated as a tan crystals (99 mg, 76%).

M.p.: 100-101 °C;^{1}H NMR (400 MHz, $CDCl_3$) δ 3.70 (6H, s), 3.79 (2H, br), 3.84 (3H, s), 3.84 (3H, s), 6.40 (1H, d, *J* = 2.0 Hz), 6.56 (2H, s), 6.58 (1H, dd, *J* = 8.5, 2.0 Hz), 6.64 (1H, d, *J* = 2.0 Hz), 6.70 (1H, d, *J* = 8.5 Hz), 7.66 (1H, d, *J* = 2.0 Hz); ^{13}C NMR (101 MHz, $CDCl_3$) δ 55.7, 56.2, 61.1, 102.8, 107.4, 110.2, 115.2, 119.3, 123.5, 136.2, 136.2, 137.1, 140.1, 143.4, 147.4, 153.1; FTIR: ν_{max} 3444 (w), 3346 (w), 3303 (w), 3198 (w), 2934 (w), 2837 (w), 1598 (m), 1500 (s), 1463 (s), 1419 (s), 1229 (s), 1120 (s), 1029 (m), 991 (m); HRMS (ESI-TOF) *m/z* $[M+H]^+$ calculated for $C_{19}H_{22}N_3O_4$: 356.1610. Found: 356.1615.

3-Phenylmethoxy-4-methoxy-1-bromobenzene, **73**:[182]

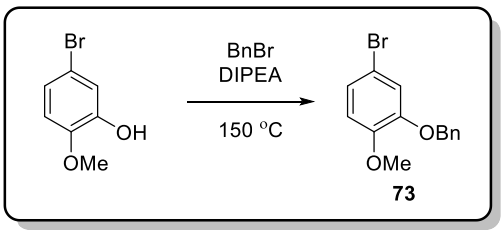

73

A flask equipped with reflux condensor was charged with 5-bromo-2-methoxyphenol (5.00 g, 24.6 mmol), benzyl bromide (6.32 g, 37.0 mmol) and Hünigs base (4.78 g, 37.0 mmol) and heated at 150 °C for 2 hours. The mixture was allowed to cool to ambient temperature and ethyl acetate and water added followed by extraction. The combined organic layers were dried over $MgSO_4$, filtered and volatiles removed *in vacuo*. The crude product was purified by flash silica chromatography (gradient starting with 100% 40-60 petroleum ether and

ending with 20% ethyl acetate in 40-60 petroleum ether) affording **73** as a colourless solid (6.85 g, 95%).

M.p.: 77-79 °C (lit.[182] 70-71 °C); ^{1}H NMR (400 MHz, $CDCl_3$) δ 3.86 (3H, s), 5.11 (2H, s), 6.77 (1H, dd, *J* = 7.0, 3.0 Hz), 7.01-7.08 (2H, m), 7.29-7.49 (5H, m); ^{13}C NMR (101 MHz, $CDCl_3$) δ 56.3, 71.3, 112.7, 113.2, 117.4, 124.1, 127.5, 128.2, 128.8, 136.6, 149.1, 149.2; FTIR: ν_{max} 2936 (w), 1584 (m), 1496 (m), 1456 (m), 1214 (s), 1186 (s), 1129 (s), 1001 (m); HRMS (ESI-TOF) *m/z* $[M+H]^+$ calculated for $C_{14}H_{14}{}^{79}BrO_2$: 292.0093. Found: 292.0088.

4-(3-phenylmethoxy-4-methoxyphenyl)-*N*-(3,4,5-trimethoxyphenyl)sydnone, **74**:

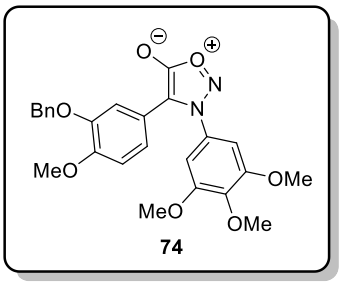

74

Following general procedure F using sydnone **19** (500 mg, 1.98 mmol) and bromide **73** (872 mg, 2.97 mmol), sydnone **74** was isolated as a colourless solid (542 mg, 59%).

M.p.: 144-146 °C; ^{1}H NMR (400 MHz, $CDCl_3$) δ 3.78 (6H, s), 3.87 (3H, s), 3.92 (3H, s), 4.97 (2H, s), 6.64 (2H, s), 6.81 (1H, d, *J* = 8.5 Hz), 6.92 (1H, dd, *J* = 8.5, 2.0 Hz), 6.98 (1H, d, *J* = 2.0 Hz), 7.27-7.35 (5H, m); ^{13}C NMR (101 MHz, $CDCl_3$) δ 56.1, 56.7, 61.3, 71.0, 102.6, 108.0, 111.8, 112.6, 117.0, 120.9, 127.8, 128.1, 128.7, 130.0, 136.6, 140.7, 148.2, 150.2, 154.2, 167.1; FTIR: ν_{max} 2939 (w), 1738 (m), 1602 (m), 1260 (s), 1234 (s), 1132 (s), 1016 (m), 993 (m); HRMS (ESI-TOF) *m/z* $[M+H]^+$ calculated for $C_{25}H_{25}N_2O_7$: 465.1656. Found: 465.1654.

1-(3,4,5-Trimethoxyphenyl)-3-(trimethylsilyl)-5-(3-phenylmethoxy-4-methoxyphenyl)-pyrazole, **75a** and 1-(3,4,5-trimethoxyphenyl)-4-(trimethylsilyl)-5-(3-phenylmethoxy-4-methoxyphenyl)-pyrazole, **75b**:

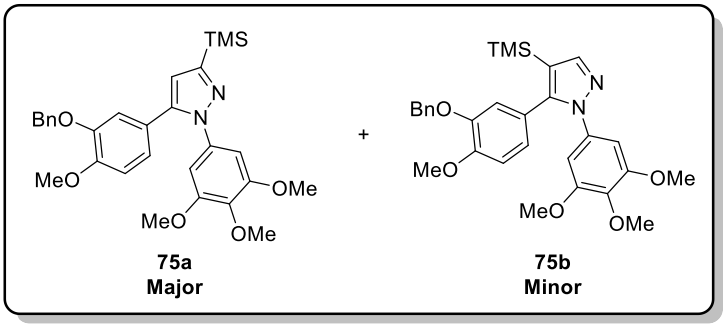

75a
Major

75b
Minor

Following general procedure G using sydnone **74** (136 mg, 0.293 mmol) and trimethylsilylacetylene (115 mg, 1.17 mmol), an inseparable mixture of pyrazole **75a** and **75b** was isolated as an orange oil (113 mg, 74%, 95:5).

^{1}H NMR (400 MHz, $CDCl_3$) δ 0.36 (9H, s), 3.69 (6H, s), 3.82 (3H, s), 3.87 (3H, s), 4.95 (2H, s), 6.51 (1H, s), 6.52 (2H, s), 6.76 (1H, d, *J* = 1.5 Hz), 6.81-6.88 (2H, m), 7.24-7.35 (5H, m); ^{13}C NMR (101 MHz, $CDCl_3$) δ -0.9, 56.0, 56.1, 61.0, 71.1, 103.3, 111.5, 113.4, 114.6, 122.0, 123.3, 127.0, 127.9, 128.6, 136.1, 136.8, 137.3, 142.9, 147.8, 149.5, 153.2, 153.7; FTIR: ν_{max} 2954 (w), 2836 (w), 1597 (m), 1505 (s), 1229 (s), 1125 (s), 1023 (m), 1005 (m), 979 (m); HRMS (ESI-TOF) *m/z* $[M+H]^+$ calculated for $C_{29}H_{35}N_2O_5Si$: 519.2310. Found: 519.2291.

1-(3,4,5-trimethoxyphenyl)-5-(3-phenylmethoxy-4-methoxyphenyl)-pyrazole, **76**:

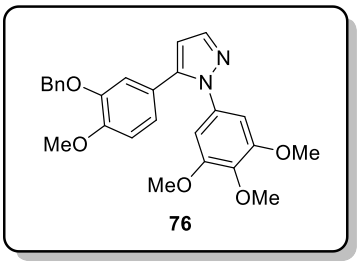

76

Following general procedure H using pyrazoles **75a** and **75b** (86 mg, 0.166 mmol, 95:5) and TBAF in THF (1.7 mL, 1.7 mmol), pyrazole **76** was isolated as a yellow oil (50 mg, 67%).

^{1}H NMR (400 MHz, $CDCl_3$) δ 3.67 (6H, s), 3.84 (3H, s), 3.88 (3H, s), 4.97 (2H, s), 6.39 (1H, d, *J* = 2.0 Hz), 6.49 (2H, s), 6.77 (1H, s), 6.83-6.85 (2H, m), 7.26-7.34 (5H, m), 7.66 (1H, d, *J* = 2.0 Hz); ^{13}C NMR (101 MHz, $CDCl_3$) δ 56.1, 56.2, 61.1, 71.3, 102.9, 107.3, 111.6, 114.8, 122.2, 123.1, 127.1, 128.1, 128.7, 135.9, 136.8, 137.3, 140.1, 142.9, 148.0, 149.9, 153.2; FTIR: ν_{max} 2936 (w), 2836 (w), 1598 (m), 1508 (s), 1454 (m), 1415 (m), 1230 (s), 1118 (s), 1019 (m), 1002 (m); HRMS (ESI-TOF) *m/z* $[M+H]^+$ calculated for $C_{26}H_{27}BN_2O_5$: 447.1914. Found: 447.1925.

1-(3,4,5-Trimethoxyphenyl)-5-(3-hydroxy-4-methoxyphenyl)-pyrazole, **64**:

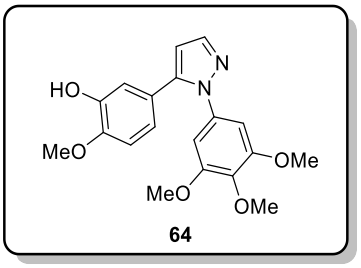

64

Following general procedure I using pyrazole **76** (139 mg, 0.311 mmol) and Pd/C (31 mg) for 24 hours, pyrazole **64** was isolated as a colourless solid (75 mg, 68%).

See above for characterisation data.

(3-Phenylmethoxy-4-methoxy)nitrobenzene:[183]

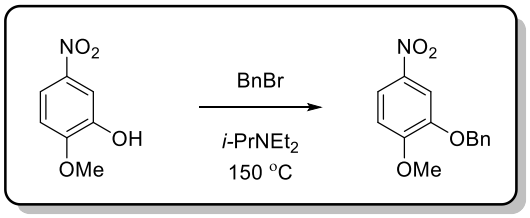

A mixture of (2-methoxy-5-nitro)phenol (5.15 g, 30.4 mmol), benzyl bromide (7.81 g, 45.7 mmol) and Hünigs base (5.90 g, 45.7 mmol) were heated at 150 °C for 2 hours. The reaction was allowed to cool to ambient temperature and water was added. The mixture was extracted with dichloromethane and the combined organic layers washed with saturated ammonium chloride and brine, before drying over $MgSO_4$ and concentrating *in vacuo*. Flash silica chromatography (gradient starting with 100% 40-60 petroleum ether and ending with 40% ethyl acetate in 40-60 petroleum ether) afforded (3-phenylmethoxy-4-methoxy)nitrobenzene as a colourless solid (6.69 g, 85%).

M.p.: 98 °C (Lit.[183] 97-98 °C); ^{1}H NMR (400 MHz, $CDCl_3$) δ 3.97 (3H, s), 5.20 (2H, s), 6.92 (1H, d, *J* = 9.0 Hz), 7.30-7.42 (3H, m), 7.44-7.50 (2H, m), 7.80 (1H, d, *J* = 2.5 Hz), 7.91 (1H, d, *J* = 9.0, 2.5 Hz); ^{13}C NMR (101 MHz, $CDCl_3$) δ 56.5, 71.3, 108.7, 110.3, 118.2, 127.7, 128.5, 128.9, 135.8, 141.4, 148.0, 155.2.

(3-Phenylmethoxy-4-methoxy)aniline:[183]

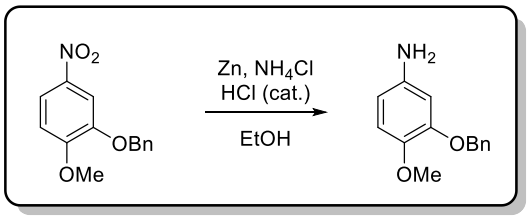

To a suspension of (3-phenylmethoxy-4-methoxy)nitrobenzene (3.37 g, 13.0 mmol), zinc dust (10.2 g, 156 mmol) and ammonium chloride (4.18 g, 78.1 mmol) in water:ethanol (3:1, 75 mL) was added concentrated hydrochloric acid (5 drops) and the reaction stirred for 14 h at room temperature. The mixture was neutralised with sodium hydrogen carbonate and extracted with ethyl acetate and the combined organic layers washed with brine, before drying over $MgSO_4$ and concentrating *in vacuo*. Flash silica chromatography (gradient starting with 100% 40-60 petroleum ether and ending with 40% ethyl acetate in 40-60 petroleum ether) afforded (3-phenylmethoxy-4-methoxy)aniline as a colourless solid (1.65 g, 55%).

M.p.: 99-101 °C (Lit.[183] 97-100 °C); ^{1}H NMR (400 MHz, $CDCl_3$) δ 3.21 (2H, br), 3.82 (3H, s), 5.11 (2H, s), 6.25 (1H, dd, *J* = 8.5, 2.5 Hz), 6.32 (1H, d, *J* = 2.5 Hz), 6.72 (1H, d, *J* = 8.5 Hz), 7.27-7.47 (5H, m); ^{13}C NMR (101 MHz, $CDCl_3$) δ 57.1, 71.0, 103.4, 107.4, 114.2, 127.3, 127.9, 128.6, 137.4, 140.8, 142.9, 149.3.

N-(3-Phenylmethoxy-4-methoxyphenyl)glycine ethyl ester:[184]

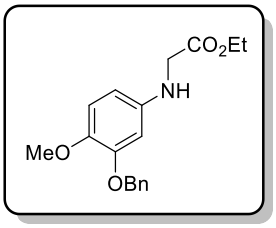

Following general procedure A using (3-phenylmethoxy-4-methoxy)aniline (800 mg, 3.49 mmol), ethylbromoacetate (583 mg, 3.49 mmol) and sodium acetate (572 mg, 6.98 mmol) for 5 hours, *N*-(3-phenylmethoxy-4-methoxyphenyl)glycine ethyl ester was isolated as a colourless solid (1.00 g, 91%).

M.p.: 66-67 °C; ^{1}H NMR (400 MHz, $CDCl_3$) δ 1.28 (3H, t, *J* = 7.0 Hz), 3.81 (2H, s), 3.82 (3H, s), 4.22 (2H, q, *J* = 7.0 Hz), 5.12 (2H, s), 6.14 (1H, dd, *J* = 8.5, 2.5 Hz), 6.29 (1H, d, *J* = 2.5 Hz), 6.79 (1H, d, *J* = 8.5 Hz), 7.27-7.47 (5H, m); ^{13}C NMR (101 MHz, $CDCl_3$) δ 14.3, 46.8, 57.1, 61.4, 71.1, 102.0, 104.7, 114.2, 127.4, 127.9, 128.7, 137.4, 142.0, 142.9, 149.5, 171.4.

N-(3-Phenylmethoxy-4-methoxyphenyl)sydnone, **77**:

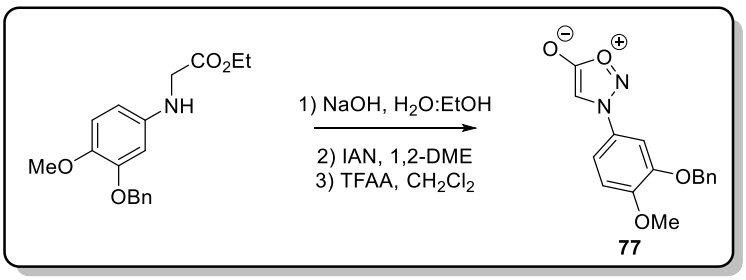

Following general procedure B using *N*-(3-phenylmethoxy-4-methoxyphenyl)glycine ethyl ester (1.46 g, 4.61 mmol), sodium hydroxide (277 mg, 6.93 mmol), *N*-(3-phenylmethoxy-4-methoxyphenyl)glycine was isolated as a tan solid (1.30 g, 98%). The product was reacted further without purification. Following general procedure C using IAN (540 mg, 4.61 mmol) and TFAA (1.45 g, 6.92 mmol), sydnone **77** was isolated as a tan solid (506 mg, 38%).

M.p.: 106-110 °C; ^{1}H NMR (400 MHz, $CDCl_3$): δ 3.97 (3H, s), 5.21 (2H, s), 6.56 (1H, s), 7.01 (1H, d, *J* = 8.5 Hz), 7.23-7.29 (m, 2H), 7.31, 7.48 (m, 5H); ^{13}C NMR (101 MHz, $CDCl_3$): δ 56.5, 71.6, 93.6, 106.9, 111.7, 114.4, 128.0, 128.6, 128.7, 129.0, 135.7, 149.2, 153.0, 169.1; FTIR: ν_{max}

3124 (w), 1735 (s), 1595 (s), 1520 (m), 1452(m), 1271 (s), 1249 (s), 1138 (s), 1019 (m), 992 (m); HRMS calculated for $C_{16}H_{14}N_2O_4$ (ES^+)($+H^+$): 299.1026. Found: 299.1029.

Attempted direct arylation *of N*-(3-phenylmethoxy-4-methoxyphenyl)sydnone, **77**:

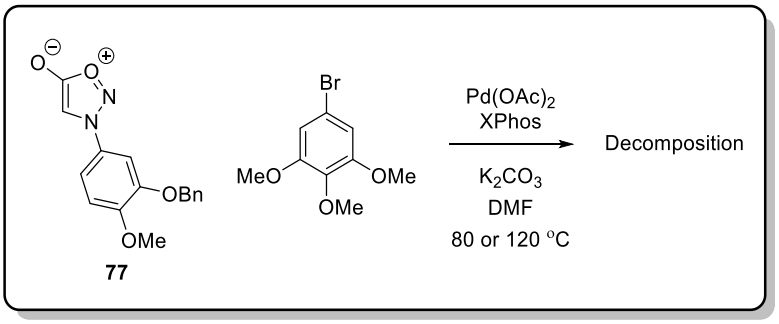

Following general procedure F using *N*-(3-phenylmethoxy-4-methoxyphenyl)sydnone 50 mg, 0.17 mmol), and 5-bromo-1,2,3-trimethoxybenzene (62 mg, 0.25 mmol), the crude reaction mixture showed no signs of *N*-(3-phenylmethoxy-4-methoxyphenyl)sydnone or target material.

4-(3,4,5-trimethoxyphenyl)-*N*-(3-phenylmethoxy-4-methoxyphenyl)sydnone, **78**:

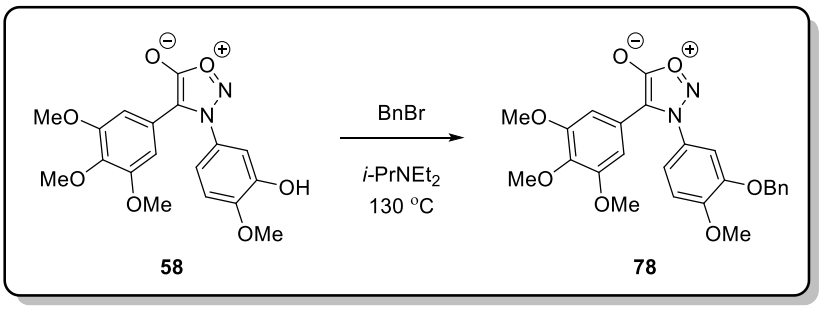

A mixture of **58** (402 mg, 1.07 mmol), benzyl bromide (368 mg, 2.15 mmol) and Hünigs base (278 mg, 2.15 mmol) were heated at 130 °C for 2 hours. The reaction was allowed to cool to ambient temperature and water was added. The mixture was extracted with dichloromethane and the combined organic layers washed with saturated ammonium chloride and brine, before drying over $MgSO_4$ and concentrating *in vacuo*. Flash silica chromatography (gradient starting with 100% 40-60 petroleum ether and ending with 40% ethyl acetate in 40-60 petroleum ether) afforded sydnone **78** as a yellow solid (296 mg, 60%).

M.p.: 58-60 °C; ^{1}H NMR (400 MHz, $CDCl_3$) δ 3.62 (6H, s), 3.83 (3H, s), 3.96 (3H, s), 5.09 (2H, s), 6.51 (2H, s), 6.98-7.03 (2H, m), 7.09 (1H, dd, *J* = 8.5, 2.5 Hz), 7.29-7.36 (5H, m); ^{13}C NMR (101 MHz, $CDCl_3$) δ 56.1, 56.6, 61.1, 71.6, 104.5, 107.8, 110.6, 111.7, 118.3, 119.9, 127.3 (x2 C), 128.6, 128.9, 135.5, 138.5, 149.1, 152.5, 153.4, 167.1; FTIR: ν_{max} 2934 (w), 2836 (w), 1728

(s), 1581 (m), 1512 (s), 1226 (s), 1123 (s), 999 (s); HRMS (ESI-TOF) *m/z* $[M+H]^+$ calculated for $C_{25}H_{25}N_2O_7$: 465.1656. Found: 465.1668.

1-(3-Phenylmethoxy-4-methoxyphenyl)-3-(trimethylsilyl)-5-(3,4,5-trimethoxyphenyl)-pyrazole, **79a** and 1-(3-phenylmethoxy-4-methoxyphenyl)-4-(trimethylsilyl)-5-(3,4,5-trimethoxyphenyl)-pyrazole, **79b**:

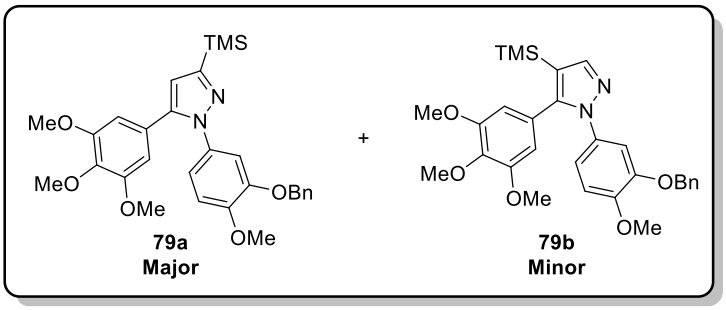

Following general procedure G using sydnone **78** (290 mg, 0.624 mmol) and trimethylsilylacetylene (245 mg, 2.50 mmol), an inseparable mixture of pyrazole **79a** and **79b** was isolated as an orange oil (256 mg, 79%, 95:5).

^{1}H NMR (400 MHz, $CDCl_3$) δ 0.36 (9H, s), 3.65 (6H, s), 3.84 (3H, s), 3.87 (3H, s), 5.02 (2H, s), 6.38 (2H, s), 6.56 (1H, s), 6.83 (1H, d, *J* = 8.5 Hz), 6.88 (1H, dd, *J* = 8.5, 2.5 Hz), 6.95 (1H, d, *J* = 2.5 Hz), 7.27-7.34 (5H, m); ^{13}C NMR (101 MHz, $CDCl_3$) δ -0.9, 56.1, 56.4, 61.0, 71.3, 106.0, 111.5, 112.0, 113.3, 118.6, 126.3, 127.3, 128.1, 128.6, 133.6, 136.6, 137.8, 143.0, 148.3, 149.2, 153.1, 153.6; FTIR: ν_{max} 2951 (w), 2834 (w), 1584 (m), 1514 (s), 1236 (s), 1126 (s), 1005 (m), 978 (m); HRMS (ESI-TOF) *m/z* $[M+H]^+$ calculated for $C_{29}H_{35}N_2O_5Si$: 519.2310. Found: 519.2314.

1-(3-Phenylmethoxy-4-methoxyphenyl)-5-(3,4,5-trimethoxyphenyl)-pyrazole, **80**:

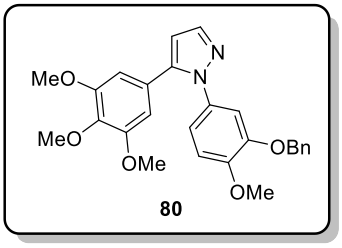

Following general procedure H using pyrazoles **79a** and **79b** (256 mg, 0.494 mmol, 95:5) and TBAF in THF (5 mL, 5 mmol), pyrazole **80** was isolated as a yellow oil (137 mg, 62%). Product was contaminated with ~10% unknown by-product.

^{1}H NMR (400 MHz, $CDCl_3$) δ 3.64 (6H, s), 3.83 (3H, s), 3.86 (3H, s), 5.01 (2H, s), 6.38 (2H, s), 6.45 (1H, d, *J* = 2.0 Hz), 6.81-6.84 (2H, m), 6.93-6.97 (1H, m), 7.25-7.36 (5H, m), 7.65 (1H, d, *J*

= 2.0 Hz); ^{13}C NMR (101 MHz, $CDCl_3$) δ 56.0, 56.3, 61.0, 71.2, 106.0, 107.0, 111.3, 111.6, 118.3, 125.9, 127.2, 127.3, 128.0, 128.6, 133.3, 136.5, 139.9, 142.9, 148.2, 149.1, 153.0; FTIR: ν_{max} 2934 (w), 2836 (w), 1584 (m), 1512 (s), 1414 (m), 1236 (s), 1121 (s), 1002 (m), 910 (m); HRMS (ESI-TOF) *m/z* $[M+H]^+$ calculated for $C_{26}H_{27}BN_2O_5$: 447.1914. Found: 447.1914.

1-(3-Hydroxy-4-methoxyphenyl)-5-(3,4,5-trimethoxyphenyl)-pyrazole, **65**:

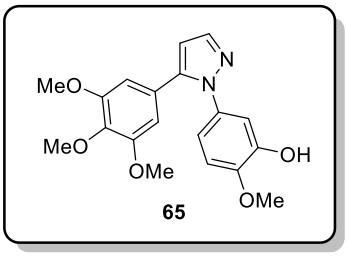

65

Following general procedure I using pyrazole **80** (137 mg, 0.307 mmol) and Pd/C (31 mg) for 24 hours, pyrazole **65** was isolated as a colourless solid (76 mg, 69%).

M.p.: 55-58 °C; ^{1}H NMR (400 MHz, $CDCl_3$) δ 3.68 (6H, s), 3.85 (3H, s), 3.88 (3H, s), 5.98 (1H, br), 6.43 (2H, s), 6.46 (1H, d, *J* = 2.0 Hz), 6.75 (1H, dd, *J* = 8.5, 2.5 Hz), 6.78 (1H, d, *J* = 8.5, Hz), 6.97 (1H, d, *J* = 2.5, Hz), 7.66 (1H, d, *J* = 2.0 Hz); ^{13}C NMR (101 MHz, $CDCl_3$) δ 56.1, 56.3, 61.1, 106.1, 107.0, 110.4, 112.7, 117.5, 126.0, 133.9, 138.0, 139.9, 143.1, 145.9, 146.3, 153.1; FTIR: ν_{max} 3146 (br), 2941 (w), 2836 (w), 1585 (m), 1511 (s), 1498 (s), 1416 (m), 1239 (s), 1120 (s), 1000 (m); HRMS (ESI-TOF) *m/z* $[M+H]^+$ calculated for $C_{19}H_{21}N_2O_5$: 357.1445. Found: 357.1444.

4,4,5,5-Tetramethyl-2-[2-(trimethylsilyl)ethynyl]-1,3,2-dioxaborolane, **81**:[185]

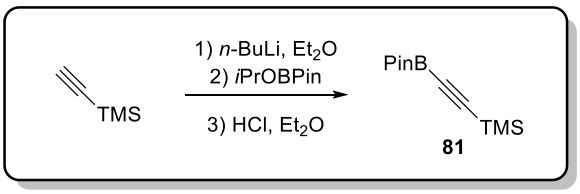

81

To a solution of trimethylsilylacetylene (10.4 g, 106 mmol) in Et_2O (100 mL) at -78 °C was added *n*-BuLi (~2.4 M, 44 mL) and the reaction stirred for 1 h. The reaction was allowed to warm to ambient temperature and 2-isopropoxy-4,4,5,5-tetramethyl-1,3,2-dioxaborolane (19.8 g, 106 mmol) was added. The reaction was stirred for 3 h at room temperature before the addition of HCl in ether (2 M, 69 mL, 138 mmol). The mixture was filtered through celite™ and washed with Et_2O. The crude residue was recrystallized from 40-60 petroleum ether affording **81** as a colourless solid (9.70 g, 41%).

M.p.: 80-82 °C; ^{1}H NMR (400 MHz, $CDCl_3$) δ 0.18 (9H, s), 1.27 (12H, s); ^{13}C NMR (101 MHz, $CDCl_3$) δ -0.4, 24.7, 84.5, 101.8 (br), 111.4.

4-(3,4,5-Trimethoxyphenyl)-*N*-methylsydnone, **86**:

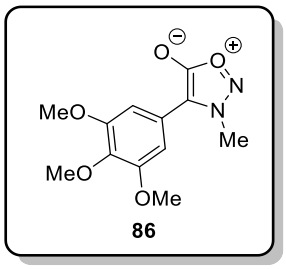

86

Following general procedure F using sydnone **40** (250 mg, 2.50 mmol) and 5-bromo-1,2,3-trimethoxybenzene (926 mg, 3.75 mmol), sydnone **86** was isolated as a colourless solid (571 mg, 86%).

M.p.: 123-124 °C; ^{1}H NMR (400 MHz, $CDCl_3$) δ 3.86 (3H, s), 3.87 (6H, s), 4.12 (3H, s), 6.74 (2H, s); ^{13}C NMR (101 MHz, $CDCl_3$) δ 39.0, 56.5, 61.1, 105.7, 108.2, 119.6, 139.2, 153.9, 167.3; FTIR: ν_{max} 2932 (w), 2858 (w), 1726 (s), 1585 (m), 1241 (m), 1225 (m), 1124 (s), 998 (m); HRMS (ESI-TOF) *m/z* $[M+H]^+$ calculated for $C_{12}H_{15}N_2O_5$: 267.0981. Found: 267.0970.

4-(3,4,5-Trimethoxyphenyl)-*N*-benzylsydnone, **87**:

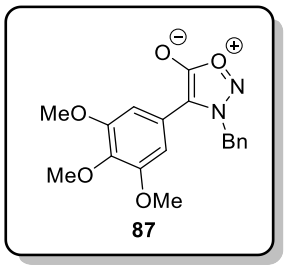

87

Following general procedure F using sydnone **44** (500 mg, 2.84 mmol) and 5-bromo-1,2,3-trimethoxybenzene (1.05 g, 4.26 mmol), sydnone **87** was isolated as a colourless solid (570 mg, 59%).

M.p.: 101 °C; ^{1}H NMR (400 MHz, $CDCl_3$) δ 3.69 (6H, s), 3.84 (3H, s), 5.52 (2H, s), 6.52 (2H, s), 7.18-7.24 (2H, m), 7.37-7.43 (3H, m); ^{13}C NMR (101 MHz, $CDCl_3$) δ 55.5, 56.2, 61.0, 106.1, 108.6, 119.4, 127.1, 129.5, 129.5, 132.0, 139.2, 153.8, 167.6; FTIR: ν_{max} 2829 (w), 1727 (s), 1712 (s), 1578 (m), 1521 (m), 1223 (s), 1131 (s), 1000 (s); HRMS (ESI-TOF) *m/z* $[M+H]^+$ calculated for $C_{18}H_{19}N_2O_5$: 343.1294. Found: 343.1278.

4-(3-Phenylmethoxy-4-methoxyphenyl)-*N*-methylsydnone, **88**:

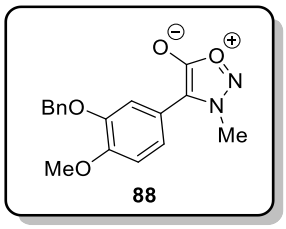

88

Following general procedure F using sydnone **40** (500 mg, 5.00 mmol) and bromide **73** (2.2 g, 7.5 mmol), sydnone **88** was isolated as a tan solid (1.105 g, 71%).

M.p.: 99 °C; ^{1}H NMR (400 MHz, $CDCl_3$) δ 3.83 (3H, s), 3.92 (3H, s), 5.19 (2H, s), 6.96 (1H, d, *J* = 8.5 Hz), 7.04 (1H, d, *J* = 2.0 Hz), 7.10 (1H, d, *J* = 8.5, 2.0 Hz), 7.27-7.33 (1H, m), 7.34-7.40 (2H, m), 7.41-7.47 (2H, m); ^{13}C NMR (101 MHz, $CDCl_3$) δ 38.6, 56.2, 71.2, 108.1, 112.2, 113.8, 116.7, 121.4, 127.4, 128.1, 128.8, 136.8, 148.3, 150.6, 167.4; FTIR: ν_{max} 2970 (w), 1723 (s), 1532 (m), 1450 (m), 1380 (m), 1305 (m), 1230 (m), 1225 (m), 1150 (s), 990 (s); HRMS (ESI-TOF) *m/z* $[M+H]^+$ calculated for $C_{17}H_{17}N_2O_4$: 313.1188. Found: 313.1185.

4-(3-phenylmethoxy-4-methoxyphenyl)-*N*-benzylsydnone, **89**:

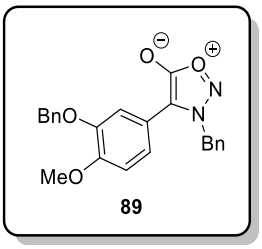

89

Following general procedure F using sydnone **44** (1.00 g, 5.68 mmol) and bromide **73** (2.50 g, 8.51 mmol), sydnone **89** was isolated as a tan solid (1.21 g, 55%).

M.p.: 144-145 °C; ^{1}H NMR (400 MHz, $CDCl_3$) δ 3.90 (3H, s), 5.01 (2H, s), 5.34 (2H, s), 6.87 (1H, d, *J* = 2.0 Hz), 6.91 (1H, d, *J* = 8.5 Hz), 6.96 (1H, dd, *J* = 8.5, 2.0 Hz), 7.06-7.11 (2H, m), 7.27-7.40 (8H, m); ^{13}C NMR (101 MHz, $CDCl_3$) δ 55.2, 56.2, 71.0, 108.0, 112.2, 114.1, 116.5, 122.4, 127.5, 127.6, 128.2, 128.8, 129.4, 129.5, 131.7, 136.6, 148.4, 150.8, 167.7; FTIR: ν_{max} 3008 (w), 2836 (w), 1720 (s), 1703 (m), 1260 (m), 1226 (m), 1176 (m), 1023 (s); HRMS (ESI-TOF) *m/z* $[M+H]^+$ calculated for $C_{23}H_{21}N_2O_4$: 389.1501. Found: 389.1519.

1-(Methyl)-3-(trimethylsilyl)-4-(pinacolatoborolane)-5-(3,4,5-trimethoxyphenyl)-pyrazole, **90a** and 1-(methyl)-3-(trimethylsilyl)-5-(3,4,5-trimethoxyphenyl)-pyrazole, **90b**:

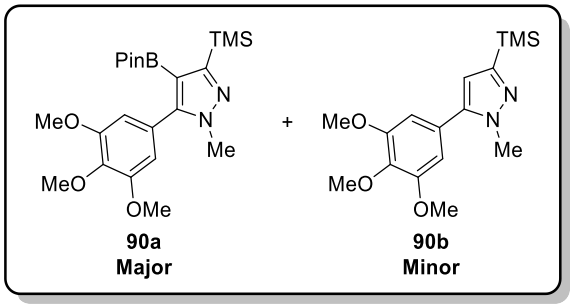

90a **Major** **90b** **Minor**

Following general procedure J using sydnone **86** (200 mg, 0.751 mmol) and alkyne **81** (337 mg, 1.50 mmol), a mixture of pyrazole **90a** and **90b** was isolated as a yellow oil (309 mg, 92% 5:1).

^{1}H NMR (400 MHz, $CDCl_3$) δ 0.36 (9H, s), 1.18 (12H, s), 3.80 (3H, s), 3.85 (6H, s), 3.90 (3H, s), 6.59 (2H, s); ^{13}C NMR (101 MHz, $CDCl_3$) δ -0.4, 25.0, 37.2, 56.2, 61.1, 83.0, 107.8, 126.9, 138.1, 150.8, 152.6, 158.8; FTIR: ν_{max} 2976 (m), 1585 (m), 1497 (s), 1411 (s), 1240 (s), 1128 (s), 1048 (m); HRMS (ESI-TOF) *m/z* $[M+H]^+$ calculated for $C_{22}H_{36}N_2O_5Si$: 447.2481. Found: 447.2488.

1-(Benzyl)-3-(trimethylsilyl)-4-(pinacolatoborolane)-5-(3,4,5-trimethoxyphenyl)-pyrazole, **91a** and 1-(benzyl)-3-(trimethylsilyl)-5-(3,4,5-trimethoxyphenyl)-pyrazole, **91b**:

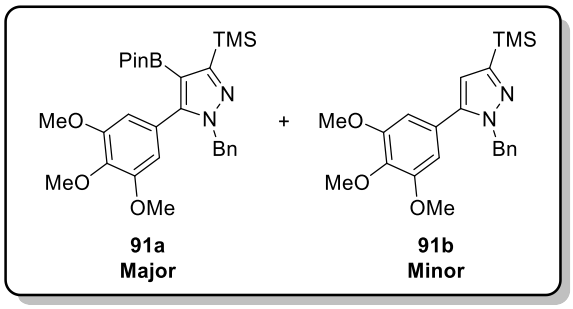

91a **Major** **91b** **Minor**

Following general procedure J using sydnone **87** (200 mg, 0.584 mmol) and alkyne **81** (262 mg, 1.17 mmol), a mixture of pyrazole **91a** and **91b** was isolated as a yellow oil (202 mg, 66%, 9:1).

^{1}H NMR (400 MHz, $CDCl_3$) δ 0.37 (9H, s), 1.19 (12H, s), 3.63 (6H, s), 3.87 (3H, s), 5.28 (2H, s), 6.40 (2H, s) 7.05 (2H, d, *J* = 7.0 Hz), 7.17-7.29 (3H, m); ^{13}C NMR (101 MHz, $CDCl_3$) δ -0.3, 25.0, 53.1, 55.9, 61.0, 83.0, 107.7, 112.8, 127.0, 127.3, 128.5, 138.0, 138.5, 150.9, 152.4, 158.8 (one sp^2 carbon not observed); FTIR: ν_{max} 2976 (w), 1585 (m), 1496 (m), 1236 (s), 1124 (s), 1038 (s); HRMS (ESI-TOF) *m/z* $[M+H]^+$ calculated for $C_{28}H_{40}{}^{11}BN_2O_5Si$: 523.2794. Found: 523.2801.

1-(Methyl)-3-(trimethylsilyl)-4-(pinacolatoborolane)-5-(3-phenylmethoxy-4-methoxyphenyl)-pyrazole, **92a** and 1-(methyl)-3-(trimethylsilyl)-5-(3-phenylmethoxy-4-methoxyphenyl)-pyrazole, **92b**:

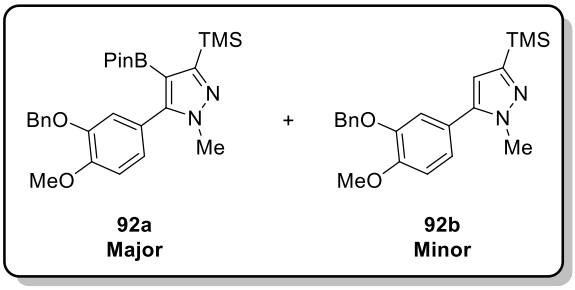

92a **Major** **92b** **Minor**

Following general procedure J using sydnone **88** (200 mg, 0.640 mmol) and alkyne **81** (287 mg, 1.28 mmol), a mixture of pyrazole **92a** and **92b** was isolated as a yellow oil (230 mg, 73%, 4:1).

^{1}H NMR (400 MHz, $CDCl_3$) δ 0.37 (9H, s), 1.20 (12H, s), 3.57 (3H, s), 3.94 (3H, s), 5.18 (2H, s), 6.91-6.94 (3H, m) 7.28-7.32 (1H, m), 7.33-7.39 (2H, m), 7.41-7.46 (2H, m); ^{13}C NMR (101 MHz, $CDCl_3$) δ -0.4, 25.0, 36.9, 56.1, 71.0, 82.9, 110.9, 116.5, 122.0, 123.6, 127.3, 128.0, 128.7, 137.1, 147.1, 149.7, 150.7, 158.7 (one sp^2 carbon not observed); FTIR: ν_{max} 2977 (w), 1498 (m), 1311 (s), 1250 (s), 1139 (s), 1046 (m), 1026 (m); HRMS (ESI-TOF) *m/z* $[M+H]^+$ calculated for $C_{27}H_{38}{}^{11}BN_2O_4Si$: 493.2694. Found: 493.2718.

1-(Benzyl)-3-(trimethylsilyl)-4-(pinacolatoborolane)-5-(3-phenylmethoxy-4-methoxyphenyl)-pyrazole, **93a** and 1-(benzyl)-3-(trimethylsilyl)-5-(3-phenylmethoxy-4-methoxyphenyl)-pyrazole **93b**:

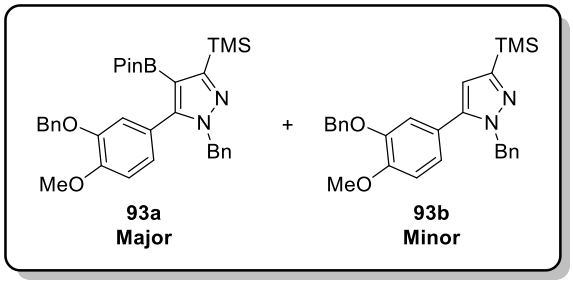

93a **Major** **93b** **Minor**

Following general procedure J using sydnone **89** (200 mg, 0.515 mmol) and alkyne **81** (231 mg, 1.03 mmol), a mixture of pyrazole **93a** and **93b** was isolated as a yellow oil (187 mg, 64%, 9:1).

^{1}H NMR (400 MHz, $CDCl_3$) δ 0.39 (9H, s), 1.19 (12H, s), 3.91 (3H, s), 4.90 (2H, s), 5.16 (2H, s), 6.78-6.82 (2H, m), 6.84 (1H, d, *J* = 8.0 Hz), 6.92-6.98 (2H, m), 7.18-7.24 (2H, m), 7.27-7.41 (6H, m); ^{13}C NMR (101 MHz, $CDCl_3$) δ -0.3, 25.0, 52.9, 56.1, 70.7, 83.0, 110.9, 115.9, 123.6, 123.9,

127.1, 127.2, 127.4, 128.0, 128.4, 128.7, 137.1, 138.3, 147.2, 149.7, 150.8, 158.7 (one sp^2 carbon not observed); FTIR: ν_{max} 2977 (w), 1497 (m), 1452 (m), 1250 (s), 1141 (s), 1029 (m) 908 (s); HRMS (ESI-TOF) *m/z* $[M+H]^+$ calculated for $C_{33}H_{42}{}^{11}BN_2O_4Si$: 569.3007. Found: 569.3010.

1-(Methyl)-3-(trimethylsilyl)-4-(3-phenylmethoxy-4-methoxyphenyl)-5-(3,4,5-trimethoxyphenyl)-pyrazole, **94** and 1-(methyl)-3-(trimethylsilyl)-5-(3,4,5-trimethoxyphenyl)-pyrazole, **90b**:

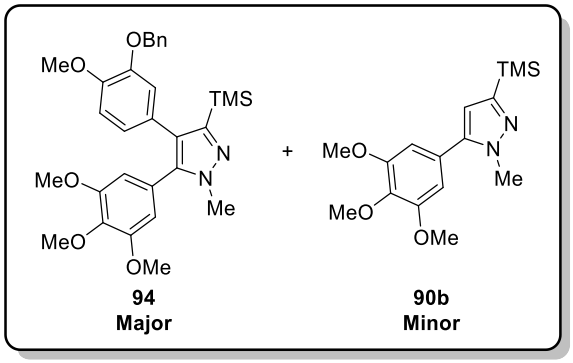

Following general procedure K using pyrazoles **90a** and **90b** (498 mg, 1.12 mmol) and bromide **73** (491 mg, 1.67 mmol), a mixture of pyrazole **94** and **90b** was isolated as a yellow oil (409 mg, 69%, 3:1).

^{1}H NMR (400 MHz, $CDCl_3$) δ 0.14 (9H, s), 3.68 (6H, s), 3.84 (3H, s), 3.87 (3H, s), 3.88 (3H, s), 5.00 (2H, s), 6.34 (2H, s) 6.68 (1H, d, *J* = 2.0 Hz), 6.71 (1H, d, *J* = 8.0, 2.0 Hz), 6.79 (1H, d, *J* = 8.0 Hz), 7.25-7.35 (5H, m); ^{13}C NMR (101 MHz, $CDCl_3$) δ -0.2, 37.7, 56.1, 56.2, 61.0, 71.1, 106.3, 107.3, 111.3, 112.6, 116.8, 123.8, 125.7, 127.1, 127.7, 127.9, 128.6, 137.2, 141.3, 147.5, 148.6, 150.5, 153.1; FTIR: ν_{max} 2957 (w), 2934 (w), 1580 (m), 1237 (s), 1127 (s), 1008 (m); HRMS (ESI-TOF) *m/z* $[M+H]^+$ calculated for $C_{30}H_{37}N_2O_5Si$: 533.2472. Found: 533.2469.

1-(Benzyl)-3-(trimethylsilyl)-4-(3-phenylmethoxy-4-methoxyphenyl)-5-(3,4,5-trimethoxyphenyl)-pyrazole, **95** and 1-(benzyl)-3-(trimethylsilyl)-5-(3,4,5-trimethoxyphenyl)-pyrazole, **91b**:

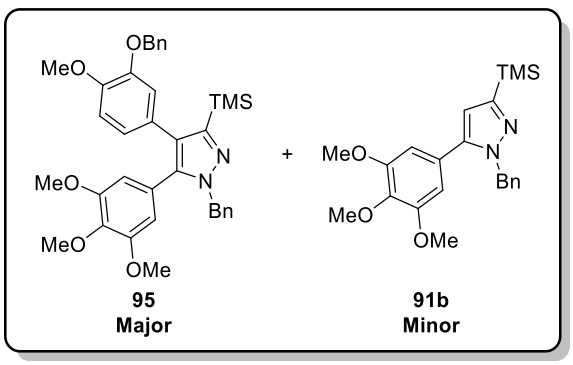

Following general procedure K using pyrazoles **91a** and **91b** (307 mg, 0.587 mmol) and bromide **73** (258 mg, 0.881 mmol), a mixture of pyrazole **95** and **91b** was isolated as a yellow oil (257 mg, 72%, 9:1).

^{1}H NMR (400 MHz, $CDCl_3$) δ 0.20 (9H, s), 3.48 (6H, s), 3.82 (3H, s), 3.86(3H, s), 4.99 (2H, s), 5.33 (2H, s), 6.18 (2H, s) 6.72-6.77 (2H, m), 6.80 (1H, d, *J* = 8.0 Hz), 7.12-7.17 (2H, m), 7.22-7.38 (8H, m); ^{13}C NMR (101 MHz, $CDCl_3$) δ -0.2, 53.6, 55.8, 56.0, 60.9, 71.1, 106.1, 107.3, 111.2, 116.6, 123.6, 125.7, 126.4, 127.0, 127.1, 127.4, 127.8, 128.5, 128.6, 137.1, 137.7, 138.5, 141.0, 147.4, 148.5, 150.7, 152.8; FTIR: ν_{max} 2956 (w), 2835 (w), 1583 (m), 1495 (m), 1244 (s), 1125 (s), 1026 (m), 1004 (m), 907 (m); HRMS (ESI-TOF) *m/z* $[M+H]^+$ calculated for $C_{36}H_{41}N_2O_5Si$: 609.2779. Found: 609.2772.

1-(Methyl)-3-(trimethylsilyl)-4-(3,4,5-trimethoxyphenyl)-5-(3-phenylmethoxy-4-methoxyphenyl)-pyrazole, **96** and 1-(methyl)-3-(trimethylsilyl)-5-(3-phenylmethoxy-4-methoxyphenyl)-pyrazole, **92b**:

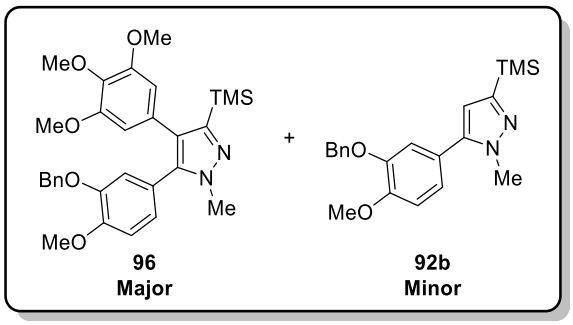

96 **Major** **92b** **Minor**

Following general procedure K using pyrazoles **92a** and **92b** (215 mg, 0.437 mmol) and bromide **73** (218 mg, 0.883 mmol), a mixture of pyrazole **96** and **92b** was isolated as a yellow oil (137 mg, 60%, 4:1).

^{1}H NMR (400 MHz, $CDCl_3$) δ 0.21 (9H, s), 3.68 (9H, s), 3.83 (3H, s), 3.87 (3H, s), 5.01 (2H, s), 6.32 (2H, s) 6.68 (1H, d, *J* = 2.0 Hz), 6.77 (1H, d, *J* = 8.5, 2.0 Hz), 6.85 (1H, d, *J* = 8.5 Hz), 7.25-7.38 (5H, m); ^{13}C NMR (101 MHz, $CDCl_3$) δ -0.2, 37.3, 56.0, 56.3, 61.0, 71.0, 104.7, 107.7, 111.5, 116.0, 122.6, 123.2, 127.0, 127.9, 128.6, 130.7, 136.8, 140.8, 147.6, 149.6, 149.8, 152.5, 153.4; FTIR: ν_{max} 2934 (w), 1580 (m), 1493 (m), 1233 (s), 1125 (s), 1006 (m); HRMS (ESI-TOF) *m/z* $[M+H]^+$ calculated for $C_{30}H_{37}N_2O_5Si$: 533.2472. Found: 533.2497.

1-(Benzyl)-3-(trimethylsilyl)-4-(3,4,5-trimethoxyphenyl)-5-(3-phenylmethoxy-4-methoxyphenyl)-pyrazole, **97** and 1-(benzyl)-3-(trimethylsilyl)-5-(3-phenylmethoxy-4-methoxyphenyl)-pyrazole, **93b**:

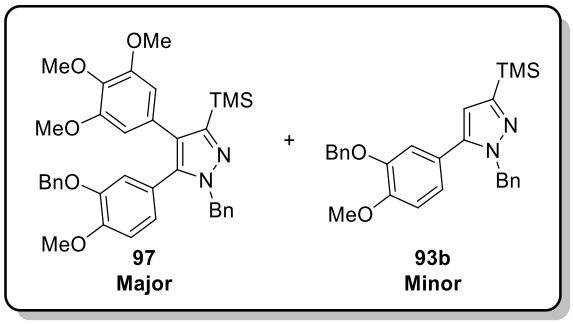

Following general procedure K using pyrazoles **93a** and **93b** (162 mg, 0.285 mmol) and bromide **73** (136 mg, 0.550 mmol), a mixture of pyrazoles **97** and **93b** was isolated as a yellow oil (85 mg, 49%, 3:1).

^{1}H NMR (400 MHz, $CDCl_3$) δ 0.24 (9H, s), 3.66 (6H, s), 3.82 (3H, s), 3.86 (3H, s), 4.78 (2H, s), 5.22 (2H, s), 6.31 (2H, s) 6.56 (1H, d, *J* = 2.0 Hz), 6.62 (1H, d, *J* = 8.5, 2.0 Hz), 6.77 (1H, d, *J* = 8.5 Hz), 7.08 (2H, dd, *J* = 9.0, 7.0 Hz), 7.22-7.35 (8H, m); ^{13}C NMR (101 MHz, $CDCl_3$) δ -0.1, 53.5, 56.1, 56.4, 61.1, 70.7, 107.7, 109.1, 111.5, 115.8, 122.1, 126.7, 127.2 (x2 C), 127.5, 128.0, 128.6 (x2 C), 130.6, 136.8, 138.2, 140.9, 147.7, 149.7, 150.3, 152.5, 154.0; FTIR: ν_{max} 2955 (w), 2934 (w), 2834 (w), 1581 (m), 1494 (m), 1232 (s), 1124 (s), 1006 (m); HRMS (ESI-TOF) *m/z* $[M+H]^+$ calculated for $C_{36}H_{41}N_2O_5Si$: 609.2784. Found: 609.2785.

1-(Methyl)-4-(3-phenylmethoxy-4-methoxyphenyl)-5-(3,4,5-trimethoxyphenyl)-pyrazole, **98a** and 1-(methyl)-5-(3,4,5-trimethoxyphenyl)-pyrazole, **98b**:

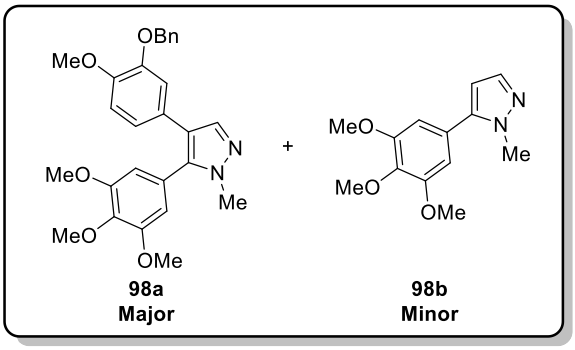

Following general procedure H using pyrazoles **94** and **90b** (211 mg, 0.396 mmol, 3:1) and TBAF in THF (4 mL, 4 mmol), a mixture of pyrazole **98a** and **98b** was isolated as a yellow oil (101 mg, 55%, 95:5).

^{1}H NMR (400 MHz, $CDCl_3$) δ 3.76 (6H, s), 3.83 (3H, s), 3.87 (3H, s), 3.89 (3H, s), 4.89 (2H, s), 6.48 (2H, s), 6.71 (1H, d, *J* = 2.0 Hz), 6.75-6.85 (2H, m), 7.20-7.32 (5H, m), 7.63 (1H, s); ^{13}C NMR (101 MHz, $CDCl_3$) δ 37.4, 56.1, 56.4, 61.1, 70.9, 106.4, 107.4, 112.0, 113.3, 120.0, 120.6, 125.8, 126.1, 127.1, 127.9, 128.6, 137.1, 137.2, 138.5, 139.4, 148.0, 148.2; FTIR: ν_{max} 2935 (w), 2835 (w), 1583 (m), 1409 (m), 1236 (s), 1123 (s), 1002 (m); HRMS (ESI-TOF) *m/z* $[M+H]^+$ calculated for $C_{27}H_{29}N_2O_5$: 461.2076. Found: 461.2090.

1-(Benzyl)-4-(3-phenylmethoxy-4-methoxyphenyl)-5-(3,4,5-trimethoxyphenyl)-pyrazole, **99**:

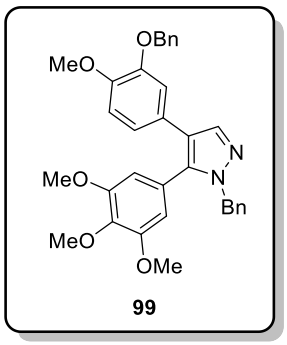

99

Following general procedure H using pyrazoles **95** and **91b** (244 mg, 0.401 mmol, 85:15) and TBAF in THF (4 mL, 4 mmol), pyrazole **99** was isolated as a yellow oil (137 mg, 64%).

^{1}H NMR (400 MHz, $CDCl_3$) δ 3.59 (6H, s), 3.84 (3H, s), 3.87 (3H, s,), 4.89 (2H, s), 5.22 (2H, s), 6.33 (2H, s), 6.76 (1H, d, *J* = 2.0 Hz), 6.79 (1H, d, *J* = 8.5 Hz), 6.85 (1H, dd, *J* = 8.5, 2.0 Hz), 7.04-7.08 (2H, m), 7.23-7.32 (8H, m), 7.74 (1H, s); ^{13}C NMR (101 MHz, $CDCl_3$) δ 53.6, 56.1 (x2 C), 61.1, 70.8, 107.5, 112.0, 113.1, 119.8, 120.8, 125.6, 125.8, 127.0, 127.1, 127.6, 127.8, 128.5, 128.6, 137.1, 137.6, 138.0, 138.4, 139.4, 148.0, 148.2, 153.5; FTIR: ν_{max} 2999 (w), 2934 (w), 2836 (w), 1580 (m), 1517 (m), 1451 (m), 1220 (s), 1136 (s), 1106 (m), 1024 (m), 1001 (m); HRMS (ESI-TOF) *m/z* $[M+H]^+$ calculated for $C_{33}H_{33}N_2O_5$: 537.2384. Found: 537.2386.

1-(Methyl)-4-(3,4,5-trimethoxyphenyl)-5-(3-phenylmethoxy-4-methoxyphenyl)-pyrazole, **100**:

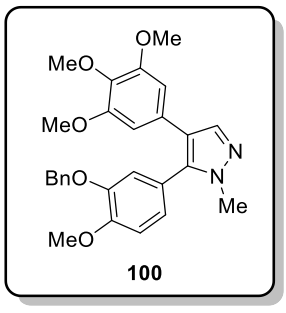

100

Following general procedure H using pyrazoles **96** and **92b** (137 mg, 0.257 mmol, 4:1) and TBAF in THF (2.6 mL, 2.6 mmol), pyrazole **100** was isolated as an orange oil (66 mg, 56%).

^{1}H NMR (400 MHz, $CDCl_3$) δ 3.59 (3H, s), 3.62 (6H, s), 3.80 (3H, s), 3.93 (3H, s), 5.11 (2H, s), 6.36 (2H, s), 6.80 (1H, d, *J* = 2.0 Hz), 6.87 (1H, dd, *J* = 8.0, 2.0 Hz), 6.96 (1H, d, *J* = 8.0 Hz), 7.24-7.38 (5H, m), 7.62 (1H, s); ^{13}C NMR (101 MHz, $CDCl_3$) δ 37.1, 55.9, 56.2, 61.0, 71.2, 104.3, 112.0, 116.2, 120.8, 122.7, 123.6, 127.2, 128.1 (x2 C), 128.7, 136.4, 136.6, 137.0, 139.7, 148.1, 150.3, 153.1; FTIR: ν_{max} 3002 (w), 2934 (w), 1584 (m), 1521 (m), 1418 (m), 1373 (m), 1253 (s), 1124 (s), 1021 (m), 1007 (m); HRMS (ESI-TOF) *m/z* $[M+H]^+$ calculated for $C_{27}H_{29}N_2O_5$: 461.2071. Found: 461.2070.

1-(Benzyl)-4-(3,4,5-trimethoxyphenyl)-5-(3-phenylmethoxy-4-methoxyphenyl)-pyrazole, **101**:

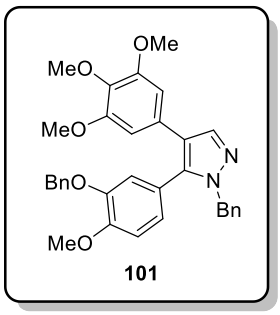

101

Following general procedure H using pyrazoles **97** and **93b** (158 mg, 0.260 mmol, 4:1) and TBAF in THF (2.6 mL, 2.6 mmol), pyrazole **101** was isolated as an orange oil (103 mg, 74%).

^{1}H NMR (400 MHz, $CDCl_3$) δ 3.61 (6H, s), 3.80 (3H, s), 3.91 (3H, s), 4.88 (2H, s), 5.13 (2H, s), 6.37 (2H, s), 6.67 (1H, d, *J* = 2.0 Hz), 6.79 (1H, dd, *J* = 8.0, 2.0 Hz), 6.90 (1H, d, *J* = 8.0 Hz), 6.98-7.03 (2H, m), 6.24-7.33 (8H, m), 7.79 (1H, s); ^{13}C NMR (101 MHz, $CDCl_3$) δ 53.3, 55.9, 56.2, 61.0, 70.8, 104.3, 111.9, 116.0, 121.2, 122.5, 123.8, 127.1, 127.3, 127.7, 128.1, 128.6, 128.7 (x2 C), 136.5, 136.6, 137.6, 137.7, 140.0, 148.1, 150.3, 153.2; FTIR: ν_{max} 2935 (w), 2835 (w), 1583 (m), 1520 (m), 1454 (m), 1373 (m), 1245 (s), 1123 (s), 1002 (s); HRMS (ESI-TOF) *m/z* $[M+H]^+$ calculated for $C_{33}H_{33}N_2O_5$: 537.2384. Found: 537.2383.

1-(Methyl)-4-(3-hydroxy-4-methoxyphenyl)-5-(3,4,5-trimethoxyphenyl)-pyrazole, **82**:

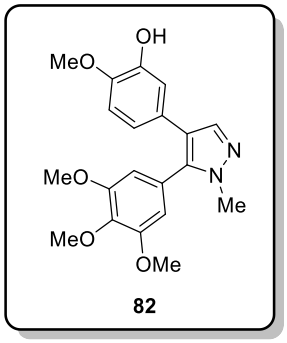

82

Following general procedure I using pyrazoles **98a** and **98b** (100 mg, 0.217 mmol) and Pd/C (22 mg), pyrazole **82** was isolated as a colourless solid (47 mg, 58%).

M.p.: 210 °C; ^{1}H NMR (400 MHz, $CDCl_3$) δ 3.77 (3H, s), 3.79 (6H, s), 3.85 (3H, s), 3.92 (3H, s), 5.57 (1H, s), 6.50 (2H, s), 6.66 (1H, dd, *J* = 8.5, 2.0 Hz), 6.72 (1H, d, *J* = 8.5 Hz), 6.85 (1H, d, *J* = 2.0 Hz), 7.67 (1H, s); ^{13}C NMR (101 MHz, $CDCl_3$) δ 37.4, 56.0, 56.3, 61.1, 107.4, 110.8, 113.8, 119.1, 120.6, 125.9, 126.5, 137.4, 138.4, 139.5, 145.3, 145.6, 153.6; FTIR: ν_{max} 3347 (br), 1582 (m), 1458 (m), 1406 (m), 1270 (m), 1232 (s), 1129 (s), 1028 (m), 997 (m); HRMS (ESI-TOF) *m/z* $[M+H]^+$ calculated for $C_{20}H_{23}N_2O_5$: 371.1607. Found: 371.1611.

4-(3-Hydroxy-4-methoxyphenyl)-5-(3,4,5-trimethoxyphenyl)-pyrazole, **83** and 1-(benzyl)-4-(3-hydroxy-4-methoxyphenyl)-5-(3,4,5-trimethoxyphenyl)-pyrazole, **102**:

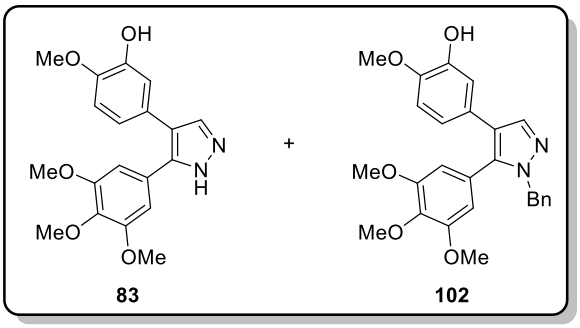

83 **102**

Following general procedure I using pyrazole **99** (126 mg, 0.235 mmol) and Pd/C (24 mg), pyrazole **83** was isolated as a colourless solid (25 mg, 30%) and pyrazole **102** was isolated as a colourless solid (23 mg, 22%).

83: M.p.: 198-200 °C; ^{1}H NMR (400 MHz, $CDCl_3$) δ 3.73 (6H, s), 3.87 (3H, s), 3.90 (3H, s), 6.71 (2H, s), 6.81 (2H, d, *J* = 1.0 Hz), 6.96 (1H, t, *J* = 1.0 Hz), 7.65 (1H, s); ^{13}C NMR (101 MHz, $CDCl_3$) δ 56.2 (x2 C), 61.1, 105.4, 105.6, 110.8, 115.2, 119.8, 120.7, 126.5, 127.1, 129.9, 138.1, 145.7, 145.8, 153.4; FTIR: ν_{max} 3251 (m), 2966 (w), 2937 (w), 1587 (m), 1412 (m), 1274 (m), 1234 (s), 1121 (s), 1028 (m), 994 (m); HRMS (ESI-TOF) *m/z* $[M+H]^+$ calculated for $C_{19}H_{20}N_2O_5$: 357.1445. Found: 357.1443.

102: M.p.: 126 °C; ^{1}H NMR (400 MHz, $CDCl_3$) δ 3.60 (6H, s), 3.84 (3H, s), 3.89 (3H, s), 5.22 (2H, s), 5.56 (1H, s), 6.33 (2H, s), 6.65-6.74 (2H, m), 6.87 (1H, d, *J* = 1.5 Hz), 7.06 (1H, d, *J* = 7.0 Hz), 7.19-7.33 (4H, m), 7.77 (1H, s); ^{13}C NMR (101 MHz, $CDCl_3$) δ 53.6, 56.1 (x 2C), 61.1, 107.6, 110.8, 113.6, 119.0, 120.8, 125.7, 126.5, 127.0, 127.6, 128.7, 138.0, 138.1, 138.5, 139.7, 145.3, 145.6, 153.4; FTIR: ν_{max} 3423 (m), 2926 (m), 2835 (w), 1579 (m), 1500 (m), 1231 (m), 1216 (m), 1124 (s), 1028 (m), 1000 (m); HRMS (ESI-TOF) *m/z* $[M+H]^+$ calculated for $C_{26}H_{26}N_2O_5$: 447.1914. Found: 447.1922.

1-(Methyl)-4-(3,4,5-trimethoxyphenyl)-5-(3-hydroxy-4-methoxyphenyl)-pyrazole, **84**:

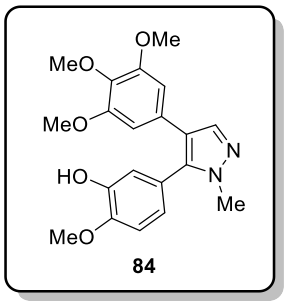

84

Following general procedure I using pyrazole **100** (177 mg, 0.384 mmol) and Pd/C (38 mg), pyrazole **84** was isolated as a colourless solid (96 mg, 67%).

M.p.: 149-150 °C; ^{1}H NMR (400 MHz, $CDCl_3$) δ 3.64 (6H, s), 3.74 (3H, s), 3.79 (3H, s), 3.92 (3H, s), 6.38 (1H, br), 6.41 (2H, s), 6.79 (1H, dd, *J* = 8.0, 2.0 Hz), 6.89-6.95 (2H, m), 7.68 (1H, s); ^{13}C NMR (101 MHz, $CDCl_3$) δ 37.2, 55.9, 56.1, 61.0, 104.4, 111.0, 116.5, 120.8, 122.4, 123.4, 128.8, 136.3, 137.0, 139.8, 146.1, 147.3, 153.1; FTIR: ν_{max} 3269 (br), 2940 (w), 1583 (m), 1373 (m), 1272 (m), 1227 (m), 1173 (m), 1123 (s), 1007 (m); HRMS (ESI-TOF) *m/z* $[M+H]^+$ calculated for $C_{20}H_{23}N_2O_5$: 371.1607. Found: 371.1605.

4-(3,4,5-Trimethoxyphenyl)-5-(3-hydroxy-4-methoxyphenyl)-pyrazole, **85** and 1-(benzyl)-4-(3,4,5-trimethoxyphenyl)-5-(3-hydroxy-4-methoxyphenyl)-pyrazole, **103**:

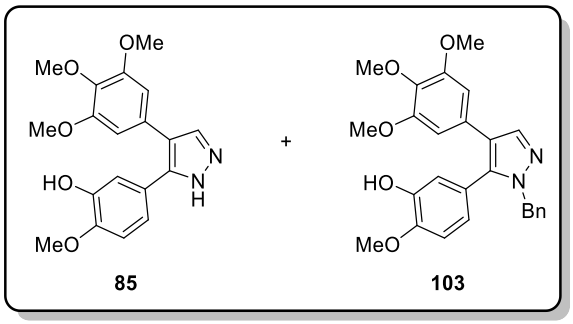

85 **103**

Following general procedure I using pyrazole **101** (66 mg, 0.123 mmol) and Pd/C (15 mg), pyrazole **85** was isolated as a colourless solid (12 mg, 27%) and pyrazole **103** was isolated as a tan solid (15 mg, 27%).

85: M.p.: 90-100 °C; ^{1}H NMR (400 MHz, $CDCl_3$) δ 3.73 (6H, s), 3.86 (3H, s), 3.88 (3H, s), 6.51 (2H, s), 6.80 (1H, d, *J* = 8.5 Hz), 6.94 (1H, dd, *J* = 8.5, 2.0 Hz), 7.13 (1H, d, *J* = 2.0 Hz), 7.67 (1H, s); ^{13}C NMR (101 MHz, $CDCl_3$) δ 56.1, 56.2, 61.1, 105.7, 110.9, 114.7, 119.6, 120.6, 124.2, 128.8, 135.9, 136.9, 142.6, 145.8, 147.1, 153.3; FTIR: ν_{max} 3282 (br), 2934 (w), 2838 (w), 1584 (m), 1449 (m), 1411 (m), 1251 (m), 1231 (m), 1122 (s), 1019 (m); HRMS (ESI-TOF) *m/z* $[M+H]^+$ calculated for $C_{19}H_{20}N_2O_5$: 357.1445. Found: 357.1440.

103: M.p.: 167-168 °C; ^{1}H NMR (400 MHz, $CDCl_3$) δ 3.65 (6H, s), 3.80 (3H, s), 3.93 (3H, s), 5.22 (2H, s), 5.66 (1H, s), 6.43 (2H, s), 6.72 (1H, dd, *J* = 8.0, 2.0 Hz), 6.83-6.88 (2H, m), 7.03-7.08 (2H, m), 7.23-7.29 (3H, m), 7.78 (1H, s); ^{13}C NMR (101 MHz, $CDCl_3$) δ 53.3, 56.0, 56.2, 61.0, 104.5, 110.9, 116.7, 121.2, 122.8, 123.6, 127.3, 127.7, 128.7, 137.5, 137.9, 140.0, 146.0, 147.2, 153.2; FTIR: ν_{max} 2929 (br), 1584 (m), 1520 (m), 1374 (m), 1246 (m), 1120 (s), 1007 (m); HRMS (ESI-TOF) *m/z* $[M+H]^+$ calculated for $C_{26}H_{26}N_2O_5$: 447.1914. Found: 447.1914.

1-(3,4,5-Trimethoxyphenyl)-5-(3-hydroxy-4-methoxyphenyl)-pyrazole, **64**:

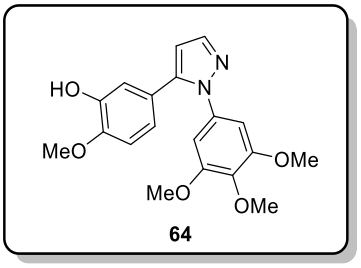

64

Following general procedure H a mixture of pyrazoles **69a** and **69b** (100 mg, 0.184 mmol) and TBAF in THF (1.8 mL, 1.8 mmol),, pyrazole **64** was isolated as a colourless solid (46 mg, 70%).

See above for characterisation data.

1-Bromo-4-fluoromethoxybenzene, **104** and 1,1'-[methylenebis(oxy)]bis[4-bromobenzene] **105**:[186]

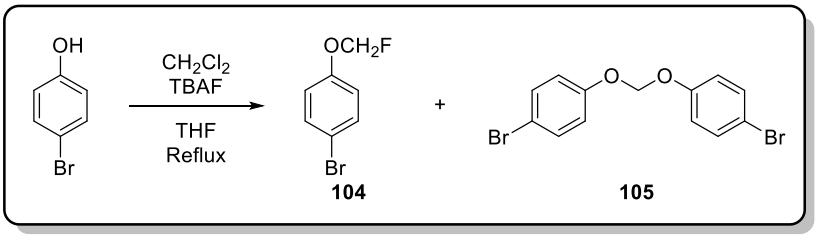

104 **105**

A flask was charged with 4-bromophenol (100 mg, 0.585 mmol), CH_2Cl_2 (0.5 mL) and TBAF in THF (1M, 6 mL, 6 mmol) and the reaction heated at reflux for 14 h. The reaction was allowed to cool to ambient temperature and poured into aq. $NaHCO_3$, extracted with ethyl acetate and volatiles removed *in vacuo*. The resulting crude material was purified by flash silica chromatography (gradient 100% petroleum ether – 10% ethyl acetate in petroleum ether) affording a mixture of **104** and **105** as a colourless oil (20 mg, 17%, 85:15). The mixture was characterised by ^{1}H and ^{19}F NMR only.

^{1}H NMR (400 MHz, $CDCl_3$) δ 5.68 (2H, d, *J* = 54.5 Hz), 6.91-7.04 (2H, m), 7.38-7.48 (2H, m); ^{19}F NMR (128 MHz, $CDCl_3$) δ -149.1 (t, *J* = 54.5 Hz).

3-Fluoromethoxy-4-methoxybenzaldehydebenzene, **106**:

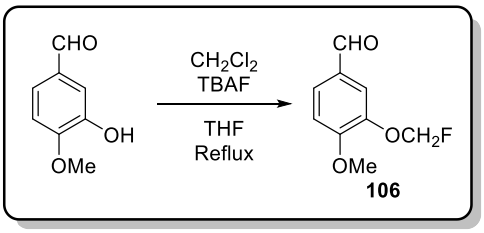

A flask was charged with 3-hydroxy-4-methoxybenzaldehyde (50 mg, 0.33 mmol), CH_2Cl_2 (0.5 mL) and TBAF in THF (1M, 3.3 mL, 3.3 mmol) and the reaction heated at reflux for 14 h. The reaction was allowed to cool to ambient temperature and poured into aq. $NaHCO_3$, extracted with ethyl acetate and volatiles removed *in vacuo*. The resulting crude material was purified by flash silica chromatography (gradient 100% petroleum ether – 40% ethyl acetate in petroleum ether) affording **106** as a colourless oil (25 mg, 41%).

M.p.: 59-61 °C; ^{1}H NMR (400 MHz, $CDCl_3$) δ 3.97 (3H, s), 5.77 (2H, d, *J* = 54.0 Hz), 7.05 (1H, d, *J* = 8.5 Hz), 7.63 (1H, d, *J* = 8.5, 2.0 Hz), 7.66-7.67 (1H, m), 9.86 (1H, s); ^{13}C NMR (101 MHz, $CDCl_3$) δ 56.4, 101.0 (d, *J* = 221.0 Hz), 111.8, 116.4, 128.5, 130.2, 146.3 (d, *J* = 2.5 Hz), 155.1, 190.5; ^{19}F NMR (128 MHz, $CDCl_3$) δ -149.8 (t, *J* = 54.0 Hz); FTIR: ν_{max} 1686 (s), 1601 (m), 1587 (m), 1508 (s), 1439 (s), 1404 (m), 1262 (s), 1228 (s), 1173 (m), 1135 (s), 1079 (m), 1016 (s), 943 (s); HRMS (ESI-TOF) *m/z* $[M+H]^+$ calculated for $C_9H_9FO_3$: 184.0530. Found: 184.0526.

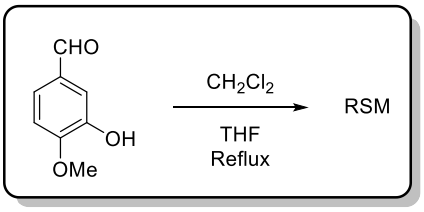

A flask was charged with 3-hydroxy-4-methoxybenzaldehyde (50 mg, 0.33 mmol), CH_2Cl_2 (0.5 mL) THF (3.3 mL) and the reaction heated at reflux for 14 h. The reaction was allowed to cool to ambient temperature and volatiles removed *in vacuo*, resulting in the recovery of starting material.

3-(Fluoro,dideuteromethoxy)-4-methoxybenzaldehydebenzene, **107**:

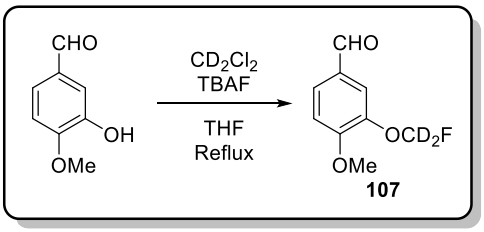

A flask was charged with 3-hydroxy-4-methoxybenzaldehyde (50 mg, 0.33 mmol), CD_2Cl_2 (0.5 mL) and TBAF in THF (1M, 3.3 mL, 3.3 mmol) and the reaction heated at reflux for 14 h. The reaction was allowed to cool to ambient temperature and poured into aq. $NaHCO_3$, extracted with ethyl acetate and volatiles removed *in vacuo*. The resulting crude material was purified by flash silica chromatography (gradient 100% petroleum ether – 40% ethyl acetate in petroleum ether) affording **107** as a colourless solid (19 mg, 31%).

M.p.: 57-59 °C; ^{1}H NMR (400 MHz, $CDCl_3$) δ 3.97 (3H, s), 5.77 (2H, d, *J* = 54.0 Hz), 7.05 (1H, d, *J* = 8.5 Hz), 7.64 (2H, m), 9.86 (1H, s); ^{13}C NMR (101 MHz, $CDCl_3$) δ 56.4, 98.5-102.1 (m), 111.8, 116.3, 128.5, 130.2, 146.3, 155.1, 190.5; ^{19}F NMR (128 MHz, $CDCl_3$) δ -151.1- -151.2 (m); FTIR: ν_{max} 1690 (s), 1603 (m), 1587 (m), 1508 (s), 1435 (s), 1266 (s), 1164 (m), 1129 (s), 1016 (s), 916 (s); HRMS (ESI-TOF) *m/z* $[M+H]^+$ calculated for $C_9H_7D_2FO_3$: 187.0734. Found: 187.0734.

3,4,5-Trimethoxyphenylacetylene:[187]

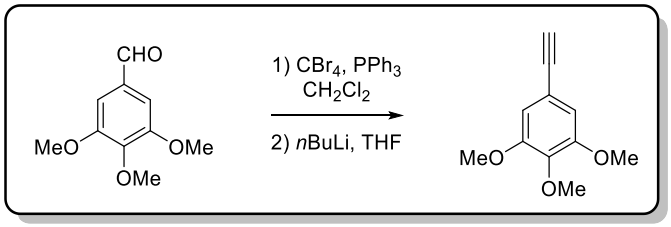

To a solution of 3,4,5-trimethoxybenzaldehyde (20.0 g, 102 mmol) and PPh_3 (60.0 g, 204 mmol) in CH_2Cl_2 (200 mL) at 0 °C was added carbon tetrabromide (36.9 g, 111 mmol) in CH_2Cl_2 (200 mL) and the reaction stirred for 2 h and ambient temperature. The mixture was poured into water and extracted with CH_2Cl_2. The combined organic layers were dried over $MgSO_4$ and volatiles removed *in vacuo*. Boiling Et_2O was added to the crude residue (3x) and the suspension filtered. The solution was cooled to -20 °C for 1 h before further filtration. Volatiles were removed *in vacuo* and the resulting material (21.02 g) dissolved in dry THF (120 mL). The solution was cooled to -78 °C and *n*BuLi (~2.5 M, 60 mL, 150 mmol) slowly added. The reaction was allowed to warm to ambient temperature and stirred for 2 h. Aqueous NH_4Cl was carefully added and extracted with EtOAc. The combined organic layers

were dried over $MgSO_4$ and volatiles removed *in vacuo*. The crude residue was purified by flash silica chromatography (gradient 100% petroleum ether to 40% ethyl acetate in petroleum ether) affording 3,4,5-trimethoxyphenylacetylene as a colourless solid (10.9 g, 56% over 2 steps).

M.p.: 42-44°C; ^{1}H NMR (400 MHz, $CDCl_3$) δ 3.03 (1H, s), 3.85 (6H, s), 3.85 (3H, s), 6.73 (2H, s); ^{13}C NMR (101 MHz, $CDCl_3$) δ 56.3, 61.1, 76.4, 83.8, 109.5, 117.2, 139.4, 153.2.

4,4,5,5-Tetramethyl-2-[2-(3,4,5-trimethoxyphenyl)ethynyl]-1,3,2-dioxaborolane, **112**:

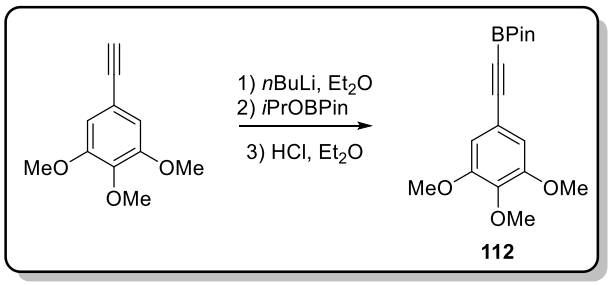

112

To a solution of 3,4,5-trimethoxyphenylacetylene (9.71 g, 50.5 mmol) in Et_2O (51 mL) at -78 °C was added *n*-BuLi (~2.3 M, 22 mL) and the reaction stirred for 1 h. The reaction was allowed to warm to ambient temperature and 2-isopropoxy-4,4,5,5-tetramethyl-1,3,2-dioxaborolane (9.40 g, 50.5 mmol) was added. The reaction was stirred for 3 h at room temperature before the addition of HCl in ether (2 M, 33 mL, 66 mmol). The mixture was filtered through celite™ and washed with Et_2O. The crude residue was passed through a short silica plug and volatiles removed *in vacuo*. The crude residue was triturated with 40-60 petroleum ether affording **112** as a colourless solid (2.17 g, 14%).

M.p.: 89-92 °C; ^{1}H NMR (400 MHz, $CDCl_3$) δ 1.32 (9H, s), 3.82 (6H, s), 3.85 (3H, s), 6.79 (2H, s); ^{13}C NMR (101 MHz, $CDCl_3$) δ 24.8, 56.2, 61.1, 84.6, 102.1 (br), 109.5, 109.9, 116.8, 139.9, 153.1; FTIR: ν_{max} 2977 (w), 2197 (w), 1578 (m), 1504 (m), 1319 (s), 1300 (s), 1239 (s), 1122 (s), 1007 (m), 960 (m), 835 (m); HRMS (ESI-TOF) *m/z* $[M+H]^+$ calculated for $C_{11}H_{14}{}^{11}BO_5$ (Product cleaved to boronic acid under LC-MS conditions): 237.0929. Found: 237.0929.

Cycloaddition of 4,4,5,5-Tetramethyl-2-[2-(3,4,5-trimethoxyphenyl)ethynyl]-1,3,2-dioxaborolane with *N*-methylsydnone:

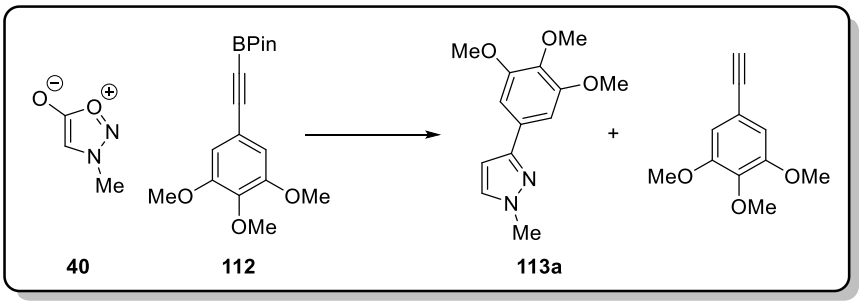

A solution of *N*-benzylsydnone (109 mg, 1.09 mmol), 4,5,5-tetramethyl-2-[2-(3,4,5-trimethoxyphenyl)ethynyl]-1,3,2-dioxaborolane (694 mg, 2.18 mmol) in xylenes (1 mL) was heated at 180 °C for 48 h affording a mixture of pyrazoles **113a** and **113b** as an orange oil (180 mg, 67%, >98:2) and 3,4,5-trimethoxyphenylacetylene as a colourless solid (37 mg, 9%).

113a: ^{1}H NMR (400 MHz, $CDCl_3$) δ 3.83 (3H, s), 3.89 (9H, s), 6.45 (1H, d, *J* = 2.0 Hz), 6.99 (2H, s), 7.33 (1H, d, *J* = 2.0 Hz); ^{13}C NMR (101 MHz, $CDCl_3$) δ 39.0, 56.1, 60.9, 102.6, 102.7, 129.4, 131.5, 137.6, 151.4, 153.4; FTIR: ν_{max} 2930 (w), 2827 (w), 1588 (m), 1507 (m), 1401 (m), 1232 (s), 1127 (s), 1008 (m); HRMS (ESI-TOF) *m/z* $[M+H]^+$ calculated for $C_{13}H_{17}N_2O_3$: 249.1234. Found: 249.1230.

3,4,5-Trimethoxyphenylacetylene: see above for characterisation data.

Cycloaddition of 4,4,5,5-Tetramethyl-2-[2-(3,4,5-trimethoxyphenyl)ethynyl]-1,3,2-dioxaborolane with *N*-benzylsydnone:

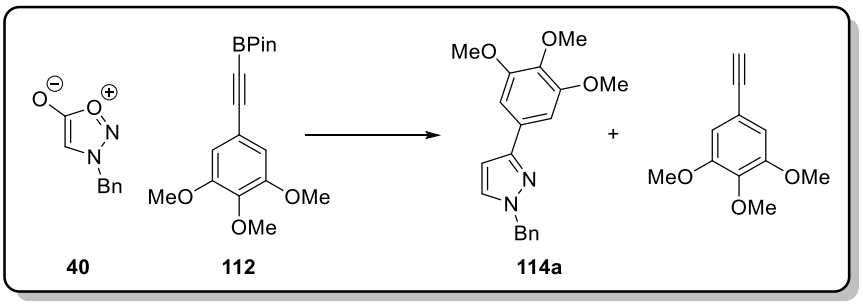

A solution of *N*-benzylsydnone (50 mg, 0.28 mmol), 4,5,5-tetramethyl-2-[2-(3,4,5-trimethoxyphenyl)ethynyl]-1,3,2-dioxaborolane (181 mg, 0.568 mmol) and galvinoxyl (10 mg, 0.024 mmol) in xylenes (0.28 mL) was heated at 160 °C in the dark for 24 h affording a mixture of pyrazoles **114a** and **114b** as an orange oil (32 mg, 35%) and 3,4,5-trimethoxyphenylacetylene as a colourless solid (22 mg, 20%).

114a: ^{1}H NMR (400 MHz, $CDCl_3$) δ 3.87 (3H, s), 3.93 (6H, s), 5.36 (2H, s), 6.53 (1H, d, *J* = 2.5 Hz), 7.05 (2H, s), 7.21-7.28 (2H, m), 7.29-7.40 (4H, m); ^{13}C NMR (101 MHz, $CDCl_3$) δ 56.2, 56.3, 61.2, 103.0, 103.4, 106.5, 127.8, 128.1, 128.9, 129.5, 130.8, 136.7, 151.6, 153.6; FTIR: ν_{max} 2934 (w), 1587 (m), 1500 (m), 1423 (m), 1228 (s), 1125 (s), 1000 (s); HRMS (ESI-TOF) *m/z* $[M+H]^+$ calculated for $C_{19}H_{21}N_2O_3$: 325.1547. Found: 325.1550.

3,4,5-Trimethoxyphenylacetylene: see above for characterisation data.

1-(Methyl)-3-(3,4,5-trimethoxyphenyl)-pyrazole, **113a** and 1-(methyl)-3-(3,4,5-trimethoxyphenyl)-pyrazole, **113b**:

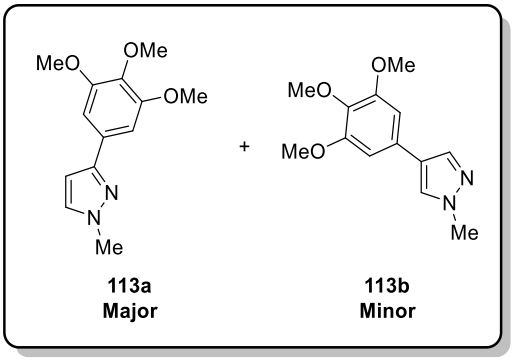

Following general procedure G using *N*-methylsydnone **40** (150 mg, 1.50 mmol) and 3,4,5-trimethoxyphenylacetylene (576 mg, 3.00 mmol), an inseparable mixture of pyrazoles **113a** and **113b** were isolated as an orange oil (236 mg, 63%, >98:2).

See above for characterisation data.

1-(Benzyl)-3-(3,4,5-trimethoxyphenyl)-pyrazole, **114a** and 1-(benzyl)-4-(3,4,5-trimethoxyphenyl)-pyrazole, **114b**:

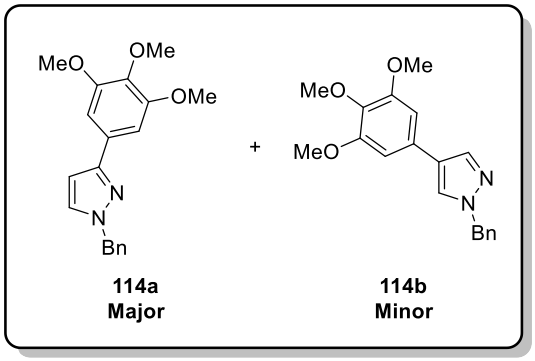

Following general procedure G using *N*-Benzylsydnone **44** (200 mg, 1.14 mmol) and 3,4,5-trimethoxyphenylacetylene (436 mg, 2.27 mmol), an inseparable mixture of pyrazoles **114a** and **114b** were isolated as an orange oil (239 mg, 64%, 9:1).

See above for characterisation data.

1-(Methyl)-3-([3-*tert*-butyldimethyloxy]-4-methoxyphenyl)-pyrazole, **115a** and 1-(methyl)-4-([3-*tert*-butyldimethyloxy]-4-methoxyphenyl)-pyrazole, **115b**:

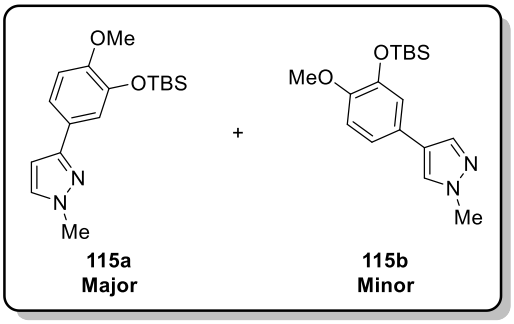

115a **Major** **115b** **Minor**

Following general procedure G using *N*-methylsydnone **40** (163 mg, 1.63 mmol) and alkyne **60** (787 mg, 3.00 mmol), an inseparable mixture of pyrazoles **115a** and **115b** were isolated as an orange oil (339 mg, 65%, 9:1).

^{1}H NMR (400 MHz, $CDCl_3$) δ 0.18 (6H, s), 1.01 (9H, s), 3.82 (3H, s), 3.93 (3H, s), 6.43 (1H, d, *J* = 2.5 Hz), 6.86 (1H, d, *J* = 8.5 Hz), 7.29 (1H, d, *J* = 2.0 Hz), 7.32-7.36 (2H, m); ^{13}C NMR (101 MHz, $CDCl_3$) δ -4.5, 18.6, 25.9, 39.1, 55.6, 102.5, 112.2, 118.6, 119.1, 126.9, 131.3, 145.2, 150.8, 151.6; FTIR: ν_{max} 2952 (w), 2930 (w), 2857 (w), 1508 (m), 1472 (m), 1271 (s), 1229 (s), 1135 (m), 992 (m), 915 (s); HRMS (ESI-TOF) *m/z* $[M+H]^+$ calculated for $C_{17}H_{27}N_2O_2Si$: 319.1836. Found: 319.1832.

1-(Benzyl)-3-([3-*tert*-butyldimethyloxy]-4-methoxyphenyl)-pyrazole, **116a** and 1-(benzyl)-4-([3-*tert*-butyldimethyloxy]-4-methoxyphenyl)-pyrazole, **116b**:

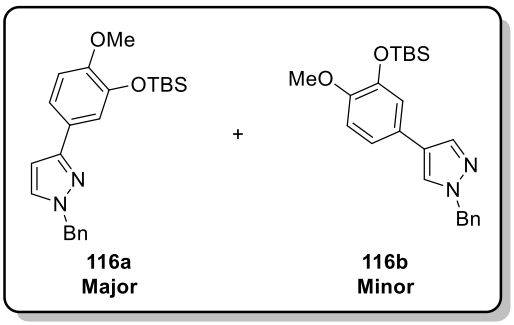

116a **Major** **116b** **Minor**

Following general procedure G using *N*-benzylsydnone **44** (200 mg, 1.14 mmol) and alkyne **60** (598 mg, 2.28 mmol), an inseparable mixture of pyrazoles **116a** and **116b** were isolated as an orange oil (263 mg, 58%, >98:2).

^{1}H NMR (400 MHz, $CDCl_3$) δ 0.21 (6H, s), 1.05 (9H, s), 3.84 (3H, s), 5.35 (2H, s), 6.49 (1H, d, *J* = 2.5 Hz), 6.89 (1H, d, *J* = 8.5 Hz), 7.24-7.28 (2H, m), 7.31-7.38 (5H, m), 7.42 (1H, dd, *J* = 8.5, 2.0 Hz); ^{13}C NMR (101 MHz, $CDCl_3$) δ -4.5, 18.6, 25.9, 55.6, 56.1, 103.0, 112.2, 118.7, 119.2, 126.9, 127.8, 128.0, 128.8, 130.5, 136.8, 145.2, 150.8, 151.4; FTIR: ν_{max} 2952 (w), 2929 (w), 2857 (w), 1504 (m), 1472 (m), 1271 (s), 1229 (s), 1134 (m), 995 (m), 915 (m); HRMS (ESI-TOF) *m/z* $[M+H]^+$ calculated for $C_{23}H_{31}N_2O_2Si$: 395.2149. Found: 395.2147.

1-(Methyl)-3-(3,4,5-trimethoxyphenyl)-4-(3-hydroxy-4-methoxyphenyl)-pyrazole, **108**:

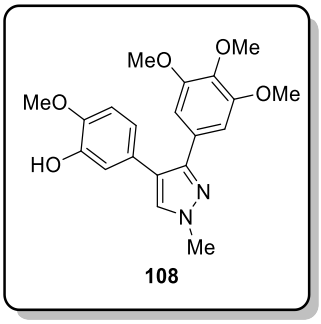

108

Following general procedure L*i* using pyrazoles **113a/b** (543 mg, 2.19 mmol), NBS (389 mg, 2.19 mmol), 3-hydroxy-4-methoxyphenylboronic acid pinacol ester (822 mg, 3.29 mmol), XPhosPdG2 (172 mg, 0.219 mmol) and Na_2CO_3 (812 mg, 7.67 mmol) for 17 hours, pyrazole **108** was isolated as a tan solid (551 mg, 68%). The product could be further purified by recrystallisation from pentane.

M.p.: 46-48 °C; ^{1}H NMR (400 MHz, $CDCl_3$) δ 3.69 (6H, s), 3.72 (3H, s), 3.83 (3H, s), 3.95 (3H, s), 5.85 (1H, s), 6.74-6.77 (3H, m), 6.82 (1H, dd, *J* = 8.0, 2.0 Hz), 6.86 (1H, d, *J* = 8.0 Hz), 7.40 (1H, s); ^{13}C NMR (101 MHz, $CDCl_3$) δ 39.1, 55.9, 56.0, 61.0, 106.3, 111.9, 114.5, 120.8, 121.9, 125.4, 129.1, 130.2, 137.5, 144.7, 146.5, 148.3, 153.0; FTIR: ν_{max} 3405 (br), 2935 (w), 2831 (w), 1587 (m), 1556 (m), 1508 (m), 1462 (m), 1413 (s), 1234 (s), 1119 (s), 1002 (m); HRMS (ESI-TOF) *m/z* $[M+H]^+$ calculated for $C_{20}H_{23}N_2O_5$: 371.1601. Found: 371.1602.

1-(Benzyl)-3-(3,4,5-trimethoxyphenyl)-4-(3-hydroxy-4-methoxyphenyl)-pyrazole, **109**:

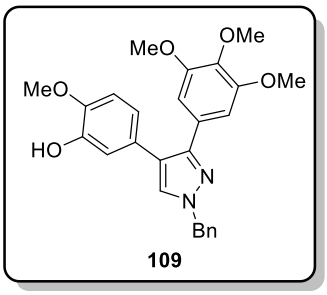

109

Following general procedure L*i* using pyrazoles **114a/b** (398 mg, 1.23 mmol), NBS (218 mg, 1.23 mmol), 3-hydroxy-4-methoxyphenylboronic acid pinacol ester (461 mg, 1.85 mmol), XPhosPdG2 (97 mg, 0.123 mmol) and Na_2CO_3 (456 mg, 4.31 mmol) for 17 hours, pyrazole **109** was isolated as a colourless solid (323 mg, 59%). The product could be further purified by recrystallization from ethyl acetate/40-60 petroleum ether.

M.p.: 168-169 °C; ^{1}H NMR (400 MHz, $CDCl_3$) δ 3.72 (6H, s), 3.72 (3H, s), 3.84 (3H, s), 5.36 (2H, s), 5.64 (1H, s), 6.74 (1H, d, *J* = 2.0 Hz), 6.79 (2H, s), 6.82 (1H, dd, *J* = 8.0, 2.0 Hz), 6.86 (1H, d, *J* = 8.0 Hz), 7.31-7.42 (5H, m), 7.38 (1H, s); ^{13}C NMR (101 MHz, $CDCl_3$) δ 56.0, 56.1, 56.3, 61.0, 105.5, 111.8, 114.5, 121.2, 122.0, 125.4, 128.1, 128.3, 129.0, 129.2 (x2 C), 136.4, 137.6, 144.7, 146.4, 148.3, 153.1; FTIR: ν_{max} 2957 (w), 2933 (w), 1588 (m), 1558 (m), 1507 (m), 1418 (m), 1265 (m), 1240 (m), 1116 (s), 1004 (m); HRMS (ESI-TOF) *m/z* $[M+H]^+$ calculated for $C_{26}H_{27}N_2O_5$: 447.1914. Found: 447.1913.

Potassium (3,4,5-trimethoxyphenyl)trifluoroborate:[188]

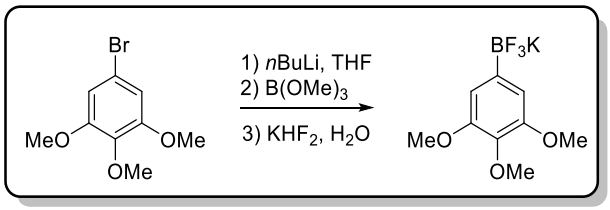

To a solution of 5-bromo-1,2,3-trimethoxybenzene (10.0 g, 40.4 mmol) in THF (80 mL) at -78 °C was added *n*-BuLi (~2.22 M, 18 mL, 40 mmol) and the reaction stirred for 1 h. Trimethylborate (6.30 g, 60.6 mmol) was slowly added over 20 min at -78 °C. The reaction was allowed to warm to -20 °C over 1 h. Potassium hydrogen difluoride (18.9 g, 242 mmol) in water (80 mL) was added and the reaction allowed to warm to ambient temperature and stirred for 1 h. The solvent was removed and the crude material refluxed in acetone, filtered and the solvent removed. Dichloromethane was added to the resulting material and the remaining colourless solid, potassium (3,4,5-trimethoxyphenyl)trifluoroborate, isolated by filtration (1.57 g, 14%).

^{1}H NMR (400 MHz, DMSO-d_6) δ 3.59 (3H, s), 3.70 (6H, s), 6.58 (2H, s); ^{13}C NMR (101 MHz, DMSO-d_6) δ 55.4, 59.8, 107.9, 135.5, 151.5 (one sp^2 carbon not observed); ^{19}F NMR (377 MHz, DMSO-d_6) δ -139.0; ^{11}B NMR (128 MHz, DMSO-d_6) δ -3.07.

1-(Methyl)-3-(3-hydroxy-4-methoxyphenyl)-4-(3,4,5-trimethoxyphenyl)-pyrazole, **110**:

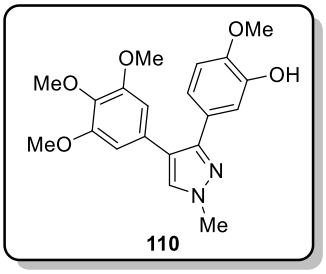

110

Following general procedure L*ii* using pyrazoles **115a/b** (125 mg, 0.392 mmol), NBS (70 mg, 0.392 mmol), potassium 3,4,5-trimethoxyphenyltrifluoroborate (159 mg, 0.580 mmol), XPhosPdG2 (31 mg, 0.039 mmol) and Na_2CO_3 (83 mg, 0.784 mmol) and K_2CO_3 (163 mg, 1.18 mmol) for 20 hours, pyrazole **110** was isolated as a colourless solid (63 mg, 43%). The product could be further purified by recrystallisation from ethyl acetate/40-60 petroleum ether.

M.p.: 171 °C; ^{1}H NMR (400 MHz, $CDCl_3$) δ 3.72 (6H, s), 3.86 (3H, s), 3.88 (3H, s), 3.95 (3H, s), 5.62 (1H, s), 6.50 (2H, s), 6.79 (1H, d, *J* = 8.5 Hz), 7.00 (1H, dd, *J* = 8.5, 2.0 Hz), 7.15 (1H, d, *J* = 2.0 Hz), 7.44 (1H, s); ^{13}C NMR (101 MHz, $CDCl_3$) δ 39.1, 56.1, 56.2, 61.1, 105.9, 110.5, 114.9, 120.6 (x2 C), 127.0, 129.0, 130.0, 136.9, 145.5, 146.4, 148.5, 153.2; FTIR: ν_{max} 3122 (br), 2965 (w), 2934 (w), 2838 (w), 1585 (m), 1462 (m), 1411 (s), 1338 (m), 1228 (s), 1127 (s), 1016 (m), 1000 (m); HRMS (ESI-TOF) *m/z* $[M+H]^+$ calculated for $C_{20}H_{23}N_2O_5$: 371.1601. Found: 371.1598.

1-(Benzyl)-3-(3-hydroxy-4-methoxyphenyl)-4-(3,4,5-trimethoxyphenyl)-pyrazole, **111**:

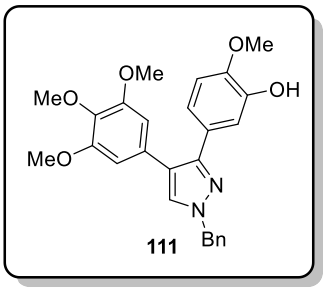

111

Following general procedure L*ii* using pyrazole **116a/b** (252 mg, 0.639 mmol), NBS (114 mg, 0.639 mmol), potassium 3,4,5-trimethoxyphenyltrifluoroborate (263 mg, 0.959 mmol), XPhosPdG2 (50 mg, 0.064 mmol) and Na_2CO_3 (135 mg, 1.28 mmol) and K_2CO_3 (265 mg, 1.92 mmol) for 20 hours, pyrazole **111** was isolated as a colourless solid (93 mg, 33%). The product could be further purified by recrystallization from ethyl acetate/40-60 petroleum ether.

M.p.: 56-58 °C; ^{1}H NMR (400 MHz, $CDCl_3$) δ 3.71 (6H, s), 3.85 (3H, s), 3.89 (3H, s), 5.35 (2H, s), 5.54 (1H, s), 6.48 (2H, s), 6.80 (1H, d, *J* = 8.5 Hz), 7.02 (1H, dd, *J* = 8.5, 2.0 Hz), 7.19 (1H, d, *J* = 2.0 Hz), 7.30-7.40 (5H, m), 7.41 (1H, s); ^{13}C NMR (101 MHz, $CDCl_3$) δ 56.1, 56.2, 56.3, 61.1, 105.9, 110.5, 115.0, 120.7, 121.0, 127.0, 128.1, 128.3, 129.0, 129.1, 136.5, 136.9, 145.5, 146.4, 148.5, 153.2 (one sp^2 carbon not observed); FTIR: ν_{max} 2935 (w), 1583 (m), 1455 (m), 1406 (m), 1234 (s), 1122 (s), 1001 (m); HRMS (ESI-TOF) *m/z* $[M+H]^+$ calculated for $C_{26}H_{27}N_2O_5$: 447.1914. Found: 447.1914.

4-(3-Hydroxy-4-methoxyphenyl)-5-(3,4,5-trimethoxyphenyl)-pyrazole, **83**:

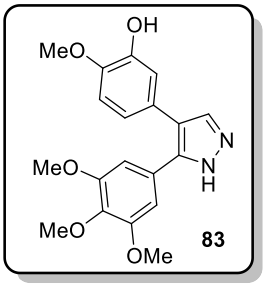

83

Following general procedure I using pyrazole **109** (79 mg, 0.18 mmol) and Pd/C (18 mg), pyrazole **83** was isolated as a colourless solid (18 mg, 29%).

See above for characterisation data.

4-(3,4,5-Trimethoxyphenyl)-5-(3-hydroxy-4-methoxyphenyl)-pyrazole, **85**:

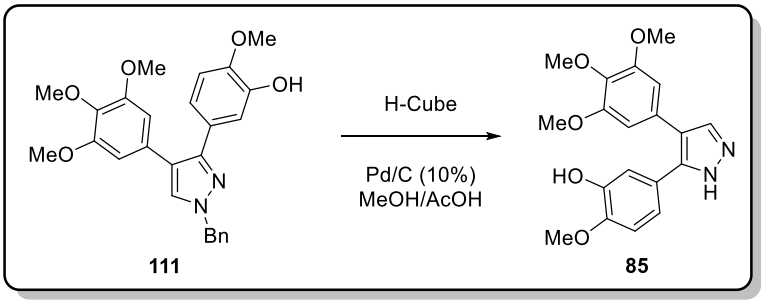

111 **85**

A solution of pyrazole **111** (274 mg, 0.614 mmol) in methanol (6 mL) and AcOH (6 drops) was flowed through a H-Cube continuous flow hydrogenator (1 mL min^{-1}) with a 10% Pd/C catalyst cartridge at 80 °C using controlled H_2 mode (80 bar) as a continuous loop. Once the reaction was complete by TLC analysis, the system was washed with methanol (10 mL). The reaction was subsequently neutralised with $NaHCO_3$ then filtered and the volatiles were removed *in vacuo*. Flash silica chromatography (gradient starting with 100% 40-60 petroleum ether and ending with 100% ethyl acetate in 40-60 petroleum ether) afforded pyrazole **85** as a colourless solid (144 mg, 66%).

See above for characterisation data.

4-(2-Pyridyl)-*N*-phenylsydnone, **128**:[103]

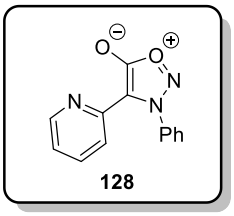

128

Following general procedure F using sydnone **36** (1.50 g, 9.25 mmol) and 2-bromopyridine (2.19 g, 13.9 mmol), 3,4-diarylsydnone **128** was isolated as colourless crystals (2.19 g, 99%).

M.p.: 111-112 °C (lit.[103] 142-143 °C); ^{1}H NMR (400 MHz, $CDCl_3$) δ 7.11 (1H, ddd, *J* = 7.5, 5.0, 1.0 Hz), 7.46-7.58 (4H, m), 7.60-7.66 (1H, m), 7.74 (1H, td, *J* = 8.0, 2.0 Hz), 8.09 (1H, dt, *J* = 8.0, 1.0 Hz), 8.23 (1H, ddd, *J* = 5.0, 2.0, 1.0 Hz); ^{13}C NMR (101 MHz, $CDCl_3$) δ 107.1, 121.8, 122.7, 125.1, 129.3, 131.6, 136.0, 136.8, 144.9, 149.1, 167.1.

Potassium(1-octyn-1-yl)triflouroborate, **129**:[189]

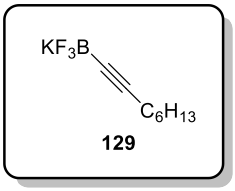

129

Following general procedure M using 1-octyne (13.5 g, 122 mmol), trimethylborate (19.0 g, 183 mmol) and potassium hydrogen difluoride (57.2 g, 732 mmol), **129** was isolated as a colourless solid (22.4 g, 85%).

M.p.: 246-250 °C (lit.[189] 275 °C dec.); ^{1}H NMR (400 MHz, DMSO-d_6) δ 1.92-2.01 (2H, m), 1.17-1.39 (8H, m), 0.86 (3H, t, *J* = 7.0 Hz); ^{13}C NMR (101 MHz, DMSO-d_6) δ 14.0, 18.9, 22.1, 28.1, 29.0, 31.0, 88.9, 93.1 (br); ^{19}F NMR (377 MHz, DMSO-d_6): δ -131.0; ^{11}B NMR (128 MHz, DMSO-d_6): δ -1.72.

1-Phenyl-3-*n*-hexyl-4-(dioctynylborane)-5-(2-pyridyl)pyrazole, **131**:

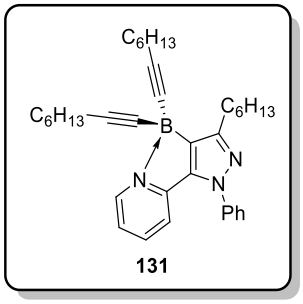

131

Following general procedure N using sydnone **128** (1.00 g, 4.18 mmol) and potassium(1-octyn-1-yl)triflouroborate (4.52 g, 20.9 mmol), pyrazole **131** was isolated as an amorphous orange solid (2.23 g, 100%).

^{1}H NMR (400 MHz, $CDCl_3$) δ 0.80-0.93 (9H, m), 1.17-1.38 (16H, m), 1.41-1.54 (6H, m), 1.94 (2H, quint, *J* = 7.5 Hz), 2.16 (4H, t, *J* = 7.0 Hz), 2.76-2.87 (2H, m), 7.28-7.35 (2H, m), 7.36-7.42 (1H, m), 7.45-7.54 (4H, m), 7.81 (1H, td, *J* = 8.0, 1.5 Hz), 8.74 (1H, d, *J* = 5.0 Hz); ^{13}C NMR (101 MHz, $CDCl_3$) δ 14.1, 14.3, 20.2, 22.7, 22.8, 28.8, 29.0, 29.2, 29.4, 29.6, 31.5, 31.9, 89.2 (b), 96.5, 117.2, 121.6, 124.7, 128.0, 129.5, 139.2 (b), 139.9, 141.3, 142.3, 145.6, 147.1, 155.5; ^{11}B NMR (128 MHz, $CDCl_3$) δ -11.4; FTIR: ν_{max} 3212 (w), 2927 (m), 2160 (w), 2030 (m), 1620 (s), 1499 (s), 1460 (s), 1123 (m), 982 (m), 769 (s), 754 (s); HRMS (ESI-TOF) *m/z* $[M+H]^+$ calculated for $C_{36}H_{49}{}^{11}BN_3$: 534.4020. Found: 534.4021.

4-(6-Methyl-2-pyridyl)-*N*-phenylsydnone, **132**:

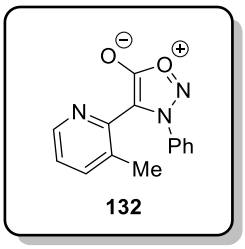

132

Following general procedure F using sydnone **36** (200 mg, 1.23 mmol) and 2-bromo-3-methylpyridine (318 mg, 1.85 mmol), 3,4-diarylsydnone **132** was isolated as tan crystals (244 mg, 78%).

M.p.: 122 °C; ^{1}H NMR (400 MHz, $CDCl_3$) δ 2.46 (3H, s), 7.15 (1H, dd, *J* = 8.0, 4.5 Hz), 7.37-7.41 (2H, m), 7.42-7.48 (2H, m), 7.51-7.62 (2H, m), 8.24 (1H, dt, *J* = 4.5, 1.5, 0.5 Hz); ^{13}C NMR (101 MHz, $CDCl_3$) δ 18.6, 107.7, 123.9, 124.2, 129.7, 131.7, 135.0, 135.1, 138.9, 143.8, 147.3 166.6; FTIR: ν_{max} 1740 (s), 1571 (m), 1458 (s), 1277 (s), 1017 (s); HRMS (ESI-TOF) *m/z* $[M+H]^+$ calculated for $C_{14}H_{12}N_3O_2$: 254.0930. Found: 254.0928.

4-(5-Methyl-2-pyridyl)-*N*-phenylsydnone, **133**:

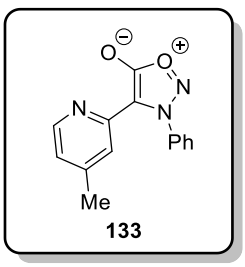

133

Following general procedure F using sydnone **36** (250 mg, 1.54 mmol) and 2-bromo-4-methylpyridine (398 mg, 2.31 mmol), 3,4-diarylsydnone **133** was isolated as colourless crystals (262 mg, 67%).

M.p.: 113-115 °C; ^{1}H NMR (400 MHz, $CDCl_3$) δ 2.36 (3H, s), 6.93 (1H, ddd, *J* = 5.0, 1.5, 0.5 Hz), 7.44-7.55 (4H, m), 7.57-7.65 (1H, m), 7.86-7.91 (1H, m), 8.07 (1H, d, *J* = 5.0 Hz); ^{13}C NMR (101 MHz, $CDCl_3$) δ 21.2, 107.2, 122.7, 123.8, 125.1, 129.3, 131.5, 136.1, 144.7, 148.2, 148.9, 167.1; FTIR: ν_{max} 1753 (s), 1598 (m), 1508 (m), 1384 (m), 1276 (m), 1213 (m), 1041 (m); HRMS (ESI-TOF) *m/z* $[M+H]^+$ calculated for $C_{14}H_{12}N_3O_2$: 254.0930. Found: 254.0922.

4-(4-Methyl-2-pyridyl)-*N*-phenylsydnone, **134**:

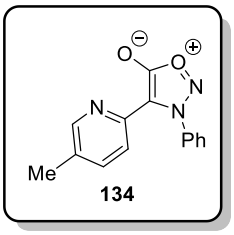

134

Following general procedure F using sydnone **36** (250 mg, 1.54 mmol) and 2-bromo-5-methylpyridine (398 mg, 2.31 mmol), 3,4-diarylsydnone **134** was isolated as an orange solid (254 mg, 65%).

M.p.: 131-132 °C; ^{1}H NMR (400 MHz, $CDCl_3$) δ 2.26 (3H, s), 7.43-7.56 (5H, m), 7.58-7.65 (1H, m), 7.94 (1H, d, *J* = 8.0 Hz), 8.07 (1H, dd, *J* = 1.5, 0.5 Hz); ^{13}C NMR (101 MHz, $CDCl_3$) δ 18.4, 107.3, 121.5, 125.1, 129.3, 131.5, 132.7, 136.0, 137.2, 142.2, 149.7, 167.1; FTIR: ν_{max} 1760 (s), 1741 (s), 1512 (m), 1274 (m), 1031 (m), 1016 (m); HRMS (ESI-TOF) *m/z* $[M+H]^+$ calculated for $C_{14}H_{12}N_3O_2$: 254.0930. Found: 254.0936.

4-(3-Methyl-2-pyridyl)-*N*-phenylsydnone, **135**:

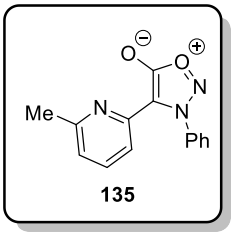

135

Following general procedure F using sydnone **36** (250 mg, 1.54 mmol) and 2-bromo-6-methylpyridine (398 mg, 2.31 mmol), 3,4-diarylsydnone **135** was isolated as colourless crystals (285 mg, 73%).

M.p.: 126 °C; ^{1}H NMR (400 MHz, $CDCl_3$) δ 2.06 (3H, s), 6.94 (1H, d, *J* = 7.5 Hz), 7.44-7.65 (6H, m), 7.89 (1H, d, *J* = 8.0 Hz); ^{13}C NMR (101 MHz, $CDCl_3$) δ 24.0, 107.3, 118.5, 122.2, 125.4, 129.0, 131.3, 136.4, 137.0, 144.0, 157.7, 167.0; FTIR: ν_{max} 1747 (s), 1573 (m), 1586 (m), 1283 (m), 1048 (m); HRMS (ESI-TOF) *m/z* $[M+H]^+$ calculated for $C_{14}H_{12}N_3O_2$: 254.0930. Found: 254.0921.

4-(5-Methoxy-2-pyridyl)-*N*-phenylsydnone, **136**:

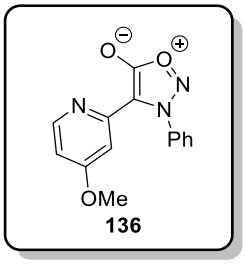

136

Following general procedure F using sydnone **36** (250 mg, 1.54 mmol) and 2-bromo-4-methoxypyridine (434 mg, 2.31 mmol), 3,4-diarylsydnone **136** was isolated as colourless crystals (259 mg, 63%).

M.p.: 124-126 °C; ^{1}H NMR (400 MHz, $CDCl_3$) δ 3.87 (3H, s), 6.63 (1H, dd, *J* = 5.5, 2.5 Hz), 7.44-7.57 (4H, m), 7.57-7.66 (2H, m), 8.02 (1H, d, *J* = 5.5 Hz); ^{13}C NMR (101 MHz, $CDCl_3$) δ 55.5, 107.02, 107.3, 109.7, 125.1, 129.3, 131.5, 136.1, 146.2, 150.2, 166.2, 167.1; FTIR: ν_{max} 1750 (s), 1588 (s), 1567 (m), 1306 (m), 1281 (m), 1019 (s); HRMS (ESI-TOF) *m/z* $[M+H]^+$ calculated for $C_{14}H_{12}N_3O_3$: 270.0879. Found: 270.0872.

4-(5-Trifluoromethyl-2-pyridyl)-*N*-phenylsydnone, **137**:

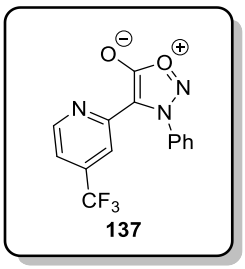

137

Following general procedure F using sydnone **36** (250 mg, 1.54 mmol) and 2-bromo-4-trifluoromethylpyridine (522 mg, 2.31 mmol), 3,4-diarylsydnone **137** was isolated as tan crystals (370 mg, 78%).

M.p.: 129-130 °C; ^{1}H NMR (400 MHz, $CDCl_3$) δ 7.29-7.33 (1H, m), 7.46-7.53 (2H, m), 7.53-7.61 (2H, m), 7.63-7.70 (1H, m), 8.35-8.39 (2H, m); ^{13}C NMR (101 MHz, $CDCl_3$) δ 106.0, 116.9 (dd, *J* = 7.0, 3.5 Hz), 117.9 (dd, *J* = 6.5, 3.0 Hz), 122.6 (q, *J* = 273.5 Hz), 125.2, 129.5, 131.9, 136.0,

139.3 (q, *J* = 34.5 Hz), 146.3, 149.9, 166.7; ^{19}F NMR (377 MHz, $CDCl_3$): δ -64.9; FTIR: ν_{max} 3071 (w), 1749 (s), 1606 (m), 1570 (m), 1506 (s), 1382 (m), 1165 (s), 1140 (s), 1038 (m); HRMS (ESI-TOF) *m/z* $[M+H]^+$ calculated for $C_{14}H_9N_3O_2F_3$: 308.0647. Found: 308.0654.

4-(4-Thiazolyl)-*N*-phenylsydnone, **138**:

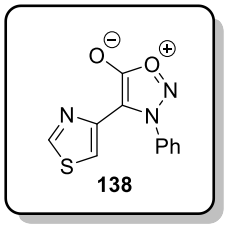

138

Following general procedure F using sydnone **36** (100 mg, 0.617 mmol) and 4-bromothiazole (152 mg, 0.925 mmol), 3,4-biarylsydnone **138** was isolated as orange needles (97 mg, 64%).

M.p.: 124-125 °C; ^{1}H NMR (400 MHz, $CDCl_3$) δ 7.50-7.62 (4H, m), 7.64-7.71 (1H, m), 8.09 (1H, d, *J* = 2.0 Hz), 8.61 (1H, d, *J* = 2.0 Hz); ^{13}C NMR (101 MHz, $CDCl_3$) δ 105.0, 117.3, 125.4, 129.5, 132.0, 135.4, 141.2, 153.2, 167.0; FTIR: ν_{max} 3064 (w), 1750 (s), 1555 (m), 1493 (w), 1251 (s), 1201 (m), 1017 (s), 767 (m); HRMS (ESI-TOF) *m/z* $[M+H]^+$ calculated for $C_{11}H_8N_3O_2S$: 246.0337. Found: 246.0332.

4-Carboxylic acid-*N*-phenylsydnone, **142**:[190]

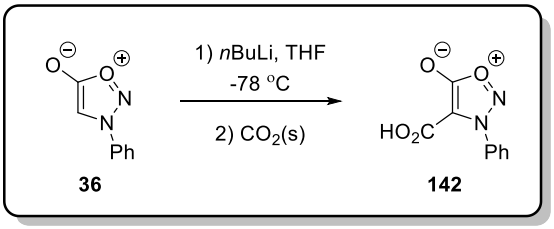

36 **142**

To a solution of *N*-phenylsydnone (3.55 g, 21.9 mmol) in THF (75 mL) at -78 °C was added a solution of *n*-butyl lithium (~2.17 M in hexanes) (11.1 mL, 24.1 mmol). The reaction mixture was stirred for 1 hour at -78 °C. The resulting solution was transferred by cannula to a flask containing excess solid CO_2 and stirred for 1 hour at -78 °C. The reaction was allowed to warm to room temperature (***caution extra venting required***) and stirred for a further 2 hours. The reaction was poured into water and the aqueous layer washed with ethyl acetate. The aqueous layer was then acidified to pH 1 and extracted with ethyl acetate. The combined organic layers were dried over $MgSO_4$, filtered and volatiles removed *in vacuo*, affording **142** as an orange solid product (4.11 g, 91%). The product could be further purified by recrystallization from ethanol.

M.p.: 190-191 °C (lit.[190] 193 °C); ^{1}H NMR (400 MHz, DMSO) δ 7.56-7.83 (5H, m), 13.37 (1H, s); ^{13}C NMR (101 MHz, $CDCl_3$) δ 100.7, 125.7, 129.2, 132.0, 135.3, 157.9, 164.5; FTIR: ν_{max} 2944 (br), 2558 (br), 2159 (br), 2031 (w), 1807 (s), 1674 (s), 1489 (s), 1308 (m), 1212 (s), 1063 (m), 1027 (m); HRMS (ESI-TOF) *m/z* $[M+H]^+$ calculated for $C_9H_7N_2O_4$: 207.0406. Found: 207.0413.

4-[(*N*-Methoxy-*N*-methyl)amide]-*N*-phenylsydnone, **143**:

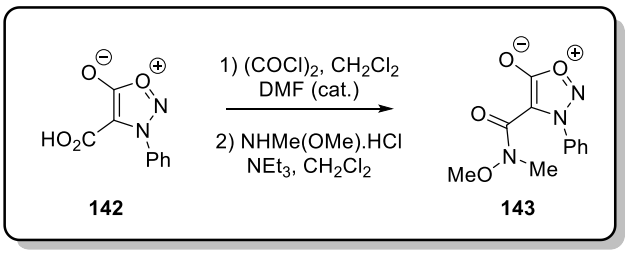

To a solution of sydnone **142** (500 mg, 2.43 mmol) in CH_2Cl_2 (10 mL) at 0 °C was added oxalyl chloride (924 mg, 7.28 mmol) and DMF (3 drops) and the mixture stirred for 10 minutes at 0 °C. The reaction was allowed to warm to room temperature and stirred for a further 3 hours. Volatiles were then removed *in vacuo* and the resulting yellow solid dissolved in CH_2Cl_2 (10 mL). Triethylamine (541 mg, 5.35 mmol) and *N*,*O*-dimethylhydroxylamine hydrogen chloride (284 mg, 2.92 mmol) were added at 0 °C and the reaction stirred for 14 hours at RT. The reaction was poured into water, extracted with CH_2Cl_2, the combined organic layers were dried over $MgSO_4$ and volatiles removed *in vacuo*. The resulting crude material was purified by flash silica chromatography (gradient 100% 40-60 petroleum ether to 60% ethyl acetate) affording **143** as a yellow oil (394 mg, 65%).

^{1}H NMR (400 MHz, $CDCl_3$) δ 3.28 (3H, s), 3.86 (3H, s), 7.50-7.61 (4H, m), 7.61-7.69 (1H, m); ^{13}C NMR (101 MHz, $CDCl_3$) δ 33.3, 62.2, 102.8, 124.0, 129.7, 132.3, 134.7, 157.3, 164.4; FTIR: ν_{max} 1765 (s), 1651 (m), 1480 (m), 1443 (w), 1269 (w), 1173 (w), 1051 (w), 990 (w); HRMS (ESI-TOF) *m/z* $[M+H]^+$ calculated for $C_{11}H_{11}N_3O_4$: 250.0822. Found: 250.0821.

4-[*N*-(2-Hydroxy-1,1-dimethylethyl)amide]-*N*-phenylsydnone, **144**:

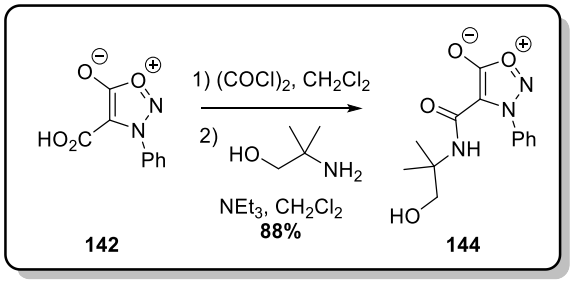

To a solution of sydnone **142** (825 mg, 4.00 mmol) in CH_2Cl_2 (40 mL) at 0 °C was added oxalyl chloride (1.52 g, 12.0 mmol) and DMF (3 drops) and the mixture stirred for 10 minutes at 0

°C. The reaction was allowed to warm to room temperature and stirred for a further 3 hours. Volatiles were then removed *in vacuo* and the resulting yellow solid dissolved in CH_2Cl_2 (40 mL). Triethylamine (486 mg, 4.80 mmol) and 2-amino-2-methylpropanol (428 mg, 4.80 mmol) were added at 0 °C and the reaction stirred for 14 hours at RT. The reaction was poured into water, extracted with CH_2Cl_2, the combined organic layers were dried over $MgSO_4$ and volatiles removed *in vacuo*. The resulting crude material was purified by flash silica chromatography (eluting solvent 100% ethyl acetate) affording **144** as a yellow solid (975 mg, 88%). The product could be further purified by recrystallisation from CH_2Cl_2/petrol.

M.p.: 184 °C; ^{1}H NMR (400 MHz, $CDCl_3$) δ 1.33 (6H, s), 3.59 (2H, s), 4.03 (1H), 7.42 – 7.86 (5H, m); ^{13}C NMR (101 MHz, $CDCl_3$) δ 24.7, 56.8, 70.2, 102.2, 125.3, 129.4, 132.5, 134.6, 155.9, 167.3; FTIR: ν_{max} 3318 (br), 1751 (s), 1675 (s), 1494 (w), 1303 (w), 1059 (w); HRMS (ESI-TOF) *m/z* $[M+H]^+$ calculated for $C_{13}H_{16}N_3O_4$: 278.1141. Found: 278.1148.

4-(4,4-Dimethyl-2-oxazoline)-*N*-phenylsydnone, **145**:

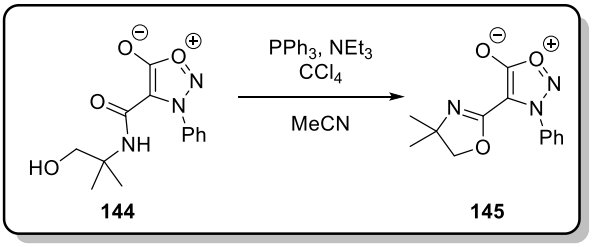

Triethylamine (5.28 g, 52.2 mmol) and carbon tetrachloride (12.3 g, 80.0 mmol) were added respectively to a suspension of **144** (964 mg, 3.48 mmol) and triphenylphosphine (3.65 g, 13.9 mmol) in acetonitrile (17 mL) at ambient temperature. The reaction was allowed to stir for 2 h before being diluted with ethyl acetate and washed with aqueous sodium hydrogen carbonate. The aqueous layer was extracted with ethyl acetate, the organics combined, dried over magnesium sulfate and the solvent removed *in vacuo*. The resulting residue was purified by flash silica chromatography (gradient 0 – 60% ethyl acetate in 40/60 petroleum ether) affording **145** as a yellow solid (475 mg, 53%).

M.p.: 131-133 °C; ^{1}H NMR (400 MHz, $CDCl_3$) δ 1.22 (6H, s), 3.87 (2H, s), 7.43 – 7.71 (5H, m); ^{13}C NMR (101 MHz, $CDCl_3$) δ 28.1, 68.2, 79.0, 98.8, 125.1, 129.5, 132.5, 135.0, 151.0, 165.5; FTIR: ν_{max} 1785 (s), 1754 (m), 1658 (m), 1485 (m); HRMS (ESI-TOF) *m/z* $[M+H]^+$ calculated for $C_{13}H_{14}N_3O_3$: 260.1035. Found: 260.1039.

4-[*N*-(3-Hydroxypropyl)amide]-*N*-phenylsydnone, **146**:

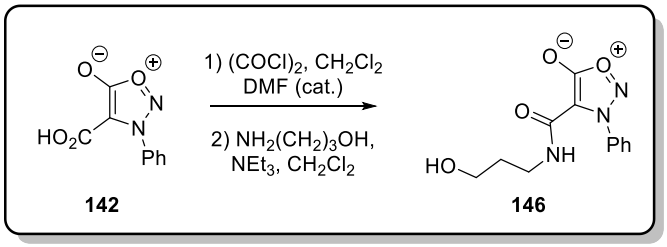

To a solution of sydnone **142** (2.00 g, 9.70 mmol) in CH_2Cl_2 (50 mL) at 0 °C was added oxalyl chloride (3.69 g, 29.1 mmol) and DMF (3 drops) and the mixture stirred for 10 minutes at 0 °C. The reaction was allowed to warm to room temperature and stirred for a further 3 hours. Volatiles were then removed *in vacuo* and the resulting yellow solid dissolved in CH_2Cl_2 (50 mL). Triethylamine (982 mg, 9.70 mmol) and 3-aminopropanol (874 mg, 11.6 mmol) were added at 0 °C and the reaction stirred for 14 hours at RT. The reaction was poured into water, extracted with CH_2Cl_2, the combined organic layers were dried over $MgSO_4$ and volatiles removed *in vacuo*. The resulting crude material was purified by flash silica chromatography (eluting solvent 100% ethyl acetate) affording **146** as a colourless solid (2.00 g, 78%). The product could be further purified by recrystallisation from CH_2Cl_2/petrol.

M.p.: 84-86 °C; ^{1}H NMR (400 MHz, $CDCl_3$) δ 1.74 (2H, td, *J* = 12.0, 6.0 Hz), 2.64 (1H, t, *J* = 6.0 Hz), 3.49 (2H, dd, *J* = 12.0, 6.0 Hz), 3.62 (2H, q, *J* = 6.0 Hz), 7.53-7.62 (4H, m), 7.68 (1H, ddt, *J* = 8.0, 6.5, 1.5 Hz), 7.75 (1H, s); ^{13}C NMR (101 MHz, $CDCl_3$) δ 32.3, 35.8, 59.5, 101.9, 125.3, 129.4, 132.5, 134.6, 156.4, 167.3; FTIR: ν_{max} 3449 (br), 3335 (m), 2930 (w), 1759 (s), 1653 (s), 1534 (s), 1493 (w), 1291 (m), 1215 (m), 956 (m); HRMS (ESI-TOF) *m/z* $[M+H]^+$ calculated for $C_{12}H_{14}N_3O_4$: 264.0984. Found: 264.0974.

4-[2-(5,6-dihydro-4*H*-1,3-oxazine)]-*N*-phenylsydnone, **147**:

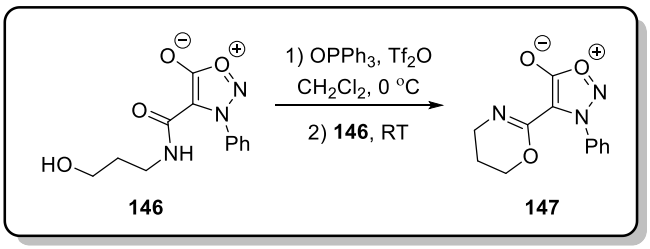

To a solution of triphenylphosphine oxide (1.90 g, 6.84 mmol) in CH_2Cl_2 (35 mL) at 0 °C was added triflic anhydride (804 mg, 2.85 mmol) and the reaction stirred for 30 minutes at 0 °C. A solution of sydnone **146** (500 mg, 1.90 mmol) in CH_2Cl_2 (15 mL) was slowly added at 0 °C and the reaction allowed to warm to room temperature and stirred for 14 hours. The reaction mixture was poured into water and the organic layer discarded. The aqueous layer was

basified with $NaHCO_3$ and extracted with ethyl acetate. The combined organic layers were dried over $MgSO_4$ and volatiles removed *in vacuo*. The crude material was purified by flash silica chromatography (eluting solvent 100% ethyl acetate) affording sydnone **147** as a colourless solid (243 mg, 52%).

M.p.: 97-101 °C; ^{1}H NMR (400 MHz, $CDCl_3$) δ 1.87 (2H, dt, *J* = 11.5, 6.0 Hz), 3.47 (2H, t, *J* = 6.0 Hz), 4.04-4.09 (2H, m), 7.47-7.73 (5H, m); ^{13}C NMR (101 MHz, $CDCl_3$) δ 21.8, 42.5, 65.5, 103.0, 124.7, 129.4, 131.9, 135.6, 146.6, 166.2; FTIR: ν_{max} 3061 (w), 2959 (w), 2856 (w), 1766 (s), 1754 (s), 1657 (s), 1635 (s), 1480 (s), 1437 (m), 1275 (s), 1140 (s), 1078 (s), 1024 (s); HRMS (ESI-TOF) *m/z* $[M+H]^+$ calculated for $C_{12}H_{12}N_3O_3$: 246.0879. Found: 246.0886.

4-[*N*-(3-Chloropropyl)amide]-*N*-phenylsydnone, **148**:

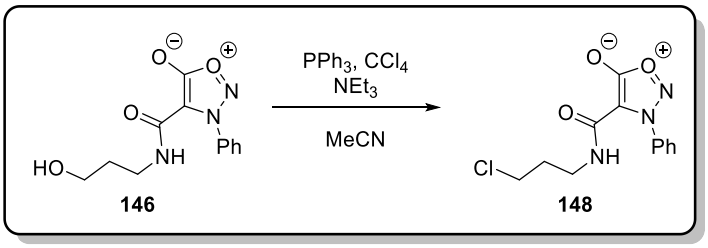

To a solution of amide **146** (200 mg, 0.760 mmol), triethylamine (1.15 g, 11.4 mmol) and carbon tetrachloride (2.63 g, 17.1 mmol) in acetonitrile (1 mL) was added triphenylphosphine (797 mg, 3.04 mmol) in acetonitrile (5 mL) and the reaction stirred for 14 h at room temperature. The reaction was poured into water and extracted with ethyl acetate, the combined organic layers dried over $MgSO_4$ and volatiles removed *in vacuo*. The crude residue was purified by flash silica chromatography (gradient 100% 40-60 petroleum ether to 40% ethyl acetate) affording sydnone **148** as a colourless solid (152 mg, 71%).

M.p.: 119-120 °C; ^{1}H NMR (400 MHz, $CDCl_3$) δ 2.02 (2H, quin, *J* = 6.5 Hz), 3.50 (2H, q, *J* = 6.5 Hz), 3.56 (2H, t, *J* = 6.5 Hz), 7.55-7.64 (4H, m), 7.66-7.72 (1H, m); ^{13}C NMR (101 MHz, $CDCl_3$) δ 32.2, 36.7, 42.2, 102.0, 125.3, 129.4, 132.6, 134.6, 155.7, 167.3; FTIR: ν_{max} 3336 (m), 3065 (w), 2959 (w), 1741 (s), 1665 (s), 1538 (s), 1466 (s), 1443 (s), 1282 (m), 1217 (m), 1070 (m), 1028 (m), 986 (m); HRMS (ESI-TOF) *m/z* $[M+H]^+$ calculated for $C_{12}H_{13}N_3O_3{}^{35}Cl$: 282.0645. Found: 282.0637.

1-Phenyl-3-*n*-hexyl-4-(dioctynylborane)-5-(6-methyl-2-pyridyl)pyrazole, **149**:

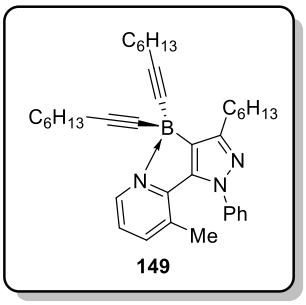

149

Following general procedure N using sydnone **132** (50 mg, 0.20 mmol) and potassium(1-octyn-1-yl)triflouroborate (213 mg, 0.987 mmol), pyrazole **149** was isolated as an amorphous orange solid (105 mg, 97%).

^{1}H NMR (400 MHz, $CDCl_3$) δ 0.83-0.91 (9H, m), 1.22-1.38 (16H, m), 1.42-1.52 (6H, m), 1.73 (3H, s), 1.95 (2H, dt, *J* = 15.5, 8.0 Hz), 2.17 (4H, dd, *J* = 7.5, 7.0 Hz), 2.77-2.86 (2H, m), 7.21-7.28 (1H, m), 7.39-7.50 (5H, m), 7.60 (1H, ddd, *J* = 7.5, 1.5, 0.5 Hz), 8.66 (1H, dd, *J* = 5.5, 0.5 Hz); ^{13}C NMR (101 MHz, $CDCl_3$) δ 14.1, 14.2, 20.1, 20.3, 22.6, 22.7, 28.7, 28.8, 29.2, 29.4, 29.6, 31.5, 31.9, 96.2, 121.3, 127.4, 128.5, 128.7, 129.0 142.4, 143.4, 143.9, 145.5, 147.0, 154.9; ^{11}B NMR (128 MHz, $CDCl_3$) δ -12.5; FTIR: ν_{max} 2955 (s), 2929 (s), 2856 (s), 2190 (w), 1605 (m), 1507 (s), 1470 (s), 1192 (m); HRMS (ESI-TOF) *m/z* $[M+H]^+$ calculated for $C_{37}H_{51}{}^{11}BN_3$: 548.4176. Found: 548.4186.

1-Phenyl-3-*n*-hexyl-4-(dioctynylborane)-5-(5-methyl-2-pyridyl)pyrazole, **150**:

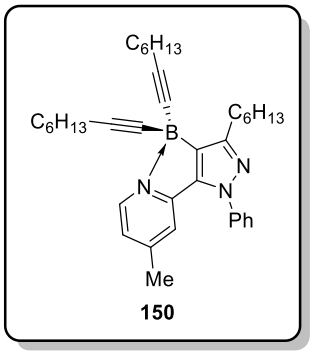

150

Following general procedure N using sydnone **133** (50 mg, 0.20 mmol) and potassium(1-octyn-1-yl)triflouroborate (213 mg, 0.987 mmol), pyrazole **150** was isolated as an amorphous orange solid (105 mg, 97%).

^{1}H NMR (400 MHz, $CDCl_3$) δ 0.82-0.93 (9H, m), 1.20-1.39 (16H, m), 1.42-1.52 (6H, m), 1.94 (2H, dt, *J* = 15.5, 7.5 Hz), 2.16 (4H, t, *J* = 7.0 Hz), 2.39 (3H, s), 2.78-2.85 (2H, m), 7.08-7.17 (2H, m), 7.37-7.44 (1H, m), 7.47-7.58 (4H, m), 8.59 (1H, d, *J* = 6.0 Hz); ^{13}C NMR (101 MHz, $CDCl_3$) δ 14.2, 14.3, 20.3, 22.1, 22.7, 22.9, 28.8, 29.1, 29.3, 29.5, 29.7, 31.6, 32.0, 89.8 (b), 96.3, 117.7,

122.7, 124.8, 128.0, 129.5, 139.4 (b), 140.1, 142.3, 144.9, 146.8, 154.0, 155.6; ^{11}B NMR (128 MHz, $CDCl_3$) δ -11.6; FTIR: ν_{max} 2956 (s), 2928 (s), 2856 (s), 2188 (w), 1632 (s), 1456 (m), 1121 (m), 1000 (m); HRMS (ESI-TOF) *m/z* $[M+H]^+$ calculated for $C_{37}H_{51}{}^{11}BN_3$: 548.4176. Found: 548.4186.

1-Phenyl-3-*n*-hexyl-4-(dioctynylborane)-5-(4-methyl-2-pyridyl)pyrazole, **151**:

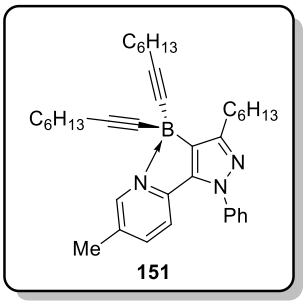

151

Following general procedure N using sydnone **134** (50 mg, 0.20 mmol) and potassium(1-octyn-1-yl)triflouroborate (213 mg, 0.987 mmol), pyrazole **151** was isolated as an amorphous orange solid (107 mg, 99%).

^{1}H NMR (400 MHz, $CDCl_3$) δ 0.83-0.91 (9H, m), 1.19-1.39 (16H, m), 1.41-1.53 (6H, m), 1.94 (2H, dt, *J* = 15.5, 7.5 Hz), 2.17 (4H, td, *J* = 7.0, 1.0 Hz), 2.42 (3H, s), 2.76-2.84 (2H, m), 7.23 (1H, d, *J* = 8.5 Hz), 7.35-7.41 (1H, m), 7.45-7.55 (4H, m), 7.59-7.65 (1H, m), 8.55-8.60 (1H, m); ^{13}C NMR (101 MHz, $CDCl_3$) δ 14.2, 14.3, 18.4, 20.2, 22.7, 22.8, 28.8, 29.0, 29.3, 29.4, 29.6, 31.5, 32.0, 89.5 (b), 96.4, 116.7, 124.6, 127.9, 129.4, 132.2, 138.4 (b), 140.0, 142.0, 142.4, 144.9, 145.4, 155.5; ^{11}B NMR (128 MHz, $CDCl_3$) δ -11.4; FTIR: ν_{max} 2955 (s), 2929 (s), 2857 (s), 2188 (w), 1750 (w), 1626 (s), 1598 (m), 1520 (s), 1497 (s), 1466 (s), 1172 (m), 1123 (m), 1063 (m), 987 (m); HRMS (ESI-TOF) *m/z* $[M+H]^+$ calculated for $C_{37}H_{51}{}^{11}BN_3$: 548.4176. Found: 548.4193.

1-Phenyl-3-*n*-hexyl-4-(dioctynylborane)-5-(3-methyl-2-pyridyl)pyrazole, **152**:

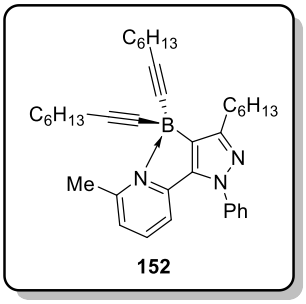

152

Following general procedure N using sydnone **135** (50 mg, 0.20 mmol) and potassium(1-octyn-1-yl)triflouroborate (213 mg, 0.987 mmol), pyrazole **152** was isolated as an amorphous orange solid (108 mg, 100%).

^{1}H NMR (400 MHz, $CDCl_3$) δ 0.81-0.93 (9H, m), 1.20-1.40 (16H, m), 1.42-1.52 (6H, m), 1.90-2.02 (2H, m), 2.14-2.23 (4H, m), 2.78-2.86 (2H, m), 3.18 (3H, s), 7.09 (1H, d, *J* = 7.5 Hz), 7.16 (1H, d, *J* = 7.5 Hz), 7.37-7.43 (1H, m), 7.46-7.56 (4H, m), 7.64-7.69 (1H, m); ^{13}C NMR (101 MHz, $CDCl_3$) δ 14.0, 14.2, 20.1, 21.5, 22.6, 22.7, 28.7, 29.0, 29.3, 29.5, 31.4, 31.8, 68.0, 87.3 (b), 96.8, 114.9, 123.6, 125.1, 128.2, 129.6, 138.1 (b), 139.5, 141.1, 142.4, 147.1, 154.8, 158.7; ^{11}B NMR (128 MHz, $CDCl_3$) δ -11.2; FTIR: ν_{max} 2955 (s), 2928 (s), 2856 (s), 2213 (w), 2188 (w), 1622 (s), 1598 (m), 1574 (m), 1514 (s), 1467 (s), 1365 (s), 1162 (m), 1122 (m), 1069 (m), 988 (m); HRMS (ESI-TOF) *m/z* $[M+H]^+$ calculated for $C_{37}H_{51}{}^{11}BN_3$: 548.4176. Found: 548.4171.

1-Phenyl-3-*n*-hexyl-4-(dioctynylborane)-5-(2-pyridyl-5-methoxy)pyrazole, **153**:

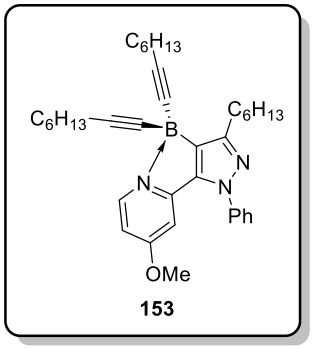

153

Following general procedure N using sydnone **136** (50 mg, 0.19 mmol) and potassium(1-octyn-1-yl)triflouroborate (201 mg, 0.928 mmol), pyrazole **153** was isolated as an amorphous yellow solid (105 mg, 100%).

^{1}H NMR (400 MHz, $CDCl_3$) δ 0.83-0.91 (9H, m), 1.21-1.38 (18H, m), 1.46 (4H, dd, *J* = 15.0, 7.5 Hz), 1.89-1.99 (2H, m), 2.16 (4H, t, *J* = 7.0 Hz), 2.75-2.88 (2H, m), 3.83 (3H, s), 6.69-6.84 (2H, m), 7.35-7.43 (1H, m), 7.46-7.61 (4H, m), 8.53 (1H, d, *J* = 6.5 Hz); ^{13}C NMR (101 MHz, $CDCl_3$) δ 14.1, 14.3, 20.2, 22.7, 22.8, 28.8, 29.0, 29.2, 29.5, 29.6, 31.5, 31.9, 56.3, 89.5 (br), 96.8, 102.8, 107.6, 124.6, 128.0, 129.4, 139.9, 142.1, 146.5, 148.5, 155.5, 169.2 (one sp^2 carbon not observed); ^{11}B NMR (128 MHz, $CDCl_3$): δ -12.6; FTIR: ν_{max} 2956 (m), 2926 (s), 2854 (m), 2186 (w), 1622 (s), 1510 (s), 1456 (s), 1249 (s), 1163 (m), 1054 (s); HRMS (ESI-TOF) *m/z* $[M+H]^+$ calculated for $C_{37}H_{51}{}^{11}BN_3O$: 564.4125. Found: 564.4128.

1-Phenyl-3-*n*-hexyl-4-(dioctynylborane)-5-(2-pyridyl-5-trifluoromethyl)pyrazole, **154**:

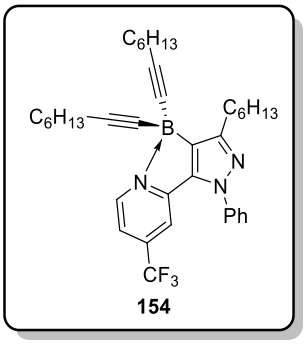

154

Following general procedure N using sydnone **137** (50 mg, 0.16 mmol) and potassium(1-octyn-1-yl)triflouroborate (176 mg, 0.814 mmol), pyrazole **154** was isolated as an amorphous yellow solid (83 mg, 85%).

^{1}H NMR (400 MHz, $CDCl_3$) δ 0.81-0.93 (9H, m), 1.21-1.37 (16H, m), 1.41-1.53 (6H, m), 1.93 (2H, dt, *J* = 15.5, 7.5 Hz), 2.13-2.20 (4H, m), 2.79-2.86 (2H, m), 7.41-7.60 (7H, m), 8.93 (1H, d, *J* = 6.0 Hz); ^{13}C NMR (101 MHz, $CDCl_3$) δ 14.1, 14.3, 20.1, 22.7, 22.8, 28.8, 28.9, 29.2, 29.3, 29.5, 31.5, 31.9, 88.0 (br), 97.2, 113.3 (d, *J* = 3.5 Hz), 117.6 (d, *J* = 3.0 Hz), 121.8 (q, *J* = 274.5 Hz), 124.5, 128.6, 129.7, 139.5, 140.9 (br), 141.4, 143.1 (q, *J* = 35.0 Hz), 147.0, 148.2, 155.8; ^{11}B NMR (128 MHz, $CDCl_3$): δ -11.2; ^{19}F NMR (377 MHz, $CDCl_3$): δ -65.4; FTIR: ν_{max} 2956 (m), 2930 (s), 2857 (m), 2189 (w), 1638 (m), 1507 (m), 1461 (s), 1301 (s), 1186 (m), 1153 (s); HRMS (ESI-TOF) *m/z* $[M+H]^+$ calculated for $C_{37}H_{48}{}^{11}BN_3F_3$: 601.3930. Found: 601.3920.

Attempted directed cycloaddition with sydnone **138**

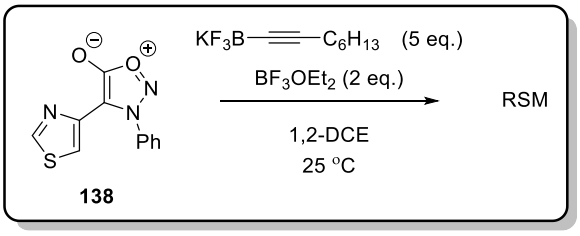

138

Following general procedure N using sydnone **138** (50 mg, 0.20 mmol) and potassium(1-octyn-1-yl)triflouroborate (220 mg, 1.02 mmol), resulted in the recovery of sydnone **138** and trace product formation.

Attempted directed cycloaddition with sydnone **143**

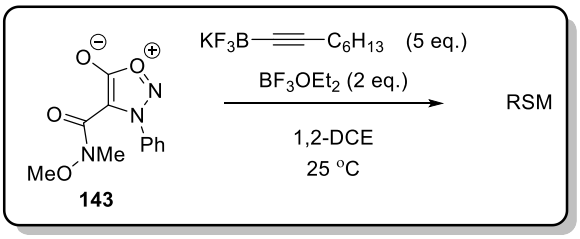

Following general procedure N using sydnone **143** (48 mg, 0.19 mmol) and potassium(1-octyn-1-yl)triflouroborate (209 mg, 0.967 mmol), resulted in the recovery of sydnone **143**.

1-Phenyl-3-*n*-hexyl-4-(boronic acid)-5-[4,4-dimethyl-2-oxazoline]pyrazole, **157**:

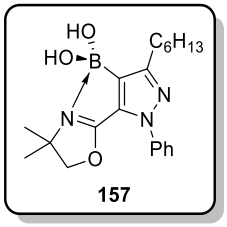

Following general procedure N using sydnone **145** (50 mg, 0.19 mmol) and potassium(1-octyn-1-yl)triflouroborate (208 mg, 0.964 mmol), pyrazole **157** was isolated as a yellow oil (2 mg, 3%).

^{1}H NMR (400 MHz, $CDCl_3$) δ 0.81-0.94 (3H, m), 1.25-1.42 (12H, m), 1.65-1.76 (2H, m), 2.90-3.00 (2H, m), 3.87 (2H, s), 7.31-7.47 (5H, m); ^{13}C NMR (101 MHz, $CDCl_3$) δ 14.2, 22.8, 28.1, 28.8, 29.5, 30.6, 31.8, 66.8, 79.7, 125.7, 128.4, 128.7, 135.5, 141.2, 158.1, 161.8 (one sp^2 carbon not observed); ^{11}B NMR (128 MHz, $CDCl_3$) δ 29.1; FTIR: ν_{max} 3355 (br), 2955 (s), 2927 (s), 2856 (s), 1642 (m), 1532 (m), 1501 (s), 1460 (s), 1432 (s), 1400 (s), 1379 (s), 1353 (m), 1036 (m); HRMS (ESI-TOF) *m/z* $[M+H]^+$ calculated for $C_{20}H_{29}{}^{11}BN_3O_3$: 370.2302. Found: 370.2285.

1-Phenyl-3-*n*-hexyl-4-(dioctynylborane)-5-(2-[5,6-dihydro-4*H*-1,3-oxazine]))pyrazole, **158**:

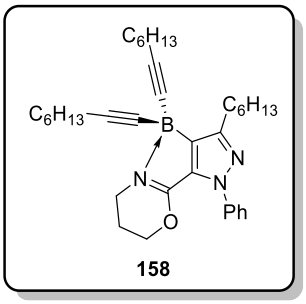

Following general procedure N using sydnone **147** (50 mg, 0.20 mmol) and potassium(1-octyn-1-yl)triflouroborate (220 mg, 1.02 mmol), pyrazole **158** was isolated as an orange oil (103 mg, 94%).

^{1}H NMR (400 MHz, $CDCl_3$) δ 0.83-0.92 (9H, m), 1.22-1.54 (22H, m), 1.89 (2H, dt, *J* = 15.5, 7.5 Hz), 2.13-2.29 (6H, t), 2.71-2.83 (2H, m), 3.80 (2H, t, *J* = 6.0 Hz), 4.48 (2H, t, *J* = 5.5 Hz), 7.29 (1H, dt, *J* = 3.5, 1.5 Hz), 7.36-7.42 (2H, m), 7.52-7.58 (2H, m); ^{13}C NMR (101 MHz, $CDCl_3$) δ 14.2, 14.3, 20.3, 20.6, 22.7, 22.8, 23.9, 28.9, 29.3, 29.5, 29.6, 31.6, 32.0, 38.6, 67.9, 87.6 (b), 96.6, 123.0, 126.9, 128.9, 136.8, 139.5, 144.2 (b), 155.1, 158.3; ^{11}B NMR (128 MHz, $CDCl_3$) δ -14.2; FTIR: ν_{max} 2925 (s), 2855 (s), 1614 (s), 1527 (m), 1499 (s), 1456 (m), 1258 (s), 1120 (m), 969 (m); HRMS (ESI-TOF) *m/z* $[M+H]^+$ calculated for $C_{35}H_{51}{}^{11}BN_3O$: 540.4111. Found: 540.4125.

4-(2-Pyridyl)-*N*-(4-methoxyphenyl)sydnone, **163**:

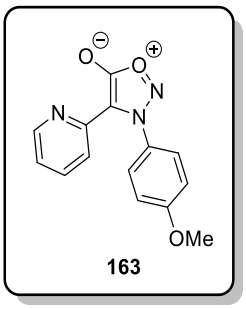

163

Following general procedure F using sydnone **25** (250 mg, 1.30 mmol) and 2-bromopyridine (313 mg, 1.95 mmol), 3,4-diarylsydnone **163** was isolated as a colourless solid (346 mg, 99%).

M.p.: 107-108 °C; ^{1}H NMR (400 MHz, $CDCl_3$) δ 3.90 (3H, s), 7.01 (2H, d, *J* = 9.0 Hz), 7.12 (1H, ddd, *J* = 7.5, 5.0, 1.0 Hz), 7.43 (2H, d, *J* = 9.0 Hz), 7.73 (1H, td, *J* = 8.0, 2.0 Hz), 8.06 (1H, dt, *J* = 8.0, 1.0 Hz), 8.29 (1H, ddd, *J* = 5.0, 2.0, 1.0 Hz); ^{13}C NMR (101 MHz, $CDCl_3$) δ 55.8, 106.9, 114.4, 122.0, 122.6, 126.5, 128.7, 136.8, 145.1, 149.2, 161.8, 167.2; FTIR: ν_{max} 2843 (w), 2035 (w), 1740 (s), 1582 (m), 1496 (s), 1176 (s), 1010 (s), 781 (s); HRMS (ESI-TOF) *m/z* $[M+H]^+$ calculated for $C_{14}H_{12}N_3O_3$: 270.0879. Found: 270.0876.

4-(2-Pyridyl)-*N*-(4-fluorophenyl)sydnone, **164**:

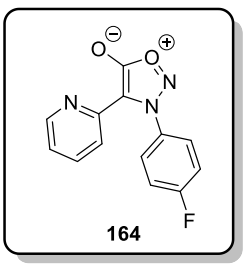

164

Following general procedure F using sydnone **38** (250 mg, 1.39 mmol) and 2-bromopyridine (329 mg, 2.08 mmol), 3,4-diarylsydnone **164** was isolated as colourless needles (350 mg, 98%).

M.p.: 108-109 °C; ^{1}H NMR (400 MHz, $CDCl_3$) δ 7.13 (1H, ddd, *J* = 7.5, 5.0, 1.0 Hz), 7.20-7.25 (2H, m), 7.48-7.55 (2H, m), 7.75 (1H, td, *J* = 8.0, 2.0 Hz), 8.12 (1H, dt, *J* = 8.0, 1.0 Hz), 8.24 (1H, ddd, *J* = 5.0, 2.0, 1.0 Hz); ^{13}C NMR (101 MHz, $CDCl_3$) δ 107.2, 116.5 (d, *J* = 23.5 Hz), 121.8, 122.8, 127.5 (d, *J* = 9.0 Hz), 132.1, 136.9, 144.8, 149.1, 164.1 (d, *J* = 253 Hz), 166.9; FTIR: ν_{max} 2159 (w), 2035 (w), 1717 (m), 1498 (m), 1276 (m), 1228 (m), 1014 (m); HRMS (ESI-TOF) *m/z* $[M+H]^+$ calculated for $C_{13}H_9FN_3O_2$: 258.0679. Found: 258.0688.

4-(2-Pyridyl)-*N*-(methyl)sydnone, **165**:

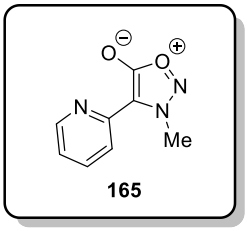

165

Following general procedure F using sydnone **40** (250 mg, 2.50 mmol) and 2-bromopyridine (592 mg, 3.75 mmol), sydnone **165** was isolated as a colourless solid (264 mg, 60%).

M.p.: 118-119 °C; ^{1}H NMR (400 MHz, $CDCl_3$) δ 4.54 (3H, s), 7.19 (1H, ddd, *J* = 7.5, 5.0, 1.0 Hz), 7.71-7.78 (1H, m), 8.19 (1H, td, *J* = 8.0, 1.0 Hz), 8.56 (1H, ddd, *J* = 5.0, 2.0, 1.0 Hz); ^{13}C NMR (101 MHz, $CDCl_3$) δ 42.2, 105.9, 120.7, 122.3, 137.0, 146.1, 149.0, 167.0; FTIR: ν_{max} 1733 (s), 1326 (m), 1166 (w), 1087 (w); HRMS (ESI-TOF) *m/z* $[M+H]^+$ calculated for $C_8H_8N_3O_2$: 178.0617. Found: 178.0624.

4-(2-Pyridyl)-*N*-(benzyl)sydnone, **166**:

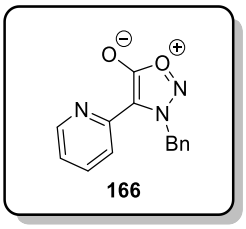

166

Following general procedure F using sydnone **44** (1.00 g, 5.68 mmol) and 2-bromopyridine (1.35 g, 8.51 mmol), sydnone **166** was isolated as orange crystals (164 mg, 11%).

M.p.: 108 °C; ^{1}H NMR (400 MHz, $CDCl_3$) δ 6.32 (2H, s), 7.19 (1H, ddd, *J* = 7.5, 5.0, 1.0 Hz), 7.29-7.36 (3H, m), 7.38-7.45 (2H, m), 7.73 (1H, td, *J* = 8.0, 2.0 Hz), 8.18 (1H, dd, *J* = 8.0, 1.0 Hz), 8.60 (1H, dd, *J* = 4.0, 1.0 Hz); ^{13}C NMR (101 MHz, $CDCl_3$) δ 56.9, 104.9, 120.8, 122.4, 128.7, 128.9, 129.2, 132.4, 137.0, 145.6, 148.7, 167.1; FTIR: ν_{max} 3025 (w), 2062 (w), 1738 (s), 1585 (m), 1510 (m), 1010 (s), 785 (s); HRMS (ESI-TOF) *m/z* $[M+H]^+$ calculated for $C_{14}H_{12}N_3O_2$: 254.0930. Found: 254.0924.

1-(4-Methoxyphenyl)-3-*n*-hexyl-4-(dioctynylborane)-5-(2-pyridyl)pyrazole, **167**:

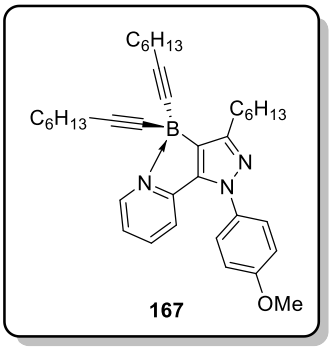

167

Following general procedure N using sydnone **163** (50 mg, 0.19 mmol) and potassium(1-octyn-1-yl)triflouroborate (201 mg, 0.928 mmol), pyrazole **167** was isolated as an amorphous orange solid (104 mg, 99%).

^{1}H NMR (400 MHz, $CDCl_3$) δ 0.80-0.95 (9H, m), 1.20-1.37 (16H, m), 1.42-1.52 (6H, m), 1.87-1.99 (2H, m), 2.16 (4H, t, *J* = 7.0 Hz), 2.72-2.88 (2H, m), 3.86 (3H, s), 7.00 (2H, d, *J* = 9.0 Hz), 7.22 (1H, dt, *J* = 8.0, 1 Hz), 7.30 (1H, ddd, *J* = 7.5, 5.5, 1.0 Hz), 7.43 (2H, d, *J* = 9.0 Hz), 7.80 (1H, ddd, *J* = 9.0, 8.0, 1.5 Hz), 8.72-8.75 (1H, m); ^{13}C NMR (101 MHz, $CDCl_3$) δ 14.2, 14.3, 20.2, 22.7, 22.8, 28.8, 29.0, 29.3, 29.4, 29.6, 31.5, 32.0, 55.7, 89.2 (b), 96.5, 114.6, 117.0, 121.5, 126.3, 133.0, 138.3 (b), 141.3, 142.6, 145.6, 147.2, 155.1, 159.4; ^{11}B NMR (128 MHz, $CDCl_3$) δ -11.5; FTIR: ν_{max} 2956 (s), 2928 (s), 2856 (s), 2190 (w), 1620 (s), 1524 (s), 1499 (s), 1456 (s), 1249 (s), 1123 (m), 1106 (m), 984 (m); HRMS (ESI-TOF) *m/z* $[M+H]^+$ calculated for $C_{37}H_{51}{}^{11}BN_3O$: 564.4125. Found: 564.4100.

1-(4-Fluorophenyl)-3-*n*-hexyl-4-(dioctynylborane)-5-(2-pyridyl)pyrazole, **168**:

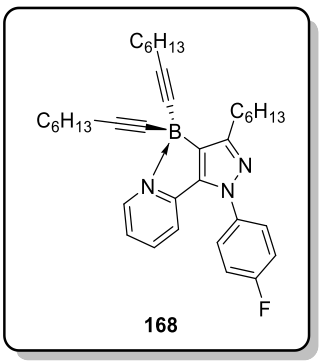

168

Following general procedure N using sydnone **164** (50 mg, 0.19 mmol) and potassium(1-octyn-1-yl)triflouroborate (210 mg, 0.972 mmol), pyrazole **168** was isolated as an amorphous orange solid (91 mg, 85%).

^{1}H NMR (400 MHz, $CDCl_3$) δ 0.81-0.94 (9H, m), 1.22-1.38 (16H, m), 1.43-1.51 (6H, m), 1.93 (2H, dt, *J* = 16.0, 8.0 Hz), 2.17 (4H, t, *J* = 7.0 Hz), 2.73-2.84 (2H, m), 7.16-7.25 (3H, m), 7.35

(1H, ddd, *J* = 7.5, 5.5, 1.0 Hz), 7.49-7.55 (2H, m), 7.85 (1H, ddd, *J* = 8.0, 7.5, 1.5 Hz), 8.77 (1H, ddd, *J* = 5.5, 1.5, 1.0 Hz); ^{13}C NMR (101 MHz, $CDCl_3$) δ 14.2, 14.3, 20.2, 22.7, 22.8, 28.8, 29.0, 29.2, 29.5, 29.6, 31.5, 32.0, 89.1 (b), 96.6, 116.4 (d, *J* = 23.0 Hz), 116.9, 121.7, 126.7 (d, *J* = 8.5 Hz), 136.1 (d, *J* = 3.0 Hz), 139.2 (b), 141.4, 142.5, 145.8, 146.9, 155.7, 162.1 (d, *J* = 248.0 Hz); ^{19}F NMR (377 MHz, $CDCl_3$) δ -113.1; ^{11}B NMR (128 MHz, $CDCl_3$) δ -11.2; FTIR: ν_{max} 2956 (s), 2929 (s), 2856 (s), 2187 (w), 1621 (m), 1524 (s), 1501 (s), 1467 (m), 1455 (m), 1224 (m), 1123 (m), 985 (m); HRMS (ESI-TOF) *m/z* $[M+H]^+$ calculated for $C_{36}H_{48}{}^{11}BN_3F$: 552.3925. Found: 552.3909.

1-(Methyl)-3-*n*-hexyl-4-(dioctynylborane)-5-(2-pyridyl)pyrazole, **169**:

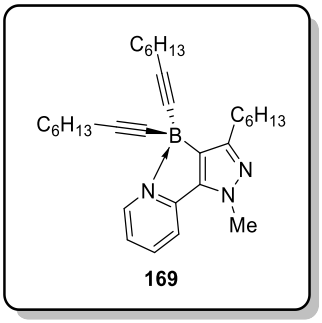

169

Following general procedure N using sydnone **165** (46 mg, 0.26 mmol) and potassium(1-octyn-1-yl)triflouroborate (305 mg, 1.41 mmol), pyrazole **169** was isolated as an colourless oil (93 mg, 76%).

^{1}H NMR (400 MHz, $CDCl_3$) δ 0.79-0.89 (9H, m), 1.17-1.35 (16H, m),), 1.37-1.49 (6H, m), 1.85 (2H, dt, *J* = 15.5, 7.5 Hz), 2.08-2.16 (4H, m), 2.66-2.74 (2H, m), 3.97 (3H, s), 7.29 (1H, ddd, *J* = 7.5, 5.5, 1.0 Hz), 7.48 (1H, dt, *J* = 8.0, 1.0 Hz), 7.91 (1H, td, *J* = 8.0, 1.0 Hz), 8.67-8.74 (1H, m); ^{13}C NMR (101 MHz, $CDCl_3$) δ 14.1, 14.3, 20.1, 22.6, 22.8, 28.7, 28.9, 29.4, 29.5, 31.5, 31.9, 37.4, 60.4, 89.2 (b), 96.3, 116.4, 121.2, 137.2 (b), 141.5, 142.9, 145.7, 146.9, 153.2; ^{11}B NMR (128 MHz, $CDCl_3$) δ -11.4; FTIR: ν_{max} 2957 (s), 2927 (s), 2856 (s), 2215 (w), 1623 (s), 1498 (m), 1461 (s), 1123 (m); HRMS (ESI-TOF) *m/z* $[M+H]^+$ calculated for $C_{31}H_{47}{}^{11}BN_3$: 472.3863. Found: 472.3861.

1-(Benzyl)-3-*n*-hexyl-4-(dioctynylborane)-5-(2-pyridyl)pyrazole, **170**:

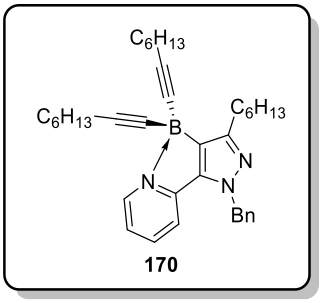

170

Following general procedure N using sydnone **166** (50 mg, 0.20 mmol) and potassium(1-octyn-1-yl)triflouroborate (213 mg, 0.987 mmol), pyrazole **170** was isolated as an colourless solid (76 mg, 70%).

M.p.: 88 °C; ^{1}H NMR (400 MHz, $CDCl_3$) δ 0.79-0.96 (9H, m), 1.10-1.53 (22H, m), 1.92 (2H, dt, *J* = 15.5, 7.5 Hz), 2.11-2.18 (4H, m), 2.74-2.82 (2H, m), 5.53 (2H, s), 7.15-7.21 (3H, m), 7.27-7.35 (4H, m), 7.81 (1H, td, *J* = 8.0, 1.5 Hz), 8.70 (1H, ddd, *J* = 5.5, 1.5, 1.0 Hz); ^{13}C NMR (101 MHz, $CDCl_3$) δ 14.1, 14.3, 20.2, 22.7, 22.8, 28.8, 29.0, 29.3, 29.4, 29.5, 31.5, 31.9, 54.4, 89.4 (b), 96.3, 116.7, 121.2, 126.6, 127.9, 129.0, 137.0, 138.4, 141.4, 142.8, 145.6, 146.8, 153.7; ^{11}B NMR (128 MHz, $CDCl_3$) δ -11.4; FTIR: ν_{max} 2957 (s), 2929 (s), 2857 (s), 2187 (w), 1623 (s), 1495 (s), 1456 (s), 1118 (m), 955 (w); HRMS (ESI-TOF) *m/z* $[M+H]^+$ calculated for $C_{37}H_{51}{}^{11}BN_3$: 548.4176. Found: 548.4189.

Potassium (phenylethynyl)triflouroborate:[191]

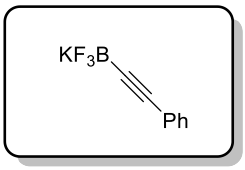

Following general procedure M using phenylacetylene (10.0 g, 97.9 mmol), trimethylborate (15.3 g, 147 mmol) and potassium hydrogen difluoride (45.9 g, 587 mmol), potassium (phenylethynyl)triflouroborate was isolated as a colourless solid (12.5 g, 61%).

M.p.: 253 °C (lit.[191] 256 °C dec.); ^{1}H NMR (400 MHz, DMSO-d_6) δ 7.21-7.35 (5H, m); ^{13}C NMR (101 MHz, DMSO-d_6) δ 89.4, 104.0 (br), 125.5, 126.9, 128.3, 131.0; ^{19}F NMR (377 MHz, DMSO-d_6): δ -131.7; ^{11}B NMR (128 MHz, DMSO-d_6): δ -1.47 (br q, *J* = 31.5 Hz).

Potassium ethynyltriflouroborate:[192]

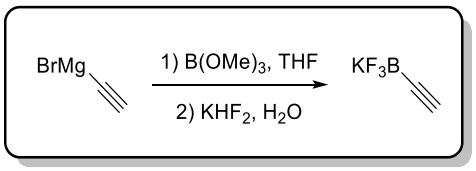

To a solution of ethynyl magnesium bromide in THF (0.5 M, 100 mL, 50 mmol) at -78 °C was added trimethylborate (7.8 g, 75 mmol) and the reaction stirred for 1 h at -78 °C. The reaction was allowed to warm to -20 °C and stirred for a further hour. A solution of potassium hydrogen difluoride (23.4 g, 300 mmol) in water (75 mL) was added at -20 °C and the mixture allowed to warm to ambient temperature and stirred for a further 2 h. Volatiles were removed *in vacuo* and the resulting solid was triturated in boiling acetone and volatiles removed *in vacuo*. The resulting solid was dissolved in minimum boiling acetone, allowed to cool to ambient temperature and product precipitated with diethyl ether. The resulting colourless solid was isolated by filtration affording potassium ethynyltriflouroborate (3.43 g, 52%).

M.p.: 212-214 °C (lit.[192] 211-212 °C dec.); ^{1}H NMR (400 MHz, DMSO-d_6) δ 3.33 (1H, s); ^{13}C NMR (101 MHz, DMSO-d_6) δ 79.0, 98.0 (br); ^{19}F NMR (377 MHz, DMSO-d_6): δ -132.4 (m); ^{11}B NMR (128 MHz, DMSO-d_6): δ -2.14 (br q, J = 36.5 Hz).

1-Phenyl-3-phenyl-4-(diphenylacetyleneborane)-5-(2-pyridyl)pyrazole, **171**:

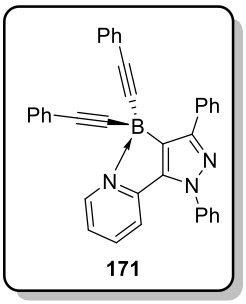

171

Following general procedure N using sydnone **128** (50 mg, 0.21 mmol) and potassium(1-phenylethyn-2-yl)triflouroborate (218 mg, 1.05 mmol), pyrazole **171** was isolated as a tan solid (107 mg, 100%).

M.p.: 246-248 °C (dec.); ^{1}H NMR (400 MHz, $CDCl_3$) δ 7.15-7.23 (6H, m), 7.29-7.54 (10H, m), 7.59 (2H, t, J = 8.5 Hz), 7.65-7.72 (2H, m), 7.90-7.99 (1H, m), 8.39 (2H, dd, J = 8.0, 1.0 Hz), 8.96-9.05 (1H, m); ^{13}C NMR (101 MHz, $CDCl_3$) δ 96.5, 98.8 (b), 117.5, 122.3, 125.0, 125.1, 127.1, 127.3, 127.9, 128.0, 128.6, 128.7, 129.7, 131.9, 133.8, 137.1 (b), 139.8, 142.0, 143.5, 145.9, 146.9, 152.9; ^{11}B NMR (128 MHz, $CDCl_3$) δ -10.0; FTIR: ν_{max} 3216 (s), 2262 (w), 2178

(w), 1623 (m), 1597 (m), 1488 (s), 1441 (s), 1195 (m), 986 (m), 919 (m); HRMS (ESI-TOF) *m/z* $[M+H]^+$ calculated for $C_{36}H_{25}{}^{11}BN_3$: 510.2142. Found: 510.2166.

1-Phenyl-4-(diethynylborane)-5-(2-pyridyl)pyrazole, **172**:

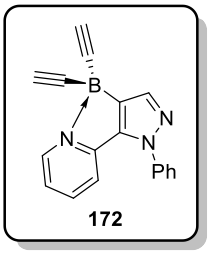

172

Following general procedure N using sydnone **128** (50 mg, 0.21 mmol) and potassium(ethynyl)triflouroborate (138 mg, 1.05 mmol), pyrazole **172** was isolated as an colourless solid (46 mg, 78%).

M.p.: 240 °C; ^{1}H NMR (400 MHz, $CDCl_3$) δ 2.25 (2H, s), 7.39 (1H, d, *J* = 8.0 Hz), 7.42-7.52 (2H, m), 7.56 (4H, d, *J* = 4.5 Hz), 7.84 (1H, s), 7.94 (1H, td, *J* = 8.0, 1.5 Hz), 8.81 (1H, d, *J* = 6.0 Hz); ^{13}C NMR (101 MHz, $CDCl_3$) δ 83.8, 93.9 (b), 117.5, 122.5, 124.8, 128.8, 129.7, 138.8 (b), 139.5, 140.8, 142.4, 145.7, 147.0; 11B NMR (128 MHz, $CDCl_3$) δ -12.5; FTIR: ν_{max} 3285 (w), 2160 (w), 1977 (w), 1619 (m), 1503 (m), 1488 (m), 979 (s), 771 (s); HRMS (ESI-TOF) *m/z* $[M+H]^+$ calculated for $C_{18}H_{13}{}^{11}BN_3$: 282.1203. Found: 282.1207.

1-Phenyl-4-(diethynylborane)-5-(2-pyridyl)pyrazole, **172**:

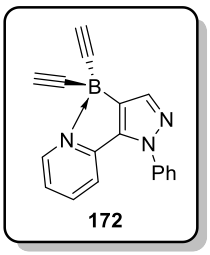

172

Following general procedure N using sydnone **128** (50 mg, 0.21 mmol) and potassium(ethynyl)triflouroborate (276 mg, 2.09 mmol), pyrazole **172** was isolated as an colourless solid (52 mg, 89%).

See above for characterisation data.

1-Phenyl-3-*n*-hexyl--5-(2-pyridyl)pyrazole, **174**:

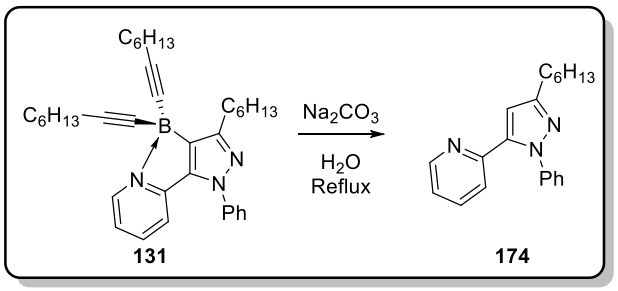

131 174

A flask was charged with pyrazole **131** (100 mg, 0.188 mmol), sodium carbonate (24 mg, 0.22 mmol) and water (2 mL) and heated at reflux for 2 hours. The mixture was allowed to cool to ambient temperature and extracted with ethyl acetate. The combined organic layers were dried over $MgSO_4$, filtered and the volatiles removed *in vacuo*. The crude residue was purified by flash silica chromatography (gradient starting with 100% 40-60 petroleum ether and ending with 20% ethyl acetate in 40-60 petroleum ether) affording pyrazole **171** as a yellow oil (52 mg, 91%).

^{1}H NMR (400 MHz, $CDCl_3$) δ 0.86 (3H, t, *J* = 7.0 Hz), 1.25-1.34 (4H, m), 1.35-1.44 (2H, m), 1.70 (2H, dt, *J* = 15.5, 7.5 Hz), 2.65-2.74 (2H, m), 6.60 (1H, s), 7.07 (1H, d, *J* = 8.0 Hz), 7.15 (1H, ddd, *J* = 7.5, 5.0, 1.0 Hz), 7.22-7.34 (5H, m), 7.53 (1H, td, *J* = 8.0, 2.0 Hz), 8.55 (1H, ddd, *J* = 5.0, 2.0, 1.0 Hz); ^{13}C NMR (101 MHz, $CDCl_3$) δ 14.2, 22.7, 28.4, 29.3, 29.7, 31.8, 107.9, 122.6, 123.6, 125.3, 127.4, 129.0, 136.2, 140.5, 142.9, 149.8, 149.9, 154.5; FTIR: ν_{max} 2960 (m), 2931 (m), 2853 (w), 1599 (m), 1588 (m), 1504 (s), 1380 (m); HRMS (ESI-TOF) *m/z* $[M+H]^+$ calculated for $C_{20}H_{24}N_3$: 306.1970. Found: 306.1973.

1-Phenyl-3-*n*-hexyl-4-(hydroxyl)-5-(2-pyridyl)pyrazole, **175**:

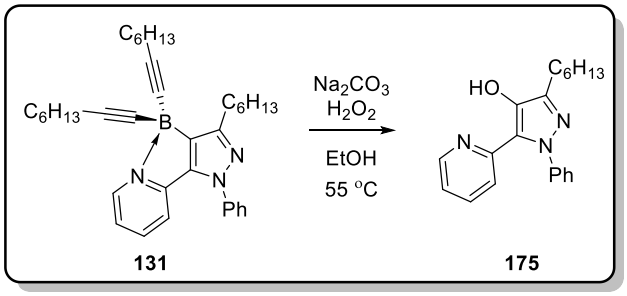

131 175

A flask was charged with pyrazole **131** (50 mg, 0.094 mmol), sodium carbonate (10 mg, 0.094 mmol), 30% hydrogen peroxide in water (0.1 ml, 0.9 mmol) and ethanol (1 mL) and heated to 55 °C for 14 hours. ***Caution: use of a blast shield is advised.*** The mixture was allowed to cool to ambient temperature and neutralised with 1 M HCl, followed by extraction with ethyl acetate. The combined organic layers were dried over $MgSO_4$, filtered and volatiles removed *in vacuo*. The crude residue was purified by flash silica chromatography (gradient starting with 100% 40-60 petroleum ether and ending with 20% ethyl acetate in 40-60 petroleum ether) affording pyrazole **175** as a yellow oil (25 mg, 83%).

^{1}H NMR (400 MHz, $CDCl_3$) δ 0.85-0.93 (3H, m), 1.27-1.36 (4H, m), 1.39-1.51 (2H, m), 1.73-1.83 (2H, m), 2.71-2.78 (2H, m), 6.70 (1H, dt, *J* = 8.5, 1.0 Hz), 7.09 (1H, ddd, *J* = 7.5, 5.0, 1.0 Hz), 7.34-7.54 (6H, m), 8.52 (1H, ddd, *J* = 5.0, 2.0, 1.0 Hz), 10.52 (1H, br); ^{13}C NMR (101 MHz, $CDCl_3$) δ 14.3, 22.8, 25.7, 28.6, 29.4, 31.8, 119.6, 121.0, 122.5, 126.1, 128.1, 129.5, 137.0, 141.3, 142.4, 144.6, 147.9, 150.6; FTIR: ν_{max} 3067 (w), 2927 (s), 1598 (s), 1501 (s), 1478 (s), 1154 (s), 968 (m); HRMS (ESI-TOF) *m/z* $[M+H]^+$ calculated for $C_{20}H_{24}N_3O$: 322.1919. Found: 322.1928.

1-Phenyl-3-*n*-hexyl-4-(pinacolborane)-5-(2-pyridyl)pyrazole, **176**:

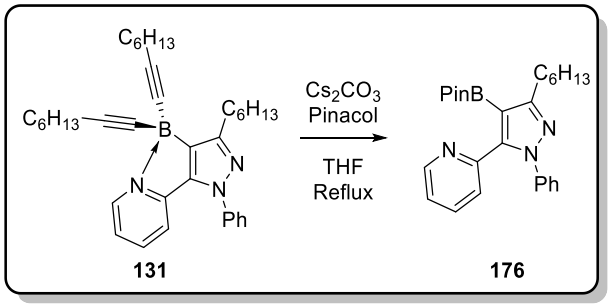

A flask was charged with pyrazole **131** (500 mg, 0.937 mmol), pinacol (554 mg, 4.69 mmol), caesium carbonate (397 mg, 1.12 mmol) and THF (10 mL) and heated at reflux for 14 hours. The mixture was allowed to cool to ambient temperature and volatiles were removed *in vacuo*. Excess pinacol was removed by Kügelrohr distillation. The crude residue was purified by flash silica chromatography (gradient starting with 100% 40-60 petroleum ether and ending with 40% ethyl acetate in 40-60 petroleum ether) affording pyrazole **176** as a clear oil (369 mg, 91%).

^{1}H NMR (400 MHz, $CDCl_3$) δ 0.86-0.93 (3H, m), 1.23 (12H, s), 1.27-1.48 (6H, m), 1.66-1.78 (2H, m), 2.80-2.88 (2H, m), 7.16-7.29 (7H, m), 7.58 (1H, td, *J* = 7.5, 2.0 Hz), 8.53 (1H, ddd, *J* = 5.0, 2.0,1.0 Hz); ^{13}C NMR (101 MHz, $CDCl_3$) δ 14.3, 22.7, 24.8, 28.7, 29.5, 30.8, 31.8, 83.1, 122.8, 125.3, 125.5, 127.2, 128.8, 135.6, 140.2, 148.6, 149.1, 150.6, 160.1 (one sp^2 carbon not observed); ^{11}B NMR (128 MHz, $CDCl_3$) δ 29.5; FTIR: ν_{max} 2956 (m), 2929 (s), 1593 (m), 1545 (s), 1504 (s), 1475 (s), 1417 (m), 1379 (s), 1312 (s), 1145 (s), 1068 (s); HRMS (ESI-TOF) *m/z* $[M+H]^+$ calculated for $C_{26}H_{35}N_3O_2{}^{11}B$: 432.2839. Found: 432.2822.

1-Phenyl-3-(*n*-hexyl)-4-(4-methoxyphenyl)-5-(2-pyridyl)pyrazole, **177**:

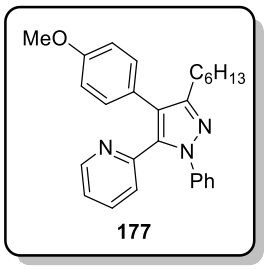

177

Following general procedure K dialkynylboronate **131** (50 mg, 0.094 mmol), 4-bromoanisole (34 mg, 0.18 mmol), XPhos G2 Precatalyst (9 mg, 0.01 mmol), sodium carbonate (25 mg, 0.24 mmol), pyrazole **177** was isolated as a yellow oil (27 mg, 70%).

^{1}H NMR (400 MHz, $CDCl_3$): δ 0.80-0.88 (3H, m), 1.19-1.37 (6H, m), 1.59-1.70 (2H, m), 2.68-2.78 (2H, m), 3.79 (3H, s), 6.79-6.88 (2H, m), 7.05 (1H, dt, *J* = 8.0, 1.0 Hz), 7.08-7.16 (3H, m), 7.20-7.32 (5H, m), 7.51 (1H, td, *J* = 8.0, 2.0 Hz), 8.49 (1H, ddd, *J* = 5.0, 2.0, 1.0 Hz); ^{13}C NMR (101 MHz, $CDCl_3$): δ 14.2, 22.7, 26.9, 29.3, 29.6, 31.7, 55.3, 113.8, 122.0, 122.6, 124.9, 125.4, 125.8, 126.8, 128.7, 131.2, 136.2, 139.3, 140.5, 149.7, 150.4, 152.2, 158.5; FTIR: ν_{max} 2952 (m), 2926 (m), 2854 (m), 1587 (m), 1557 (m), 1502 (s), 1375 (m), 1285 (m), 1245 (s), 1174 (s); HRMS (ESI-TOF) *m/z* $[M+H]^+$ calculated for $C_{27}H_{30}N_3O$: 412.2389. Found: 412.2401.

1-Phenyl-3-(*n*-hexyl)-4-(4-methoxyphenyl)-5-[2-(5,6-dihydro-4*H*-1,3-oxazine)]pyrazole, **178a** and 1-phenyl-3-(*n*-hexyl)-5-[2-(5,6-dihydro-4*H*-1,3-oxazine)]pyrazole, **178b**:

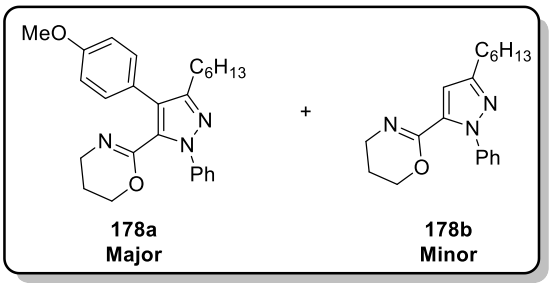

178a
Major

178b
Minor

Following general procedure N using sydnone **147** (1.00 g, 4.08 mmol) and potassium(1-octyn-1-yl)triflouroborate (4.40 g, 20.4 mmol) were stirred for 3 hours at 25 °C, pyrazole **158** was isolated as an orange oil. The crude material was carried forward without further purification. Following general procedure K, using crude dialkynylboronate **158** (4.08 mmol), 4-bromoanisole (1.14 g, 6.12 mmol), XPhos G2 Precatalyst (0.321 g, 0.408 mmol), sodium carbonate (0.865 g, 8.16 mmol), pyrazole **178a** and protodeboronated product **178b** were isolated as an orange oil (1.19 g, 70%, 9:1).

178a: ^{1}H NMR (400 MHz, $CDCl_3$): δ 0.80-0.87 (3H, m), 1.18-1.35 (6H, m), 1.56-1.65 (2H, m), 1.79-1.87 (2H, m), 2.65-2.71 (2H, m), 3.39 (2H, t, *J* = 6.0 Hz), 3.85 (3H, s), 4.04 (2H, t, *J* = 5.5 Hz), 6.94 (2H, d, *J* = 9.0 Hz), 7.30-7.35 (3H, m), 7.42 (2H, t, *J* = 8.0 Hz), 7.53-7.58 (2H, m); ^{13}C

NMR (101 MHz, $CDCl_3$): δ 14.2, 21.8, 22.7, 26.8, 29.3, 29.5, 31.7, 43.0, 55.4, 65.5, 113.7, 122.3, 123.8, 125.2, 127.2, 128.9, 130.6, 134.5, 140.6, 150.4, 151.9, 158.6; FTIR: ν_{max} 2926 (m), 2855 (m), 1668 (m) 1502 (s), 1462 (m) 1377 (m), 1246 (s), 1173 (s); HRMS (ESI-TOF) *m/z* $[M+H]^+$ calculated for $C_{26}H_{32}N_3O_2$: 418.2495. Found: 418.2495.

1-Phenyl-3-(*n*-hexyl)-4-(4-methoxyphenyl)-5-(N-3-chloropropylamide)pyrazole, **179**:

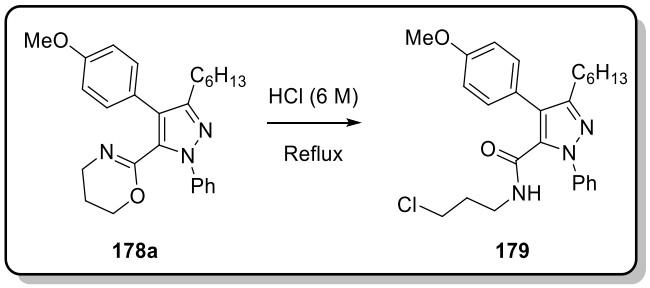

178a **179**

A flask equipped with reflux condenser was charged with pyrazole **178a** (340 mg, 0.814 mmol) and HCl (6 M, 33 mmol, 5.4 mL) and heated at reflux for 2 hours. The reaction was allowed to cool to ambient temperature, poured into water and extracted with ethyl acetate. The combined organic layers were dried over $MgSO_4$, filtered and volatiles removed *in vacuo*. The crude residue was purified by flash silica chromatography (gradient starting with 100% 40-60 petroleum ether and ending with 40% ethyl acetate in 40-60 petroleum ether) affording **179** (221 mg, 62%) as an amorphous yellow solid.

^{1}H NMR (400 MHz, $CDCl_3$): δ 0.84 (3H, t, *J* = 7.0 Hz), 1.17-1.32 (6H, m), 1.56 (2H, dt, *J* = 15.5, 7.5 Hz), 1.74 (2H, p, *J* = 6.5 Hz), 2.56-2.64 (2H, m), 3.19 (2H, t, *J* = 6.5 Hz), 3.31 (2H, q, *J* = 6.5 Hz), 3.87 (3H, s), 5.65 (1H, t, *J* = 5.5 Hz), 7.00 (2H, d, *J* = 9.0 Hz), 7.28 (2H, d, *J* = 9.0 Hz), 7.33-7.38 (1H, m), 7.40-7.56 (2H, m), 7.48-7.52 (2H, m); ^{13}C NMR (101 MHz, $CDCl_3$): δ 14.2, 22.7, 26.6, 29.2, 29.5, 31.6, 31.7, 37.0, 42.0, 55.5, 121.6, 122.1, 124.2, 124.8, 128.0, 129.0, 131.1, 134.6, 140.5, 152.2, 159.6, 160.7; FTIR: ν_{max} 3266 (m), 2956 (m), 2927 (m), 2855 (w), 1640 (s) 1501 (s), 1461 (m) 1378 (m), 1248 (s), 1178 (m) 1021 (m); HRMS (ESI-TOF) *m/z* $[M+H]^+$ calculated for $C_{26}H_{33}N_3O_2{}^{35}Cl$: 454.2261. Found: 454.2262.

Attempted deprotection of **178a** by Yu's method:[162]

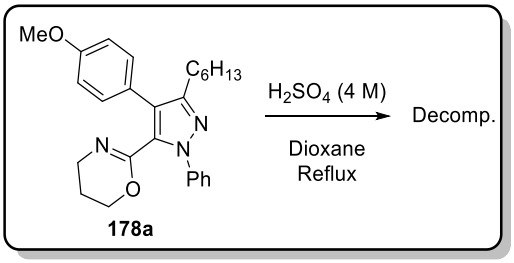

178a

A flask equipped with reflux condenser was charged with pyrazole **178a** (112 mg, 0.274 mmol), H_2SO_4 (4 M, 0.65 mL) and 1,4-dioxane (2.4 mL) and heated at reflux for 14 hours. The reaction was allowed to cool to ambient temperature, poured into water and extracted with ethyl acetate. The aqueous layer was neutralised and extracted with ethyl acetate. The combined organic layers were dried over $MgSO_4$, filtered and volatiles removed *in vacuo*. The crude residue contained a complex mixture of decomposition products and pyrazole **178a**.

1-Phenyl-3-(*n*-hexyl)-4-(4-methoxyphenyl)-5-[*N*-(methyl)-(3-chloropropylamide)]pyrazole, **180**:

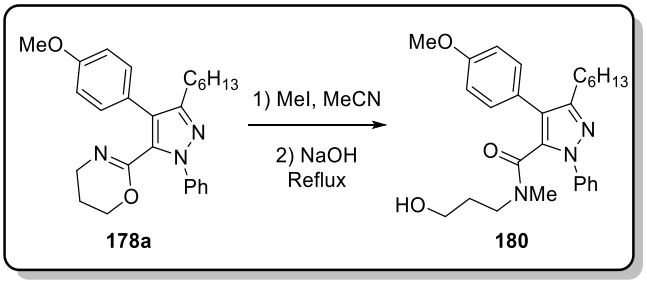

178a **180**

To a solution of oxazine **178a** (105 mg, 0.251 mmol) in MeCN (1 mL) was added methyl iodide (54 mg, 0.377 mmol) and the mixture stirred for 14 h at ambient temperature. Volatiles were removed in vacuo and the resulting residue heated at reflux with sodium hydroxide (50 mg, 1.25 mmol) in water (1 mL) for 8 h. The reaction was allowed to cool to ambient temperature, diluted with water and extracted with CH_2Cl_2. The combined organic layers were dried over $MgSO_4$ and volatiles removed *in vacuo*. The crude residue was purified by flash silica chromatography (gradient starting with 100% 40-60 petroleum ether and ending with 60% ethyl acetate in 40-60 petroleum ether) affording **180** (38 mg, 34%) as a yellow oil.

^{1}H NMR (400 MHz, $CDCl_3$): δ 0.79-0.84 (3H, m), 1.19-1.35 (6H, m), 1.53-1.70 (4H, m), 2.52 (3H, s), 2.72 (2H, t, *J* = 7.5 Hz), 3.23-3.31 (2H, m), 3.39-3.51 (2H, m), 3.79 (1H, dd, *J* = 3.0, 1.5 Hz), 3.84 (3H, s), 6.94 (2H, d, *J* = 9.0 Hz), 7.29 (2H, d, *J* = 9.0 Hz), 7.32-7.36 (1H, m), 7.43 (2H, t, *J* = 8.0 Hz), 7.52-7.57 (2H, m); ^{13}C NMR (101 MHz, $CDCl_3$): δ 14.2, 22.7, 26.8, 29.2, 29.3, 29.3, 31.6, 35.8, 43.7, 55.4, 58.0, 114.2, 123.2, 124.2, 127.8, 129.3, 129.4, 130.2, 134.4, 139.8, 152.1, 159.1, 164.7; FTIR: ν_{max} 3412 (br), 2927 (m), 2856 (m), 1625 (s), 1556 (m), 1503 (s), 1461 (m), 1374 (m), 1287 (m), 1247 (s), 1176 (m), 1020 (m), 839 (m); HRMS (ESI-TOF) *m/z* $[M+H]^+$ calculated for $C_{27}H_{35}N_3O_3$: 450.2751. Found: 450.2757.

1-Phenyl-3-(*n*-hexyl)-4-(4-methoxyphenyl)-5-(*N*-3-chloropropylamide)pyrazole, **179**:

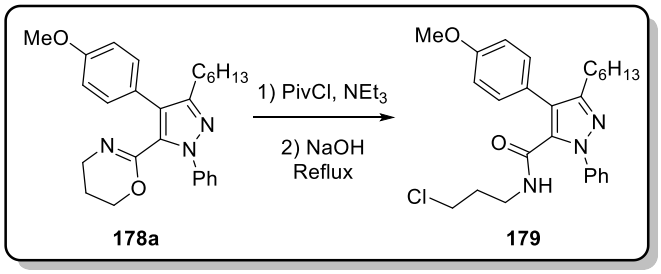

To a solution of oxazine **178a** (167 mg, 0.400 mmol) and NEt_3 (97 mg, 0.96 mmol) in THF (2 mL) at 0 ^oC was added pivaloyl chloride (106 mg, 0.880 mmol). The reaction mixture was then heated at reflux for 6 h. Sodium hydroxide (160 mg, 4.00 mmol) in water 2 mL was added and the mixture heated at reflux for 14 h. The reaction was allowed to cool to ambient temperature and extracted with EtOAc. The combined organic layers were dried over $MgSO_4$ and volatiles removed *in vacuo*. The crude residue was purified by flash silica chromatography (gradient starting with 100% 40-60 petroleum ether and ending with 40% ethyl acetate in 40-60 petroleum ether) affording **179** (87 mg, 48%) as an amorphous yellow solid and recovered **178a** (97 mg 58%, ~85% purity).

See above for characterisation data.

1-Phenyl-3-(*n*-hexyl)-4-(4-methoxyphenyl)-5-[*N*-(pivaloyl)-(3-chloropropylamide)]pyrazole **181** and 1-Phenyl-3-(*n*-hexyl)-4-(4-methoxyphenyl)-5-(*N*-3-chloropropylamide)pyrazole, **179**:

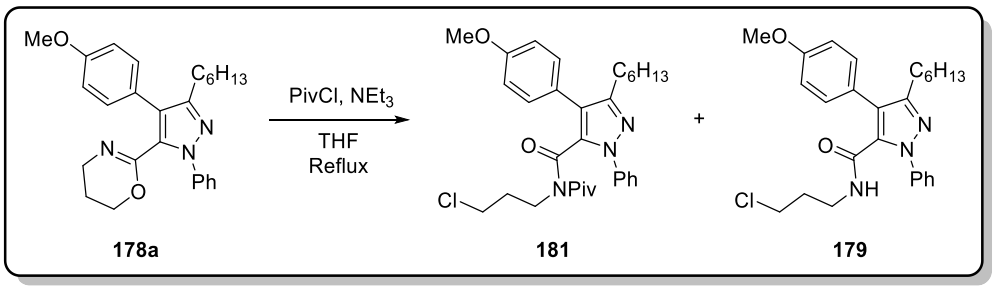

To a solution of oxazine **178a** (201 mg, 0.481 mmol) and NEt_3 (117 mg, 1.15 mmol) in THF (2 mL) at 0 ^oC was added pivaloyl chloride (128 mg, 1.06 mmol). The reaction mixture was then heated at reflux for 14 h during which the THF evaporated. The reaction was allowed to cool to ambient temperature, water added and extracted with EtOAc. The combined organic layers were dried over $MgSO_4$ and volatiles removed *in vacuo*. The crude residue was purified by flash silica chromatography (gradient starting with 100% 40-60 petroleum ether and ending with 40% ethyl acetate in 40-60 petroleum ether) affording **181** as a yellow oil (75 mg,

29%), amide **179** as an amorphous yellow solid (58 mg, 27%) and recovered **178a** (57 mg, 28%).

181: ^{1}H NMR (400 MHz, $CDCl_3$): δ 0.83 (3H, t, *J* = 7.0 Hz), 0.95 (9H, s), 1.17-1.34 (6H, m), 1.53-1.65 (2H, m), 1.84 (2H, br), 2.62-2.71 (2H, m), 3.42 (2H, t, *J* = 6.0 Hz), 3.67 (2H, br), 3.83 (3H, s), 6.94 (2H, d, *J* = 8.5 Hz), 7.23 (2H, d, *J* = 9.0 Hz), 7.29-7.36 (1H, m), 7.42 (2H, t, *J* = 7.5 Hz), 7.55-7.60 (2H, m); ^{13}C NMR (101 MHz, $CDCl_3$): δ 14.2, 22.7, 26.7, 27.8, 29.3, 29.3, 30.7, 31.6, 42.1, 42.4, 44.0, 55.5, 114.3, 120.5, 124.2, 124.3, 127.8, 129.2, 130.8, 135.3, 140.1, 151.9, 159.3, 165.5, 184.8; FTIR: ν_{max} 2929 (m), 2857 (m), 2160 (w), 2029 (w), 1703 (m), 1672 (s) 1554 (m), 1501 (s), 1462 (m) 1335 (m), 1289 (m), 1247 (s), 1176 (m), 1122 (s), 1020 (m); HRMS (ESI-TOF) *m/z* $[M+H]^+$ calculated for $C_{31}H_{40}N_3O_3Na^{35}Cl$: 560.2656. Found: 560.2643.

See above for characterisation data of **179**.

Attempted reaction of **178a** with pivaloyl chloride:

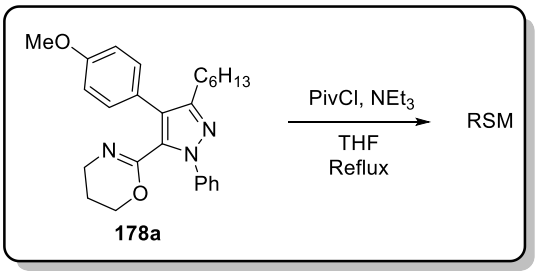

To a solution of oxazine **178a** (200 mg, 0.479 mmol) and NEt_3 (116 mg, 1.15 mmol) in THF (2 mL) at 0 °C was added pivaloyl chloride (127 mg, 1.05 mmol). The reaction mixture was then heated at reflux for 14 h. The reaction was allowed to cool to ambient temperature, water added and extracted with EtOAc. The combined organic layers were dried over $MgSO_4$ and volatiles removed *in vacuo*. Starting material **178a** was recovered.

1-Phenyl-3-(*n*-hexyl)-4-(4-methoxyphenyl)-5-[*N*-(pivaloyl)-(3-chloropropylamide)]pyrazole **181**:

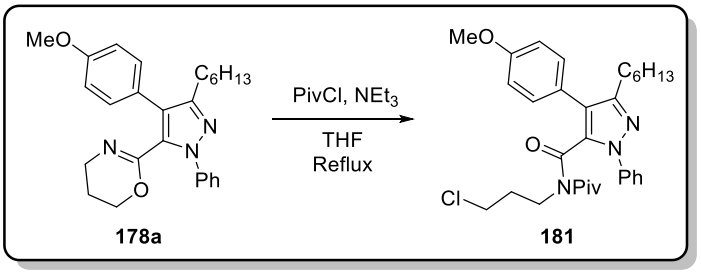

To a solution of oxazine **178a** (200 mg, 0.479 mmol) and NEt_3 (267 mg, 2.63 mmol) in THF (1 mL) at 0 °C was added pivaloyl chloride (289 mg, 2.39 mmol). The reaction mixture was then

heated at reflux for 14 h. The reaction was allowed to cool to ambient temperature, water added and extracted with EtOAc. The combined organic layers were dried over $MgSO_4$ and volatiles removed *in vacuo*. The crude residue was purified by flash silica chromatography (gradient starting with 100% 40-60 petroleum ether and ending with 40% ethyl acetate in 40-60 petroleum ether) affording **181** as a yellow oil (62 mg, 24%).

See above for characterisation data.

1-Phenyl-3-(*n*-hexyl)-4-(4-methoxyphenyl)-5-[*N*-(pivaloyl)-(3-chloropropylamide)]pyrazole **181**:

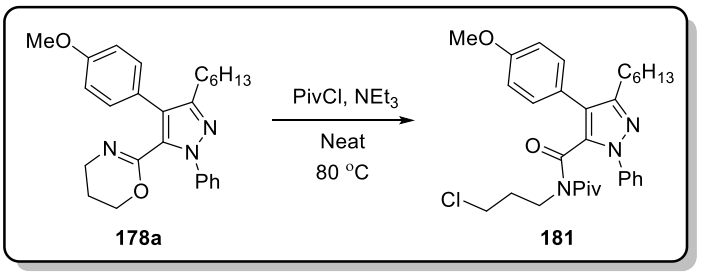

Oxazine **178a** (107 mg, 0.256 mmol), NEt_3 (285 mg, 2.82 mmol) and pivaloyl chloride (309 mg, 2.56 mmol) were heated at 80 °C for 14 h. The reaction was allowed to cool to ambient temperature, water added and extracted with EtOAc. The combined organic layers were dried over $MgSO_4$ and volatiles removed *in vacuo*. The crude residue was purified by flash silica chromatography (gradient starting with 100% 40-60 petroleum ether and ending with 40% ethyl acetate in 40-60 petroleum ether) affording **181** as a yellow oil (48 mg, 35%) and recovered **178a** (42 mg, 39%).

See above for characterisation data.

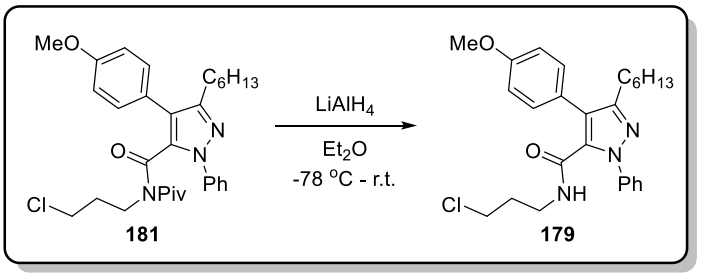

To a suspension of $LiAlH_4$ (33 mg, 0.88 mmol) in Et_2O (1 mL) at -78 °C was added imide **181** (95 mg, 0.18 mmol) in Et_2O (1 mL) and the reaction allowed to warm to ambient temperature and stirred for 14 h. The reaction was quenched with aq. HCl (1 M) and extracted with EtOAc. The combined organic layers were dried over $MgSO_4$ and volatiles removed *in vacuo*. The crude residue was purified by flash silica chromatography (gradient starting with 100% 40-60

petroleum ether and ending with 40% ethyl acetate in 40-60 petroleum ether) affording **179** as a yellow solid (44 mg, 55%).

See above for characterisation data.

Resubjection of **131** to directed cycloaddition conditions:

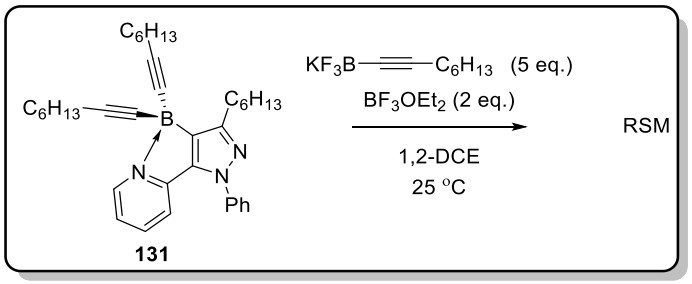

Following general procedure N using pyrazole **131** (50 mg, 0.094 mmol) and potassium(1-octyn-1-yl)triflouroborate (101 mg, 0.469 mmol), resulted in the recovery of pyrazole **131**.

Subjection of **131** to boron trifluoride:

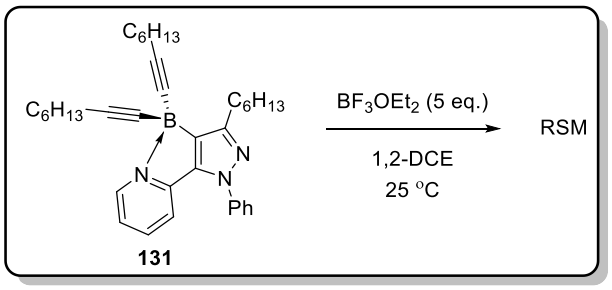

A flask was charged with pyrazole **131** (50 mg, 0.094 mmol) in 1,2-dichloroethane (2 mL) and borontrifluoride diethyl etherate (67 mg, 0.47 mmol) added. The solution was stirred for 2 h at 25 °C. The reaction was poured into brine, extracted with dichloromethane, the combined organic layers dried over $MgSO_4$ and volatiles removed *in vacuo*, resulting in the recovery of pyrazole **131**.

Subjection of **131** to boron trichloride:

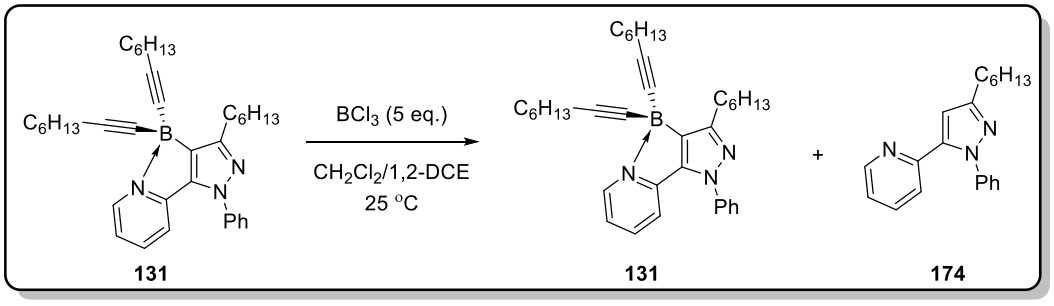

A flask was charged with pyrazole **131** (50 mg, 0.094 mmol) in 1,2-dichloroethane (1.5 mL) and borontrichloride in dichloromethane (1 M, 0.5 mL, 0.5 mmol) added. The solution was stirred for 2 h at 25 °C. The reaction was poured into brine, extracted with dichloromethane, the combined organic layers dried over $MgSO_4$ and volatiles removed *in vacuo*, resulting in the recovery of pyrazole **131** and protdeboronated product **174**.

Subjection of **131** to boron tribromide:

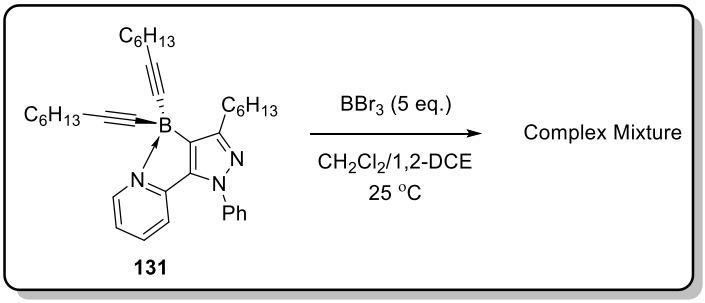

A flask was charged with pyrazole **131** (50 mg, 0.094 mmol) in 1,2-dichloroethane (1.5 mL) and borontribromide in dichloromethane (1 M, 0.5 mL, 0.5 mmol) added. The solution was stirred for 2 h at 25 °C. The reaction was poured into brine, extracted with dichloromethane, the combined organic layers dried over $MgSO_4$ and volatiles removed *in vacuo*, resulting in a complex mixture of apparent polymerisation products and protodeboronation product **174**.

Subjection of **131** to boron trifluoride at 40 °C:

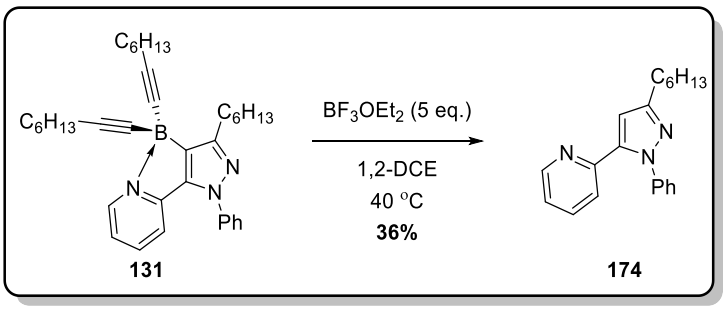

A flask was charged with pyrazole **131** (50 mg, 0.094 mmol) in 1,2-dichloroethane (2 mL) and borontrifluoride diethyl etherate (67 mg, 0.47 mmol) added. The solution was stirred for 2 h at 40 °C. The reaction was poured into brine, extracted with dichloromethane, the combined organic layers dried over $MgSO_4$ and volatiles removed *in vacuo*, affording pyrazole **174** (10 mg, 36%) as a yellow oil.

See above for characterisation data.

Subjection of **131** to KHF_2:

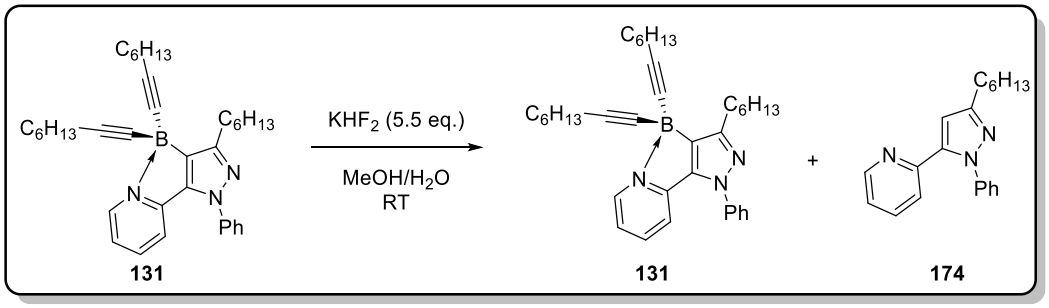

A flask was charged with pyrazole **131** (50 mg, 0.094 mmol) in methanol (0.3 mL) and potassium hydrogen fluoride (40 mg, 0.52 mmol) in water (0.15 mL) was added. The solution was stirred for 30 min at ambient temperature. The reaction was poured into water, extracted with dichloromethane, the combined organic layers dried over $MgSO_4$ and volatiles removed *in vacuo*, resulting in the recovery of pyrazole **131** and protdeboronated product **131**.

1-Phenyl-3-phenyl-4-(diphenylacetyleneborane)-5-(2-pyridyl)pyrazole boron trifluoride adduct, **195**:

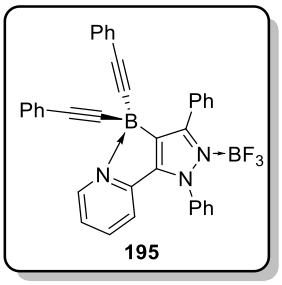

A number of stock solutions were prepared. The solutions were then combined to afford different reaction mixtures and analysed by ^{1}H-, ^{19}F- and ^{11}B NMR spectroscopy. For each stoichiometry analysed, two dilutions were used to obtain defined spectra. Low dilution used **171** (0.025 M) and high dilution used **171** (0.0061 M). Control spectra of $BF_3.OEt_2$ in CD_2Cl_2 and **171** in CD_2Cl_2 alone were also obtained.

Stock solution A) **171** (250 mg, 0.49 mmol) in CD_2Cl_2 (4 mL).

Stock Solution B) $BF_3.OEt_2$ (350 mg, 2.45 mmol) in CD_2Cl_2 (4 mL).

Stock Solution C) $BF_3.OEt_2$ (280 mg, 1.96 mmol) in CD_2Cl_2 (4 mL).

Stock Solution D) $BF_3.OEt_2$ (210 mg, 1.47 mmol) in CD_2Cl_2 (4 mL).

Stock Solution E) $BF_3.OEt_2$ (140 mg, 0.98 mmol) in CD_2Cl_2 (4 mL).

Stock Solution F) $BF_3.OEt_2$ (70 mg, 0.49 mmol) in CD_2Cl_2 (4 mL).

Entry	Stoichiometry (BF_3:**171**)	Stock A volume	Stock (volume)	CD_2Cl_2 volume
1	5:1	0.4 mL	B (0.4 mL)	N/A
2	5:1	0.1 mL	B (0.1 mL)	0.6 mL
3	4:1	0.4 mL	C (0.4 mL)	N/A
4	4:1	0.1 mL	C (0.1 mL)	0.6 mL
5	3:1	0.4 mL	D (0.4 mL)	N/A
6	3:1	0.1 mL	D (0.1 mL)	0.6 mL
7	2:1	0.4 mL	E (0.4 mL)	N/A
8	2:1	0.1 mL	E (0.1 mL)	0.6 mL
9	1:1	0.4 mL	F (0.4 mL)	N/A
10	1:1	0.1 mL	F (0.1 mL)	0.6 mL

References

1. Alberts, B.; Johnson, A.; Lewis, J.; Raff, M.; Roberts, K.; Walter, P.; Wilson, J.; Hunt, T., *Cancer Drug Discovery and Development; The Role of Microtubules in Cell Biology, Neurobiology and Oncology*; 5th ed.; Garland Science: New York, 2008; Vol. 15.
2. Hanahan, D.; Weinberg, R. A., *Cell,* **2000**, *100*, 57-70.
3. Wilson, S.; Jones, L.; Couseens, C.; Haana, K.; *Cancer and the Environment:Gene-Environment Interactions*; The National Academies Press: Washington D. C., 2002; Vol. 1.
4. Weinberg, R. A., *The Biology of Cancer*, 1st Ed.; Garland Science: New York, 2007; Vol. 15; pp 57-60.
5. Ford, D.; Easton, D. F.; Stratton, M.; Narod, S.; Goldgar, D.; Devilee, P.; Bishop, D. T.; Weber, B.; Lenoir, G.; Chang-Claude, J.; Sobol, H.; Teare, M. D.; Struewing, J.; Arason, A.; Scherneck, S.; Peto, J.; Rebbeck, T. R.; Tonin, P.; Neuhausen, S.; Barkardottir, R.; Eyfjord, J.; Lynch, H.; Ponder, B. A. J.; Gayther, S. A.; Birch, J. M.; Lindblom, A.; Stoppa-Lyonnet, D.; Bignon, Y.; Borg, A.; Hamann, U.; Haites, N.; Scott, R. J.; Maugard, C. M.; Vasen, H.; Seitz, S.; Cannon-Albright, L. A.; Schofield, A.; Zelada-Hedman, M., *Am. J. Hum. Genet.,* **1998**, *62*, 676-689.
6. Hanahan, D.; Weinberg, Robert A., *Cell,* **2011**, *144*, 646-674.
7. Chaplin, D. J.; Hill, S. A., *Int. J.of Rad. Oncol.* **2002**, *54*, 1491-1496.
8. Baluk, P.; Hashizume, H.; McDonald, D. M., *Curr. Opin. Genet. & Dev.* **2005**, *15*, 102-111.
9. Sevick, E. M.; Jain, R. K., *Cancer Res.,* **1989,** *49*, 3506-3512.
10. Hashizume, H.; Baluk, P.; Morikawa, S.; McLean, J. W.; Thurston, G.; Roberge, S.; Jain, R. K.; McDonald, D. M., *Am. J. Pathol.,* **2000**, *156*, 1363-1380.
11. Baluk, P.; Morikawa, S.; Haskell, A.; Mancuso, M.; McDonald, D. M., *Am. J. Pathol.* **2003,** *163*, 1801-1815.
12. Peterson, H. I.; Appelgren, L., *Bibliotheca anatomica* **1977**, 262-5.
13. Dvorak, H. F.; Nagy, J. A.; Dvorak, J. T.; Dvorak, A. M., *Am. J. Pathol.* **1988**, *133*, 95-109.
14. Jain, R. K.; Munn, L. L.; Fukumura, D., *Nat. Rev. Cancer,* **2002**, *2*, 266-276.
15. Folkman, J.; Hanahan, D., *Princess Takamatsu Symp.,* **1991**, *22*, 339-47.
16. Weis, S. M.; Cheresh, D. A., *Nat. Med.,* **2011**, *17*, 1359-1370.
17. Thorpe, P. E., *Clin. Cancer Res.* **2004**, *10*, 415-427.
18. Folkman, J., *J. Natl. Cancer Inst.* **1990**, *82*, 4-7.
19. Bergers, G.; Javaherian, K.; Lo, K.-M.; Folkman, J.; Hanahan, D., *Science,* **1999,** *284*, 808-812.
20. Cai, S. X., *Recent Pat. Anticancer Drug. Discov.,* **2007,** *2*, 79-101.
21. Carmeliet, P.; Jain, R. K., *Nature,* **2000,** *407*, 249-257.
22. Folkman, J., *N. Eng. J. Med.* **1971**, *285*, 1182-1186.
23. Cristofanilli, M.; Charnsangavej, C.; Hortobagyi, G. N., *Nat. Rev. Drug Discov.,* **2002**, *1*, 415-426.
24. Folkman, J., *N. Engl. J. Med.,* **1995**, *333*, 1757-1763.
25. Fojo, A. T.; *Cancer Drug Discovery and Development; The Role of Microtubules in Cell Biology, Neurobiology and Oncology*; Humana Press: Totowa, NJ, 2008, Vol. 9.
26. Denekamp, J., *Br. J. Cancer,* **1982**, *45*, 136-139.
27. Denekamp, J., *Acta Oncologica,* **1984**, *23*, 217-225.
28. Tozer, G. M.; Kanthou, C.; Baguley, B. C., *Nat. Rev. Cancer,* **2005**, *5*, 423-435.
29. Prise, V. E.; Honess, D. J.; Stratford, M. R. L.; Wilson, J.; M, T. G., *Int. J. Oncol.,* **2002**, *21*, 717-726.
30. Kanthou, C.; Tozer, G. M., *Expert Opin. Ther. Targ.* **2007**, *11*, 1443-1457.
31. Boehle, A. S.; Sipos, B.; Kliche, U.; Kalthoff, H.; Dohrmann, P., *Ann. Thorac. Surg.,* **2001,** *71*, 1657-1665.
32. Young, S. L.; Chaplin, D. J., *Expert Opin. Investig. Drugs,* **2004**, *13*, 1171-1182.

33. Shaked, Y.; Ciarrocchi, A.; Franco, M.; Lee, C. R.; Man, S.; Cheung, A. M.; Hicklin, D. J.; Chaplin, D.; Foster, F. S.; Benezra, R.; Kerbel, R. S., *Science,* **2006,** *313*, 1785-1787.
34. Laws, A. L.; Matthew, A. M.; Double, J. A.; Bibby, M. C., *Br. J. Cancer,* **1995**, *71*, 1204-1209.
35. Beauregard, D. A.; Pedley, R. B.; Hill, S. A.; Brindle, K. M., *NMR in Biomed.,* **2002,** *15*, 99-105.
36. Jassar, A. S.; Suzuki, E.; Kapoor, V.; Sun, J.; Silverberg, M. B.; Cheung, L.; Burdick, M. D.; Strieter, R. M.; Ching, L.-M.; Kaiser, L. R.; Albelda, S. M., *Cancer Res.,* **2005,** *65*, 11752-11761.
37. Hulpiau, P.; van Roy, F., *Int. J. Biochem. & Cell Biol.,* **2009,** *41*, 349-369.
38. Gerhardt, H.; Betsholtz, C., *Cell Tissue Res.,* **2003**, *314*, 15-23.
39. Orest W. Blaschuk, W.; Barbara J. Gour, B. US 6031072, 2000.
40. Shintani, Y.; Fukumoto, Y.; Chaika, N.; Grandgenett, P. M.; Hollingsworth, M. A.; Wheelock, M. J.; Johnson, K. R., *Int. J. Cancer,* **2008**, *122*, 71-77.
41. Ducki, S.; Rennison, D.; Woo, M.; Kendall, A.; Chabert, J. F. D.; McGown, A. T.; Lawrence, N. J., *Bioorg. Med. Chem.,* **2009**, *17*, 7698-7710.
42. Mitchison, T.; Kirschner, M., *Nature,* **1984,** *312*, 237-242.
43. Jordan, M. A.; Wilson, L., *Nat. Rev. Cancer,* **2004,** *4*, 253-265.
44. Belotti, D.; Vergani, V.; Drudis, T.; Borsotti, P.; Pitelli, M. R.; Viale, G.; Giavazzi, R.; Taraboletti, G., *Clin. Cancer Res.,* **1996**, *2*, 1843-1849.
45. Holwell, S. E.; Hill, B. T.; Bibby, M. C., *Br. J. Cancer,* **2001**, *84*, 290-295.
46. Micheletti, G.; Poli, M.; Borsotti, P.; Martinelli, M.; Imberti, B.; Taraboletti, G.; Giavazzi, R., *Cancer Res.,* **2003,** *63*, 1534-1537.
47. Kanthou, C.; Tozer, G. M., *Blood,* **2002,** *99*, 2060-2069.
48. Pasquier, E.; Honoré, S.; Braguer, D., *Drug Resist. Update,* **2006**, *9*, 74-86.
49. Boyland, E.; Boyland, M. E., *Biochem. J.,* **1937,** *31*, 454-460.
50. Ludford, R. J., *Br. J. Cancer,* **1948,** *2*, 75-86.
51. Pettit, G. R.; Cragg, G. M.; Singh, S. B., *J. Nat. Prod.,* **1987,** *50*, 386-391.
52. Lin, C. M.; Singh, S. B.; Chu, P. S.; Dempcy, R. O.; Schmidt, J. M.; Pettit, G. R.; Hamel, E., *Mol. Pharmacol.,* **1988,** *34*, 200-208.
53. Chaplin, D. J.; Pettit, G. R.; Parkins, C. S.; Hill, S. A., *Brit. J. Cancer Suppl.,* **1996**, *27*, S86-S88.
54. Dark, G. G.; Hill, S. A.; Prise, V. E.; Tozer, G. M.; Pettit, G. R.; Chaplin, D. J., *Cancer Res.,* **1997**, *57*, 1829-1834.
55. Pettit, G. R.; Temple, C.; Narayanan, V. L.; Varma, R.; Simpson, M. J.; Boyd, M. R.; Rener, G. A.; Bansal, N., *Anticancer Drug Des.,* **1995**, *10*, 299-309.
56. Patterson, D. M.; Rustin, G. J. S., *Clin. Oncol.,* **2007**, *19*, 443-456.
57. Pettit, G. R.; Lippert, J. W., *Anticancer Drug Des.* **2000**, *15*, 203-216.
58. Hill, S. A.; Tozer, G. M.; Chaplin, D. J., *Anticancer Res.,* **2002**, *22*, 1453-1458.
59. Patterson, D. M.; Ross, P.; Koetz, B.; Saleem, A.; Stratford, M.; Stirling, J.; Padhani, A.; Asselin, M.; Price, P.; Rustin, G. J., *J. Clin. Oncol., ASCO Annual Meeting Proceedings Part I,* **2007**, *25*, 14146.
60. Tozer, G. M.; Prise, V. E.; Wilson, J.; Cemazar, M.; Shan, S.; Dewhirst, M. W.; Barber, P. R.; Vojnovic, B.; Chaplin, D. J., *Cancer Res.,* **2001**, *61*, 6413-6422.
61. Lin, C. M.; Ho, H. H.; Pettit, G. R.; Hamel, E., *Biochem.,* **1989**, *28*, 6984-6991.
62. Ahmed, B.; van Eijk, L. I.; Bouma-ter Steege, J. C. A.; van der Schaft, D. W. J.; van Esch, A. M.; Joosten-Achjanie, S. R.; Lambin, P.; Landuyt, W.; Griffioen, A. W., *Int. J. Cancer,* **2003**, *105*, 20-25.
63. Lunt, S.-J.; Akerman, S.; Hill, S. A.; Fisher, M.; Wright, V. J.; Reyes-Aldasoro, C. C.; Tozer, G. M.; Kanthou, C., *Int. J. Cancer,* **2011**, *129*, 1979-1989.
64. Tron, G. C.; Pirali, T.; Sorba, G.; Pagliai, F.; Busacca, S.; Genazzani, A. A., *J. Med. Chem.,* **2006,** *49*, 3033-3044.
65. Semenova, M. N.; Kiselyov, A.; Semenov, V. V., *BioTechniques,* **2006**, *40*, 765-774.

66. Semenov, V. V.; Kiselyov, A. S.; Titov, I. Y.; Sagamanova, I. K.; Ikizalp, N. N.; Chernysheva, N. B.; Tsyganov, D. V.; Konyushkin, L. D.; Firgang, S. I.; Semenov, R. V.; Karmanova, I. B.; Raihstat, M. M.; Semenova, M. N., *J. Nat. Prod.,* **2010**, *73*, 1796-1802.
67. Titov, I. Y.; Sagamanova, I. K.; Gritsenko, R. T.; Karmanova, I. B.; Atamanenko, O. P.; Semenova, M. N.; Semenov, V. V., *Bioorg. Med. Chem. Lett.,* **2011**, *21*, 1578-1581.
68. Cushman, M.; Nagarathnam, D.; Gopal, D.; Chakraborti, A. K.; Lin, C. M.; Hamel, E., *J. Med. Chem.,* **1991**, *34*, 2579-2588.
69. Ohsumi, K.; Nakagawa, R.; Fukuda, Y.; Hatanaka, T.; Morinaga, Y.; Nihei, Y.; Ohishi, K.; Suga, Y.; Akiyama, Y.; Tsuji, T., *J. Med. Chem.,* **1998**, *41*, 3022-3032.
70. Simoni, D.; Romagnoli, R.; Baruchello, R.; Rondanin, R.; Grisolia, G.; Eleopra, M.; Rizzi, M.; Tolomeo, M.; Giannini, G.; Alloatti, D.; Castorina, M.; Marcellini, M.; Pisano, C., *J. Med. Chem.,* **2008**, *51*, 6211-6215.
71. Lawrence, N. J.; Ghani, F. A.; Hepworth, L. A.; Hadfield, J. A.; McGown, A. T.; Pritchard, R. G., *Synthesis,* **1999,** *1999*, 1656-1660.
72. Lara-Ochoa, F.; Espinosa-Pérez, G., *Tet. Lett.,* **2007**, *48*, 7007-7010.
73. Petrov, O. I.; Gerova, M. S.; Chanev, C. D.; Petrova, K. V., *Synthesis,* **2011**, *2011*, 3711-3715.
74. Brown, H. C.; Zweifel, G., *J. Am. Chem. Soc.,* **1961**, *83*, 3834-3840.
75. Giraud, A.; Provot, O.; Hamzé, A.; Brion, J.-D.; Alami, M., *Tet. Lett.,* **2008**, *49*, 1107-1110.
76. Cushman, M.; Nagarathnam, D.; Gopal, D.; He, H. M.; Lin, C. M.; Hamel, E., *J. Med. Chem.,* **1992**, *35*, 2293-2306.
77. Getahun, Z.; Jurd, L.; Chu, P. S.; Lin, C. M.; Hamel, E., *J. Med. Chem.,* **1992**, *35*, 1058-1067.
78. Zhang, Q.; Peng, Y.; Wang, X. I.; Keenan, S. M.; Arora, S.; Welsh, W. J., *J. Med. Chem.* **2007,** *50*, 749-754.
79. Odlo, K.; Hentzen, J.; dit Chabert, J. F.; Ducki, S.; Gani, O. A. B. S. M.; Sylte, I.; Skrede, M.; Fløtenes, V. A.; Hansen, T. V., *Bioorg. Med. Chem.,* **2008**, *16*, 4829-4838.
80. Romagnoli, R.; Baraldi, P. G.; Cruz-Lopez, O.; Lopez Cara, C.; Carrion, M. D.; Brancale, A.; Hamel, E.; Chen, L.; Bortolozzi, R.; Basso, G.; Viola, G., *J. Med. Chem.,* **2010**, *53*, 4248-4258.
81. Beale, T. M.; Bond, P. J.; Brenton, J. D.; Charnock-Jones, D. S.; Ley, S. V.; Myers, R. M., *Bioorg. Med. Chem.,* **2012**, *20*, 1749-1759.
82. Romagnoli, R.; Baraldi, P. G.; Salvador, M. K.; Preti, D.; Aghazadeh Tabrizi, M.; Brancale, A.; Fu, X.-H.; Li, J.; Zhang, S.-Z.; Hamel, E.; Bortolozzi, R.; Basso, G.; Viola, G., *J. Med. Chem.,* **2011**, *55*, 475-488.
83. Bhat, B. A.; Dhar, K. L.; Puri, S. C.; Saxena, A. K.; Shanmugavel, M.; Qazi, G. N., *Bioorg. Med. Chem. Lett.,* **2005**, *15*, 3177-3180.
84. LeBlanc, R.; Dickson, J.; Brown, T.; Stewart, M.; Pati, H. N.; VanDerveer, D.; Arman, H.; Harris, J.; Pennington, W.; Holt Jr, H. L.; Lee, M., *Bioorg. Med. Chem.,* **2005**, *13*, 6025-6034.
85. Wang, L.; Woods, K. W.; Li, Q.; Barr, K. J.; McCroskey, R. W.; Hannick, S. M.; Gherke, L.; Credo, R. B.; Hui, Y.-H.; Marsh, K.; Warner, R.; Lee, J. Y.; Zielinski-Mozng, N.; Frost, D.; Rosenberg, S. H.; Sham, H. L., *J. Med. Chem.,* **2002**, *45*, 1697-1711.
86. Liu, T.; Cui, R.; Chen, J.; Zhang, J.; He, Q.; Yang, B.; Hu, Y., *Arch. Pharm.* **2011**, *344*, 279-286.
87. Zaninetti, R.; Cortese, S. V.; Aprile, S.; Massarotti, A.; Canonico, P. L.; Sorba, G.; Grosa, G.; Genazzani, A. A.; Pirali, T., *ChemMedChem,* **2013**, *8*, 633-643.
88. Xu, Q.; Qi, H.; Sun, M.; Zuo, D.; Jiang, X.; Wen, Z.; Wang, Z.; Wu, Y.; Zhang, W., *PLoS ONE,* **2015**, *10*, e0128710.
89. Fustero, S.; Sánchez-Roselló, M.; Barrio, P.; Simón-Fuentes, A., *Chem. Rev.* **2011**, *111*, 6984-7034.
90. Earl, J. C.; Mackney, A. W., *J. Chem. Soc.,* **1935**, 899-900.

91. McNaught, A. D.; Wilkinson, A., *IUPAC. Compendium of Chemical Terminology*, 2nd ed. (the "Gold Book"). Blackwell Scientific Publications, Oxford: XML on-line corrected version: http://goldbook.iupac.org (2006-) created by M. Nic, J. Jirat, B. Kosata; updates compiled by A. Jenkins., 1997, (accessed 01/08/2013).
92. Browne, D. L.; Harrity, J. P. A., *Tetrahedron* **2010**, *66*, 553-568.
93. Greco, C. V.; O'Reilly, B. P., *J. Heterocyclic Chem.,* **1970**, *7*, 1433-1434.
94. Applegate, J.; Turnbull, K., *Synthesis,* **1988**, *1988*, 1011-1012.
95. Baker, W.; Ollis, W. D.; Poole, V. D., *J. Chem. Soc. (Resumed),* **1950**, 1542-1551.
96. Azarifar, D.; Ghasemnejad-Bosra, H., *Synthesis,* **2006,** *2006*, 1123-1126.
97. Baker, W.; Ollis, W. D.; Poole, V. D., *J. Chem. Soc.(Resumed),* **1949,** 307-314.
98. Kato, H.; M, O., *Bull. Chem. Soc. Jpn.,* **1962,** *35*, 1418-1419.
99. Dumitraşcu, F.; Drâghici, C.; Dumitrescu, D.; Tarko, L.; Râileanu, D., *Liebigs Annalen,* **1997**, *1997*, 2613-2616.
100. Dumitraşcu, F. M., C. I.; Dumitrascu, D.; Drăghici, C.; Căproiu, M. T., *ARKIVOC,* **2002**, *ii*, 80-86.
101. Browne, D. L.; Taylor, J. B.; Plant, A.; Harrity, J. P. A., *J. Org. Chem.* **2008**, *74*, 396-400.
102. Turnbull, K.; Krein, D. M.; Tullis, S. A., *Synth. Commun.,* **2003**, *33*, 2209-2214.
103. Rodriguez, A. M., W. J., *Synthesis,* **2009**, *4*, 650-654.
104. Rodriguez, A.; Fennessy, R. V.; Moran, W. J., *Tet. Lett.,* **2009**, *50*, 3942-3944.
105. Yang, Y. G., H.; Kuang, C., *Synthesis,* **2013**, *45*, 1469-1474.
106. Huisgen, R.; Grashey, R.; Gotthardt, H.; Schmidt, R., *Angew. Chem. Int. Ed.,* **1962**, *1*, 48-49.
107. Maffrand, J.-P., *Heterocycles,* **1981**, *16*, 35-37.
108. Padwa, A.; Burgess, E. M.; Gingrich, H. L.; Roush, D. M., *J. Org. Chem.,* **1982**, *47*, 786-791.
109. En-Ming Chang, F. F. W., Tse-Hsin Chen, Kuo-Chen Chiang, and Mou-Yung Yeh, *Heterocycles,* **2006**, *68*, 1007-1015.
110. Browne, D. L.; Helm, M. D.; Plant, A.; Harrity, J. P. A., *Angew. Chem. Int.Ed.,* **2007**, *46*, 8656-8658.
111. Browne, D. L.; Vivat, J. F.; Plant, A.; Gomez-Bengoa, E.; Harrity, J. P. A., *J. Am. Chem. Soc.,* **2009**, *131*, 7762-7769.
112. Foster, R. S. H., J.; Vivat, J. F.; Browne, D. L.; Harrity, J. P. A., *Org. Biomol. Chem.,* **2009**, *7*, 4052-4056.
113. Kolodych, S.; Rasolofonjatovo, E.; Chaumontet, M.; Nevers, M.-C.; Créminon, C.; Taran, F., *Angew. Chem. Int. Ed.* **2013**, *52*, 12056-12060.
114. Specklin, S.; Decuypere, E.; Plougastel, L.; Aliani, S.; Taran, F., *J. Org. Chem.* **2014**, *79*, 7772-7777.
115. Decuypere, E.; Specklin, S.; Gabillet, S.; Audisio, D.; Liu, H.; Plougastel, L.; Kolodych, S.; Taran, F., *Org. Lett.* **2014**, *17*, 362-365.
116. Comas-Barceló, J.; Foster, R. S.; Fiser, B.; Gomez-Bengoa, E.; Harrity, J. P. A., *Chem. Eur. J.,* **2015**, *21*, 3257-3263.
117. Ackermann, L.; Vicente, R.; Kapdi, A. R., *Angew. Chem. Int. Ed.,* **2009**, *48*, 9792-9826.
118. Yoshikai, N.; Matsumoto, A.; Norinder, J.; Nakamura, E., *Angew. Chem. Int. Ed.,* **2009**, *48*, 2925-2928.
119. Watanabe, T.; Ueda, S.; Inuki, S.; Oishi, S.; Fujii, N.; Ohno, H., *Chem. Commun.,* **2007**, 4516-4518.
120. Satoh, T.; Kawamura, Y.; Miura, M.; Nomura, M., *Angew. Chem. Int. Ed.,* **1997**, *109*, 1820-1822.
121. Yang, J., *Organic & Biomol. Chem.,* **2015**, *13*, 1930-1941.
122. Chen, X.; Engle, K. M.; Wang, D.-H.; Yu, J.-Q., *Angew. Chem. Int. Ed.,* **2009**, *48*, 5094-5115.
123. Arockiam, P. B.; Bruneau, C.; Dixneuf, P. H., *Chem. Rev.,* **2012**, *112*, 5879-5918.

124. Maiden, T. M. M.; Swanson, S.; Procopiou, P. A.; Harrity, J. P. A., *Chem. Eur. J.,* **2015**, *21*, 14342-14346.
125. Zhang, S.-Y.; Li, Q.; He, G.; Nack, W. A.; Chen, G., *J. Am. Chem. Soc.,* **2015**, *137*, 531-539.
126. Wang, G.-W.; Yuan, T.-T.; Wu, X.-L., *J. Org. Chem.* **2008**, *73*, 4717-4720.
127. Tang, D.-T. D.; Collins, K. D.; Glorius, F., *J. Am. Chem. Soc.* **2013**, *135*, 7450-7453.
128. Berman, A. M.; Lewis, J. C.; Bergman, R. G.; Ellman, J. A., *J. Am. Chem. Soc.* **2008**, *130*, 14926-14927.
129. Maiden, T. M. M.; Swanson, S.; Procopiou, P. A.; Harrity, J. P. A., *Org. Lett.* **2016**, *18*, 3434-3437.
130. Alberico, D.; Scott, M. E.; Lautens, M., *Chem. Rev.* **2007**, *107*, 174-238.
131. Seregin, I. V.; Gevorgyan, V., *Chem. Soc. Rev.* **2007**, *36*, 1173-1193.
132. Lafrance, M.; Fagnou, K., *J. Am. Chem. Soc.,* **2006**, *128*, 16496-16497.
133. Liégault, B. t.; Lapointe, D.; Caron, L.; Vlassova, A.; Fagnou, K., *J. Org. Chem.,* **2009**, *74*, 1826-1834.
134. Campo, M. A.; Larock, R. C., *J. Am. Chem. Soc.,* **2002**, *124*, 14326-14327.
135. Zhao, D.; Wang, W.; Lian, S.; Yang, F.; Lan, J.; You, J., *Chem. Eur. J.,* **2009**, *15*, 1337-1340.
136. Goodson, F. E.; Wallow, T. I.; Novak, B. M., *J. Am. Chem. Soc.,* **1997**, *119*, 12441-12453.
137. Surry, D. S.; Buchwald, S. L., *Angew. Chem. Int. Ed.,* **2008**, *47*, 6338-6361.
138. Billingsley, K.; Buchwald, S. L., *J. Am. Chem. Soc.,* **2007**, *129*, 3358-3366.
139. Barder, T. E.; Buchwald, S. L., *J. Am. Chem. Soc.,* **2007**, *129*, 5096-5101.
140. Strieter, E. R.; Buchwald, S. L., *Angew. Chem. Int. Ed.,* **2006**, *118*, 939-942.
141. Romagnoli, R.; Baraldi, P. G.; Brancale, A.; Ricci, A.; Hamel, E.; Bortolozzi, R.; Basso, G.; Viola, G., *J. Med. Chem.,* **2011**, *54*, 5144-5153.
142. Goode, B. L.; Drubin, D. G.; Barnes, G., *Curr. Opin. Cell Bio.,* **2000**, *12*, 63-71.
143. McGown, A. T.; Fox, B. W., *Anti-cancer Drug Des.,* **1989**, *3*, 249-54.
144. Galbraith, S. M.; Chaplin, D. J.; Lee, F.; Stratford, M. R.; Locke, R. J.; Vojnovic, B.; Tozer, G. M., *Anticancer Res.,* **2001**, *21*, 93-102.
145. Towbin, H.; Staehelin, T.; Gordon, J., *Proc. Natl. Acad. Sci.,* **1979**, *76*, 4350-4354.
146. Renart, J.; Reiser, J.; Stark, G. R., *Proc. Natl. Acad. Sci.,* **1979**, *76*, 3116-3120.
147. Chalkley, H. W., *J. Natl. Cancer Inst.* **1943**, *4*, 47-53.
148. Foster, R. S.; Adams, H.; Jakobi, H.; Harrity, J. P. A., *J. Org. Chem.,* **2013**, *78*, 4049-4064.
149. Brown, A. W.; Harrity, J. P. A., *J. Org. Chem.,* **2015**, *80*, 2467-2472.
150. Langlois, B. R., *Tet. Lett.,* **1991**, *32*, 3691-3694.
151. Zhang, W.; Zhu, L.; Hu, J., *Tetrahedron,* **2007**, *63*, 10569-10575.
152. Vivat, J. F.; Adams, H.; Harrity, J. P. A., *Org. Lett.,* **2010**, *12*, 160-163.
153. Kirkham, J. D.; Butlin, R. J.; Harrity, J. P. A., *Angew. Chem. Int. Ed.,* **2012**, *51*, 6402-6405.
154. Delaney, P. M.; Browne, D. L.; Adams, H.; Plant, A.; Harrity, J. P. A., *Tetrahedron,* **2008**, *64*, 866-873.
155. Crépin, D. F. P.; Harrity, J. P. A.; Jiang, J.; Meijer, A. J. H. M.; Nassoy, A.-C. M. A.; Raubo, P., *J. Am. Chem. Soc.,* **2014**, *136*, 8642-8653.
156. Bayer, Michael J.; Pritzkow, H.; Siebert, W., *Eur. J. Inorg. Chem.,* **2002**, *2002*, 1293-1300.
157. Crépin, D. F.; Harrity, J. P. A., *Org. Lett.,* **2013**, *15*, 4222-4225.
158. Bachollet, S. P. J. T.; Vivat, J. F.; Cocker, D. C.; Adams, H.; Harrity, J. P. A., *Chem. Eur. J.,* **2014**, *20*, 12889-12893.
159. Kirkham, J. D.; Edeson, S. J.; Stokes, S.; Harrity, J. P. A., *Org. Lett.,* **2012**, *14*, 5354-5357.
160. Shih, C.; Swenton, J. S., *J. Org. Chem.,* **1982**, *47*, 2668-2670.
161. Meyers, A. I.; Temple, D. L., *J. Am. Chem. Soc.,* **1970**, *92*, 6644-6646.

162. Giri, R.; Chen, X.; Yu, J.-Q., *Angew. Chem. Int. Ed.,* **2005**, *44*, 2112-2115.
163. Meyers, A. I.; Reuman, M.; Gabel, R. A., *J. Org. Chem.,* **1981**, *46*, 783-788.
164. Sidduri, A.; Tilley, J. W.; Lou, J. P.; Chen, L.; Kaplan, G.; Mennona, F.; Campbell, R.; Guthrie, R.; Huang, T.-N.; Rowan, K.; Schwinge, V.; Renzetti, L. M., *Bioorg. Med. Chem. Lett.,* **2002**, *12*, 2479-2482.
165. Song, Y.; De Silva, H. I.; Henry, W. P.; Ye, G.; Chatterjee, S.; Pittman Jr, C. U., *Tet. Lett.,* **2011**, *52*, 4507-4511.
166. Orgel, L. E.; Cottrell, T. L.; Dick, W.; Sutton, L. E., *J. Chem. Soc. Faraday Trans.,* **1951**, *47*, 113-119.
167. Bregadze, V. I.; Furmanova, N. G.; Golubinskaya, L. M.; Kompan, O. Y.; Struchkov, Y. T.; Bren, V. A.; Bren, Z. V.; Lyubarskaya, A. E.; Minkin, V. I.; Sitkina, L. M., *J. Organomet. Chem.,* **1980**, *192*, 1-15.
168. Dou, C.; Long, X.; Ding, Z.; Xie, Z.; Liu, J.; Wang, L., *Angew. Chem. Int. Ed.,* **2016**, *55*, 1436-1440.
169. D.D.Perrin; W.L.F.Armarego, Armarego, W. L. F.; Chai, C. L. L., Eds. Butterworth-Heinemann: *Purification of Laboratory Chemicals*, 6th Ed.; Oxford, 2009; pp xiv-xv.
170. Saalfrank, R. W.; Weiß, B., *Chem. Ber.,* **1985**, *118*, 2626-2634.
171. Joshi, P. C.; Parmar, S. S.; Rastogi, V. K., *J. Heterocyclic Chem.,* **1979**, *16*, 607-608.
172. Satheesha Rai, N.; Kalluraya, B.; Lingappa, B.; Shenoy, S.; Puranic, V. G., *Eur. J. Med. Chem.,* **2008**, *43*, 1715-1720.
173. Yashunski, V. G.; Vasil'eva, V. F.; Sheinker, Y. N., *Zh. Obshch. Khim.,* **1959**, *29*, 2712-2718.
174. Bellas, M.; Suschitzky, H., *J. Chem. Soc. C: Org.,* **1966**, 189-192.
175. Fang, Y.; Wu, C.; Larock, R. C.; Shi, F., *J. Org. Chem.,* **2011**, *76*, 8840-8851.
176. Nakajima, M.; Anselme, J. P., *J. Org. Chem.,* **1983**, *48*, 1444-1448.
177. Yang, Y.; Gong, H.; Kuang, C., *Synthesis,* **2013**, *45*, 1469-1474.
178. Wang, X.; Meng, F.; Wang, Y.; Han, Z.; Chen, Y.-J.; Liu, L.; Wang, Z.; Ding, K., *Angew. Chem.Int. Ed.,* **2012**, *51*, 9276-9282.
179. Kaffy, J.; Pontikis, R.; Florent, J.-C.; Monneret, C., *Org. Biomol. Chem.,* **2005**, *3*, 2657-2660.
180. Chen, Y.; Zou, Y.; Sun, H.-Y.; Liu, X.-K.; Xiao, C.-F.; Sun, J.; He, S.-J.; Li, J., *Synthesis,* **2011**, *2011*, 217-222.
181. Pettit, G. R., US 5561122 A: 1996.
182. Yu, Y.; Singh, S. K.; Liu, A.; Li, T.-K.; Liu, L. F.; LaVoie, E. J., *Bioorg. Med. Chem.,* **2003**, *11*, 1475-1491.
183. White, R. L.; Schwan, T. J.; Alaimo, R. J., *J. Heterocyclic Chem.,* **1980**, *17*, 817-818.
184. Bromidge, S., M., Lovell, P., J., Goodacre, C., WO 03057220, 2003.
185. Gandon, V.; Leca, D.; Aechtner, T.; Vollhardt, K. P. C.; Malacria, M.; Aubert, C., *Org. Lett.,* **2004**, *6*, 3405-3407.
186. Rueda-Becerril, M.; Mahé, O.; Drouin, M.; Majewski, M. B.; West, J. G.; Wolf, M. O.; Sammis, G. M.; Paquin, J.-F., *J. Am. Chem. Soc.,* **2014**, *136*, 2637-2641.
187. Pelphrey, P. M.; Popov, V. M.; Joska, T. M.; Beierlein, J. M.; Bolstad, E. S. D.; Fillingham, Y. A.; Wright, D. L.; Anderson, A. C., *J. Med. Chem.,* **2007**, *50*, 940-950.
188. Santos-Filho, E. F.; Sousa, J. C.; Bezerra, N. M. M.; Menezes, P. H.; Oliveira, R. A., *Tet. Lett.,* **2011**, *52*, 5288-5291.
189. Jouvin, K.; Couty, F.; Evano, G., *Org. Lett.,* **2010**, *12*, 3272-3275.
190. Kato, H.; Ohta, M., *Bull. Chem. Soc. Jap.,* **1959**, *32*, 282-284.
191. Vieira, A. S.; Fiorante, P. F.; Hough, T. L. S.; Ferreira, F. P.; Lüdtke, D. S.; Stefani, H. A., *Org. Lett.,* **2008**, *10*, 5215-5218.
192. Yamamoto, Y.; Hattori, K.; Ishii, J.-i.; Nishiyama, H., *Tetrahedron,* **2006**, *62*, 4294-4305.

Appendices

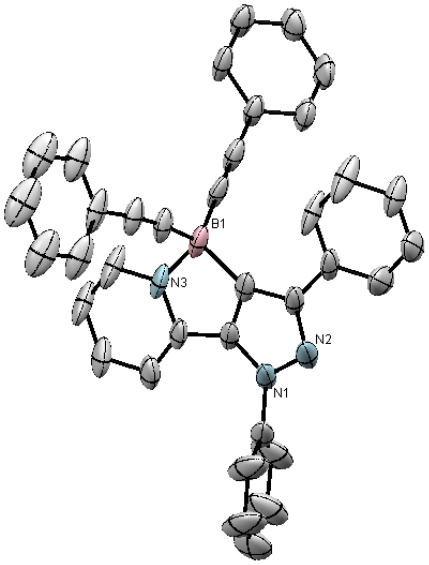

Table 1. Crystal data and structure refinement for zhu18-twin.

Identification code	zhu18-twin	
Empirical formula	C36 H24 B N3	
Formula weight	509.39	
Temperature	446(2) K	
Wavelength	0.71073 Å	
Crystal system	Monoclinic	
Space group	C2/c	
Unit cell dimensions	a = 33.043(4) Å	α= 90°.
	b = 9.1771(10) Å	β= 115.283(9)°.
	c = 20.128(2) Å	γ = 90°.
Volume	5519.1(12) $Å^3$	
Z	8	
Density (calculated)	1.226 Mg/m^3	
Absorption coefficient	0.072 mm^{-1}	
F(000)	2128	
Crystal size	0.200 x 0.200 x 0.120 mm^3	
Theta range for data collection	2.238 to 27.691°.	
Index ranges	-42<=h<=42, -11<=k<=11, -26<=l<=26	
Reflections collected	24047	

Independent reflections	24047 [R(int) = ?]
Completeness to theta = 25.242°	99.6 %
Absorption correction	None
Refinement method	Full-matrix least-squares on F^2
Data / restraints / parameters	24047 / 144 / 363
Goodness-of-fit on F^2	1.045
Final R indices [I>2sigma(I)]	R1 = 0.1065, wR2 = 0.2272
R indices (all data)	R1 = 0.1844, wR2 = 0.2726
Extinction coefficient	0.0008(2)
Largest diff. peak and hole	0.771 and -0.830 e.$Å^{-3}$

Table 2. Atomic coordinates (x 10^4) and equivalent isotropic displacement parameters ($Å^2$x 10^3) for zhu18-twin. U(eq) is defined as one third of the trace of the orthogonalized U^{ij} tensor.

	x	y	z	U(eq)
B(1)	1121(2)	11064(5)	3714(3)	47(2)
N(1)	402(2)	8004(4)	3687(3)	67(2)
N(2)	744(2)	7062(4)	3764(3)	74(2)
N(3)	643(2)	11804(4)	3612(2)	48(1)
C(1)	1082(2)	7905(5)	3770(3)	57(2)
C(2)	962(2)	9402(4)	3705(2)	47(2)
C(3)	537(2)	9392(4)	3653(2)	48(2)
C(4)	330(2)	10816(5)	3592(2)	47(2)
C(5)	-84(2)	11268(5)	3519(3)	61(2)
C(6)	-180(2)	12745(5)	3467(3)	66(2)
C(7)	141(2)	13728(6)	3482(3)	73(2)
C(8)	547(2)	13227(5)	3561(3)	69(2)
C(9)	3(3)	7515(5)	3741(4)	71(2)
C(10)	-383(3)	7509(7)	3164(4)	95(2)
C(11)	-763(3)	7077(7)	3228(4)	98(2)
C(12)	-752(3)	6620(7)	3866(4)	90(2)
C(13)	-344(3)	6593(8)	4466(4)	107(2)
C(14)	45(3)	7059(7)	4413(4)	103(2)
C(15)	1503(2)	7252(4)	3841(3)	55(1)
C(16)	1560(2)	5761(5)	3807(4)	90(2)
C(17)	1969(2)	5165(6)	3907(4)	80(2)
C(18)	2317(2)	6017(5)	4022(3)	62(1)
C(19)	2268(2)	7498(5)	4051(3)	81(2)
C(20)	1863(2)	8108(5)	3959(3)	67(2)
C(21)	1481(2)	11592(4)	4478(3)	50(2)
C(22)	1730(2)	12012(4)	5081(3)	53(2)
C(23)	2003(2)	12488(5)	5825(3)	61(1)
C(24)	1882(2)	12091(5)	6385(3)	69(2)
C(25)	2127(2)	12582(5)	7097(3)	80(2)
C(26)	2494(2)	13466(6)	7255(3)	86(2)
C(27)	2617(2)	13863(6)	6710(3)	82(2)
C(28)	2375(2)	13369(5)	5991(3)	69(2)
C(29)	1207(2)	11527(4)	3033(3)	51(2)
C(30)	1263(2)	11852(4)	2501(2)	51(2)
C(31)	1336(2)	12224(4)	1865(2)	46(1)

C(32)	1541(2)	13525(4)	1836(2)	57(2)
C(33)	1620(2)	13861(5)	1232(2)	58(2)
C(34)	1494(2)	12902(5)	650(3)	62(2)
C(35)	1287(2)	11609(6)	676(3)	67(2)
C(36)	1207(2)	11266(5)	1273(3)	60(2)

Table 3. Bond lengths [Å] and angles [°] for zhu18-twin.

B(1)-C(21)	1.566(7)
B(1)-C(29)	1.573(7)
B(1)-C(2)	1.610(6)
B(1)-N(3)	1.649(8)
N(1)-C(3)	1.362(5)
N(1)-N(2)	1.378(6)
N(1)-C(9)	1.438(7)
N(2)-C(1)	1.356(7)
N(3)-C(8)	1.337(6)
N(3)-C(4)	1.365(6)
C(1)-C(2)	1.420(6)
C(1)-C(15)	1.463(8)
C(2)-C(3)	1.364(7)
C(3)-C(4)	1.457(6)
C(4)-C(5)	1.376(7)
C(5)-C(6)	1.386(6)
C(5)-H(5)	0.9300
C(6)-C(7)	1.384(8)
C(6)-H(6)	0.9300
C(7)-C(8)	1.362(8)
C(7)-H(7)	0.9300
C(8)-H(8)	0.9300
C(9)-C(10)	1.308(9)
C(9)-C(14)	1.366(7)
C(10)-C(11)	1.376(9)
C(10)-H(10)	0.9300
C(11)-C(12)	1.337(7)
C(11)-H(11)	0.9300
C(12)-C(13)	1.373(10)
C(12)-H(12)	0.9300
C(13)-C(14)	1.401(9)
C(13)-H(13)	0.9300
C(14)-H(14)	0.9300
C(15)-C(20)	1.362(8)
C(15)-C(16)	1.387(6)
C(16)-C(17)	1.390(8)
C(16)-H(16)	0.9300
C(17)-C(18)	1.327(8)

C(17)-H(17)	0.9300
C(18)-C(19)	1.373(6)
C(18)-H(18)	0.9300
C(19)-C(20)	1.386(8)
C(19)-H(19)	0.9300
C(20)-H(20)	0.9300
C(21)-C(22)	1.203(6)
C(22)-C(23)	1.447(7)
C(23)-C(28)	1.387(8)
C(23)-C(24)	1.395(8)
C(24)-C(25)	1.387(7)
C(24)-H(24)	0.9300
C(25)-C(26)	1.380(8)
C(25)-H(25)	0.9300
C(26)-C(27)	1.371(9)
C(26)-H(26)	0.9300
C(27)-C(28)	1.396(7)
C(27)-H(27)	0.9300
C(28)-H(28)	0.9300
C(29)-C(30)	1.200(6)
C(30)-C(31)	1.441(6)
C(31)-C(32)	1.387(6)
C(31)-C(36)	1.393(6)
C(32)-C(33)	1.380(6)
C(32)-H(32)	0.9300
C(33)-C(34)	1.380(6)
C(33)-H(33)	0.9300
C(34)-C(35)	1.381(7)
C(34)-H(34)	0.9300
C(35)-C(36)	1.374(7)
C(35)-H(35)	0.9300
C(36)-H(36)	0.9300

C(21)-B(1)-C(29)	115.4(5)
C(21)-B(1)-C(2)	114.3(4)
C(29)-B(1)-C(2)	115.2(4)
C(21)-B(1)-N(3)	106.2(4)
C(29)-B(1)-N(3)	107.4(4)
C(2)-B(1)-N(3)	95.7(4)
C(3)-N(1)-N(2)	108.8(5)

C(3)-N(1)-C(9)	128.8(5)
N(2)-N(1)-C(9)	121.9(4)
C(1)-N(2)-N(1)	106.0(4)
C(8)-N(3)-C(4)	119.6(5)
C(8)-N(3)-B(1)	126.6(5)
C(4)-N(3)-B(1)	113.9(4)
N(2)-C(1)-C(2)	110.8(5)
N(2)-C(1)-C(15)	120.8(4)
C(2)-C(1)-C(15)	128.4(5)
C(3)-C(2)-C(1)	103.7(4)
C(3)-C(2)-B(1)	109.1(4)
C(1)-C(2)-B(1)	147.0(6)
N(1)-C(3)-C(2)	110.6(4)
N(1)-C(3)-C(4)	133.7(5)
C(2)-C(3)-C(4)	115.7(4)
N(3)-C(4)-C(5)	120.7(4)
N(3)-C(4)-C(3)	105.6(5)
C(5)-C(4)-C(3)	133.6(5)
C(4)-C(5)-C(6)	119.2(6)
C(4)-C(5)-H(5)	120.4
C(6)-C(5)-H(5)	120.4
C(7)-C(6)-C(5)	119.2(6)
C(7)-C(6)-H(6)	120.4
C(5)-C(6)-H(6)	120.4
C(8)-C(7)-C(6)	119.4(5)
C(8)-C(7)-H(7)	120.3
C(6)-C(7)-H(7)	120.3
N(3)-C(8)-C(7)	122.0(6)
N(3)-C(8)-H(8)	119.0
C(7)-C(8)-H(8)	119.0
C(10)-C(9)-C(14)	121.7(6)
C(10)-C(9)-N(1)	120.8(5)
C(14)-C(9)-N(1)	117.6(7)
C(9)-C(10)-C(11)	120.1(6)
C(9)-C(10)-H(10)	119.9
C(11)-C(10)-H(10)	119.9
C(12)-C(11)-C(10)	121.9(8)
C(12)-C(11)-H(11)	119.0
C(10)-C(11)-H(11)	119.0
C(11)-C(12)-C(13)	117.6(7)

C(11)-C(12)-H(12)	121.2
C(13)-C(12)-H(12)	121.2
C(12)-C(13)-C(14)	121.1(6)
C(12)-C(13)-H(13)	119.4
C(14)-C(13)-H(13)	119.4
C(9)-C(14)-C(13)	117.5(7)
C(9)-C(14)-H(14)	121.3
C(13)-C(14)-H(14)	121.3
C(20)-C(15)-C(16)	116.7(6)
C(20)-C(15)-C(1)	120.3(4)
C(16)-C(15)-C(1)	122.9(5)
C(15)-C(16)-C(17)	121.7(6)
C(15)-C(16)-H(16)	119.1
C(17)-C(16)-H(16)	119.1
C(18)-C(17)-C(16)	120.6(5)
C(18)-C(17)-H(17)	119.7
C(16)-C(17)-H(17)	119.7
C(17)-C(18)-C(19)	118.8(6)
C(17)-C(18)-H(18)	120.6
C(19)-C(18)-H(18)	120.6
C(18)-C(19)-C(20)	121.2(6)
C(18)-C(19)-H(19)	119.4
C(20)-C(19)-H(19)	119.4
C(15)-C(20)-C(19)	120.8(5)
C(15)-C(20)-H(20)	119.6
C(19)-C(20)-H(20)	119.6
C(22)-C(21)-B(1)	174.8(6)
C(21)-C(22)-C(23)	175.7(7)
C(28)-C(23)-C(24)	119.2(5)
C(28)-C(23)-C(22)	121.6(5)
C(24)-C(23)-C(22)	119.2(6)
C(25)-C(24)-C(23)	120.6(6)
C(25)-C(24)-H(24)	119.7
C(23)-C(24)-H(24)	119.7
C(26)-C(25)-C(24)	119.8(6)
C(26)-C(25)-H(25)	120.1
C(24)-C(25)-H(25)	120.1
C(27)-C(26)-C(25)	120.2(5)
C(27)-C(26)-H(26)	119.9
C(25)-C(26)-H(26)	119.9

C(26)-C(27)-C(28)	120.6(6)
C(26)-C(27)-H(27)	119.7
C(28)-C(27)-H(27)	119.7
C(23)-C(28)-C(27)	119.7(6)
C(23)-C(28)-H(28)	120.2
C(27)-C(28)-H(28)	120.2
C(30)-C(29)-B(1)	178.1(5)
C(29)-C(30)-C(31)	179.0(6)
C(32)-C(31)-C(36)	119.0(4)
C(32)-C(31)-C(30)	120.8(4)
C(36)-C(31)-C(30)	120.2(4)
C(33)-C(32)-C(31)	120.6(4)
C(33)-C(32)-H(32)	119.7
C(31)-C(32)-H(32)	119.7
C(32)-C(33)-C(34)	120.2(5)
C(32)-C(33)-H(33)	119.9
C(34)-C(33)-H(33)	119.9
C(33)-C(34)-C(35)	119.3(5)
C(33)-C(34)-H(34)	120.3
C(35)-C(34)-H(34)	120.3
C(36)-C(35)-C(34)	121.0(4)
C(36)-C(35)-H(35)	119.5
C(34)-C(35)-H(35)	119.5
C(35)-C(36)-C(31)	119.9(5)
C(35)-C(36)-H(36)	120.0
C(31)-C(36)-H(36)	120.0

Symmetry transformations used to generate equivalent atoms:

Table 4. Anisotropic displacement parameters ($Å^2 x\ 10^3$) for zhu18-twin. The anisotropic displacement factor exponent takes the form: $-2\pi^2[\ h^2\ a^{*2}U^{11} + ... + 2\ h\ k\ a^*\ b^*\ U^{12}\ ]$

	U^{11}	U^{22}	U^{33}	U^{23}	U^{13}	U^{12}
B(1)	89(5)	18(2)	34(3)	-2(2)	25(3)	-5(3)
N(1)	133(5)	21(2)	98(4)	0(2)	99(4)	-4(3)
N(2)	149(5)	22(2)	110(4)	4(2)	112(4)	-1(3)
N(3)	88(4)	20(2)	30(2)	-8(2)	18(2)	-4(2)
C(1)	120(5)	21(2)	63(3)	1(2)	71(4)	-1(3)
C(2)	99(5)	25(2)	33(3)	-1(2)	43(3)	-4(3)
C(3)	102(5)	23(2)	43(3)	-2(2)	53(3)	-5(3)
C(4)	95(5)	26(2)	33(3)	-9(2)	39(3)	-6(3)
C(5)	113(6)	37(3)	52(3)	-8(2)	55(4)	2(3)
C(6)	98(5)	41(3)	54(3)	-22(2)	27(3)	3(3)
C(7)	83(5)	27(3)	75(4)	-22(3)	2(4)	0(3)
C(8)	84(5)	23(3)	61(4)	-12(2)	-6(3)	-2(3)
C(9)	141(4)	35(2)	88(3)	-11(2)	98(3)	-21(3)
C(10)	132(4)	101(3)	101(3)	41(3)	97(3)	23(3)
C(11)	128(4)	107(4)	104(3)	42(3)	93(3)	24(3)
C(12)	133(4)	90(3)	93(3)	15(3)	92(3)	-2(4)
C(13)	156(5)	119(4)	82(3)	-13(3)	85(3)	-75(4)
C(14)	157(4)	111(3)	77(3)	-30(3)	85(3)	-81(3)
C(15)	117(4)	18(2)	57(3)	3(2)	62(3)	3(2)
C(16)	125(4)	26(2)	167(4)	-2(3)	108(3)	-3(3)
C(17)	123(4)	23(2)	139(4)	-1(2)	98(3)	6(2)
C(18)	97(4)	27(2)	45(2)	-2(2)	13(3)	6(2)
C(19)	88(4)	29(2)	72(3)	-5(2)	-17(3)	7(2)
C(20)	91(4)	17(2)	53(3)	-3(2)	-6(3)	6(2)
C(21)	90(5)	18(2)	41(3)	0(2)	26(3)	5(3)
C(22)	82(5)	21(2)	44(3)	2(2)	14(3)	11(3)
C(23)	95(4)	18(2)	38(2)	4(2)	-2(2)	16(2)
C(24)	107(4)	27(2)	38(2)	10(2)	-3(2)	6(2)
C(25)	115(4)	42(3)	37(2)	14(2)	-11(3)	2(3)
C(26)	111(4)	47(3)	43(3)	15(2)	-22(3)	3(3)
C(27)	98(4)	42(3)	53(3)	12(2)	-18(3)	7(3)
C(28)	91(4)	30(2)	49(2)	6(2)	-5(3)	14(2)
C(29)	91(5)	15(2)	42(3)	-1(2)	25(3)	-11(2)
C(30)	90(5)	20(2)	39(3)	-2(2)	22(3)	-8(3)
C(31)	84(4)	20(2)	37(3)	1(2)	27(3)	-3(2)

C(32)	116(5)	20(2)	38(3)	-2(2)	36(3)	-7(3)
C(33)	109(5)	27(2)	46(3)	2(2)	41(3)	-8(3)
C(34)	103(5)	49(3)	48(3)	-5(2)	47(3)	-1(3)
C(35)	106(6)	52(3)	55(3)	-29(3)	46(4)	-16(3)
C(36)	102(5)	34(3)	56(3)	-17(2)	43(3)	-14(3)

Table 5. Hydrogen coordinates (x 10^4) and isotropic displacement parameters ($Å^2$x 10^3) for zhu18-twin.

	x	y	z	U(eq)
H(5)	-297	10590	3505	73
H(6)	-457	13071	3421	80
H(7)	80	14722	3439	88
H(8)	764	13893	3580	82
H(10)	-400	7797	2710	114
H(11)	-1036	7104	2815	118
H(12)	-1012	6331	3903	108
H(13)	-326	6259	4914	128
H(14)	321	7058	4821	123
H(16)	1318	5144	3715	108
H(17)	1998	4159	3893	97
H(18)	2589	5618	4081	75
H(19)	2511	8103	4135	97
H(20)	1838	9115	3976	80
H(24)	1635	11492	6279	83
H(25)	2043	12317	7467	96
H(26)	2660	13793	7733	103
H(27)	2863	14466	6820	98
H(28)	2463	13630	5626	83
H(32)	1627	14177	2226	68
H(33)	1758	14736	1218	69
H(34)	1548	13124	244	74
H(35)	1202	10962	285	80
H(36)	1065	10395	1282	72